# Lithostratigraphic and Geochemical Characterisation of the Waterberg Coalfield: Implications to Acid Mine Drainage, Limpopo Province, South Africa

BY

Ramphabana Khethani Tom

Student No: 17002715

**A dissertation submitted to the Department of Earth Sciences, Faculty of Science, Engineering and Agriculture, in fulfilment of the requirements for the degree of Master of Earth Sciences in Mining and Environmental Geology**

Supervisor : Dr. H.R. Mundalamo

Co-supervisor : Emeritus Prof. J.S. Ogola

Co-supervisor : Mr. K.T.R. Netshitungulwana

**August 2023**

# DECLARATION

I, **Ramphabana Khethani Tom**, declare that the work presented in this dissertation is mine, and it has not been submitted for any other degree or professional qualification. I also confirm that the work submitted to the Department of Earth Sciences is mine, and any ideas, arguments and data used have been acknowledged.

Student's signature

15/08/2023

Date

# DEDICATION

I dedicate this dissertation to my family and friends for the moral support they provided in completion of my Masters of Earth Sciences in Mining and Environmental Geology.

# ACKNOWLEDGEMENT

Firstly, I am grateful to the almighty God for giving me strength, attentiveness and understanding to complete this project.

I express my profound gratitude to my supervisor Dr. H.R. Mundalamo for her hard work, patience, training and guidance throughout this project. To my Co-supervisors, Emeritus Professor J.S. Ogola and Mr. K.T.R. Netshitungulwana thanks for your invaluable scientific guidance, persistence, and motivation throughout the research work. This work would not have been possible without your mammoth contributions. To Professor N. Wagner, I would like to confer my sincerest gratitude for organic petrology training provided at the University of Johannesburg.

My sincerest gratitude to my sponsors, the National Research Foundation (NRF) (reference: MND200626537137), DSI-NRF-Centre of Excellence for Integrated Mineral and Energy Resource Analysis (CIMERA) and Council for Geoscience (CGS) for their financial support through the course of my study.

Special thanks to Dr. K. Singo of Singo Consulting and Mr. G.M. Mapholi of Sekoko Lephalale Coal Concession mine for their wonderful assistance in provision of access to the box-cut within the aforementioned mine.

Mr. T. Mphanana, my mentor and friend, has been invaluable in assisting me with fieldwork and sample collection. He has truly taught me a lot. Mrs. N. Lilimu, the laboratory technician from the Department of Earth Science at the University of Venda, deserves my heartfelt thanks for her assistance during laboratory preparations. Special thanks to the University of Venda's Department of Earth Science for providing access to laboratory equipment and other university resources used in this study. I'd also like to thank Waterlab (Pty) Ltd, the University of Pretoria, the University of Johannesburg, Bureau Veritas, and the University of Cape Town for their invaluable assistance with laboratory analyses.

# ABSTRACT

The study conducted at Sekoko coal mine in the Waterberg coalfield of South Africa aimed to establish the quality of coal and its host rocks, as well as the potential for acid mine water generation.

A total of 18 samples were collected from a box-cut and analysed using various methods such as, Scanning electron microscopy, X-ray diffraction spectroscopy, X-ray fluorescence spectroscopy, proximate analysis, Modified Sobek Acid Base Accounting test as well as petrographic study. The major rock types identified in the study area included shale, sandstone and gritstone. Coal was overlain by these rocks.

The study revealed significant concentrations of framboidal pyrite in coal, which increases with depth as determined by X-ray Diffraction spectroscopy and scanning electron microscopy. Whole rock geochemistry indicates that $Fe_2O_3$ was higher in coal (1.18 wt%) than in host rocks (0.45 wt%) and increased with depth. Average mean of 1.23% a.d. for sulphur content was revealed thus, classifying the coal as medium sulphur coal. Sulphur occurred as pyritic, organic, and as sulphate, in that order of abundance. Using both proximate analysis and calorific value (with mean value of 21.2 Mj/kg) coal was classified as below grade D. From the vitrinite reflectance value (ranging between 0.6 to 0.7), coal was ranked as medium-grade bituminous C. Paste pH and EC results indicated that the Sekoko coal is already undergoing oxidation, and modified Sobek tests indicated that over 72% of the analysed samples have sufficient sulphur to generate long-term acid mine drainage. The potential for acid generation increases with depth (1.09 to 181 kg/t) and was high on the southern side (181 kg/t) than the western side (52 kg/t). Results indicate that there aren't enough neutralization materials to counter the acid production potential as the neutralisation potential is negative for all samples.

The study concluded that the coal from Sekoko coal deposit is enriched with pyrite minerals, hence this causes an increase in the potential for acid mine water generation. Screening of coal prior to utilization is recommended so as to reduce the content of pyrite in coal.

**Keywords:** *Waterberg Coalfield, Acid Mine Drainage, Acid Base Accounting, Coal Quality*

## TABLE OF CONTENT

# LIST OF FIGURES

# LIST OF TABLES

## LIST OF ACRONYMS AND ABBREVIATIONS

| | |
|---|---|
| **ABA** | Acid Base Accounting |
| **ABACUS** | Acid Base Accounting Cumulative Screening Tool |
| **ad** | air dried |
| **AMD** | Acid Mine Drainage |
| **AP** | Acid Production |
| **ASTM** | American Society for Testing |
| **CBM** | Coal Bed Methane |
| **CIA** | Chemical Index of Alteration |
| **CIW** | Chemical Index of Weathering |
| **daf** | dry ash free |
| **db** | dry basis |
| **EC** | Electrical Conductivity |
| **EDX** | Energy dispersive X-ray Analysis |
| **EPA** | Environmental Protection Agency |
| **FFF** | Fossil Fuel Foundation |
| **F-R** | West Right |
| **GARD** | Global Acid Rock Drainage |
| **ICCP** | International Committee for Coal Petrology |
| **ICP-OES** | Inductively Coupled Plasma-Optical Emission Spectroscopy |
| **Inc. mm** | Including Mineral Matter |
| **ISO** | International Organisation for Standards |
| **Kg** | Kilograms |
| **LMB** | Limpopo Mobile Belt |
| **MKB** | Main Karoo Basin |
| **mmf** | Mineral Matter Free |
| **NNP** | Net Neutralising Potential |
| **NP** | Neutralising Potential |
| **NPR** | Neutralisation Potential Ratio |
| **PIA** | Plagioclase Index of Alteration |
| **SACRM** | South African Coal Road Map |
| **SANS** | South African National Standards |
| **SEM** | Scanning Electron Microscopy |
| **SHOS** | Super High Organic Sulphur |
| **S-L** | South Left |

| | |
|---|---|
| **WCA** | World Coal Association |
| **WHO** | World Health Organization |
| **XRD** | X-Ray Diffraction |
| **XRF** | X-Ray Fluorescence |

# CHAPTER 1: INTRODUCTION

## 1.1 Background

Coal is a combustible, sedimentary organic rock mainly composed of carbon, hydrogen and oxygen (White and Thiessen, 1913). O'Keefe *et al.* (2013) further elucidated that coal is a complex ignitable sedimentary rock composed mainly but not completely of aquatic plant remains. It is formed from organic matter that has been buried under high pressure and heat (WCA, 2015). The formation of coal began during the carboniferous period (360 to 290 million years ago) also known as the first coal age (WCA, 2015). The formation of coal in South Africa took place during the Permian Period which lasted from 299 to 252 million years ago (Arnold, 2023). The energy that we get from coal was accumulated by organic matter from the sun (Thomas, 2013; Wagner *et al.,* 2018).

The formation of coal takes place gradually over millions of years. This occurs when sediments pileup on organic matter causing an increase in pressure and temperature increase. This causes the organic matter to undergo various transformation from peat to anthracite (Wagner *et.al.*, 2018).

There is an increase in environmental awareness such as depletion of natural resources and impact on the environment. Coal plays a significant role in society, however, coal resources are gradually getting depleted due to rapid increase in population which necessitates generation of more energy and consequently put pressure on coal resources (Deysel, 2015). South Africa depends largely on coal to fulfil its energy demand and as a result mining of coal is unavoidable (Deysel, 2015).

South Africa is facing an uncertain future as a result of global climate change causing changes in temparatures (Murdoch, 2018). Since 2003, South Africa's coal production has been stagnant, owing to the gradual depletion of the Witbank, Ermelo, and Highveld Coalfields in Mpumalanga province (Creamer media's mining weekly, 2010). As a result, the South African coal Road Map (SACRM), created in 2013, investigated short-, medium-, and long-term activities to support the South African coal industry (Fossil Fuel Foundation, 2013; Ramane, 2014). There is a scenario in the SACRM that suggests that the medium- and long-term development of the South African coal industry is dependent on the opening of the Waterberg Coalfield in the Ellisras Basin (Murdoch, 2018). However, if this scenario is implemented, the environmental consequences of mining should be considered. According to Deysel (2015),

coal mining has a significant environmental impact because it has the potential to cause Acid Mine Drainage (AMD), affect water quality both on the surface and underground, and cause air pollution.

South Africa relies heavily on mining for economic growth; however, Acid Mine Drainage is a major threat to the environment (Ferguson and Erikson, 1988). According to Nengovhela *et al*. (2006), AMD is caused by the oxidation of sulphide minerals when exposed to water and oxygen. They went on to say that AMD has serious environmental consequences such as water contamination and soil degradation. As a result, the focus of this research was on the lithostratigraphic and geochemical characterisation of the Waterberg Coalfield, as well as the implications for acid mine water generation.

## 1.2 Study Area

### 1.2.1 Location

The Waterberg Coalfield is located 400 km northwest of Johannesburg in the Limpopo Province (Fig. 1.1). The Coalfield extends approximately 90 km east-west and 40 km north-south and covers 360 000 hectares (Henderson, 1986). The Waterberg Coalfield ranges from the Palala shear zone in the east to the Botswana border in the west (Hancox, 1998). The northern boundary of the Coalfield is defined by the Melinda fault zone (Falcon, 1988), whereas the southern boundary is defined by the Eenzaamheid fault zone where rocks of the Waterberg Group occur (Fourie *et al.*, 2014).

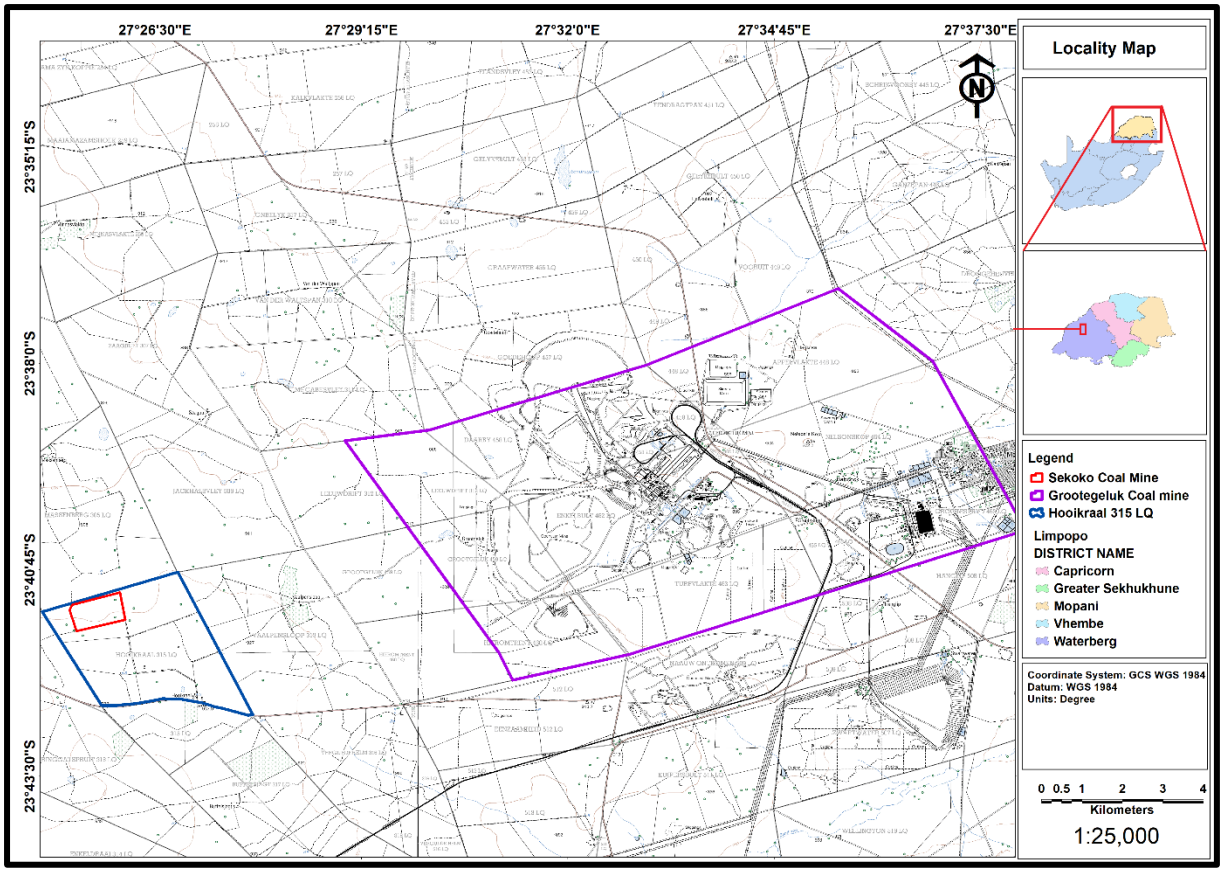


Figure 1.1: Locality map of Sekoko coal mine (ArcGIS 10.8, 2022).

### 1.2.2 Climate

The northern and western regions of the area experience a hot and semi-arid climate whereas the southern and eastern regions are more humid and slightly cooler (Waterberg Municipality, 2013). The mean circulation of the atmosphere over southern Africa is anti-cyclonic throughout the year (SAWS, 2016).

The municipality area falls within the summer rainfall region of Limpopo province with rainy season lasting from November to March. The average rainfall is between 600 and 650 mm (Fig. 1.2) with the highest measurements in January and December (SAWS, 2016). The south-east of the Waterberg Formation receives more rainfall than the other surrounding areas (Waterberg Municipality, 2013). The Waterberg (Lephalale) region has mean temperature ranging from 27°C in January, 15°C in June and 25°C in December (SAWS, 2016) (Fig. 1.3).

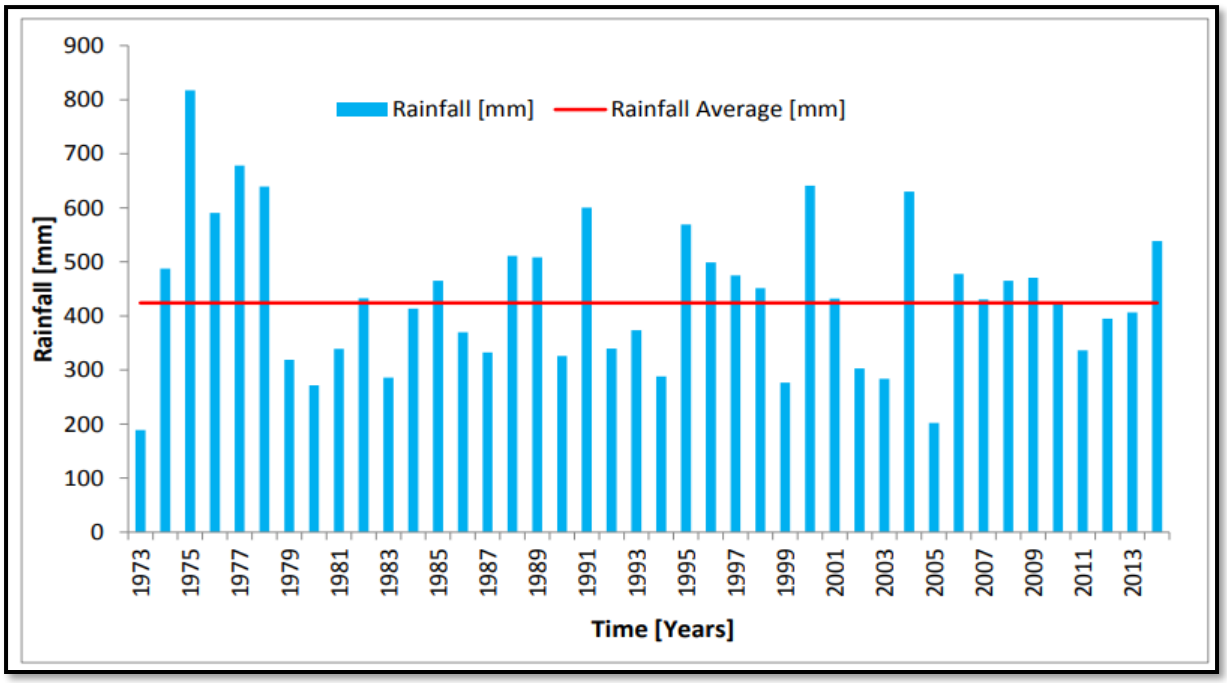


Figure 1.2: Rainfall pattern within the study area (Roux, 2015).

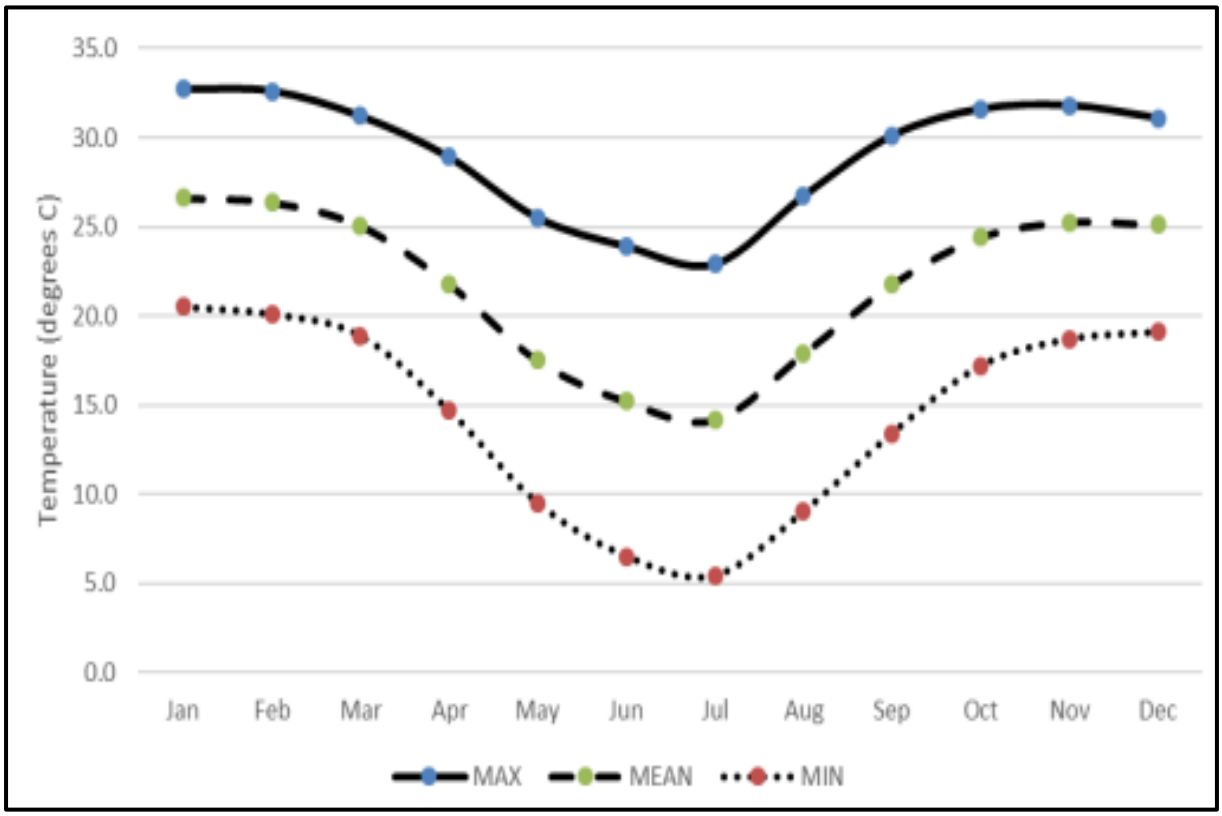


Figure 1.3: Temperature of the Lephalale region (SAWS, 2016).

### 1.2.3 Topography and Drainage

The landscape of the Waterberg District is a unique feature that distinguishes it from any other place in South Africa. There are four main landscape features in the Waterberg District, namely; the Waterberg Plateau, the Transvaal Plateau Basin, the Pietersburg Plain and the Limpopo Depression (Waterberg Municipality, 2013).

Waterberg District derives its name from the Waterberg Mountains and was given by the indigenous people of the area because of the many water streams flowing down the mountain slopes (Waterberg Municipality, 2013). The study area is characterised by a gently dipping terrain. The study area is located on a higher altitude (935 m) compared to the surrounding catchments and rivers (915 m) (Fig. 1.4). This shows that contaminated water could possibly drain to the surrounding rivers.

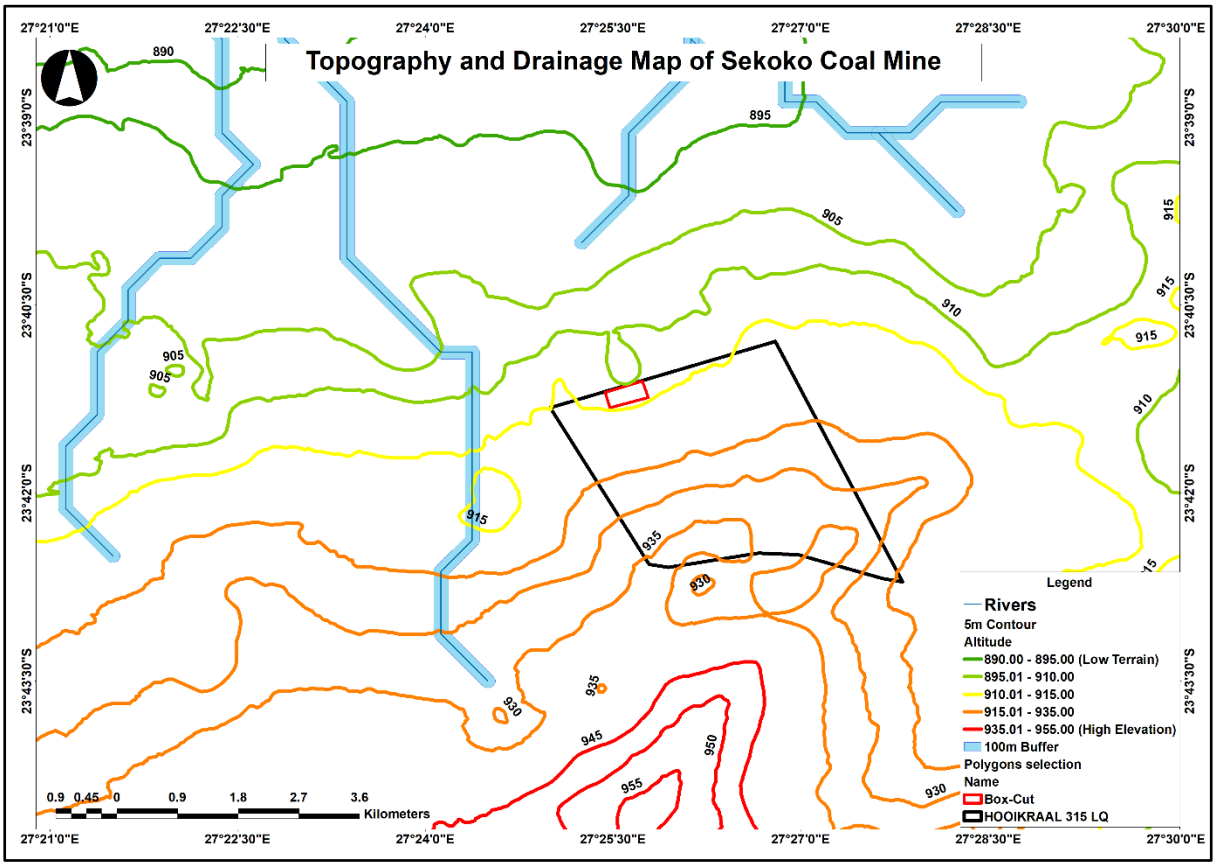


Figure 1.4: Topography and drainage map of Sekoko coal mine (Arcmap 10.8, 2023).

### 1.2.4 Soil and Vegetation

The soil of the area is diverse. Major soil associations have been identified. These include weakly developed soils on mountainous catchments; uplands and rocky areas; dystrophic; red and yellow; freely draining sandy soils; and plinthic upland duplex and Para duplex soils on

undulating mid-level, rugged terrain (Waterberg Municipal, 2013). The soil is mostly deep and greyish in colour overlying granite, quartzite or sandstone (Bredenkamp *et al.,* 1996). The vegetation is short and shrubby (Mtimkulu, 2009). Sandy areas are dominated by trees such as: Silver Clusterleaf *Terminalia sericea*, Yellow Pomegranate *Rhigozum obovatum*, Wild Raisin Grewia flava and *Acacia tortilis.*

## 1.3 Problem Statement

Although it is imminent that the Waterberg Coalfield is going to be the next major coal producer in South Africa, not much work has been undertaken in the entire coalfield to determine the potential of acid mine water generation as a result of future coal mining. The general assumption is that the coal quality from the Grootegeluk deposit is representative of the coal in the entire Coalfield (Hancox and Gotz, 2014), the same applies to the knowledge of acid mine water generation potential at this area, this indicates a gap.

## 1.4 Justification

South Africa depends greatly on coal resources for energy generation. Coal is estimated to produce over 40% and over 80% of global and South African electricity respectively. According to Creswell (2019) the South African coal industry still has a relevant future for decades to come through export markets. Zero Hedge (2021) further indicated that the demand for coal is rising despite the call to reduce the use of coal. For example, in 2021 the price of coal (thermal) rose about three times compared to the price in September 2020, also the price for coking coal increased by 80% this year (2022) alone (International Energy Agency, 2022).

The Waterberg Coalfield contains an enormous portion of South Africa's future coal resources (Ramane, 2014). According to Deysel (2015) the Waterberg Coalfield showed potential for acid mine water generation in areas with clay lithologies, whereas in overburden material it showed neutralizing potential. This is mainly because clay lithologies contained sulfide minerals such as pyrite. According to Hancox (2016) there is a lack of detailed study on the quality of coal from the Waterberg Coalfield. It is crucial to examine the Waterberg Coalfield in greater depth to comprehend the quality of coal and its potential use.

The Waterberg Coalfield contains a significant amount of South Africa's future coal resources and is therefore a vital area for energy production. However, prior to mining, it is vital to determine the potential for acid mine water generation in both the host rock and coal. This includes understanding the chemical composition and mineralogy of coal, as well as the

geology and geochemistry of the host rock. The presence of acid-generating minerals, such as pyrite, can cause acid mine drainage, leading to severe environmental impacts such as water pollution and damage to ecosystems. Furthermore, it is essential to evaluate the potential environmental effects of mining in the Waterberg Coalfield, including acid mine drainage and its impact on water resources. Acid mine water can negatively affect water quality, making it unfit for human consumption or irrigation, and harm aquatic life. Additionally, acid mine drainage can result in the leaching of heavy metals from the host rock, which can have toxic effects on plants and animals.

Lastly, it is important to research the quality of coal from the Waterberg Coalfield and its potential use. The composition and characteristics of coal, including its calorific value, ash, sulphur, and moisture content, can affect its efficiency and cost-effectiveness as a fuel source. The coal quality and host rock can also impact the mining method used, and the cost of mining and transport.

## 1.5 Research Questions

- What is the mineralogical composition of host rock and coal from Sekoko mine lithostratigraphy?
- What are the chemical properties of host rock and coal within the Sekoko mine lithostratigraphy?
- What is the potential of acid mine water generation of host rock and coal at Sekoko coal mine?

## 1.6 Objectives

### 1.6.1 Main Objective

To establish the potential for acid mine water generation within the lithostratigraphy at Sekoko coal mine of the Waterberg Coalfield through mineralogical and geochemical investigation.

### 1.6.2 Specific Objectives

- To determine the mineral composition of host rock and coal:
- To determine the chemical properties of host rock and coal:
- Determine acid mine water generation by conducting Acid Base Accounting:

## 1.7 Limitations of the Study

Every study has limitations that hinder or delay the activities to be undertaken, in this study the following were the limitations encountered:

- Lack of availability of exploration boreholes; and
- Fenced farms restricting access to surface coal outcrops.

# CHAPTER 2: LITERATURE REVIEW

This chapter focused on desktop studies to review the previous work relevant to the study area and the research topic.

## 2.1 Regional Geology of South African Coalfields

Carboniferous deposits along the northern coast and the widespread Karoo deposits of late carboniferous-Permian age found throughout central and southern Africa are the primary coal occurrences in Africa (Haughton, 1969). South Africa's coal deposits, according to Thomas (2013), are located in a series of basins in the country's north and east. The Karoo sequences were formed when the Gondwana Supercontinent split apart during the Mesozoic period (Thomas, 2013).

Thomas (2013) states that the Main Karoo Basin (MKB) stretches 200 km from the Free State province to the south and 400 km from Mpumalanga to KwaZulu-Natal in South Africa. The Karoo sequence was deposited directly onto the basement, with shallow, almost horizontal coal seams. The Karoo sequence has been impacted by igneous intrusions, which are thought to be the cause of the coal quality variation (Dreyer, 1994; Thomas, 2013; Hancox and Gotz, 2014).

The Karoo basin is part of the major series of Gondwana basins that formed as a result of subduction, compression, and terrane accretion along Gondwana (Cole, 1992). According to Hancox and Gotz (2014), the Karoo basin has economic significance in energy resources such as coal, methane, shale gas, and geothermal energy. Rowsell and Connan (1979) noted that there is oil present, but it is of uneconomic value.

The sedimentary part of the Karoo basin is divided into four major lithostratigraphic units from the bottom; Dwyka, Ecca, Beaufort, and Stormberg (Hancox and Gotz, 2014) (Fig. 2.1). These lithostratigraphic units are capped by a 1.4 km thick layer of Drakensberg basaltic lava (Veevers *et al*., 1994; Johnson *et al*., 1996). According to Hancox and Gotz (2014), the Karoo deposits ranged from glacial (Dwyka) to shallow marine and coastal plains (Ecca Group) to non-marine fluvial and Aeolian (Beaufort and Stormberg Groups). Cox (1992) concluded that the basaltic lava intrusion is related to the breakup of Gondwana.

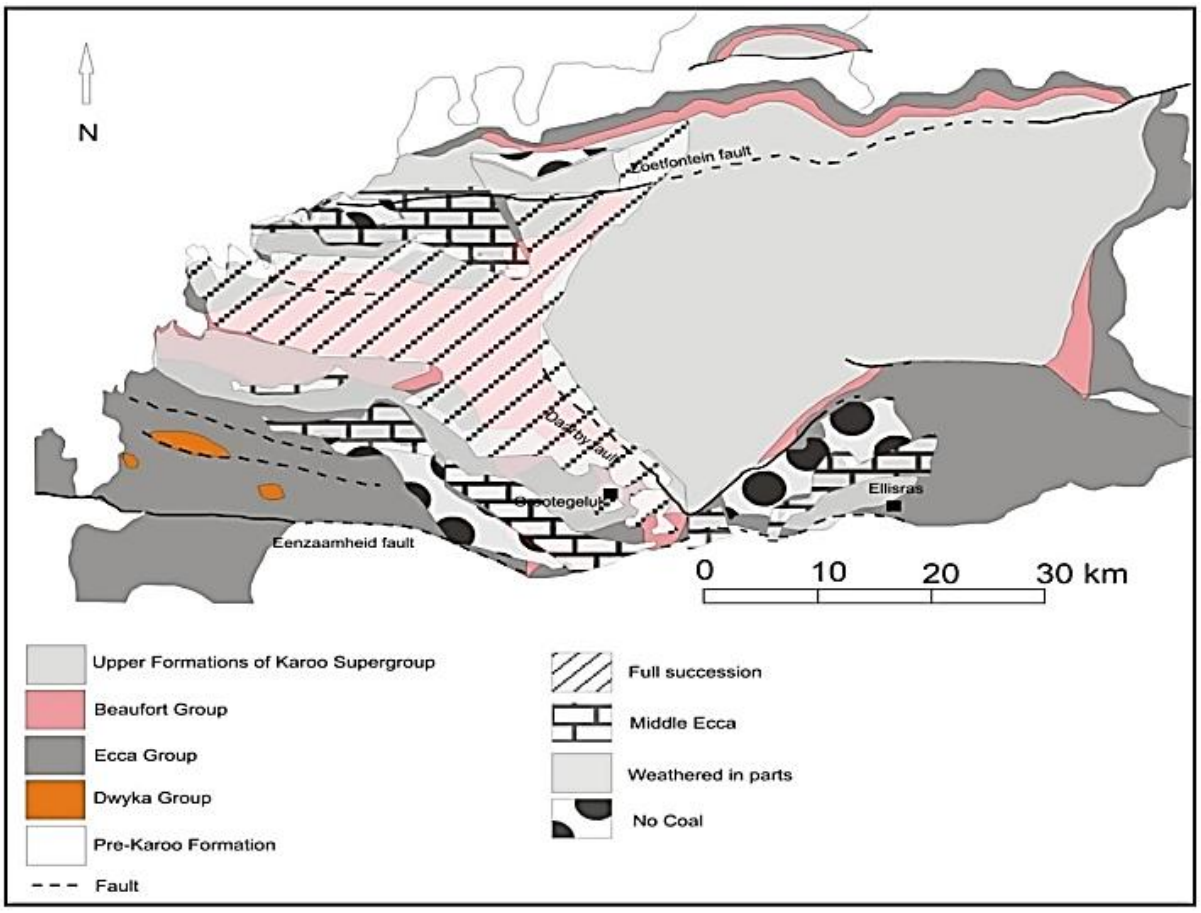


Figure 2.1: Geological successions of the Waterberg Coalfield (Deysel, 2015).

**Dwyka Group**

The Dwyka Group was formed as a result of glacial deposition (Hancox and Gotz, 2014). The rocks of this Group are found in some of Gondwana's most significant glacial deposits. According to Visser (1990), the Dwyka Group dates back between 302 and 288 million years. Bangert *et al*. (1999) concluded that this Group formed during the late Carboniferous and early Permian periods. The thickness of the Dwyka Group deposit ranges from centimetres to meters (Dreyer, 1994) (Table 2.1). Hancox and Gotz (2014) observed that deposition in the Dwyka Group occurred under high water-table conditions, as evidenced by the presence of glacial or periglacial lakes.

**Ecca Group**

The South African Committee for Stratigraphy (SACS, 1980) established a formal lithostratigraphic nomenclature for the Ecca Group, replacing the previous lower, middle, and upper subdivisions with the Pietermaritzburg shale Formation, Vryheid Formation, and Volksrust shale Formation (Table 2.1). The Ecca Group, according to Cadle (1993) can be

subdivided into several informal units due to the alternating nature of the sedimentary fills. These subdivisions are discussed further below.

Pietermaritzburg Formation

The Pietermaritzburg Formation is almost entirely composed of 400 m thick dark grey laminated siltstone and mudstone (Du Toit, 1954). No coal seams exist in the Pietermaritzburg Formation (Hancox and Gotz, 2014).

Vryheid Formation

The vast majority of economically extracted coal in South Africa, according to Hancox and Gotz (2014), occurs in the Vryheid Formation rocks. The thickness of the Vryheid Formation ranges from 70 to 500 m within the Main Karoo Basin (MKB) (Hancox and Gotz, 2014). South of Newcastle and Vryheid, the formation thickens (Hancox and Gotz, 2014). Cadle (1982) and Du Toit (1954) discovered that the Formation was thickest in the south due to the most subsidence and the deepest basin.

Volksrust Formation

SACS (1980) renamed the upper Ecca beds Volksrust Formation (Table 2.1). This formation has a thickness that ranges between 150 and 250 m. According to Hancox and Gotz (2014) and Dreyer (1994), this unit is dominated by dark grey-green siltstones and mudstones (Table 2.1). This formation exhibits an overall coarsening-upward trend (Cadle, 1993). Hancox and Gotz (2014) explained that coal occurs with mudstones and that the Formation itself is thought to have formed in shallow-deep water basinal conditions.

**Beaufort Group**

The Beaufort Group, according to Johnson (1976), Dreyer (1994), marks a transition from subaqueous (Ecca Group) to fully subaerial deposition with predominantly fluvial sedimentation. The Beaufort Group is made up of fine-grained lithofeldspathic sandstone and mudstone that alternate in a fining-upwards series (Johnson, 1976) (Table 2.1). Lower Adelaine and upper Tarkastad are subgroups of the Beaufort Group. Only the Adelaine Group contains coal (Johnson *et al*., 2006; Hancox and Gotz, 2014).

**Stormberg Group**

The Stormberg Group consist of the Molteno, Elliot and Clarens Formations (Du Toit, 1954).

Molteno Formation

The Stormberg Group's basal unit is the Molteno Formation, which consists of northward twinning wedges of clastic sedimentary rocks (Hancox and Gotz, 2014). The Molteno Formation is divided into two members; lower Bamboesberg and Indwe sandstone (Hancox and Gotz, 2014). The Bamboesberg member is made up of up to five stalled fining-upward sequences ranging in thickness from 5 to 50 m. These sequences are made up of sandstones that are laterally extensive and capped by thin lenticular siltstones. According to Hancox (1998), the Bamboesberg member contains three coal seams.

Elliot Formation

The lower part of this formation shows deposition occurred under perennial, moderately meandering fluvial styles whereas the upper part shows evidence of ephemeral fluvial processes (Hancox and Gotz, 2014). The Elliot Formation according to Hancox and Gotz (2014) doesn't host any coal deposits.

Clarens Formation

Beukes (1969) determined and concluded the thickness of this unit to be 305 m. Most authors concur that the Clarens Formation dominated by sandstones represents aeolian depositional systems with minor fluvial input (Eriksson, 1981; Dreyer, 1994; Hancox and Gots, 2014). Hancox and Gotz (2014) also indicated that there is no coal deposit in the Clarens Formation.

The western area of the Main Karoo Basin consists of Vereeniging-Sasolburg and South Rand Coalfields which consist of coal seams which range between the thicknesses of 10 to 25 metres. Witbank and Highveld Coalfields are located north of the MKB. These Coalfields host five coal seams of the five, two seams have been exploited up to 10 metres.

The southern Kwazulu-Natal area however includes the Vryheid and Utrecht Coalfields with five seams of which two are worked together with the two coal seams of the Kliprivier Coalfield (Thomas, 2013). The MKB as a whole produces high volatile bituminous coal with high ash and variable sulphur contents. Thomas (2013) indicated that anthracite coal is produced in the eastern parts of Mpumalanga and Kwazulu-Natal. There are other Coalfield basins in the northeast of the country which are less developed, of these the Waterberg Coalfield and the Springbok flats area appear to have a future potential for coal mining (Thomas, 2013).

Table 2.1: Subdivision of the Karoo basin stratigraphy (after Dreyer, 1994)

| Group | Formation (SACS, 1980) | Formation (Cilliers, 1951) | Representative Rock Type | Average Thickness (m) |
|---|---|---|---|---|
| Stormberg | Drakensberg Basalt | Drakensberg | Lava, Purplish to red amygdaloidal | 95 |
| | Clarens Sandstone | Cave sandstone | Sandstone, fine grained white to yellow-brown to reddish | 80 |
| | Elliot | Red beds | Mudstone, red to chocolate brown clayey | 90 |
| | Molteno | Molteno | Sandstone, white, medium to coarse grained, scattered pebbles | 15 |
| Beaufort | Beaufort | Beaufort | Mudstone, purple and greenish grey, alternating at top, light grey at base | 90 |
| Ecca | Volktrust | Upper Ecca | Intercalated shale and bright coal | 60 |
| | Vryheid | Middle Ecca | Sandstone and grit, Intercalated carbonaceous shale, siltstone, few thick coal seams | 55 |
| | Pietermaritzburg | Lower Ecca | Shale and sandstone, grit in lower portions | 150 |
| Dwyka | Dwyka | Dwyka | Tillite | 3 |

## 2.2 Prominent Coalfields of South Africa

South Africa has 19 known coalfields (Fig. 2.2). They are found in Kwazulu-Natal, Limpopo, and Mpumalanga, with a few exceptions in the provinces of Free State, Gauteng, Eastern Cape, North West, and Western Cape. Witbank, Waterberg, Highveld, and Soutpansberg are among the major South African coalfields discussed.

### Soutpansberg Coalfield

The Soutpansberg Coalfield is located in Limpopo province, with a strike length of 190 km that cuts through Waterpoort in the Kruger National Park (Dreyer, 1994). Sullivan et al. (1994) indicated that geological structures such as faults and dolerite inclusion disturb the coal in this field, with the dull coal occupying the bottom of the multi-seam in the Waterpoort area and the top part of the lower seam on the other side of the Tshikondeni area.

According to Sullivan *et al.* (1994), the structural geology of Soutpansberg is characterized by parallel strips of Karoo rocks. Tshikondeni Exxaro Mine began exploitation of the Madzaringwe Formation in 2013, with high quality coking coal discovered on the bottom part of the upper seam of the Formation (Fig. 2.3).

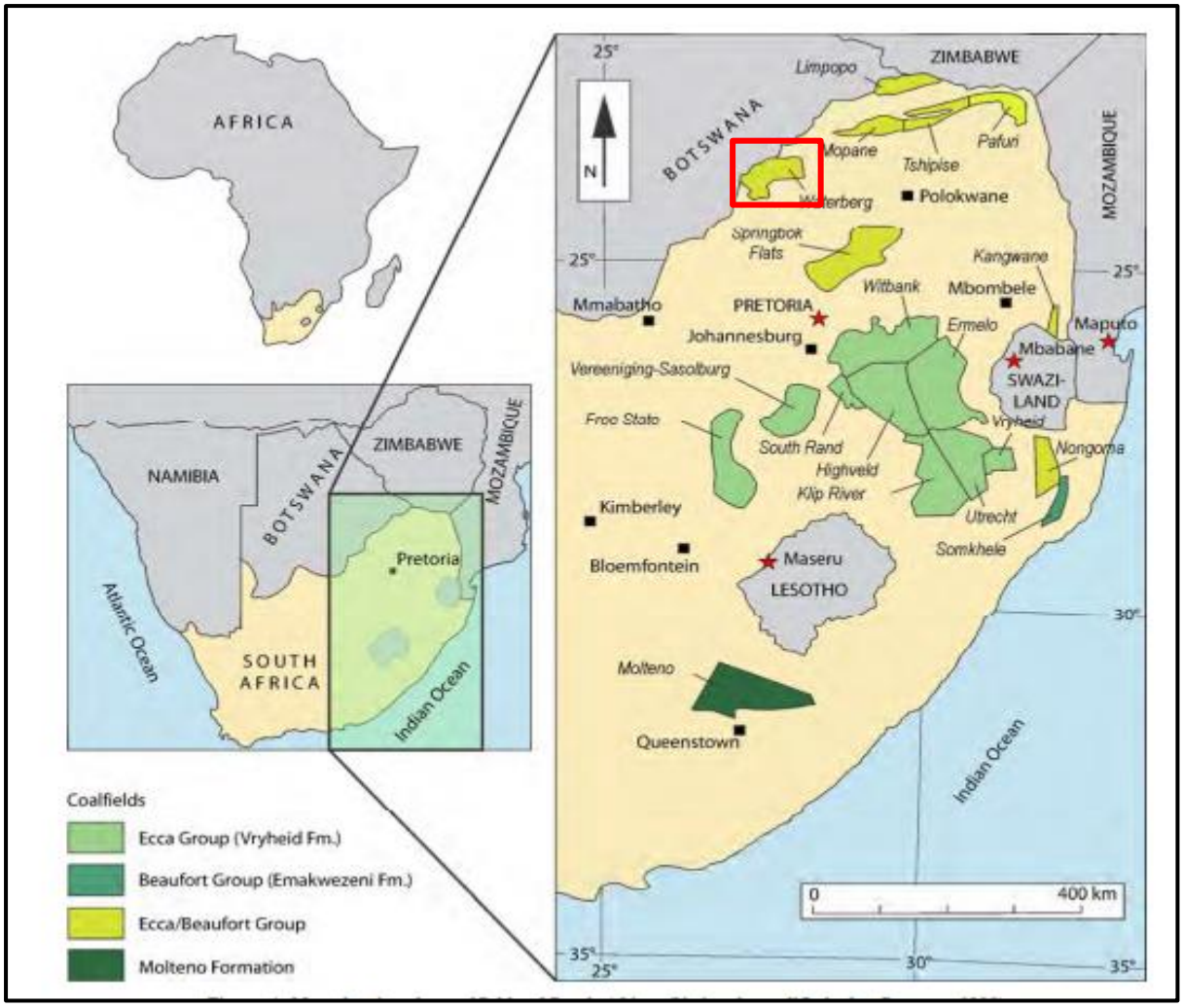


Figure 2.2: Coalfields of South Africa (after Hancox and Gotz, 2014).

Coal of Africa discovered a green field at this coalfield with prospects of extracting five million tonnes of coal, but the operation is prohibited due to the proximity of the Mapungubwe and Kruger National Parks, making the area environmentally sensitive, despite the fact that they had already been granted a licence.

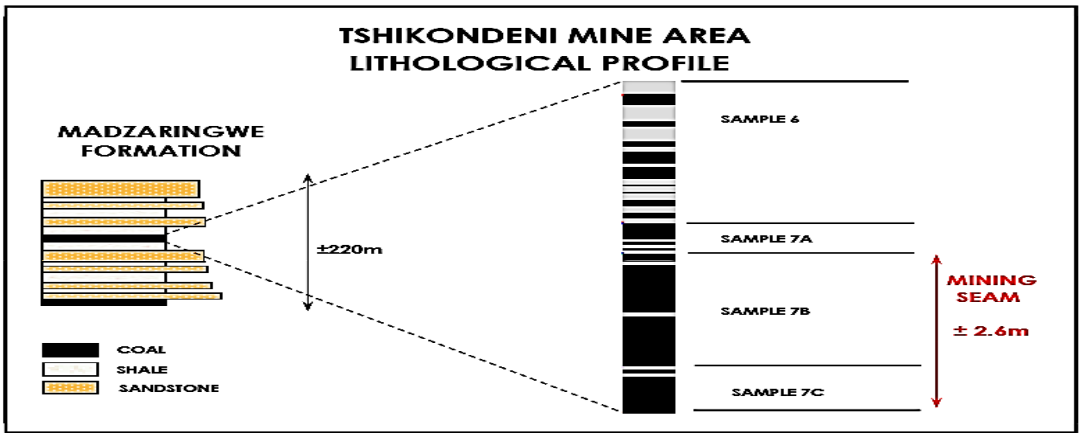


Figure 2.3: Madzaringwe Formation lithological profile (Sullivan, *et al.*, 1994).

**Witbank Coalfield**

This is the largest coalfield in South Africa, stretching approximately 180 kilometers east-west from springs to Belfast (Hancox and Gotz, 2014). Geologically coal in this coalfield is affected by igneous intrusions. When igneous intrusions occur close to coal deposits it gets devolatised and displaced (Snyman, 1986). The dyke is known as Ogies, which is also the name of the farm (Ogiesfontein) in South Africa's Mpumalanga province (Smith and Whittaker, 1986).

The Witbank Coalfield has six major seams that are numbered from bottom to top, with the sixth seam been uncommon in most areas due to erosion (Fig. 2.4). The deepest seam is 100 m deep, whereas the shallowest is 30 m below the surface. The geological condition surrounding these seams is moderately stable, with a competent hanging wall and strong foot wall sandstone, allowing mining to take place (Jeffrey, 2005). The thickness of these seams ranges from 0.5 m to 6 m. (Chabedi, 2013). The rocks found in this Coalfield include shale, siltstone, sandstone and conglomerate, and Dwyka tillite.

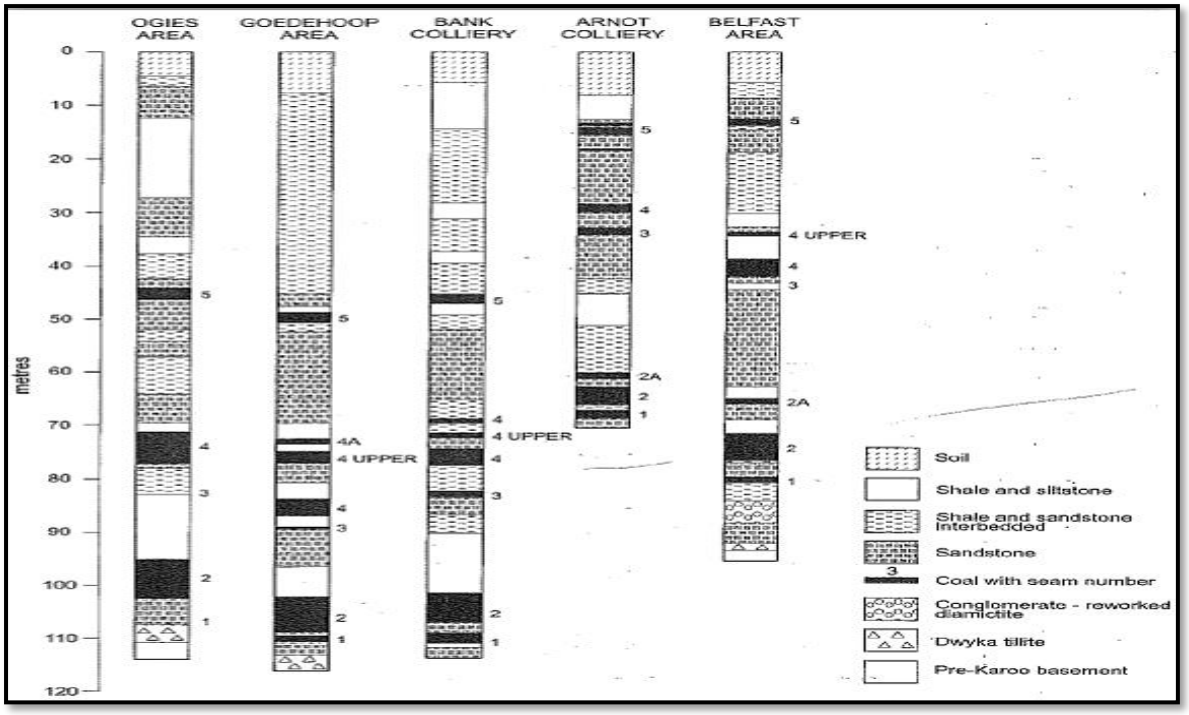


Figure 2.4: A representation of the stratigraphic column in the Witbank Coalfield (Snyman, 1986).

### Highveld Coalfield

The Highveld Coalfield is 7 000 square km located south of the larger Witbank Coalfield (Snyman, 1986). This coalfield is dominated by sedimentary rocks. Plant debris deposition was controlled by pre-Karoo glacial valleys, according to evidence (Synman, 1986).

The depth of the coal from the surface is approximately 0-300 m. This Coalfield, like the Witbank Coalfield, has six major coal seams on the Vryheid Formation (Jordan, 1986; Jeffrey, 2005). According to Jordan (1986), the Coalfield contains two major dolerite sills that are named based on their age (Table 2.2).

Table 2.2: Difference between the older and the younger dolerite sills (Jeffery, 2005)

| Older Dolerite sill | Younger dolerite sill |
|---|---|
| • Non-porphyritic and coarse grained sill<br>• Average thickness of 90 m<br>• Highly/heavily jointed<br>• Near the earth surface | • Porphyritic and fine grained sill<br>• Thickness varies from 5 to 80 m<br>• Heavily splitted sill into 40 m thick composite sills<br>• Deeper than the older sill. |

## 2.3 Waterberg Coalfield

This coalfield is located approximately 25 kilometres outside of Lephalale in South Africa's Limpopo province. It has a small surface area in comparison to other coalfields, but the coalfield is approximately 110 m thick. According to Jeffrey (2005), the Waterberg Coalfield geology consists of two Formations with major faults disrupting the basin.

The Waterberg Coalfield is fault-bounded within the Ellisras sub-basin, which is considered an embayment of the much larger Kalahari Basin, which underpins a large portion of Botswana (Catuneanu *et al*., 2005). This sub-basin is classified as either a half-graben (Fourie *et al*., 2014) or a graben structure (Sullivan *et al*., 2013). The Archaean Beit Bridge Complex in the north and the Proterozoic Waterberg Group in the south form the basement (Brandl, 1996). The Constantia Suite and BIC (Villa Nora and Nebo granites) are being developed to the north-east and east.

The Vryheid Formation is approximately 55 m thick. It is a multiple seam deposit with four zones of coal and five seams ranging in thickness from 1.5 to 9.0 m thick (Fig. 2.5). According to Hancox (2016), the Waterberg Coalfield contains 40-50% of South Africa's remaining coal resources, making it the country's largest remaining coalfield. The Ellisras Basin has an area

of about 3600 km$^2$. The basin is bounded by three major faults: the Zoetfontein, Daarby, and Eenzaamheid faults (Jeffrey, 2005; Fourie *et al*., 2014; Hancox and Götz, 2014).

Coal seams in the region have been divided into near surface deposits and more deeply buried seams by the Daarby Fault. The deeply buried coal seams are explored for coal bed methane (CBM) (Fourie *et al*., 2014). Shallow deposits are currently exploited by Exxaro at their Grootegeluk mine that produces a range of coal products including thermal and metallurgical coal which are supplied to local and export markets (Fourie *et al.,* 2014). Grootegeluk has a total measured coal resource of 4 719 Mt (Exxaro, 2018).

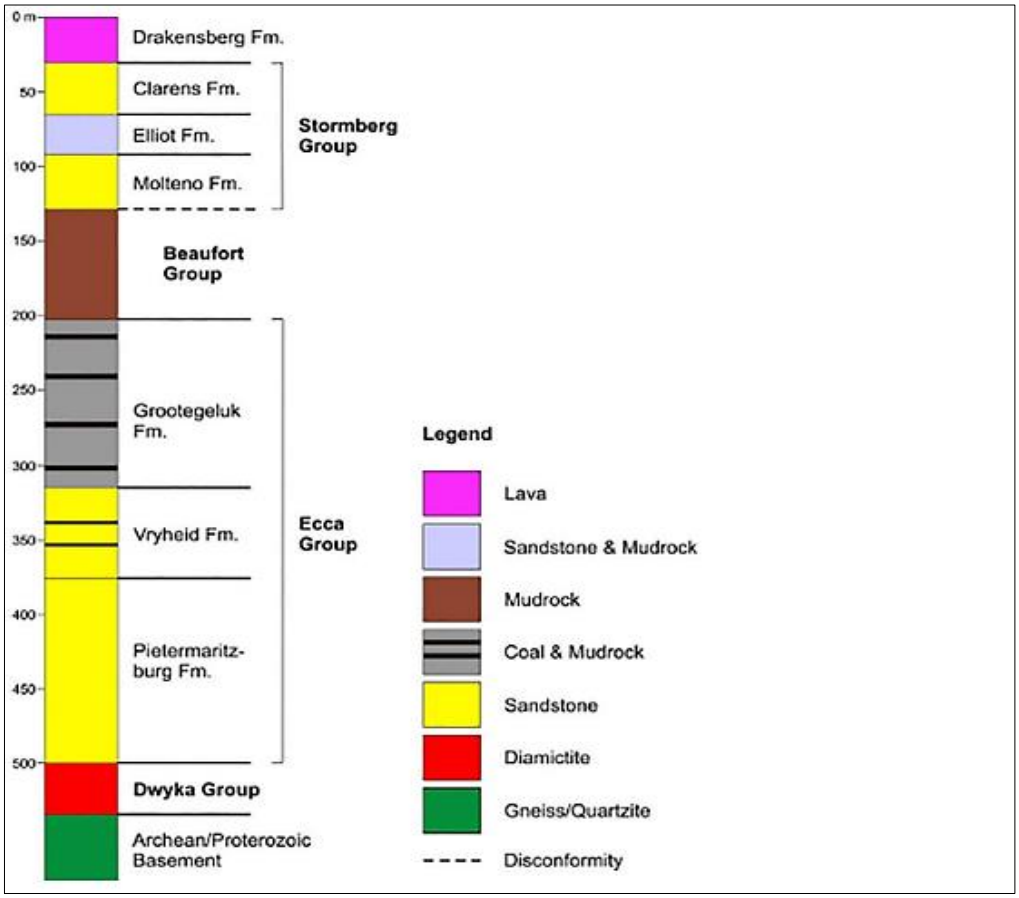


Figure 2.5: Stratigraphic column of the geology of the Waterberg Coalfield (Hancox and Gotz, 2014).

The Waterberg Coalfield, like the Limpopo Coalfield, formed as an intra-cratonic rift during the late Permian period (Cairncross, 2001). This tectonic setting produced floodplain deposits similar to those of the MKB; however, the Waterberg Karoo package is dominated by carbonaceous mudstones interbedded with coal seams (Smith *et al*., 1993; Snyman and Botha, 1993). As a result, the Waterberg Coalfield deposits should not be confused with the

Proterozoic rocks of the Waterberg Group or the Waterberg Basin in Namibia (Johnson *et al*., 2006).

The Waterkloof and Wellington Formations are the lowermost units of the Karoo sequence in the Ellisras Basin and the equivalent of the Dwyka Group in the main Karoo basin. The contact between these units with the basement varies laterally such that in the south of the Ellisras Basin, they unconformably overlie the sediments of the Waterberg Group, meta-sediments of the Limpopo Mobile Belt (LMB), Bushveld lavas in the north-eastern margin, and meta-sediments of the LMB in the northern margin (Fourie *et al*., 2014). Above the sequences of the Waterkloof and Wellington Formations, are units corresponding to the Ecca Group in the main Karoo basin (MKB), namely the Swartrant, Goedgedacht and Grootegeluk Formations. The siltstones and sandstones of the Swartrant Formation, which overlie the Waterkloof and Wellington Formations, are equivalents of the Pietermaritzburg Formation in the MKB.

Eleven economic coal seams are distributed between the Goedgedacht Formation (Vryheid Formation equivalent in the MKB) and Grootegeluk Formation (Volksrust Formation equivalent in the MKB). Of these the Grootegeluk Formation is the principal economic target due to the presence of more well developed (brighter) and thicker coal seams which are interbedded with sandstone and shale, attaining a maximum thickness of 90 m (Faure *et al.*, 1996). The Goedgedacht Formation consists of 55 m of coarse sandstones and carbonaceous mudstones interbedded with coal seams of varying thicknesses. The alternating lithologies in the Goedgedacht and Grootegeluk Formations contribute to the high ash content which ranges between 21-62.9 %, necessitating rigorous beneficiation.

Coal deposition in the Waterberg Basin occurred in flood plain settings in which coal in the Goedgedacht Formation was deposited further from the sediment source, in low energy conditions (Snyman and Botha, 1993). Coals in the Goedgedacht Formation are inertinite-rich, for example, Wagner and Tlotleng (2012) reported that coal in Bench 11 consisted of 74.7 vol% inertinite. The overlying coal seams of the Grootegeluk Formation are characterized by a high proportion of vitrinite macerals of up to 90 vol% (Faure *et al.*, 1996; Hancox and Götz, 2014). These vitrinite rich coals suggest deposition in a low energy environment.

### 2.3.1 Stratigraphy of the Waterberg Coalfield

Mtimukulu (2009) describes the base of the basin-fill at the Waterberg basin as an erosional surface. Johnson (1996) discussed the Karoo depositional cycle and revealed that tillites and fluvioglacial conglomerates are the first sediments encountered on the top of the Waterberg basin erosional surface. Several authors and the Council for Geoscience have attempted to develop the lithostratigraphy of the Ellisras basin (Beukes, 1985; Beukes *et al*., 1991; Faure

*et al*., 1996). According to Beukes (1985), the Waterberg basin develops the classic lithostratigraphic units of the Karoo in the main basin. MacRae (1988) challenged Beukes' findings, claiming that there is no connection between the Waterberg and main basins, making correlation difficult.

The Ecca Group is divided into several parts including the upper, middle and lower Ecca, according to Faure *et al*. (1996). Coal zones 1 to 4A of the Waterberg Coalfield has a correlation Zones 1 to 4A of the Vryheid Formation of the MKB (Fig. 2.6). This however, is not the case when taking into consideration coal zones 5 to 11. The first coal zone is generally thin, about 2 m thick, and consists of dull heavy coal with shale on occasion (De Jager, 1976). De Jager (1976) further explained that the second coal zone has a consistent thickness ranging from 1 to 4.5 m on the shallow western part and up to 5.2 m in the deeper parts of the basin. According to De Jager (1976), the first and second zones are frequently overlain by conglomerate and separated by coarse-grained white feldspathic sandstone up to 5 m thick. A 5 m thick impure fine and medium-grained sandstone separates the third zone from the second zone.

The fourth zone (4 and 4A) establishes a transition between the middle Ecca and upper Ecca stages in this field and the seams are 4-9 m thick. Faure *et al.* (1996) indicated that the upper Ecca consist of bright coal with massive carbonaceous shale. These zones are numbered 5-11, and they occur in the Grootegeluk formation. Dreyer (1994) and Faure *et al.* (1996) further indicated that the presence of the Daarby fault also has influence on the stratigraphy of the Waterberg basin (Fig. 2.6).

The stratigraphic correlation developed by Faure *et al*. (1996) (Fig. 2.6) is similar to that of the SACS. The Vryheid Formation consists of 4 zones and mainly comprises sandstones, coal, shale, siltstone and mudstones and at times Dwyka tillites are also observed. Zones 5-11 occur on the Grootegeluk Formation and the coal occurs interbedded with shale (Dreyer, 1994).

**Goedgedacht Formation**

Siepker (1986) indicated that the Goedgedacht Formation only prevails over the north and northwest part of the Ellisras basin where it decreases from a maximum thickness of 80 m in the north towards the south where it interfingers with the Swartrant Formation. Siepker (1986) noted that this formation lies unconformably on granitoids-gneiss-mafic rocks. Furthermore,

this formation consists of units of mudrocks with graded beddings as well as angular quartz in their basal parts which may be capped by thin impure vitrinite-rich coal.

**Grootegeluk Formation**

Faure *et al.* (1996) indicated that this formation has varying thickness; it is up to 110 m in the south, 40-60 m in the north and northwest, 50 m in the southeast and 10-20 m in the northeast. He further indicated that this Formation overlies the Swartrant Formation in the east and extreme south. The bottom end of the Grootegeluk Formation is believed to be intercalated with the Goedgedacht Formation which consists of mudstone, carbonaceous shale and coal; these layers occur in a cyclic manner as indicated by Faure et al. (1996).

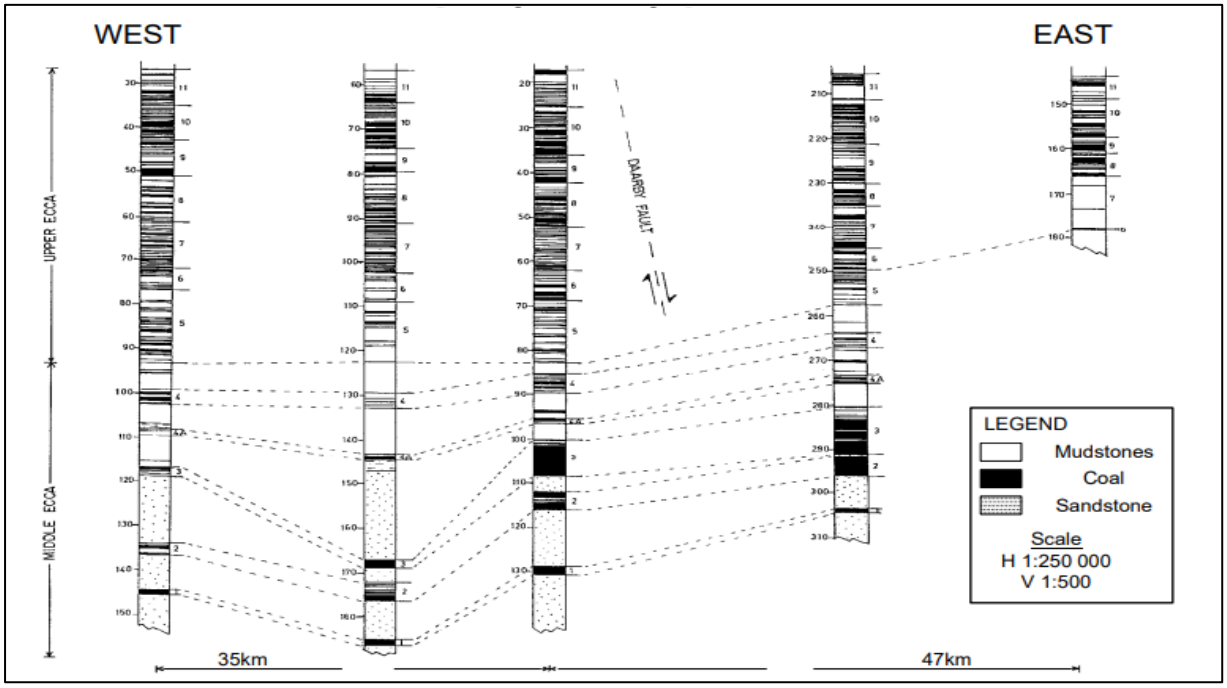


Figure 2.6: West to east Stratigraphic Correlation of the Waterberg basin (Faure *et al.*, 1996).

Coal seams in this formation are prominent in the lower half of the succession where shale is also prominent. Faure *et al*. (1996) further elucidated that where the succession was complete, it is divided into 38 zones. Zones 1-6 are situated at the base and consist of dark, highly carbonaceous mudstone and dull coal. Zones 7-28 consist of alternating layers of bright and dull coal together with carbonaceous shale (Mtimukulu, 2009). Siepker (1986) indicated that zones 29-38 consist of bright vitrinite rich coal (up to 88%) and carboniferous shale. The amount of vitrinite is believed to increase from 2% at the base to 65% at the top.

### 2.3.2 Mining History

Waterberg Coalfield has 75 billion tonnes of coal resources, representing 40% of South Africa's remaining coal resources (Moumakwa, 2009). Department of Mineral Resources report indicates that the Waterberg Coalfield hosts coke and power generation coal from the Upper and Middle Ecca Zones of the Karoo Supergroup (Moumakwa, 2009).

Alberts (1982) clarified that Exarro's Grootegeluk mine has been mining coal in the Waterberg Coalfield since 1980. Semi-soft coking coal, thermal coal, and metallurgical coal are all found in the mine. The measured resource is approximately 4600 mt, but only about 2800 mt is accessible. The Grootegeluk mine produces approximately 14.5 million tonnes of coal per year, which is supplied to the Matimba power station, which is a dry cooled coal power station (Moumakwa, 2009). Every year, the Grootegeluk mine produces and sells 1.5 million tonnes of metallurgical coal to metal industries (Grootegeluk, 2007).

According to Moumakwa (2009), 60% of the remaining coal resources in the Waterberg Coalfield will require underground operations, while the remaining 40% will be extracted through opencast methods. The coal in the Grootegeluk mine is said to be mostly from the upper Ecca zone (Grootegeluk Formation).

### 2.3.3 Future Development at the Waterberg Coalfields

According to the Department of Mineral Resources (DMR), electricity demand will rise by 1200 Mw per year over the next 20 years, necessitating the construction of eight new power plants (Moumakwa, 2009). The gradual depletion of some of South Africa's major coalfields is having serious ramifications for Eskom coal supply, which is expected to decrease over the next 15 years (Moumakwa, 2009). The Waterberg Coalfield must be developed in order to meet energy demands (Moumakwa, 2009).

**Sekoko Lephalale Coal Mine**

Sekoko coal mine is a South African black-owned company that is currently exploiting coal in the Waterberg Coalfield near the Grootegeluk Exarro coal mine (Sekoko coal, 2011; Maromo, 2011; Mining Review Africa, 2021). The company began exploration drilling in 2007, and it was granted mining rights in 2011. Sekoko Resources owns over eight farms totaling 7500 acres. The two economic formations include the Grootegeluk and Vryheid Formations which contains 11 coal seams. Sekoko coal (2011) indicated that Eskom is the existing customer. Coal produced from Sekoko coal mine is sold to Tutuka and Majuba power stations located in Mpumalanga province. Mining Review Africa (2021) indicated that Sekoko coal mine will also

supply Matimba power station with coal. Sekoko contains enough coal to produce 120 mt of coal suitable for metallurgical and thermal export markets.

The average ash content of seams 11 to 7 is 29%, the calorific value is 22%, and the volatile content is 29%. (Sekoko coal, 2011). From seam 11 to 1, the average sulphur and moisture content is about 1 and 3%, respectively (Sekoko coal, 2011).Sekoko coal (2011) further indicated that ash content in seam 6 to 4 is at an average of 35%, while the calorific value is at an avarage of 35% and volatiles 24%. The bottom seams (seam 3 to 1) are reported to have ash content of 22% calorific value of 24% and volatile content of 22%.

## 2.4 Coal Geology

White and Thiessen (1913) defined coal as transformed peat. This definition has been further elucidated by other recent studies including but not limited to O'Keefe *et al*. (2013) which indicates that coal is a combustible sedimentary rock composed on aquatic plant remains. The study further indicates that coal is formed through decomposition of plant remains in swamps and deltas. White and Thiessen (1913) indicated that the degree to which the plant remains will be lithified depends on oxygen supply, temperature, exposure to air as well as drainage. White and Thiessen (1913); Thomas (2013) and Wagner *et al.* (2018) indicated that coal is composed of organic and inorganic constituents. The organic constituents of coal are recognized as macerals while the inorganic content is composed of mineral matter of either syngenetic and/or epigenetic origin.

Coals are divided into two main Groups namely, humic and sapropelic coals International Committee for Coal and Organic Petrology (ICCP, 2001). Sapropelic coal according to O'Keefe *et al.* (2013) is deposited through the putrefication of non-woody plant remains such as algae, spores, pollen and cuticles. In contrast, humic coals may contain alternating bands of bright and dull coal (ICCP, 2001). O'Keefe *et al*. (2013) further elucidated that humic coal is formed through peatification of woody plant debris.

### 2.4.1 Coal Petrography

Petrography is a sub-branch of petrology concerned with the microscopic examination of rocks. Wagner *et al*. (2018) went on to say that coal petrography entails the microscopic study of both the organic and inorganic constituents of coal.

Schapiro and Gray (1964); Taylor *et al*. (1967); Stach *et al*. (1982) and Wagner (2007) all stated that coal research is critical in determining the technological properties of coal as well

as the thermal maturity of sedimentary basins for shale gas exploration. According to Thomas (2013), studying coal under the microscope has allowed for a better understanding of its organic and mineral components, as well as determining whether the coal is suitable for industrial use.

Carboniferous coals have a characteristically bright lustrous appearance and are composed primarily of vitrinite and clarite, according to Thiessen (1920) and Teichmuller and Teichmuller (1982). Alternatively, Permian coals were formed in the Gondwana Supercontinent, with the exception of early Permian coals in China, and these coals have a dull appearance and a high content of inertinite (Taylor *et al*., 1998; Thomas, 2013). Taylor *et al*. (1998) elaborated that the Gondwana coal's inertinite nature may have been influenced by the climate, in which freezing-drying conditions caused oxygen to be bound with the organic structure. Taylor *et al*. (1998) went on to say that inorganic constituents are also abundant.

**Organic Constituents of Coal**

All ranks of coal have identifiable organic constituents (macerals) that make up the coal mass. vitrinite, liptinite, and inertinite are the three groups of macerals (ICCP, 1963, 1975; Wagner *et al*., 2018) (Fig. 2.7). When these associations are examined under a microscope, they are referred to as microlithotypes (Taylor *et al*., 1998; Thomas, 2013). The three types of macerals are discussed further below.

**Vitrinite**

Thomas (2013) and Wagner *et al.* (2018) indicated that vitrinite originated in anaerobic conditions due to high groundwater table level in the peat. According to Thomas (2013) vitrinite makes up to 40-50% of the carboniferous coals in the northern hemisphere, while in the Gondwana coals it doesn’t exceed 20-30%.

Taylor *et al. (*1998) indicated that the carbon content in vitrinite macerals is proven to increase consistently with increasing rank. As such vitrinite is used as a universal standard to measure the reflectance levels of coals for determination of rank (Gray *et al.*, 1976; Teichmuller, 1989; ICCP, 1998). Taylor *et al.* (1998) and Thomas (2013) indicated that for coal to be used for coke production it must have >40% of fusible macerals (vitrinite) to form a well fused coke.

**Liptinite**

This maceral is derived from hydrogen rich plant organs (Taylor *et al.*, 1998 and Pickel *et al.*, 2017). Liptinite exhibit a lower reflectance as compared to the vitrinite maceral group (McHugh *et al.*, 1991).

**Inertinite**

This maceral group contains >95% inertinite macerals which include inertodetrinite, semifusinite and fusinite (Fig. 2.7 and Table 2.3). Fusinite in coals ranges between 5-10% (Thomas, 2013) and fusinite rich coals are thought to be the result of the onset of aerobic conditions in peat formation. Inertodetrinite is present in the northern hemisphere, and it contains 95% of inertodetrite. A study by Mahooana *et al*. (2022) recently revealed that this maceral and microlithotype is available in South African coal. Taylor *et al.*, (1998) indicated that the high concentration of inertinite in gondwana coals has been attributed to the oxidation of peat.

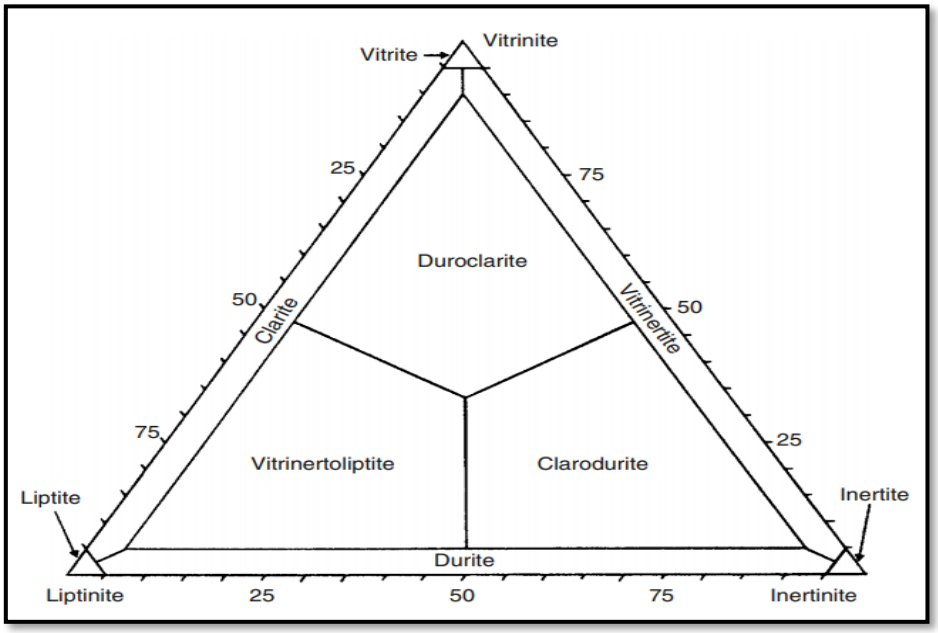


Figure 2.7: Diagrammatic representation of microlithotypes classification (Thomas, 2013).

Table 2.3: Macerals and group macerals recognized in hard coals (Teichmüller, 1989)

| Macerals | | Origin |
|---|---|---|
| Group | Maceral | |
| Vitrinite | Telinite | Plant cell walls (with visible structure) |
| | Collotelinite | Plant cell walls (gelified, structureless) |
| | Vitrodetrinite | Small particles of plant attritus (worn-down particles of plant humus) |
| | Collodetrinite | Mottled peat groundmass (originally attritus [worn-down particles]) |
| | Corpogelinite | Primary and secondary cell infillings from humic gels |
| | Gelinite | Amorphous humic matter in crack fillings |
| Liptinite | Sporinite | Outer cell walls of plant spores and pollen |
| | Cutinite | Outer coatings (cuticles) of leaves, roots, stems |
| | Suberinite | Degraded (suberinized) cell walls of cork in bark and roots |
| | Resinite | Plant resins, balsams, latexes, fats, and waxes |
| | Alginite | Algae |
| | Bituminite | Amorphous fluorescent material of either algal or bacterial origin |
| | Exsudatinite | Secondary crack-filling material formed from maturation after oil generation |
| | Fluorinite | Secondary crack-filling material formed from maturation after oil generation |
| | Liptodetrinite | Fragments or degradation residues of liptinites |
| Inertinite | Fusinite | Carbonized (fusinized) plant cell walls (from fires and other processes) |
| | Semifusinite | Partly humified and dehydrated plant tissues |
| | Funginite | Fungal spores and other fungal tissues |
| | Secretinite | Possible oxidation product of resins |
| | Macrinite | Dehydrated small, clumped (flocculated) peat matrix substances |
| | Inertodetrinite | Tiny, carbonized (fusinized) inertinite precursors |
| | Micrinite | Secondary coalification residues of liptinitic substances |

**Inorganic Constituents of Coal**

The mineral matter or content available in coal is incombustible inorganic fraction (Thomas, 2013). Wagner *et al.* (2018) indicated that minerals in coal can be categorized into two main groups namely; syngenetic and epigenetic. The first category is called syngenetic (meaning those minerals that are inherent in the plant tissues including trace elements). Detrital minerals which were eroded and incorporated in the peat have been categorized as syngenetic (Ward, 2016). These are minerals formed at the same time as the initial accumulation of the peat. Alternatively, epigenetic minerals can be referred to as introduced forms of minerals. These minerals are introduced into the coal after the initial accumulation of the peat (Wagner *et al.*, 2018).

Different minerals occur in coal, these include quartz, carbonate, iron and clay minerals (Vassilev and Vassilev, 1996; Wagner *et al.*, 2018). Precipitated minerals may also be disseminated through the peat or present as aggregates whereas mineral rich fluids present during the last stage of coalification tend to precipitate minerals on joints and any open voids within the coal (Thomas, 2013). This process occurs continuously even after coal is deposited. Falcon (2013) further indicated that of the minerals present in coal, clay minerals are the most abundant making up 60-80% of the total mineral matter.

According to Martinez and Escobar (1995), mineral matter in coal is undesirable because it raises the cost of beneficiation and causes equipment wear. According to Tlou-Sebola (2018), South African coals are rich in mineral matter, causing them to be classified as low grade and making the beneficiation process more complex and costly.

### 2.4.2 Coal Quality

Wagner *et al*. (2018) found that variations in the deposition environment have a significant impact on coal quality. Detritus can enter peat through marine invasions, overbank flooding, or airborne contemporaneous volcanism. As a result of such occurrences, all or part of the coal seam will have a higher ash level (Thomas, 2013). If marine waters infiltrate the peat mire for an extended period of time, minerals will likely precipitate into the uppermost part of the peat, increasing the sulphur content (Chou, 2012; Thomas, 2013).

According to Thomas (2013), coal quality parameters will not only indicate their distribution, but also the paleo-environmental influences that existed during the depositional and post-depositional phases of coal formation. The interpretation will aid in predicting the quality of coal in specific areas. Areas far from the sea will have low sulphur content, and coal deposited away from the main distributary channels and only exposed to low energy currents will have low ash content (Speight, 2005; Thomas, 2013).

Speight (2005) summarized this relationship as follows, rapid subsidence during sedimentation generally results in abrupt variations in coal seams however it is accompanied by low sulphur and trace element concentration whereas slower subsidence favours greater lateral continuity but higher content of chemically precipitated materials. Taylor *et al.* (1998) indicated that the coal quality parameters which are relevant are volatile matter, ash and sulphur content. If the coal has deficiency of volatile matter, but high ash and sulphur contents, the coal can be concluded to be uneconomic due to increased preparation costs (Taylor *et al.*, 1998).

Coal is used all over the world to generate electricity and to make iron and steel. Iron and steel production is primarily dependent on coal; however, coal-generated electricity is being challenged by other alternative energy sources, despite the fact that coal generates 42% of global electricity (Thomas, 2013). Taylor *et al*. (1998) stated that for coal to be used in industry, it must contain a high proportion of fusible macerals (>40% vitrinite) in order to form a well fused coke, as well as low concentrations of sulphur, phosphorus, and mineral matter.

### 2.4.3 Future of Coal Mining

Coal is the world's primary energy producer, accounting for more than 40% of global electricity generation. Coal accounts for more than 80% of electricity generation in South Africa. According to Deysel (2015), continuous coal mining in South Africa is required because future electricity generation projects indicate that coal will generate 71% of electricity in the future.

Gandolphe (2019) showed that the coal sector yielded good results in 2018 wherein the demand for coal increased by 0.7%. The six major coal producing countries, China, India, United States, Indonesia, Australia and Russia account for 83% of the world's coal production and they reported a strong growth (Gandolphe, 2019). Zero Hedge (2021) reported that the coal market in 2021 was yielding strong results. The price of the Australian thermal coal surged to $151 per ton which is three times what it was in September 2020 moreover the coking coal price increased by 80% so far. The price of coal in 2023 rose to $145 per tonne, however, it is projected to fall below $120 by 2025 (Trading Economics, 2023).

The world coal association (WCA, 2015) reported that the world coal production in 2013 reached a record level of 7822.8 Mt showing an increase by 0.4% from 2012. Since 2003 South Africa has been producing around 240 Mt coal per year, thus indicating stagnation in production (Deysel, 2015). This stagnation is primarily due to the gradual depletion of the Ermelo, Highveld and Witbank Coalfields in Mpumalanga province. Although it is still a significant participant in the global coal markets, South Africa moved from the fourth largest producer in 2001 to the seventh largest producer in 2013 (Table 2.4) (Garside, 2021).

China according to Garside (2021) is the leading producer with over 3.5 billion tons in 2018 (Table 2.4, whereas in 2019 it was the largest consumer of coal with 82 exajoules. Zero Hedge (2021) indicated that China consumes 4 billion tons of coal yearly and imports 300 million tons. The top exporters and importers are indicated (Tables 2.5 and 2.6 respectively).

South Africa currently exports 70 million tons plus of coal and 40 million tons of this is exported to India annually at $ 100 per ton (Creamer, 2021). Creamer (2021) indicated the demand for South African coal is continuing to increase in Pakistan and Sri Lanka. According to Chamber of Mines (2018) South Africa is a net exporter of coal and accounts for 6% of total global exports. South Africa is ranked number 6 as the largest exporters (Table 2.5). Chamber of Mines (2018) indicated that South Africa produced 253.1 Mt of coal in 2016 and 181.4 Mt valued at R 61.5 billion was sold within the country whereas 68.9 Mt was exported at R 50 billion.

Table 2.4: Top 10 coal producers in the world (Garside, 2021)

| Country | Coal produced in Million tons (2018) |
|---|---|
| China | 3530 |
| India | 730.3 |
| United States | 634.2 |
| Indonesia | 497.8 |
| Australia | 452.8 |
| Russia | 352.6 |
| South Africa | 253.6 |
| Kazakhstan | 111.9 |
| Colombia | 84.3 |
| Poland | 63.6 |

Table 2.5: World's biggest coal exporters (Buchholz, 2021)

| Exporters | Coal in Million tons (2019) |
|---|---|
| Indonesia | 455 |
| Australia | 393 |
| Russia | 217 |
| United States | 84 |
| South Africa | 81 |
| Colombia | 72 |
| Canada | 36 |
| Mongolia | 28 |

Table 2.6: World's biggest coal importers(IEA, 2019).

| Importers | Coal Million tons (2018) |
|---|---|
| PR China | 295.4 |
| India | 240.2 |
| Japan | 185.1 |
| Korea | 142 |
| Chinese Taipei | 66.5 |
| Germany | 44.4 |
| Turkey | 38.3 |
| Malaysia | 33 |
| Russia | 28.2 |
| Thailand | 24.9 |

## 2.5 Effects of Coal Mining

Matshusa (2007) and Munnik *et al.* (2010) noted that coal mining inflicts many external impacts on its surroundings. It is by its nature destructive to the environment. Munnik *et al.* (2010) further explained that coal mining involves the removal of enormous quantities of overburden to have access to the ore. This according to Goswami (2015) produces a lot of waste and discard which result in severely degraded land, water, air and subsequently the quality of life. The mining industry in general puts tremendous pressure on the local fauna and flora. Goswami (2013, 2015) indicated that the effects of mining on groundwater quality, silting of water bodies and destruction of the habitat is of great concern.

When coal is combusted, it releases harmful gases and substances such as sulphur dioxide, nitrogen oxide, carbon dioxide, dust and ash (Fig. 2.8) (Goswami, 2015). The introduction of such noxious gases into the atmosphere causes acid rain which can cause extensive environmental impacts. Agarwal and Narain (1991) and Mamurekli (2010) indicated that coal mining also affect global environment as coal mining activities are associated with the release of enormous quantities of coal bed methane which according to Goswami (2013, 2015) has 30 times harmful impacts as a greenhouse gas than carbon dioxide.

To reduce the negative effects of coal mining, it is critical that clean mining activities be practised (Goswami, 2015). According to Goswami (2015), coal mining also exposes sulphide minerals such as pyrite, which react with oxygen and water and become oxidised, resulting in acid mine drainage, a global problem (AMD). The acid produced can leach and raise the pH of water, rendering it unfit for consumption, irrigation, and other industrial applications (Fig. 2.8) (Goswami, 2013).

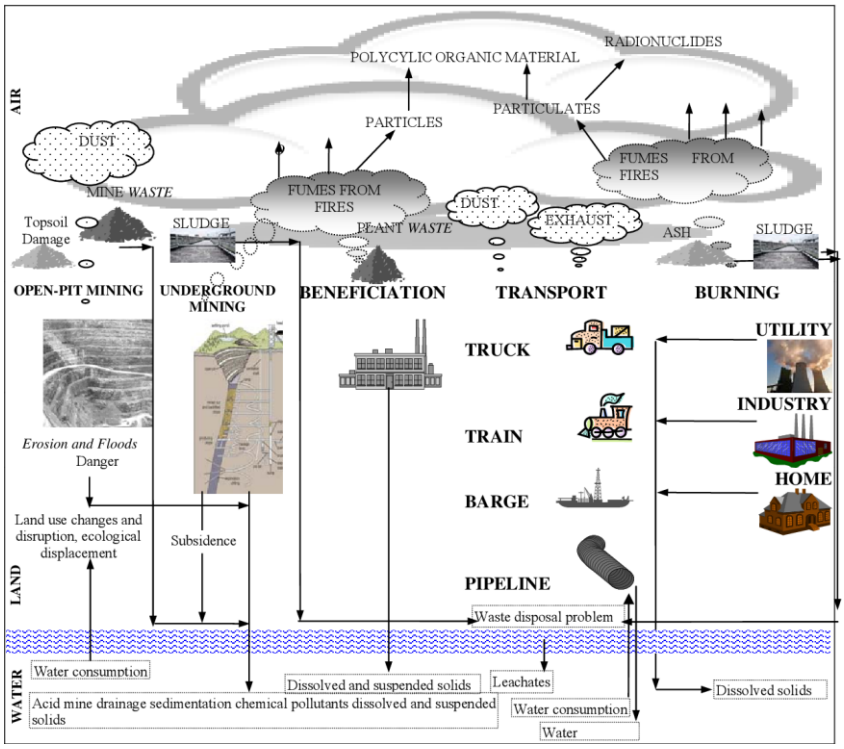


Figure 2.8: Environmental impacts of coal mining (Mamurekli, 1997).

## 2.6 Acid Mine Drainage

Acid mine drainage is a natural by-product of mining activities that occurs when a deposit (metal or coal) is excavated below groundwater level, exposing sulphide minerals to water and oxygen (McGinnes, 1999; Akcil and Koldas, 2006; Nengovhela *et al*. 2006). Nengovhela *et al*. (2006) concluded that, while oxygen and water are both responsible for sulphide mineral oxidation, their contribution to acid generation differs. They also discovered that within the Witwatersrand gold tailings, oxygen plays a larger role in the oxidation of sulphides. According to McGinnes (1999), when mines close, pumps are removed to reduce costs, which causes groundwater to return to pre-mining levels, resulting in flooding of mine openings and acid mine water generation. According to Kleinmann (1990), McGinnes (1999), and Nengovhela *et al*. (2006), acid mine drainage occurs as a result of sulphide oxidation (mostly pyrite) when

exposed to water and oxygen, and sometimes as a result of biological reactions enabled by bacterial activities.

Wang *et al.* (2021) indicated that AMD has become a worldwide environmental problem. Taking into consideration the contamination of the Tinto River in the Rio region in Spain and the acid generated in closed pits of the Witwatersrand mine which according to (Netshitungulwana *et al.*, 2013) is of great concern. Minerals contained in waste material or exposed rocks (mostly sulphides, pyrite) react with water and oxygen to produce sulphuric acid. Fey (2003) indicated that this acid is itself detrimental to water quality. Acid leaches metals from material and introduces them into environment (Fey, 2003). This process takes place naturally at a lesser scale in a process called Acid Rock Drainage.

The excessive removal of the overburden in the mining industry does however exacerbate this process (Fey, 2003; Johnson and Hallberg, 2005; Udayabhanu and Prasad, 2010). Udayabhanu and Prasad (2010) indicated that AMD is the most problematic environmental impact associated with the mining industry. This is due to the fact that the contaminants from the mine can persist in the environment for long periods of time even after the mining activities have ceased (Modis *et al.*, 1998; Demchark *et al.*, 2004). Maiyana (2003) noted that the morphology of sulphide minerals can influence the rate of acid mine production. Udayabhanu and Prasad (2010) further indicated that the amount of AMD generated is dependent upon the size of the exposed sulphide minerals.

**Sources and factors influencing Acid Mine Drainage**

According to Natarajan (2008), there are both primary and secondary causes of AMD. The primary source is waste rock dumps and tailings impoundments. Secondary sources include treatment sludge ponds and rock cuts. According to Udayabhanu and Prasad (2010) and Nengovhela *et al*. (2006), there are several factors that improve and accelerate the AMD process. The presence of oxidants, pH levels, temperature, chemical reactivity, surface area of exposed sulphide minerals, and biological activity are the major factors driving AMD. (Nengovhela *et al*., 2006; Natarajan, 2008; Udayabhanu and Prasad, 2010). Sulphide minerals responsible for acid mine water generation are listed in Table 2.7.

Ferguson and Erikson (1988) are amongst one of the pioneers in investigating the influence of biological activity in the exacerbation of oxidation. Nengovhela *et al*. (2006); Natarajan (2008) further indicated that bacterial (biological) activities can rapidly exacerbate AMD. Thiobacillus ferroxidase and Thiobacillus trioxidanes are ubiquitously present in sulphide mineral bearing ore deposits, mine tailings and abandoned mines. These bacteria play a significant role in acid production because of their ability to rapidly oxidize reduced forms of

iron and sulphur (Ferguson and Erikson, 1988; Natarajan, 2008; Nengovhela *et al*., 2006; Udayabhanu and Prasad, 2010). Zipper *et al.* (2018) further indicated that the presence of such bacteria exacerbates the rate of sulphur oxidation. Without the presence of these catalytic bacteria the rate of oxidation of iron would be slow.

Oxygen is also an important factor in acid mine water generation (Ferguson and Erikson, 1988; Nengovhela *et al*., 2006). When the mine waste contains sufficient oxygen from the atmosphere the rate of reaction tends to increase (Ferguson and Erikson, 1988). Hawley (1977); Maiyana (2003) also indicated that the forms of pyrite present also contribute to the rate of acid generation. Hawley (1977) further noted that isometric pyrite is not as chemically reactive as orthorhombic or hexagonal Pyrrhotite. Maiyana (2003) focused on the morphology of pyrite and noted that euhedral pyrite is less reactive when compared to framboidal pyrite.

Table 2.7: Sulphide minerals responsible for acid mine water generation (Udayabhanu and Prasad, 2010; Fey, 2003)

| **Sulphides** | **Formula** |
|---|---|
| Pyrite | $FeS_2$ |
| Pyrrhotite | $Fe_XS_X$ |
| Chalcocite | $Cu_2S$ |
| Covelite | CuS |
| Chalcopyrite | $CuFeS_2$ |
| Arsenopyrite | $FeAsS_2$ |
| Molibdenite | $MoS_2$ |
| Galena | PbS |
| Millerite | NiS |
| Sphalerite | ZnS |

### 2.6.1 Chemistry of Acid Mine Drainage Generation

Weathering of sulphide is responsible for vast majority of surface and groundwater contamination incidents. Pyrite in particular is the most ubiquitous sulphide mineral and is responsible for acid generation from coal mines and metal mines (Udayabhanu and Prasad, 2010). The iron sulphide is oxidised and acid is subsequently generated and released. Ferguson and Erikson (1988) indicated that the oxidation of pyrite during acid mine water generation follows four steps (Equations 1, 2, 3, 4). Nengovhela *et al.* (2006), Fey (2003) and Udayabhanu and Prasad (2010) further indicated that the process of AMD is initiated by the breakdown of pyrite in the presence of oxygen and water to yield ferrous iron, sulphate and acidity (Equation 1).

$$FeS_2 + 7/2O_2 + H_2O \rightarrow Fe_2 + 2SO_4^{2-} + 2H^+ \qquad \text{Equation (1)}$$

When sufficient oxygen has been dissolved in water, the oxidation of ferrous to ferric iron occurs (Equation 2). This reaction is rapidly accelerated by a bacterium called Thiobacillus ferroxidase (Ferguson and Erikson, 1988; Fey, 2003, Nengovhela *et al*., 2006; Udayabhanu, 2010).

$Fe^{2+} + 1/4O_2 + H^- \rightarrow Fe^{3+} + 1/2H_2O$ Equation (2)

Ferguson and Erikson (1988) and Udayabhanu and Prasad (2010) indicated that the third step involves hydrolysis of ferric iron to produce the solid ferric hydroxide and release of additional acidity. Jambor and Blowes (1998) indicated that this step is pH dependent. When pH is below 3.5 the solid material does not form and ferric iron remains in solution, alternatively, when pH is above 3.5 a precipitate of $Fe(OH)_3$ forms which is commonly referred to as yellow boy (Equation 3).

$Fe^{3+} + 3H_2O \rightarrow Fe(OH)_3 + 3H^+$ Equation (3)

When the acidity increases the reaction reinitiates because the ferric iron remains in solution and is reduced by pyrite which result in the release of ferrous iron and acidity (Equation 4).

$FeS_2 + 14\ Fe^{3+} + 8H_2O \rightarrow 15\ Fe^{2+} + 2SO_4^{2-} + 2H^+$ Equation (4)

This cyclic spread of acid generation by ferric iron takes place rapidly and continues until supply of ferric iron of pyrite is completely exhausted. The overall sequence of reactions is acid producing (Equation 5) (Udayabhanu and Prasad, 2010). This section focused chiefly on the oxidation of pyrite as it is the common known sulphide mineral in coal deposits.

$4FeS_2 + 15O_2 + 14\ H_2O \rightarrow Fe(OH)_3 + 8H_2SO_4$ Equation (5)

Pyrite + Oxygen + Water → Yellow Boy + Sulphuric Acid

Metals such as aluminium (Al) and manganese (Mn) also contribute in the formation of acid mine drainage (Zipper *et al.*, 2018). Aluminium ($Al^{3+}$) contributes to the acidity of the solution because aluminium has the ability to hydrolyse when hydroxide ($OH^-$) ions are added (Equation 6). When the aluminium hydrolyses it precipitates in a solid phase and releases hydrogen (Equation 6) (Zipper *et al.*, 2018). Manganese has a similar case as ferric hydroxide, as it precipitates (in solid form) it releases hydrogen ions ($H^+$) (Equation 7) (Zipper *et al.*, 2018).

$Al^{3+} + 3H_2O \rightarrow Al(OH)_3 + 3H^+$ Equation (6)

$Mn^{2+} + 0.5\ O_2 + 1.5\ H_2O \rightarrow MnOOH + 2H^+$ Equation (7)

### 2.6.2 Acid Neutralising Minerals

Udayabhanu and Prasad (2010) indicated that there are several acid treatment methods. These methods are collectively Grouped into active (using chemicals) and passive (Using natural materials). Limestone has been studied by different researchers such as Wilmoth *et al*. (1972); Ford (1974); Caruccio and Geidel (1985) who concluded that limestone can neutralise the pH of acidic water. Younger *et al.* (2002) further noted that limestone (rich in calcium) can increase the pH of water by consuming the hydrogen ions and adding alkalinity through bicarbonate ions (Equation 8). Udayabhanu and Prasad (2010) further elucidated that when the pH of acidic water is raised, hydroxides and oxy-hydroxides are produced through precipitation of metals (Equation 9). When the pH is increased, the environment becomes unfavourable for bacterial activity which then inhibits the formation of acidic solution (Kleinmann, 1990). There are several minerals which can neutralize the acidity of water (Table 2.8). Carbonate minerals are some of the detailed studied acid neutralising minerals. Phosphate have been studied and documented as one of the minerals that slow the rate of pyrite oxidation (Kleinmann, 1990).

Table 2.8: Minerals with ability to neutralise acid (Kleinmann, 1990)

| **Name** | **Formula** |
|---|---|
| Sodium Hydroxide | NaOH |
| Sodium Carbonate | $Na_2CO_3$ |
| Phosphate | $PO_4$ |
| Calcium Carbonate | $CaCO_3$ |

$CaCO_3 + 2H^+ \rightarrow Ca^{2+} + H_2O + CO_2$ Equation (8)

$CaCO_3 + H_2CO_3 \rightarrow Ca^{2+} + 2HCO_3$ Equation (9)

The neutralisation of the acidic water takes place through the dissolution of limestone and the exsolution of carbon dioxide from the water (Udayabhanu and Prasad, 2010).

### 2.6.3 Acid Mine Drainage in South Africa

South African acid mine drainage research has focused on gold and coal resources (Lishman, 2009). Since 1894, the Witbank Coalfield has been a major coal producer in South Africa. Due

to a large number of abandoned coal mines in this area, acid mine water has been generated (McCarthy, 2011).

According to Bell *et al*. (2001), AMD seeping from an abandoned mine in the Witbank Coalfield contaminated the Blesbokspruit stream, a tributary of the larger Olifants River. They also discovered that the water flowing from the mine in Witbank has a lower pH, high electrical conductivity, and a high concentration of dissolved solids. Geldenhuis and Bell (1998) conducted research in the Witbank's Loubert mine. According to the study's findings, the mine produces acid mine water from backfilled open cast mine workings. Pinetown et al. (2007) further indicated that acid mine water generation within the Witbank Coalfield is chiefly attributed to the bottom two seams (seams 1 and 2). Hobbs *et al.* (2008) further indicated that the upper Olifants River catchment is South Africa's most important source of coal. However, AMD from old abandoned coal mines in this area has been identified as having a long-term impact on water quality. Bega (2022) recently reported toxic water spilling from the Khwezela colliery into the Wilge River (Fig. 2.9). The study further indicated that millions of litres of acid mine water spilled from an old coal mine (Khwezela colliery) after an old shaft collapsed in February 2022, wreaking havoc on aquatic life in the Wilge River.

Figure 2.9: Toxic water from the Khwezela colliery near Emalahleni (Bega, 2022).

## 2.7 Acid Base Accounting

Hossner and Brandt (1997) indicated that the term Acid Base Accounting (ABA) means different things to different people. This is because this method is used to assess the suitability of overburden materials for mine soils, whereas others are used to predict post-mining environmental effects. According to Ferguson and Erikson (1988), there are static and kinetic acid base accounting tests, and the static tests provide a rough indication of the acid generation potential of the numerous lithological units, whereas the kinetic test is performed

to estimate if the samples are prone to produce acid over a 20-week period. Ferguson and Erikson (1988) tabulated the costs of acid mine drainage prediction techniques in their study and discovered that static acid base accounting is the least expensive method with good reliability. Static acid base accounting tests were used in this study to estimate or predict the acid generating potential of both coal and host rocks.

According to Sobek *et al*. (1978), Ferguson and Erikson (1988), Brady *et al*. (1994), and Cruywagen (1999), acid base accounting (ABA) is a classification procedure that determines the acid producing potential (AP) and neutralising potential (NP) of materials. Brady *et al*. (1994) defined the net neutralisation potential (NNP) as the difference between the neutralisation potential (NP) and the acid generating potential (AP), which is the sum of the total carbonates and bases available to neutralise acidity. Static acid base accounting produces the worst-case scenario for acid generation potential, as well as the worst-case, most likely-case, or best-case value for potential neutralisation (Usher *et al*., 2003).

**Static Tests**

The static tests according to Sobek *et al*. (1978); EPA (1994) predict drainage by comparing the sample's maximum acid production potential (AP) with its maximum neutralization potential (NP). EPA (1994) further indicated that the acid production potential (AP) is determined by multiplying the percent of total sulphur by the conversion factor (31.25) (Equation 10) whereas the neutralization potential is determined by either adding acid to the sample and back titrating to determine the amount of acid consumed. The neutralization potential is conducted to measure the concentration of carbonate material available to neutralize acid (Ferguson and Morin, 1991). The Net neutralization potential (NNP) or acid/base account (ABA) is determined by finding the difference between neutralizing potential (NP) and acid production (AP) (Equation 11):

$$AP = \%\ \text{Sulphur X}\ 31.25 \qquad \text{Equation (10)}$$

$$NNP = \text{NP} - \text{AP} \qquad \text{Equation (11)}$$

EPA (1994) and Fey (2003) indicated that there are different types of static test methods and these include acid base accounting (ABA), modified acid base accounting, British Columbia research initial, alkaline production potential and the net acid production (Table 2.9). For the purpose of this study the acid base accounting method was used to predict the potential for acid generation while the neutralization potential was determined using modified Sobek method.

Table 2.9: Summary of static test methods, their advantages and disadvantages (EPA, 1994)

| **Acid Base Accounting** (Sobek *et al* , 1978) | **MODIFIED Acid Base Accounting** (Coastech, 1989) | **BC RESEARCH INITIAL** (Duncan and Bruynesteyn, 1979) | **Alkaline Production Potential: Sulfur** (Caruccio *et al* , 1981) | **Net Acid Production** (Coastech 1989) |
|---|---|---|---|---|
| **ACID PRODUCTION DETERMINATION** | | | | |
| Acid Producing Potential = 31.25 * Total S | Acid Producing Potential = 31.25 * Total S | Total Acid Production = 31.25 * Total S | Total S used as indicator | 300 mL H2 2 O added to 5 g rock to directly oxidize sulfides present |
| **NEUTRALIZATION POTENTIAL DETERMINATION** | | | | |
| -60 mesh (0.24 mm) sample add HCl as indicated by fizz test, boil one minute than cool titration endpt pH 7.0 cost: 34-110 | -60 mesh (0.24 mm) sample add HCl as indicated by fizz test agitate for 23 hours at room temperature pH 1.4 - 2.0 required after six hours agitation titration endpt pH 8.3 cost: 34-110 | -300 mesh (0.038 mm) sample titrate sample to pH 3.4 with 1.0 N H2 3 SO titration endpt not applicable cost: 65-170 | -0.023 mm sample 20 mL 0.1 N HCl to 0.4g solid for 2 hours at room temperature titration endpt pH 4.0 cost: 34-110 | particle size not presented acid produced by iron sulfide oxidization dissolves buffering minerals titration endpt pH 7.0 cost: 25-68 |
| **ADVANTAGES AND DISADVANTAGES** | | | | |
| simple and short time no special equipment and easy interpretation many samples can be tested does not relate to kinetic assumes parallel acid/ alkaline release if APP and NP are close, hard to interpret and different particle size not reflected | simple, short time, no special equipment, and easy interpretation does not relate to kinetic assumes parallel acid/ alkaline release if AP and NP are close, hard to interpret and different particle size not reflected | simple and fairly short time no special equipment and easy interpretation many samples can be tested assumes parallel acid/ alkaline release, different particle size not reflected, and if APP and NP are close, hard to interpret | simple, short time, and no special equipm moderate interpre | simple, short time, no special equipment, and easy interpretation limited reproducibility uncertain if extent of sulfide oxidation simulates that in field |

# CHAPTER 3: MATERIALS AND METHODS

This study was divided into several stages such as preliminary work, fieldwork, laboratory work, sample analysis which subsequently led to data analysis and discussion (Fig. 3.1).

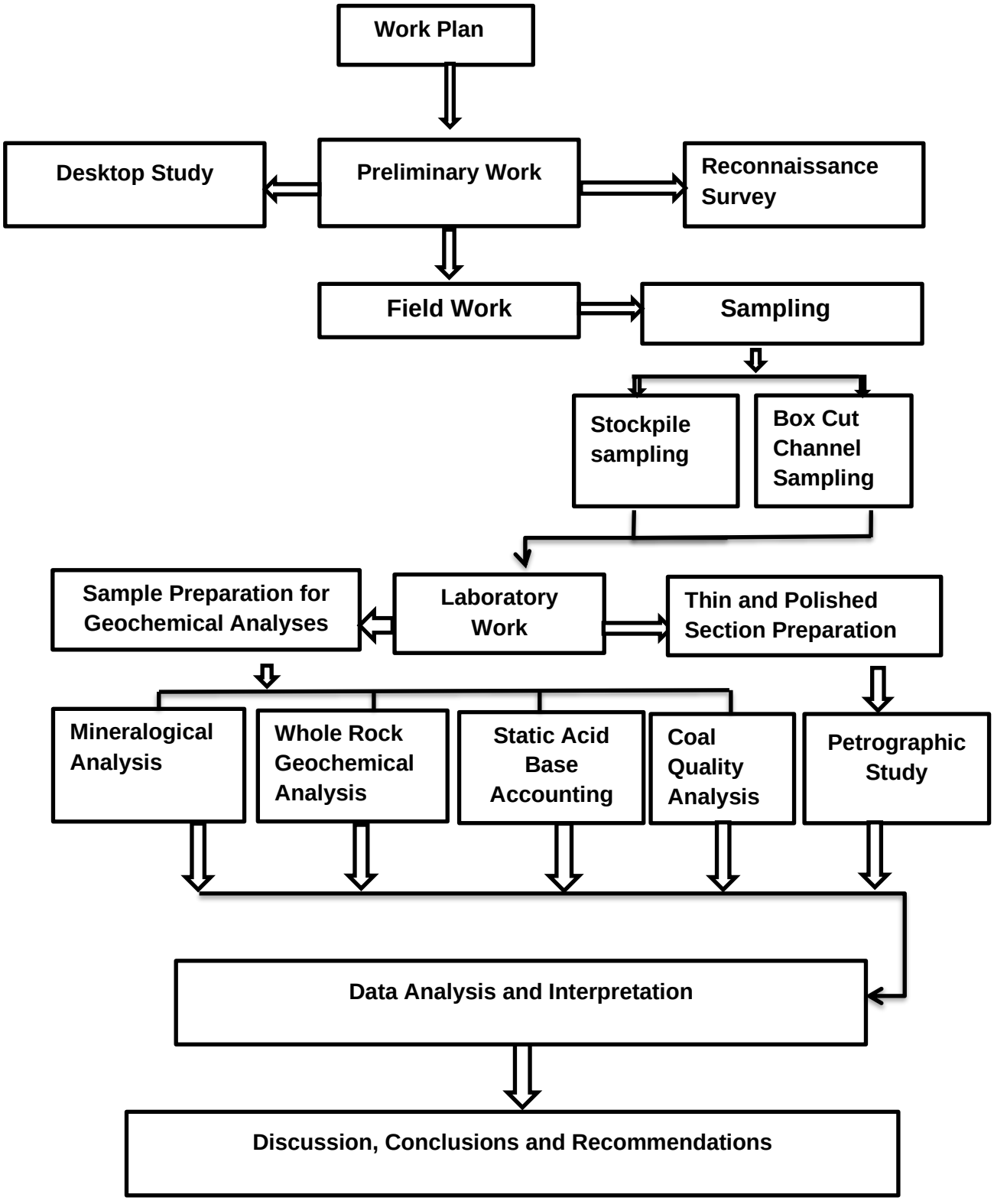


Figure 3.1: Flow chart summarising the methods and procedures applied in this study.

## 3.1 Preliminary Study

Preliminary work mostly refers to the preparatory activities undertaken before the actual fieldwork. These activities were carried out to identify materials and methods to be used during the study. Information gathered in this stage provided the knowledge about the study area and any challenges to be encountered during the study. Preliminary work included desktop study and reconnaissance survey.

### 3.1.1 Desktop Study

Desktop study was prepared in order to acquire first-hand information about the location, characteristics and accessibility to the study area. This information was gathered from various sources which included, but not limited to books, published and unpublished documents, records, internet sources, Journals, topographical and geological maps.

The information was collected through intensive literature review which provided the information about the study area and to assist in the selection of the best materials and methods to be used.

### 3.1.2 Reconnaissance Survey

Reconnaissance survey involved a visit to the study area. At this stage local authorities, mine owners and relevant stakeholders were visited to seek permission to conduct fieldwork. Demarcation of the study area was done in order to conceptualize procedures for fieldwork. It was crucial to conduct reconnaissance survey as it helped with outlining the fieldwork plan. Consequently, methods and procedures for fieldwork were established for example, sampling method to be used during box-cut sampling.

## 3.2 Fieldwork

This is the backbone of the research work that the component of the research ensures that the objectives of the study are achieved. This is the actual work in the field, wherein the field was explored, verified, mapped and collection of samples was done as it is the vital part of the fieldwork.

Channel sampling for coal and host rock samples was conducted at Sekoko Lephalale Coal Concession which is 10 km from the Grootegeluk mine (Fig. 3.2). Sekoko coal mine is bounded within the Swartrant and Grootegeluk Formations, the former is stratigraphically equivalent to the Pietermaritzburg Formation of the main karoo basin (MKB) (Fig. 3.3). Seam

10 was first mapped then sampled from the box cut. Seam 11 however due to limited access, was sampled from the stockpile.

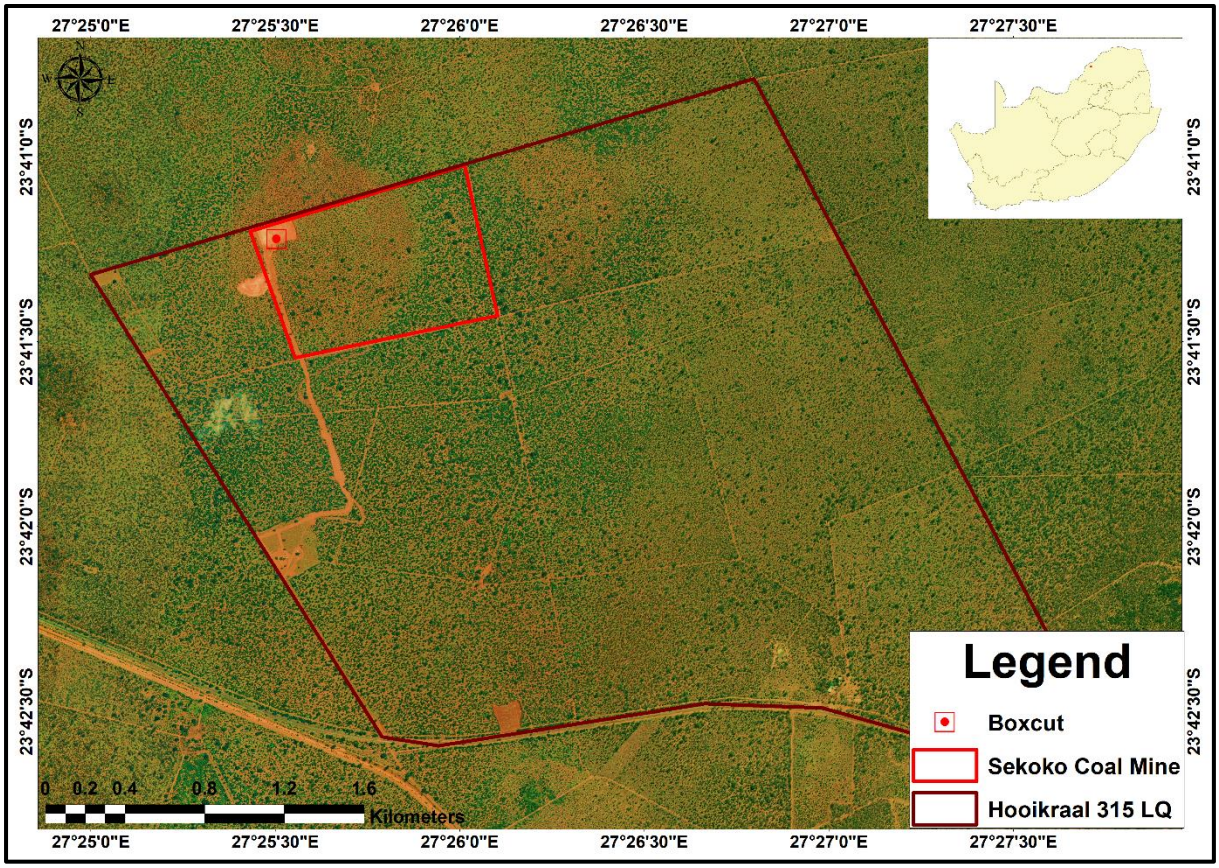


Figure 3.2: Location of Sekoko coal mine within the Hooikraal 315 LQ Farm (Google earth pro).

### 3.2.1 Coal Face Mapping

The box-cut at Sekoko Lephalale Coal Concession exposed two coal seams (11 and 10) respectively (Fig. 3.4). Due to restricted access, only seam 10 was mapped. During mapping the roof, coal seams and interburden were marked and described. Supplementary data such as coordinates, location in the pit, seam number, thickness, minerals and weathering were indicated. Mapping was conducted on the west and south portion of the box cut (Fig. 3.5). Coal seam 10 is overlain by grey medium- to course-grained sandstone stained with sulphur (Fig. 3.4). This coal seam has alternating bands of bright and dull coal with carbonaceous shale and shale occurring as the interburden. Sulphur (yellow) is prominent on the face of the pit (Fig. 3.4). Characteristic of host rock and coal were noted and summarized (Tables 3.1 and 3.2).

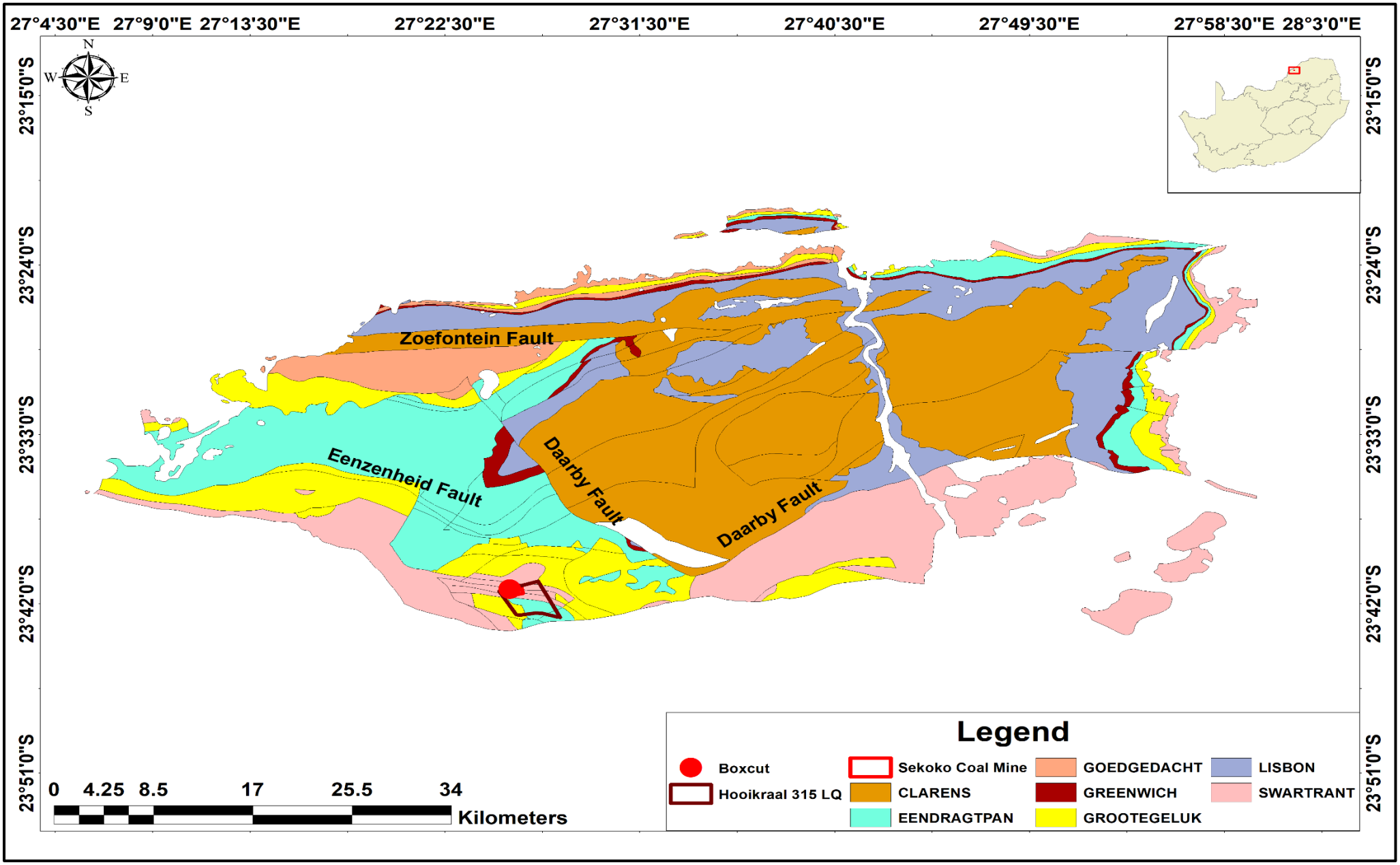


Figure 3.3: Geological location of Sekoko Coal Mine (ArcGIS 10.8, Data sourced from Council for Geoscience).

Table 3.1: Characteristics of host rocks and coal seam mapped on the west side of the box cut

| Ply | Lithological Description | Thickness (m) | True coal | Coal type: Bright/Dull | Mineralogy | Roof strata | Floor strata | weathering | Description |
|---|---|---|---|---|---|---|---|---|---|
| A | Sandstone | 2 | | | | | | | Grey course textured sandstone |
| Shale F-R | Shale | 10 | --- | ----- | Pyrite | Shale | | --- | A Gray fissile, fine grained, hard laminated clastic argillaceous sedimentary rock overlain by white quartz rich sandstone. Yellow stains of sulphur. |
| B | Coal | 0.73 | 0.73 | Dull coal | | | | Moderately weathered on exposed face | Black earthy bituminous coal showing moderate fracturing on the face. |
| C | Coal | 0.25 | 0.25 | Bright coal | | | | | Black shiny bituminous coal, fresh and intact. Not showing signs of weathering. |
| D | Coal | 0.37 | 0.37 | Bright coal | Pyrite | | | Gradually weathered towards the centre with calcite and sulphur reactions showing | Black shiny bituminous coal. Showing reaction of sulphur (yellow) and calcite (white) due to contact with water. |
| E | Shale | 0.1 | 0.1 | Carbonaceous shale | Pyrite | | | | A black fissile, fine grained, hard laminated clastic argillaceous sedimentary rock intercalated with coal. |
| G | Coal | 0.82 | 0.82 | Dull coal | Pyrite | | | Moderately weathered, crumbling | Dull coal occurring interchangeably with thin bright coal layers. Showing gradual change from bright to dull coal with sulphur reaction on the face. |
| H | Coal | 0.52 | 0.52 | Bright Coal | | | | | Black shiny bituminous coal, fresh and intact. Not showing signs of weathering. |

Table 3.2: Characteristics of host rocks and coal seam mapped on the south side of the box-cut

| Ply | Lithological Description | Thickness (meters) | True coal thickness | Coal type: Bright/Dull | Mineralogy | Roof strata | Floor strata | weathering | Description |
|---|---|---|---|---|---|---|---|---|---|
| A | Sandstone | 30 | ----- | ------ | Pyrite | Sandstone | | ---- | A white fine-grained quartz-rich sandstone with sulfur stains. |
| B | Coal | 1.76 | 1.76 | Dull coal | | | | | Black earthy bituminous coal shows moderate fracturing on the face. |
| C | Coal | 0.11 | 0.11 | Bright coal | | | | | Black shiny bituminous coal, fresh and intact. Not showing signs of weathering. |
| D | Coal shale | 0.62 | 0.62 | Coal shale | | | | | Black carbonaceous shale showing fissility. |
| E | Shale | 0.30 | 0.30 | Shale | | | | | A Gray fissile, fine-grained, hard platy clastic argillaceous sedimentary rock intercalated with coal. |
| F | Coal | 0.80 | 0.80 | Bright coal | | | | | Black shiny bituminous coal with thin layers of dull coal. |
| G | Shale | 0.20 | 0.20 | Platy shale | | | | | Shale intercalated with thin layers of |
| H | Coal | 0.16 | 0.16 | Bright coal | calcite | | | Reaction of calcite | Black shiny bituminous coal, fresh and intact. They are showing a reaction of calcite on the face. |

### 3.2.2 Host Rock and Coal Sampling

Sampling was conducted at the Sekoko coal mine located 10 km from the Grootegeluk coal mine in the Lephalale region. Two exposed coal seams were sampled within the box cut at the Sekoko Coal Mine. Host rocks overlying the coal seam and different partings of seam 10 were sampled. Seam 11 was sampled from the stockpile.

**Host Rock and Coal Sampling at the Box Cut**

Channel sampling was carried out at the box cut. Channel sampling was conducted because it gives a representative sample of coal seam in the area. Host rocks and coal beds were horizontal and channel sampling was conducted perpendicular to the bedding. A composite sample was collected to provide the composite quality analysis of the coal seam. Since coal seams are rarely homogeneous throughout the thickness, seam 10 was subdivided into distinct lithological sections (Ply) (Fig. 3.3).

A geological hammer together with a tape and scoop were used to uniformly sample 2 kg of the different plies of seam 10 (Fig. 3.6A). Samples were placed in a plastic sample bag which was tied and labelled with a permanent marker. The plastic sample bag was placed within another plastic bag to prevent addition of moisture (Fig. 3.6B) and a labelled tag was inserted inside for accurate identification of the sample.

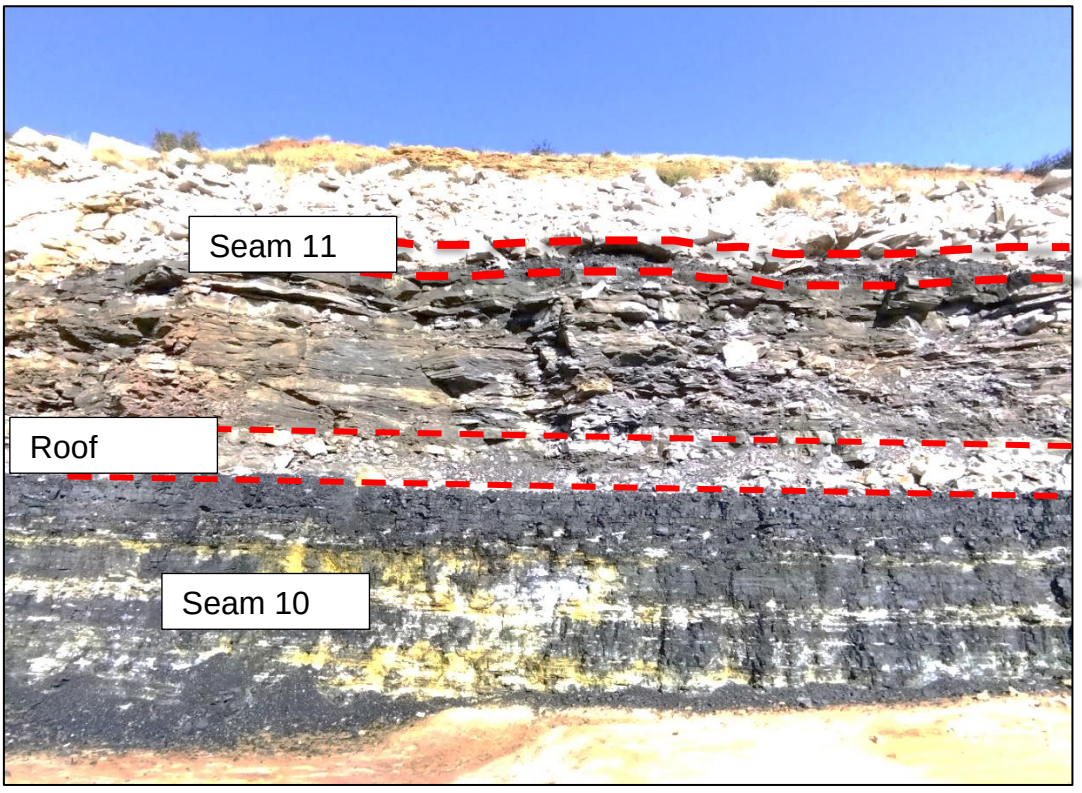


Figure 3.4: Exposed coal seams at Sekoko Lephalale Coal Concession.

Figure 3.5: Mapping of seam 10 on the west side of the box cut.

A B

Figure 3.6: Channel sampling at the box cut.

**Stockpile Sampling**

Ex-situ sample was collected from the stockpile. This was done for seam 11 since it was inaccessible from the pit. A scoop was used to collect a composite representative sample of unprocessed coal (Fig. 3.7). To ensure that the sample is representative, four scoops were collected along each side of the stockpile at equidistant points and two scoops were taken from the top. A 2 kg sample was collected from the stockpile. The coal on top was first removed to gain access to fresh samples. A plastic sample bag was used to store the samples and tied to prevent moisture loss.

Figure 3.7: Sample collection from the stockpile.

During this stage of sampling, a total of 18 samples were collected, from the 18 collected samples, 3 were host rocks and 15 were coal samples wherein 17 samples were collected from the box-cut and 1 composite sample from stockpile.

## 3.3 Laboratory Work

Laboratory work involved preparation of samples as well as analysis.

### 3.3.1 Sample Preparation

Sample preparation involved all the standard procedures followed in preparing samples for petrographic studies, geochemical analysis, coal quality and static acid base accounting tests.

#### 3.3.1.1 Preparation for Petrographic Studies

Thin section and polished blocks were prepared for petrographic study. Host rock specimens were prepared for thin section while polished blocks were prepared for coal samples.

**Thin Section**

Thin section preparation was done for petrographic study. A total of three rock specimens were prepared at the Department of Earth Science, University of Venda. A mechanical

diamond saw (Fig. 3.8A) was used to cut three rock specimens into smaller sized slab. Samples were then trimmed using Buehler's PetroTrim machine (Fig. 3.8B) to obtain a flat slide sized slab for mounting on a glass slide. Subsequently, slabs were grinded using silica carbide (220 to 1000 grit size) (Fig. 3.8C) to remove saw marks as well as remaining edges on samples. Before mounting glass slides were polished using silica carbide to provide a rough surface to mount on. Thereafter, samples were left to air dry overnight. The reason behind air drying is that when samples are oven dried at 50ºC or higher, organic materials reacts.

A mixture of hardener and resin (Fig. 3.8D) on a ratio of 1:7 was used to mount samples on glass slides. Subsequently, bonding jig (Fig. 3.8E) was used to apply pressure on samples overnight. After 24 hours of drying, Buehler's PetroThin-section (Fig. 3.8F) machine was used to further cut the sample to achieve a block size of 1 mm for competent material like sandstone and 5 mm for friable material like shale. After cutting, samples were grinded using Buehler's PetroThin-section machine to achieve a size of 100 µm thickness (Beuhler, 2012). Thereafter, Struers RotoPol-35 Pdm-force-20 lapping machine (Fig. 3.8G) was used to polish samples with aid of Akasel's DiaDoublo mono 6 µm diamond suspension and Struers MD-Plan 300 mm diameter lapping disk (Fig. 3.8H) to achieve 20 to 30 µm in thickness (Beuhler, 2012).

**Polished Block preparation**

A total number of six coal samples were selected for polished block preparation at the University of Johannesburg. Coal samples were crushed to pass the 1 mm sieve. Thereafter, bonding material was prepared using a ratio of 1:7 for hardener and resin respectively. The bonding material was poured into a mounting cup. Subsequently, the crushed coal was added into the same mounting cup and stirred. Samples were placed in a vacuum to remove bubbles for 24 hours. Upon drying, polished blocks were polished using Struers Rotopol 35 PdM-Force-20 (Fig. 3.8G) to achieve a smooth surface. Polished blocks were placed in a closed container awaiting petrographic analysis.

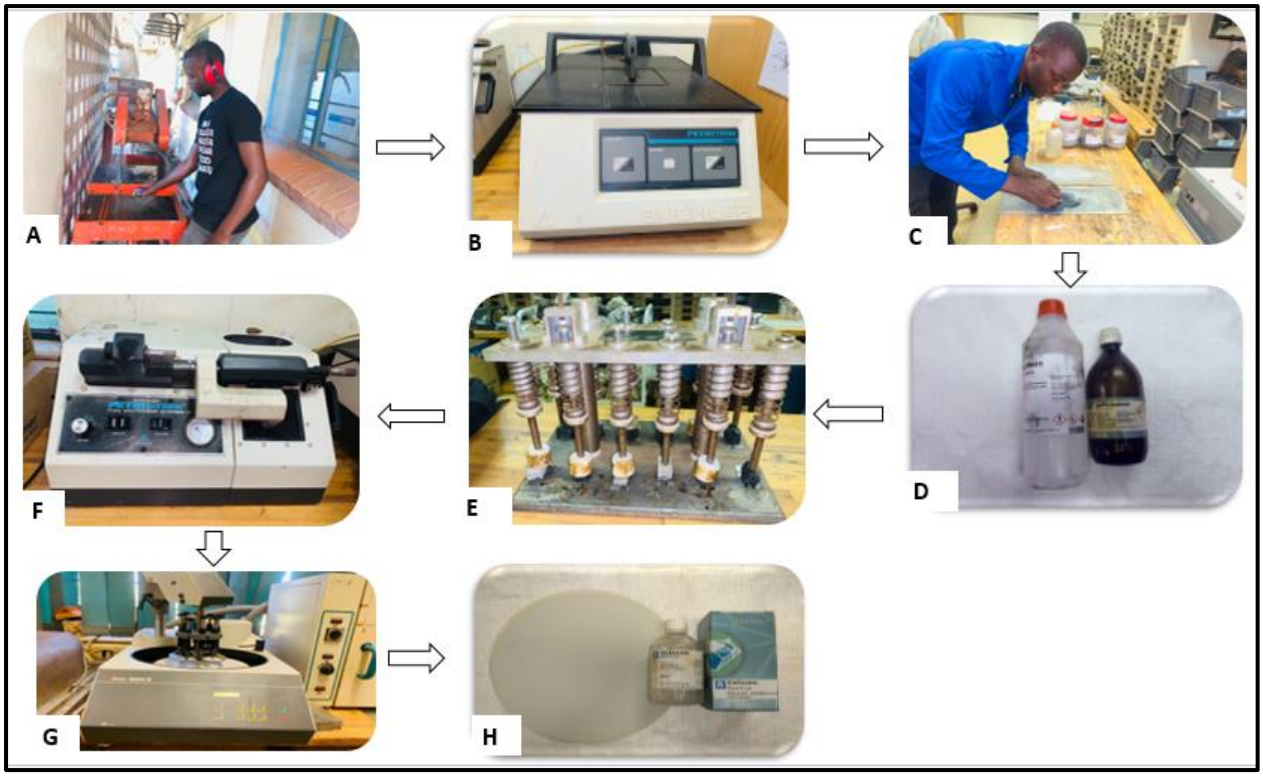


Figure 3.8: A figure depicting steps undertaken in thin-section preparation: (A) Cutting of rock specimens using a mechanical jaw crusher, (B) Trimming rock specimens using Beuhler PetroTrim machine, (C) polishing slabs on a glass plate, (D) Epoxy and rasin mixture, (E) Bonding of rock specimens using a bonding Jig, (F) Grinding of rock specimens, (G) Polishing rock specimens using a lapping machine with aid of diamond suspension and lapping disc (H).

### 3.3.1.2 Preparation for Scanning Electron Microscopic Study

A total of 5 coal Samples were prepared for scanning electron microscopic study. Samples were crushed to pass the 1 mm sieve. Following (Syed *et al*., 2017; Kannan, 2018) coal samples were mounted on Bakelite using a hot mounting method with phenolic resin (Syed *et al*., 2017). Samples were washed with water and alcohol and then dried prior to polishing. Samples were subjected to polishing; this involved mechanical grinding of the sample using grits (Silicon carbide) and mechanically polishing the sample in slurry of alumina particles ($Al_2O_3$). This was done to ensure a smooth surface. Samples were then ready for SEM-EDX analyses.

### 3.3.1.3 Preparation for Geochemical Analyses

Rock specimens and coal samples were prepared for mineralogical and major elemental oxides analyses.

**Preparation for Mineralogical Analysis using X-Ray Diffraction Spectrometry**

The X-Ray Diffraction (XRD) technique was used for mineralogical analysis on both rock specimens and coal samples. The presence of pyrite and other sulphide minerals, as well as calcite and dolomite, can be determined using XRD (Chauhan and Chauhan, 2014). This technique was selected because of its accuracy. According to Zhu (2014) the XRD is reported to produce results which are accurate with ±15% of the actual values.

A total of 8 samples (3 rock specimens and 5 coal samples) were prepared for x-ray diffraction spectroscopy at the Department of Earth Science, University of Venda. Samples were air dried prior any laboratory preparations. Thereafter, a mechanical jaw crusher (Fig. 3.9A) was used to crush a total of 8 samples into small particle size. To minimize cross contamination, quartz was used to clean the jaw crusher before working on the next sample. Thereafter, a riffle splitter (Fig. 3.9B) was used to homogenize samples as coal is known to be heterogeneous. Subsequently, samples were further pulverized using Retsch mechanical milling machine (Fig. 3.9C). Milling was undertaken to achieve a particle size of -75 µm or less for x-ray diffraction spectroscopy. Samples were sent to the University of Pretoria where they were prepared according to the standardized PANalytical backloading system, which provides a nearly random distribution of the particles.

**Preparation for geochemical analysis using X-Ray Fluorescence Spectroscopy**

Major elemental oxides in both rock specimens and coal samples were determined by using X-Ray Fluorescence (XRF) spectroscopy, which is used to determine the chemical composition of a rock sample by analysing several elements at once (Taggart *et al.*, 1987; Andrew, 2004).

Air dried samples were prepared for X-Ray fluorescence spectroscopy at the Department of Earth Science, University of Venda. Using a jaw crusher (Fig. 3.9A) a total of 18 samples (3 rock specimens and 15 coal samples) were crushed. To homogenize samples, a riffle splitter (Fig. 3.9B) was used. This was done to thoroughly mix samples as coal is heterogeneous. Thereafter, Retsch mechanical milling machine (Fig. 3.9C) was used to further pulverize samples to achieve a particle size of 75 µm or less. Samples were sent to the University of Pretoria where they were calcined prior analysis (Fig. 3.9D). Thereafter, pressed pellets were prepared using a hydraulic press (Fig. 3.9E) to undertake x-ray fluorescence spectroscopy.

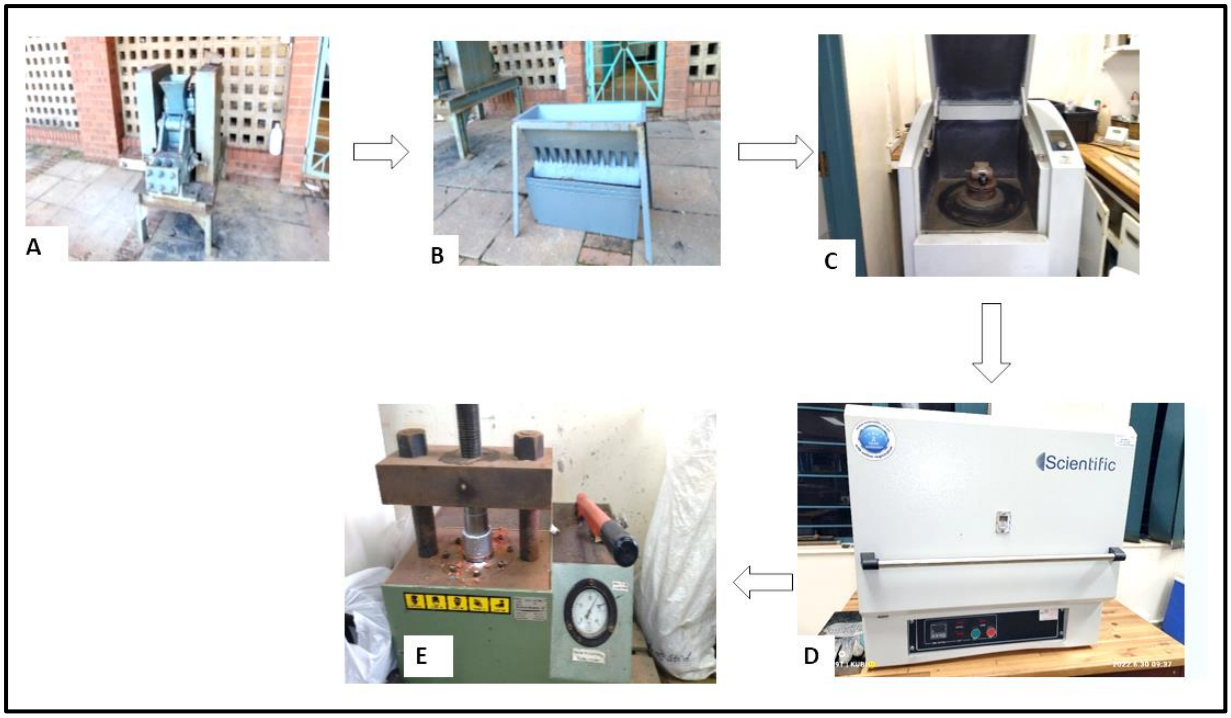


Figure 3.9: Sample preparation for x-ray diffraction and x-ray-fluorescence: (A) mechanical jaw crusher, (B) A riffle splitter for homogenization, (C) Retsch milling machine, (D) Furnace for sample calcination, (E) Hydraulic press for pellets preparation.

### 3.3.1.4 Preparation for Coal Quality Analyses

There are two broad chemical analyses for coal namely proximate and ultimate analysis (Zhu, 2014). The study further indicated that the proximate analysis focuses on the moisture content, the volatile matter, the ash and the fixed carbon of coal while the ultimate analysis include carbon, hydrogen, nitrogen, ash and oxygen content. To meet the objectives this study focused on proximate, total sulphur and calorific value analyses. A total of 15 coal samples were crushed and milled to pass the 75 µm sieve. Samples were then packaged and sent for analysis at Bureau Veritas laboratory in Johannesburg.

### 3.3.1.5 Preparation for Static Acid Base Accounting

The Acid base accounting according to EPA (1994) was first developed in 1974 to evaluate coal mine waste. It was later modified by Sobek *et al.* (1978). Fey (2003) indicated that this method is based on the sulphur content to estimate the acid generation potential.

Assumptions of this method as indicated by EPA (1994) include:

- All reported sulphur occurs as pyrite
- Pyrite is completely oxidized to sulphate and ferric hydroxide

- Hydrogen ions produced are neutralized by $CaCO_3$
- All reactions are instantaneous

A total of 18 samples were air dried for 24 hours prior preparation. Subsequently, samples were then crushed. Samples were sent to the Waterlab (PTY) Ltd at Pretoria for analysis. Total sulphur was determined for acid generating potential for all collected samples.

### 3.3.2 Sample Analysis

Host rock specimens and coal samples were subjected to several laboratory analyses including, petrographic studies, geochemical analyses, coal quality and static acid base accounting tests.

#### 3.3.2.1 Petrographic and Mineralogical Analysis

Microscopic and mineralogical characteristics of both host rock specimens and coal samples was undertaken. Transmitted light petrographic microscopy was undertaken for 3 host rock specimens while organic petrography was done 6 coal samples. Quantitative mineralogical studies were undertaken for 8 samples (3 rock specimens and 5 coal samples).

**Petrographic Analysis**

The microscopic study of rock specimens allowed for a better understanding of its mineral components (Craig and Vaughan, 1994). An Olympus Zeiss AxioCam transmitted light petrographic microscope (Fig. 3.10) was used for petrographic analysis at the Department of Earth Sciences, University of Venda. These specimens were studied at 200 µm scale. Photomicrographs for the three studied rock specimens were further interpreted and discussed (Figs. 4.1; 4.2; 4.3).

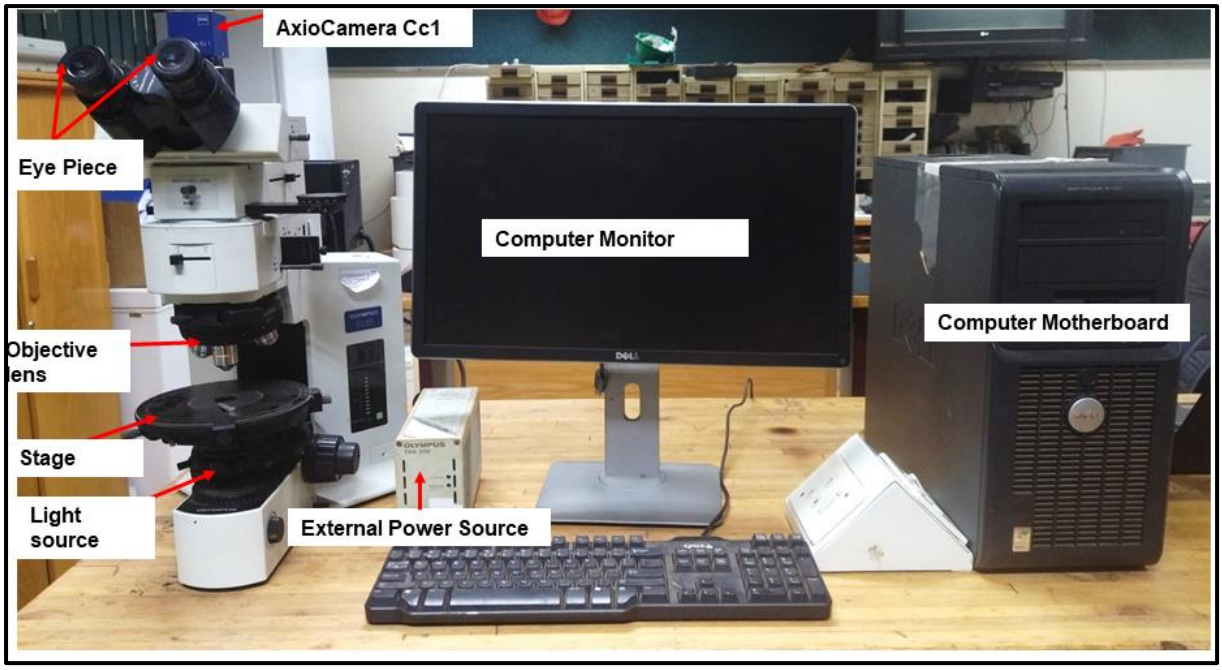


Figure 3.10: Olympus BX51 transmitted and reflected light petrographic microscope used for petrographic study of rock specimens.

**Organic Petrology Analysis**

Maceral analyses were performed on polished blocks under a reflected light microscope equipped with an oil immersion objective lens and an automatic point counting stage that traverses the sample at 0.4 mm intervals in accordance with ISO 7404-3. Under the cross hair, a minimum of 500 points are counted. To calculate the coal rank, an objective lens with a magnification of x50 is used, and the stage or light path is rotated 360 degrees. A minimum of 100 readings on vitrinite bands within the measurement area are taken. Vitrinite is used because it has a constant and linear loss of volatile matter as well as an increase in carbon content (Wagner *et al.*, 2018). High quality sample preparation is required to ensure good results.

Coal samples were analysed using Zeiss Axioimager M2m polarized reflected light microscope with a 50X oil immersion objective lens fitted with Fossil monochrome and colour cameras (Fig. 3.11). Organic petrology training was provided by a certified coal petrographer, Professor N. Wagner from the Geology Department, University of Johannesburg. This involved studying the macerals as well as the inorganic constituent of coal. Prior analysis, yttrium-aluminum-garnet 0.900 disk was used to calibrate the microscope with aid of immersion oil. A 500 point count was undertaken for macerals and mineral matter analysis while a 100 point count was undertaken for vitrinite reflectance. Samples were analysed following ISO 7404-3 and results were reported in volume percentage. Maceral point count

and vitrinite reflectance results were tabulated (Tables 4.1; 4.2). Photomicrographs for coal samples are interpreted and discussed (Figs. 4.5 - 4.10).

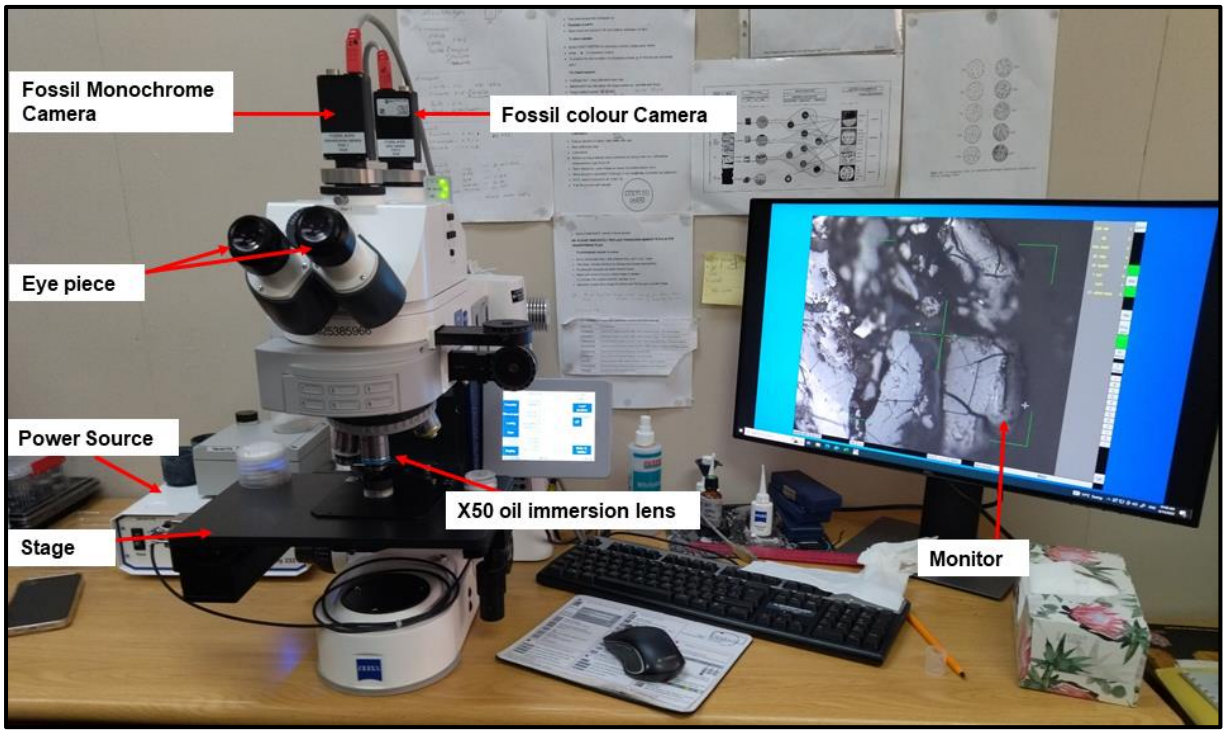


Figure 3.11: Zeiss Axioimager organic petrography microscope used for maceral point count and vitrinite reflectance studies.

**Mineralogical Analysis**

Coal samples were heated at 100 ºC prior analysis to remove excess organic matter that would mask the mineral phases. Subsequently, 25 mm pressed pellets were prepared for XRD. samples were then analysed in θ–θ configuration using a PANalytical X-Pert Pro powder diffractometer with an X-Celerator detector and variable divergence and fixed receiving slits with iron filtered Co-Kα radiation (λ=1.789Å). X-pert highscore plus software was used to identify mineral phases by selecting the best fitting pattern from the ICSD database to the measured diffraction pattern. The identified quantitative mineral phases are tabulated (Table 4.3).

### 3.3.2.2 Scanning Electron Microscopy Analysis

A total of 5 coal samples were selected for SEM-EDX analyses which was undertaken at the University of Cape Town. These samples were selected following the preliminary mineralogy and organic petrology results to investigate the morphology of pyrite in coal. Pyrite and its modes of occurrence were identified using scanning electron microscopy with energy

dispersive X-ray spectrometry (SEM-EDX) analyses. The observations were carried out on 5 polished pellets and included detection modes for secondary electrons and back scattered electrons, as well as EDX analysis for the determination of chemical compositions of high quality. A Tescan MIRA3 FEG scanning electron microscope (SEM) was used for the SEM-EDX analysis. Photomicrographs as well as EDX results were grouped together (Figs. 4.13 – 4.17).

#### 3.3.2.3 Whole Rock Geochemistry Analysis

Powdered host rock specimens and coal samples were sent to the University of Pretoria. Bruker s2 Ranger x-ray fluorescence (XRF) spectrometer was used to analyze the powdered and pelletized samples for major elemental oxides. Before analysis can be undertaken the XRF spectrometer was calibrated using a copper disk to ensure accurate results. After analysis, the data was retrieved to a computer system. All the data was then exported to Microsoft excel for further interpretation (Tables 4.5; 4.7).

#### 3.3.2.4 Coal Quality Analysis

Proximate analyses (Moisture, ash, volatile matter and fixed carbon content) were analysed for 15 coal samples. Complementary analyses such as total sulphur and calorific value were undertaken for 15 coal samples at Bureau Veritas laboratory in Johannesburg. Coal quality results are noted and tabulated in Table 4.11.

**Proximate analyses**

Moisture Content

Moisture analysis is conducted to determine the inherent moisture of coal. The moisture content was determined following the ISO 11722: 1999 method. Wet coal was first air dried to remove surface moisture.

The mass of the crucibles was measured on a weighing scale and calibrated. One gram of each sample was weighed into the crucible (M1) and then placed in the oven and heated at 105-110ºC. Samples were dried for two and half an hour. Crucibles were then removed from the oven and tightly covered with their lids to prevent introduction of moisture. Samples were cooled in a desiccator for 30 minutes then weighed (M2). Moisture content was calculated following Equation 12. Moisture is calculated on air dried (ad) basis.

$$Moisture\ ad = \frac{M1-M2}{M1}\ X\ 100 \qquad \text{Equation (12)}$$

Ash Content

According to Donahue and Rais (2009) and Thomas (2013) ash in coal is the residue (inorganic) material left behind after loss of moisture and volatile moisture. Thomas (2013) further indicated that the determined ash content is not equivalent to the mineral matter content of the coal, but it does, however represent the mineral matter in coal after losing the volatile component ($CO_2$, $SO_2$, $H_2O$). Zhu (2014) indicated that the ash usually consists of silica, alumina, iron oxide and small quantities of lime and magnesia.

The ash content was determined following the ISO 1171: 2010 method. The porcelain crucible was weighed and calibrated on a weighing machine. A weighed sample (1 g) was placed in the crucible (M1) and weighed. The sample was heated gradually at a rate that temperature would reach 450-500ºC by the end of the first hour. By the end of the second hour the temperature must have reached 700-750ºC. The sample was allowed to cool and weighed again (M2). The ash content was calculated on the basis of air dried basis (ad) according to ISO 1171: 2010 Equations 13 and 14.

$$Ash\ ad = \frac{\mathrm{M1-M2}}{\mathrm{M1}}\ X\ 100 \qquad \text{Equation (13)}$$

To avoid the effect of moisture, air dried values was converted into dry basis following Equation 14.

$$Ash\ db = \frac{\text{Ash ad}}{\text{100−moisture ad}}\ X\ 100 \qquad \text{Equation (14)}$$

Volatile Matter

Volatile matter was determined following the ISO 562:2010 standard. A total of 15 samples were placed in a crucible and measured on a balance scale. A measured sample (1 g) was placed in the crucible prior to heating (M1). Samples were then heated at 950±20ºC for 7 minutes. Following that, samples were then removed and allowed to cool for 15 to 30 minutes then weighed again (M2). The volatile matter was calculated following Equations (15, 16 and 17).

$$Volatile\ matter\ ad = \frac{\mathrm{M1-M2}}{\mathrm{M1}}\ X\ 100 \qquad \text{Equation (15)}$$

The air-dried (ad) value was converted to dry basis as follows:

$$Volatile\ matter\ db = \frac{\text{Volatile matter ad}}{\text{100−moisture ad}}\ X\ 100 \qquad \text{Equation (16)}$$

Thereafter, the dry ash free (daf) value was obtained by:

$$Volatile\ matter\ daf = \frac{100}{100-\text{ash db}}\ X\ volatile\ matter\ db$$ Equation (17)

Fixed Carbon Content

The fixed carbon content was determined indirectly by finding the difference between the sum of moisture content, ash content and volatile matter and 100 %. Calculating the fixed carbon through difference yields values in air dried basis. However, it is necessary to convert air dried values to dry and dry ash free basis so as to obtain representative values of the amount of carbon in coal (SANS 10320:2004) Equations 18 and 19.

$$\%\ \text{FC}\ db = \frac{FC\ (ad)}{100-\text{moisture ad}}\ X\ 100$$ Equation (18)

$$\%\ FC\ daf = \frac{100}{100-\text{Ash (db)}}\ X\ \%\ FC$$ Equation (19)

**Calorific value**

The calorific value of coal refers to the amount of heat given off when coal is combusted (Falcon and Snyman, 1986; Suárez-Ruiz and Ward, 2008). Samples were sent to Bureau Veritas testing and inspecting laboratory in Johannesburg for calorific value analysis. The gross calorific value was determined using the Parr 6200 calorimeter and the complimentary Parr 6510 water handling system in accordance with ISO 1928: 2004.

**Total Sulphur**

The gravimetric Eschka method in accordance with ISO 334:1992 was used in preparation for total sulphur. Coal samples were sent to Bureau Veritas in Johannesburg for total sulphur determination. The sulphur content was analysed using Leco SC632 equipment following ISO 334: 1992.

**Forms of Sulphur**

Thiessen (1945) conducted a study on the forms of sulphur in coal. He noted that sulphur does not occur elementally in coal, it does however occur in different forms namely; organic, pyritic and, sulphate sulphur. Coals contain varying concentrations of sulphur ranging from 0.5 to 5% (Chou, 2012).

Using preliminary mineralogical data, 5 coal samples were chosen and analysed for sulphur forms. In accordance with ISO 157: 1996, sulphur forms were determined using ICP-OES Perkin Elmer Optima 5300 and Perkin Elmer Lamda 265 Gebruik. Sulphate sulphur was determined from a second split by HCL extraction. Organic sulphur (non-extractable) is the total sulphur content of the $HNO_3$ split. Organic sulphur was determined from a third split by

$HNO_3$ extraction. However, acid soluble sulphide sulphur (pyrite) was determined by finding the difference between the total sulphur contents of the HCL treated and $HNO_3$ treated splits (Lepakko, 1993; EPA, 1994).

#### 3.3.2.5 Acid Mine Water Generation

To achieve this objective, the paste pH and electric conductivity of host rock specimens and coal samples were determined. Thereafter, acid base accounting tests were conducted.

**Paste pH and Electrical Conductivity**

To determine the paste pH and EC, 25 g of pulverized host rock specimens and coal samples was weighed using Radway PS 6000/C/2 balance scale. Thereafter, samples were transferred into a 250 ml beaker which was then filled with de-ionized water. The mixture was vigorously stirred. This was done following Wu (2021). Thereafter, pH and EC were measured directly from the slurry for 4 days. This was done to access the effect of time on the acidity of samples.

**Acid Production Potential**

The acid generation potential was determined following the Sobek acid base accounting test (Sobek *et al.*, 1978). Using the Leco SC 632, total sulphur was determined from a split (sample mass of 0.5 to 2 g). The AP (Acid generation potential) was calculated by multiplying the sulphur content in percentage by the conversion factor of 31.25 as indicated by Sobek *et al*. (1978).

**Neutralization Potential**

The neutralization potential was determined following the modified Sobek method. A mass of 0.5 g pulverized 75 µm was placed in a piece of aluminum foil. Thereafter, on a ratio of 1:3 HCl was added to the sample and fizzing was observed. Fizz readings as provided by Sobek *et al.* (1978) (Table 3.3) were used to quantify the required acid.

Table 3.3: Fizz ratings and acid addition parameters (Sobek *et al.*, 1978)

| Fizz Ratings | HCL (ml) | HCL (Normality) |
|---|---|---|
| 0 none | 20 | 0.1 |
| 1 slight | 40 | 0.1 |
| 2 moderate | 40 | 0.5 |
| 3 strong | 80 | 0.5 |

After conducting the fizz test, fizz rating indicated slight to none. Thereafter, 2g of 75 µm sample was weighed into a 250 ml erlenmeyer flask. Using the results from the fizz test, 0.1 N of HCl was added into the samples. Samples were heated to nearly boiling while swirling the flask every 5 minutes until the reaction was complete. Distilled water was then added to make a total of 125 ml, thereafter, gently boiled for one minute and cooled at room temperature. Boiling chips were placed inside the beaker and covered with a watch glass. Boiling was carried out for gently for 5 minutes, then solution was allowed to cool. The solution was filtered using No. 40 Whatman filter paper. Subsequently, 5 ml of 30% hydrogen peroxide ($H_2O_2$) was added into the filtrates which were then boiled gently for an additional 5 minutes. Back titration was carried out using 0.1 N NaOH to pH of 7 standard units. The neutralizing potential was calculated using HCl normality, NaOH normality and weight of samples using Equation (20).

$$NP = \frac{(Acid\ Normality\ x\ V) - (Base\ Normality\ x\ V) x\ 50}{Mass\ of\ sample} \qquad \text{Equation (20)}$$

If less than 3 ml of NaOH is required to achieve a pH of 7, then it is possible that HCl added was not enough to neutralize all the base present was not enough to neutralize all the base present in the 2 g sample.

The Net neutralizing potential was determined by finding the difference between the acid generating and neutralizing potential as shown in equation 21 (Sobek *et al.*, 1978; Usher *et al*., 2003).

$$NNP = NP - AP \qquad \text{Equation (21)}$$

**Screening Criteria**

The criteria to be used following Price *et al.* (1997) and Usher *et al.* (2003) are:

- Paste pH and EC
- Net neutralizing potential (NNP)
- Neutralizing potential ratio (NPR)
- % S (Total sulphur) vs NPR

Net Neutralizing Potential

Sobek *et al*. (1978), Price (1997), Fey (2003) and Usher *et al*. (2003) indicated that if the NNP is greater than 20 kg/ton $CaCO_3$ then it is considered to be safe and non-acidic producing, alternatively if the NNP is less than - 20 kg/ton $CaCO_3$ then the material is capable of generating acid. EPA (1994) and Fey (2003) further indicated that if the NNP is between -20

and +20 kg/ton $CaCO_3$ then this represents a range of uncertainty and necessitate further testing using kinetic tests.

Neutralizing Potential Ratio

The ratio of NP to AP can also be used (Ferguson and Morin, 1991). If ratios are used and the ratio of NP to AP is greater than 4:1 then there is a lower chance that acid will be generated (Price, 1997) (Table 3.4). Alternatively, ratios with 1:1 or less are more likely to generate acid (EPA, 1994).

Table 3.4: Guideline for screening of acid generation potential based on Price (1997) and Usher *et al.* (2003)

| Potential for ARD | Initial NPR Screening Criteria | Comments |
|---|---|---|
| **Likely** | **< 1:1** | Likely AMD generating |
| **Possibly** | **1:1 – 2:1** | Possibly AMD generating if NP is insufficiently reactive or is depleted at a faster rate than sulphides |
| **Low** | **2:1 – 4:1** | Not potentially AMD generating unless significant preferential exposure of sulphides along fracture planes, or extremely reactive sulphides in combination with insufficiently reactive NP |
| **None** | **>4:1** | No further AMD testing required unless materials are to be used as a source of alkalinity |

Sulphur Vs NPR

For sustainable long-term acid generation, at least 0.3% sulphide-S is needed. Values below this can yield acidity, but it is likely to be only of short-term significance. From these facts, and using the NPR values, several rules can be derived (Price, 1997) and Usher *et al.* (2003):

- Sample with less than 0.3% sulphide-S are regarded as having insufficient oxidisable sulphide-S to sustain acid generation,
- NPR ratios of >4:1 are considered to have enough neutralising capacity.
- NPR ratios of 3:1 to 1:1 are consider inconclusive.
- NPR ratios below 1:1 with sulphide-S above 3% are potentially acid-generating (Soregaroli and Lawrence, 1998; Usher *et al.*, 2003).

### 3.4 Quality Control and Quality Assurance

All glassware were washed with soap and then soaked in dilute nitric acid (10%) and thoroughly rinsed before use with deionized water. The XRF and XRD had to pass the required tuning test before calibration with freshly prepared standards done. The correlation coefficients for most of the elements should be close to 1 for the data collected to be reproducible and reliable. All measurements were done in duplicates and an average value was taken.

# CHAPTER 4: RESULTS INTERPRETATION

This chapter presents the results interpretations for petrology, element geochemistry, and acid mine prediction.

## 4.1 Petrographic and Mineralogical Characterisation of Host Rocks and Coal

Host rock specimens and coal samples were characterised petrographically, quantitative mineralogical data was used to support petrography results.

### 4.1.1 Description of Host Rocks

The selected three host rock specimens and six coal samples from the Sekoko coal mine in the Waterberg Coalfield are described in detail in the petrographic results. To fully comprehend the samples, they were first visually examined by describing the physical properties of observable minerals. The optical properties of minerals in each sample were studied using a petrographic microscope on a scale of 200 µm. Mineralogical results confirmed the results of the petrology.

**Shale (Shale F-R)**

Shale F-R through field description was characterized by fine clay sized particles with a grey colour (Fig. 4.1A). The rock specimen is a clastic, argillaceous sedimentary rock. It is competent and characterized by laminations (thin parallel beds of less than 1 cm each) and breaks easily along the parallel layers (fissile). This specimen was collected from the roof material of seam 10 on the west portion. It was interbedded with a white to grey sandstone. Shale F-R is dominated by clay minerals as seen in Figure 4.1 (B,C). Quartz is the second dominant mineral occurring within fractures (Fig. 4.1C). The rock is dominated by fine grains of kaolinite (Fig. 4.1B,C). Based on the physical and petrographic description the specimen was identified as shale.

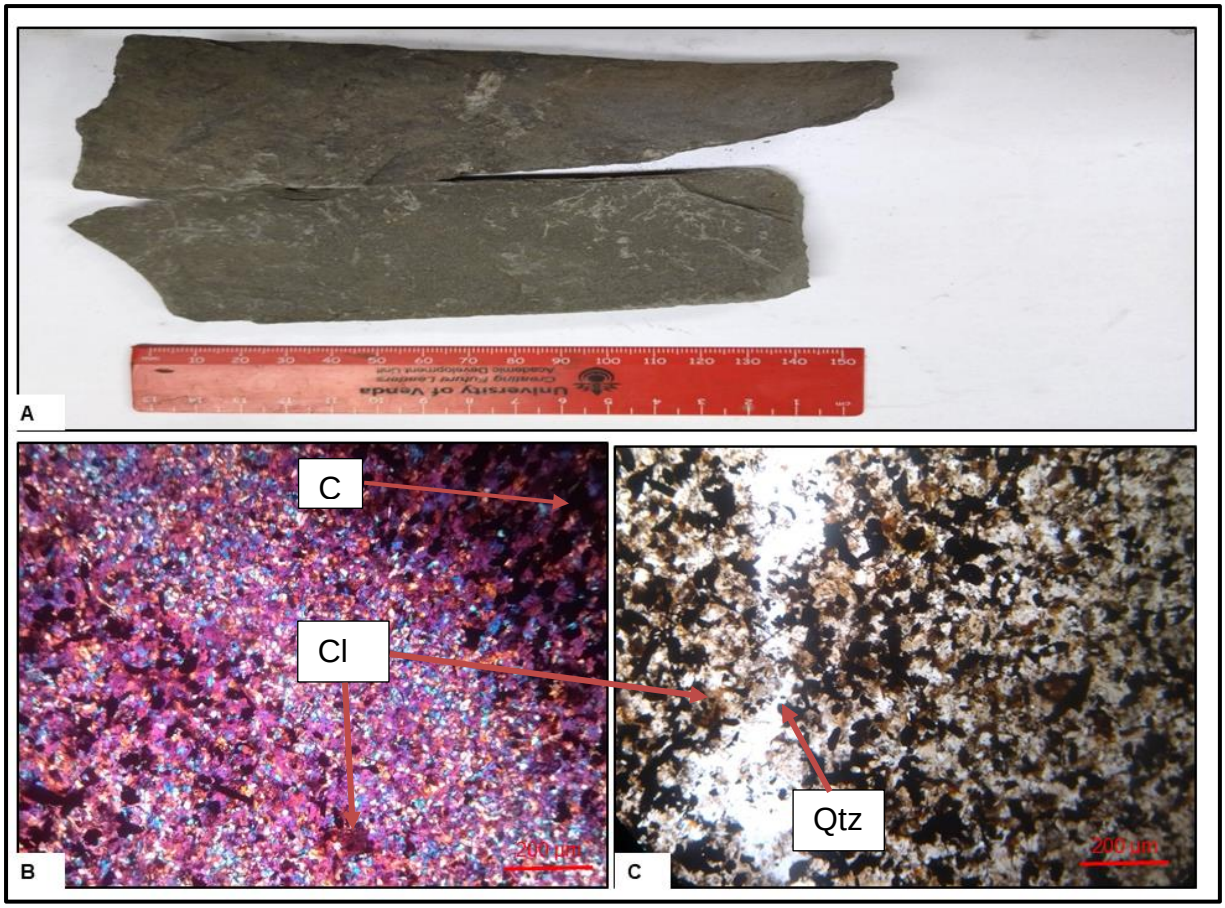


Figure 4.1: A diagram showing a shale specimen (Shale F-R): (A) hand specimen of shale collected from the roof of seam 10; (B) Photomicrograph of shale under plane polarised light; (C) Photomicrograph of shale under cross polarised light.: F-R= Far right, Qtz = Quartz, Cl= Clay, C= organic matter.

**Gritstone (Ply A F-R)**

The rock is an arenaceous sedimentary rock, characterized by course texture (Fig. 4.2A). The rock had a whitish to greyish colour, with yellowish colour on the surface due to sulphur stains. It revealed well packed grains that were matrix supported. It was found to be dominated by residual quartz minerals. Specimen was collected from the west portion of the box cut interbedded with the shale. Quartz was the dominant mineral (Fig. 4.2B,C), Kaolinite clay occurred as cementing material (Fig.4.2B). Grains of K-feldspar feldspar were seen (Fig. 4.2C) but not as dominant as quartz and clay. Minor content of muscovite grains were identified and were surrounded by quartz grains (Fig. 4.2C). Based on the physical and petrographic description the specimen was identified as a gritstone.

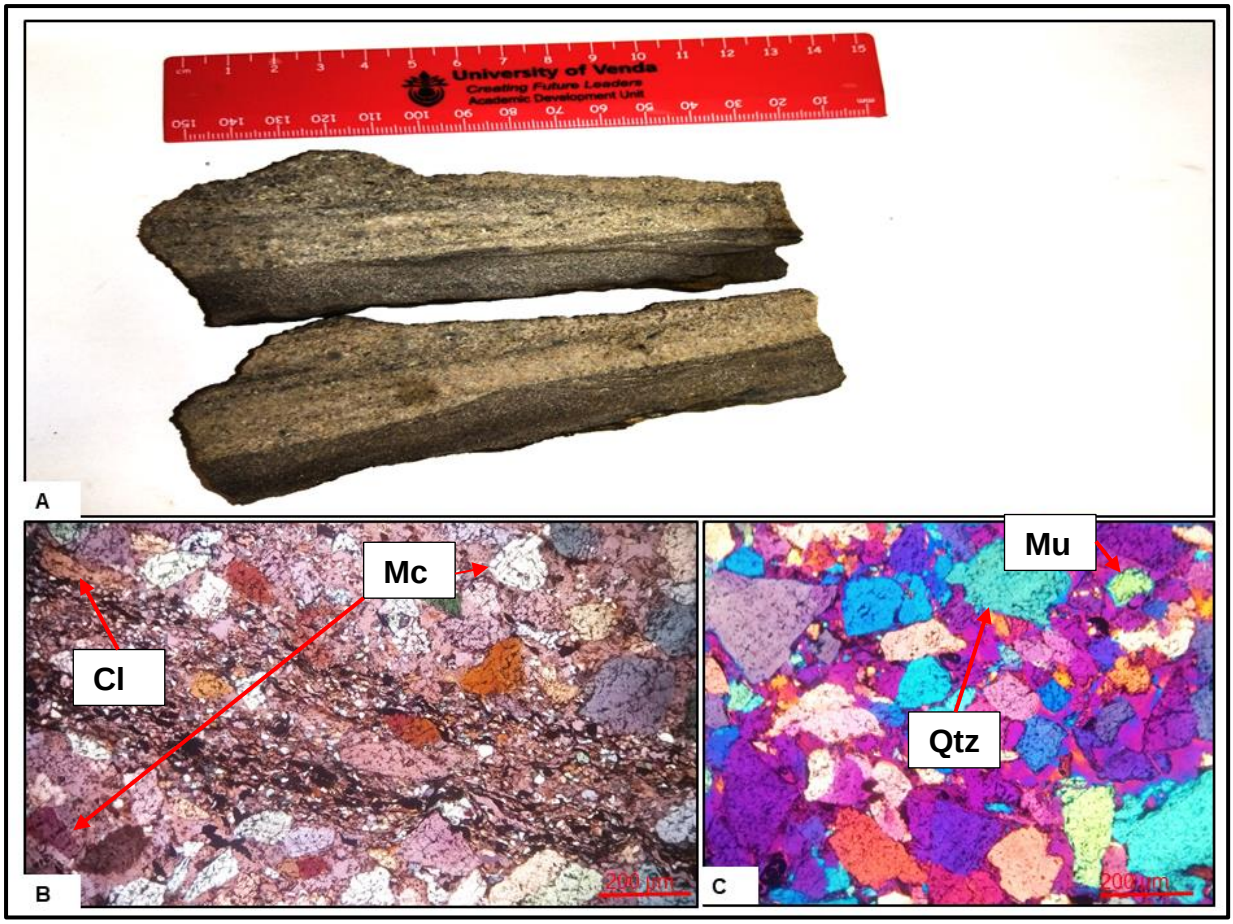


Figure 4.2: Hand specimen of gritstone (Ply A F-R) (A) collected from the roof of seam 10 on the west portion of the box cut: (B) Photomicrograph of gritstone under crossed polarised light, (C) Photomicrograph of gritstone under plane polarised light; F-R= Far right; Mc= K-feldspar; Qtz= Quartz; Cl= Clay; Mu=Muscovite.

**Sandstone (Ply A S-L)**

The specimen was collected from the box-cut. The grains displayed medium to fine texture (Fig. 4.3A). The specimen was dominated by a white colour due to the abundance of quartz grains. Grain sizes ranged from 100 to 200 µm and were well packed. A lump of fine-grained kaolinite was found to be enclosed by quartz grains (Fig. 4.3B,C) implying that kaolinite occurred as secondary minerals due to weathering during diagenesis process. Minor content of muscovite were present with medium relief and planar cleavage (Fig. 4.3C).

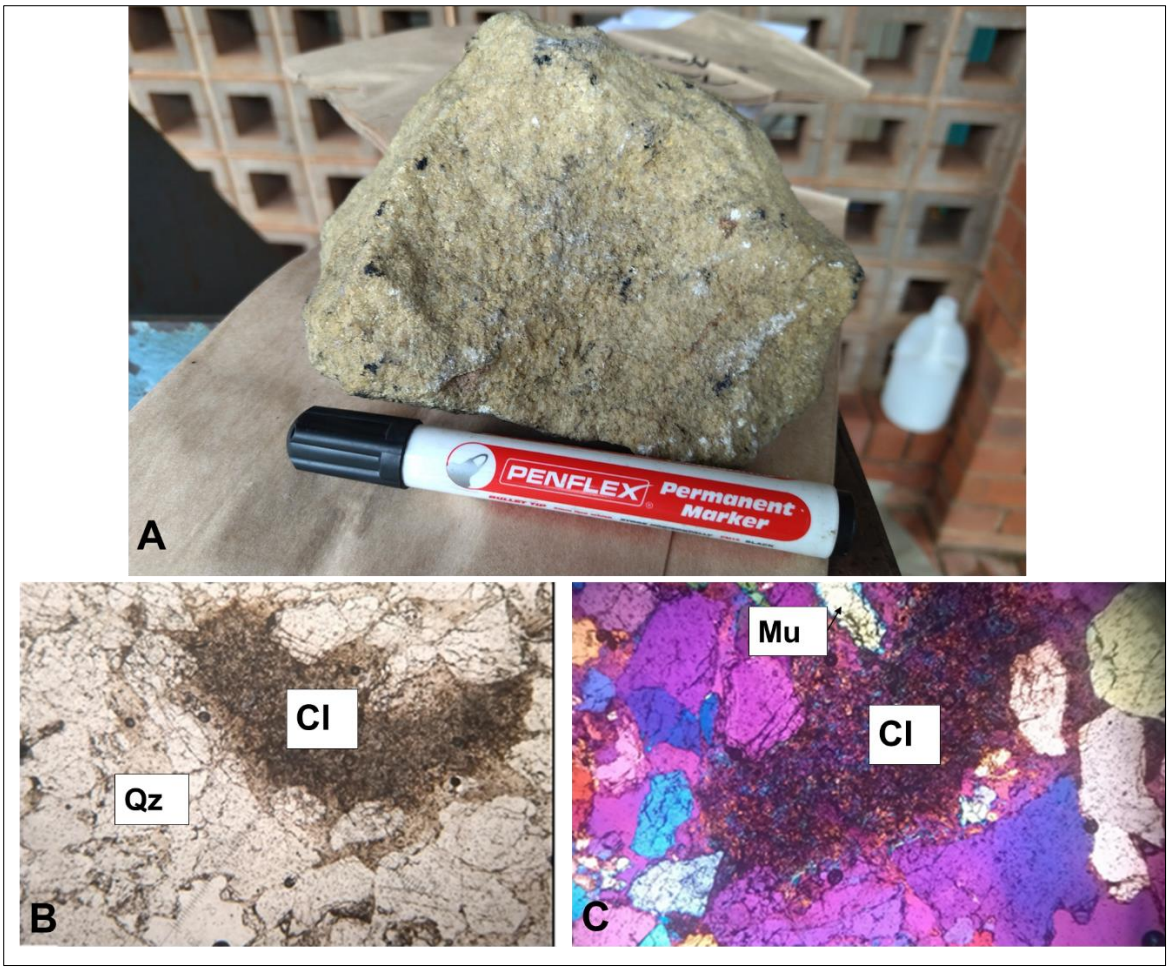


Figure 4.3: Hand specimen of sandstone (Ply A S-L) (A) collected from the roof of seam 10 on the south portion of the box cut: (A) Photomicrograph of sandstone under cross polarised light, (C) Photomicrograph of sandstone under plane polarised light and Photomicrographs (B and C) of the specimen under a petrographic microscope. Mc= K-feldspar, Qz= Quartz and Cl= Clay.

### 4.1.2 Description of Coal Samples

The Waterberg coalfield is characterized by coal consisting of alternating bands of bright and dull coal (Fig. 4.4A,B). On the west portion of seam 10, layers of both bright and dull coal were found to be thin as compared to those on the southern portion. The coal specimen was mostly bright with prominent stains of sulphur and calcite stains on the face of the box cut. Physically, the coal is characterized by high density and it breaks evenly.

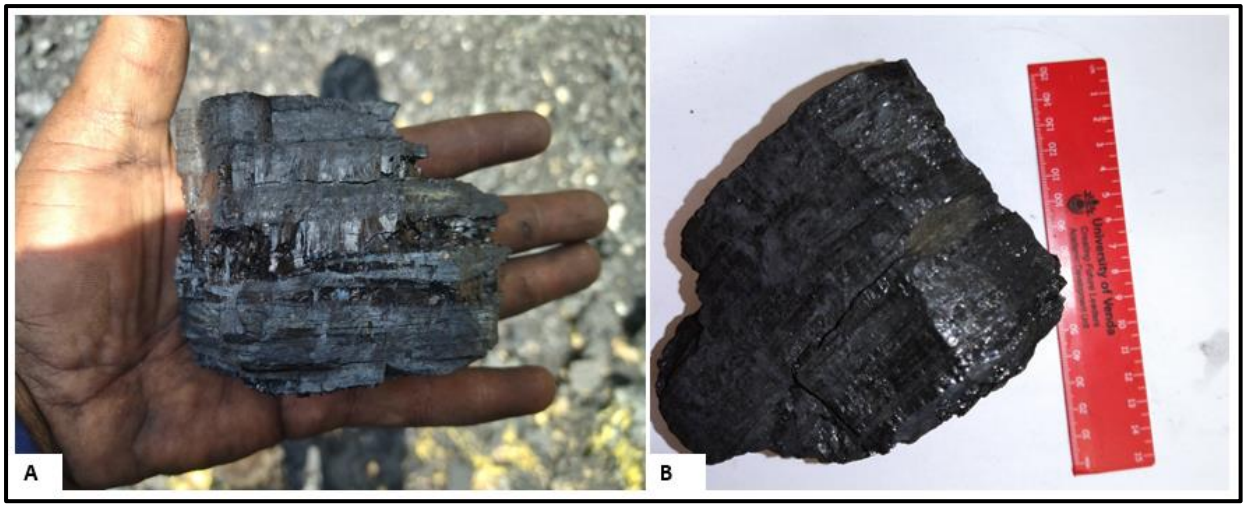


Figure 4.4: Hand specimen showing alternating bands of bright and dull coal: (A) alternating bands of dull and bright coal, (B) thin bands of bright and dull coal.

### 4.1.3 Mineralogical Characterisation of Host Rocks and Coal

X-ray diffraction patterns of selected 8 samples were established (Table 4.1). The quantitative results for the XRD analyses are as follows:

- Quartz and kaolinite are the dominant mineral phases in clastic sedimentary rocks (A S-L, A F-R, shale F-R) with mean concentrations of 58.23 and 35.40 Wt% respectively. Coal samples, however, are dominated by kaolinite (Fig. 4.5) with a mean concentration of 17.44 Wt% (Table 4.1).
- The concentration of kaolinite decreases with depth on the south portion of seam 10 (from ply E to H S-L) and it is more dominant in seam 11 than 10 (Table 4.1).
- K-feldspar, muscovite and Anatase are present in clastic sedimentary rocks overlying seam 10 (Fig. 4.5). K-feldspar is only present in ply A S-L at 10.50 Wt % (Table 4.1).
- Pyrite is present in all coal samples with a minimum concentration of 1.10 Wt % (seam 11 composite) and a maximum concentration of 9.40 Wt% (H S-L). Seam 10 contains more pyrite (1.30 Wt %) as compared to seam 11 (1.10 Wt %). The mean concentration of pyrite in all coal samples is 4 Wt%.
- Magnetite is present in ply E S-L at 1.00 Wt % (Fig. 4.5).

Table 4.1: Quantitative mineralogy of host rocks (Clastic rocks: interburden) and coal (South left portion to composites)

| | | Clastic rocks: Interburden | | | Mean (Host Rocks) | South left portion | | West far right | Composites | | Mean (Coal) |
|---|---|---|---|---|---|---|---|---|---|---|---|
| **Mineral** | **Formula** | **A_S-L** | **A_F-R** | **Shale F-R** | | **E_S-L** | **H_S-L** | **C_F-R** | **Seam 10** | **Seam 11** | |
| **Quartz** | $SiO_2$ | 75,10 | 63,60 | 36,00 | 58,23 | 2,6 | 3,8 | 4,4 | 9,4 | 7,8 | 5,6 |
| **Kaolinite** | $Al_2Si_2O_5(OH)_4$ | 23,50 | 22,20 | 60,50 | 35,40 | 13 | 11,8 | 15,3 | 21,9 | 25,2 | 17,44 |
| **Pyrite** | $FeS_2$ | 0,00 | 0,00 | 0,00 | 0,00 | 6,9 | 9,4 | 1,3 | 1,3 | 1,1 | 4 |
| **Muscovite** | $KAl_2(AlSi_3O_{10}(FOH)_2)$ | 0,90 | 3,40 | 3,00 | 2,43 | 0 | 0 | 0 | 0 | 0 | 0 |
| **K-feldspar** | $KAlSi_3O_8$ | 0,00 | 10,50 | 0,00 | 3,50 | 0 | 0 | 0 | 0 | 0 | 0 |
| **Anatase** | $TiO_2$ | 0,50 | 0,30 | 0,50 | 0,43 | 0 | 0 | 0 | 0 | 0 | 0 |
| **Magnetite** | $Fe_3O_4$ | 0,00 | 0,00 | 0,00 | 0,00 | 1 | 0 | 0 | 0 | 0 | 0,2 |
| **Amorphous** | Organic matter | 0,00 | 0,00 | 0,00 | 0,00 | 76,5 | 75,1 | 78,9 | 67,3 | 66 | 72,76 |

### 4.1.3.1 Clastic Sedimentary Rocks

Ply A S-L

This is a clastic sedimentary rock (sandstone) overlying coal seam 10 on the south portion. It is dominated by quartz with a concentration of 75.10 Wt% (Table 4.1, Fig. 4.5). The second dominant mineral phase is kaolinite (clay) which occurs at a concentration of 23.50 Wt%. Muscovite (0.90 Wt%) and Anatase (0.50 Wt%) are in minor quantities (Table 4.1; Fig. 4.5).

Ply A F-R

This is also a clastic sedimentary rock dominated by quartz with concentration of 63.60 Wt%. Kaolinite (22.20 Wt %) is the second dominant mineral phase then followed by K-feldspar with a concentration of 10.50 Wt %. The concentration of quartz and kaolinite mineral phases are lower in gritstone as compared to those in the sandstone, however, Ply A F-R contains more K-feldspar (10.50 Wt %) and muscovite (3.40 Wt %) compared to that of the sandstone (A S-L) (Table 4.1; Fig. 4.5). Physically, this specimen is coarser as compared to the sandstone, it is characteristically grey in colour with whitish cementing agent. Clay (kaolinite) inherited from chemical alteration of the source rock is the cementing agent.

Shale F-R

This rock is dominated by kaolinite with a concentration of 60.50 Wt% without organic matter (Fig. 4.5). The concentration of quartz (36%) is the second dominant mineral phase. Muscovite and Anatase are present in minor quantities of 3 Wt% and 0.50 Wt% respectively (Fig. 4.5).

#### 4.1.3.2 Coal Samples

Ply E S-L

Kaolinite is the dominant mineral phase with a concentration of 13 Wt% followed by pyrite at 6.90 Wt%. Quartz and magnetite mineral phases are also present at 2.60 and 1.00 Wt% respectively (Table 4.1; Fig. 4.5).

Ply H S-L

Kaolinite (11.80 Wt %) is the main mineral component, but it is less compared to that of Ply E S-L overlying it (Fig. 4.5). The concentration of pyrite is increasing with depth in the south portion of seam 10, from 6.90 to 9.40 Wt % in Ply E and H S-L respectively. The concentration of quartz increases with depth in the south portion of seam 10, from 2.60 to 3.80 Wt% in Ply E and H S-L respectively.

Ply C F-R

The coal sample from the west portion of seam 10 contains kaolinite as the dominant mineral phase with a concentration of 15.30 Wt %. Quartz (4.40 Wt%) is the second dominant mineral phase and it is more abundant than the specimen collected from the south portion. Pyrite is present in coal at 1.30 Wt % which is less when compared to those in the south (Fig. 4.5).

Seam 11 Composite

Mineralogically, the composite sample of seam 11 is dominated by kaolinite (25.20 Wt %) as an inorganic constituent. The second dominant mineral phase is quartz which occurs at 7.80 Wt. %. Pyrite mineral phase is present in coal at 1.10 Wt% (Fig. 4.5).

Seam 10 Composite

Composite sample of seam 10 is chiefly composed of kaolinite mineral with a concentration of 21.90 Wt%. Quartz is the second dominant mineral with concentration of 9.40 Wt%. Pyrite in seam 10 (1.30 Wt%) composite is occurring in higher concentration as compared to seam 11. This shows that the concentration of pyrite is increasing with depth (Table 4.1).

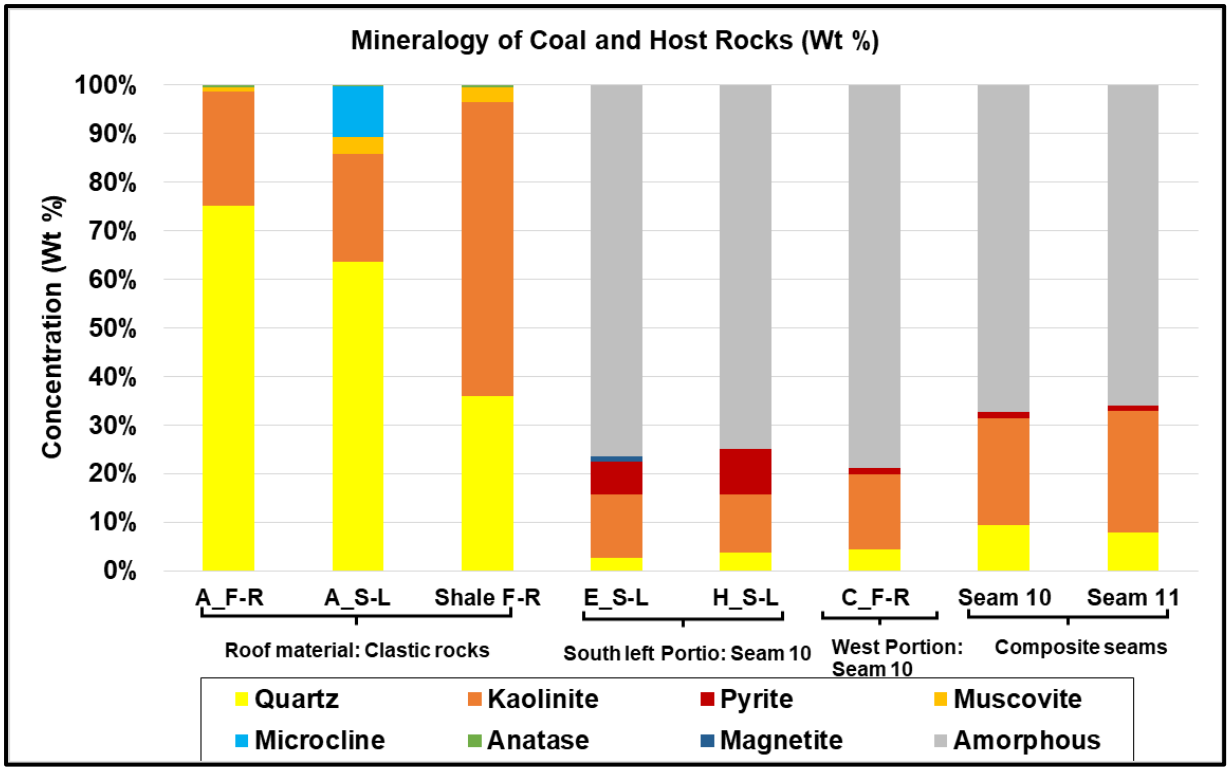


Figure 4.5: Quantitative mineralogy of selected host rock specimens and coal samples.

## 4.2 Major Oxides of Host Rocks and Coal

This involved the use of x-ray fluorescence to determine the major oxides in host rock specimens and coal samples.

### 4.2.1 Host Rocks

Results of major oxides in clastic sedimentary rocks indicate an average mean value in weight % of $SiO_2$ (77.43); $Al_2O_3$ (13.22); $K_2O$ (0.54), $TiO_2$ (0.49); $Fe_2O_3$ (0.45); $ZrO_2$ (0.19); $P_2O_5$ (0.15); $Cr_2O_3$ (0.10); MgO (0.05); SrO (0.05) and CaO (0.04) in their order of abundance (Table 4.3). Other oxides like, $V_2O_5$; MnO, NiO, and $Y_2O_3$ all had an average concentration of 0.01 Wt% (Table 4.2). Concentrations of sulphur (S) were occurring at extremely low concentration with a maximum concentration of 0.2 wt % in Ply A F-R (Table 4.2). The concentration of $SiO_2$ in clastic sedimentary rocks is the dominant major oxide ranging between 61.63 (Shale F-R) and 85.61 Wt % (PLY A S-L) to (Table. 4.2; Fig. 4.6).

The concentration of $TiO_2$ in clastic sedimentary rocks ranged between 0.15 to 0.95 Wt% (Fig. 4.6). The concentration of $Fe_2O_3$ ranged between 0.44 to 0.47 Wt% (Table. 4.3). The concentration of $Fe_2O_3$ is higher in shale F-R than the other clastic rocks. The concentrations of the other oxides like $K_2O$, MgO, CaO and MnO are relatively low ranging between 0.17 to 1.36; 0.00 to 0.25; 0.00 to 0.08 and 0.00 to 0.01 Wt% (Table 4.3; Fig. 4.6).

Table 4.2: Concentrations of major oxides in clastic sedimentary rocks (ND= Not determined as major oxides but as elements)

| Major Oxides | A-F-R | Ply A-S-L | Shale F-R | UCC |
|---|---|---|---|---|
| $SiO_2$ | 85.05 | 85.61 | 61.63 | 61.5 |
| $Al_2O_3$ | 7.89 | 8.3 | 23.48 | 15.1 |
| MgO | 0.02 | 0.02 | 0.11 | 3.7 |
| $Na_2O$ | <0,01 | <0,01 | <0,01 | 3.2 |
| $P_2O_5$ | 0.29 | 0.06 | 0.1 | 0.18 |
| $Fe_2O_3$ | 0.44 | 0.46 | 0.47 | 6.28 |
| $K_2O$ | 0.1 | 1.12 | 0.4 | 2.4 |
| CaO | 0.04 | 0.03 | 0.05 | 5.5 |
| $TiO_2$ | 0.38 | 0.15 | 0.95 | 0.68 |
| $V_2O_5$ | 0.01 | <0,01 | 0.03 | ND |
| $Cr_2O_3$ | 0.18 | 0.07 | 0.04 | ND |
| MnO | 0.02 | 0.01 | <0,01 | 0.1 |
| NiO | 0.03 | 0.01 | <0,01 | ND |
| CuO | <0,01 | <0,01 | <0,01 | ND |
| $ZrO_2$ | 0.2 | 0.09 | 0.27 | ND |
| S | 0.02 | 0.01 | <0,01 | ND |
| ZnO | 0.01 | <0,01 | 0.02 | ND |
| SrO | 0.08 | 0.02 | 0.04 | ND |
| $Y_2O_3$ | 0.01 | <0,01 | 0.02 | ND |
| LOI | 5.22 | 4.04 | 12.38 | |
| TOTAL | 99.99 | 99.99 | 99.97 | |

Table 4.3: Descriptive statistics of major oxides (Wt %) in overburden

| Major Oxides (Wt %) | Mean | SD | Standard Error | Minimum | Maximum | Sum | Coefficient of variation (SD/mean) |
|---|---|---|---|---|---|---|---|
| $SiO_2$ | 77,43 | 13,69 | 7,90 | 61,63 | 85,61 | 232,29 | 0,18 |
| $Al_2O_3$ | 13,22 | 8,88 | 5,13 | 7,89 | 23,48 | 39,67 | 0,67 |
| MgO | 0,05 | 0,05 | 0,03 | 0,02 | 0,11 | 0,15 | 0,95 |
| $P_2O_5$ | 0,15 | 0,12 | 0,07 | 0,06 | 0,29 | 0,45 | 0,82 |
| $Fe_2O_3$ | 0,45 | 0,02 | 0,01 | 0,44 | 0,47 | 1,36 | 0,04 |
| $K_2O$ | 0,54 | 0,53 | 0,30 | 0,10 | 1,12 | 1,62 | 0,97 |
| CaO | 0,04 | 0,01 | 0,00 | 0,03 | 0,05 | 0,12 | 0,19 |
| $TiO_2$ | 0,49 | 0,41 | 0,24 | 0,15 | 0,95 | 1,48 | 0,83 |
| $V_2O_5$ | 0,01 | 0,01 | 0,01 | 0,00 | 0,03 | 0,04 | 1,08 |
| $Cr_2O_3$ | 0,10 | 0,08 | 0,04 | 0,04 | 0,18 | 0,29 | 0,79 |
| MnO | 0,01 | 0,01 | 0,00 | 0,00 | 0,02 | 0,02 | 1,06 |
| NiO | 0,01 | 0,01 | 0,01 | 0,00 | 0,03 | 0,04 | 1,08 |
| $ZrO_2$ | 0,19 | 0,09 | 0,05 | 0,09 | 0,27 | 0,56 | 0,49 |
| S | 0,01 | 0,01 | 0,01 | 0,00 | 0,02 | 0,03 | 1,27 |
| ZnO | 0,01 | 0,01 | 0,01 | 0,00 | 0,02 | 0,02 | 1,13 |
| SrO | 0,05 | 0,03 | 0,02 | 0,02 | 0,08 | 0,14 | 0,70 |
| $Y_2O_3$ | 0,01 | 0,01 | 0,01 | 0,00 | 0,02 | 0,03 | 0,88 |
| LOI | 7,21 | 4,51 | 2,61 | 4,04 | 12,38 | 21,64 | 0,63 |

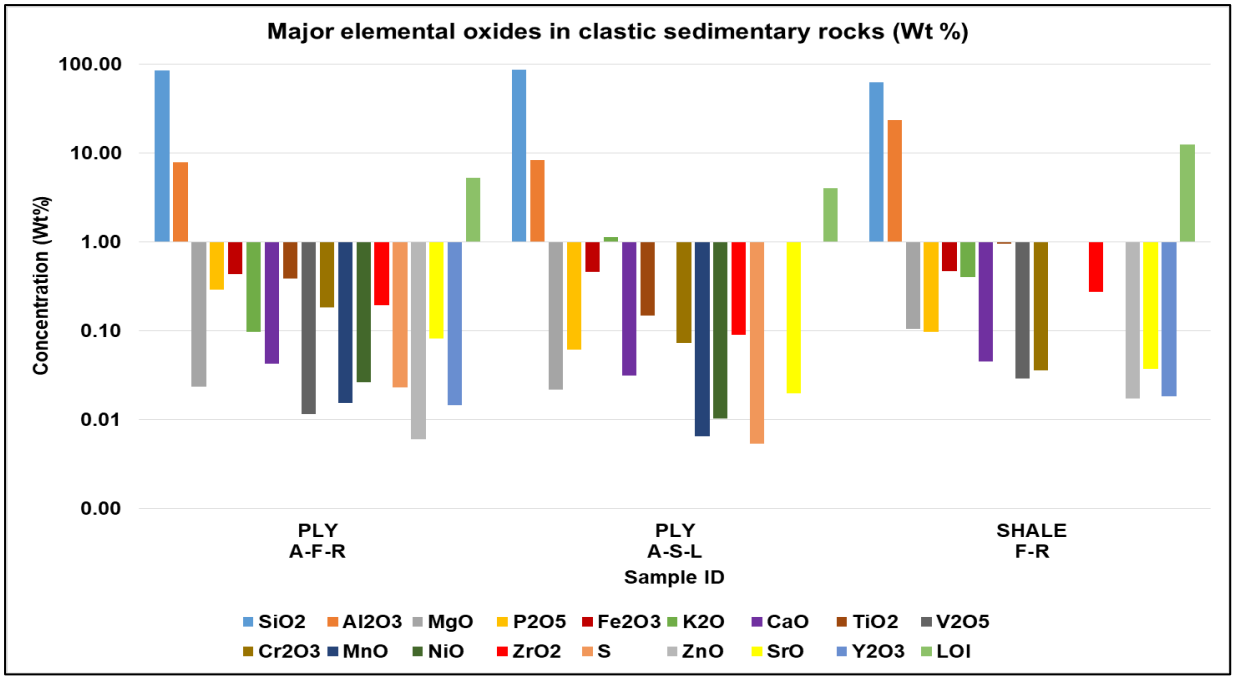


Figure 4.6: Concentration of major oxides in clastic sedimentary rocks.

### 4.2.2 Coal

Results for major oxides in coal are indicated in Table 4.4. Descriptive statistics of major oxides in coal indicate an average mean value in weight % of $SiO_2$ (14.98), $Al_2O_3$ (7.58), $Fe_2O_3$ (1.18), $TiO_2$ (0.35), $ZrO_2$ (0.08), $K_2O$ (0.06), CaO (0.02), MgO (0.02), $P_2O_5$ (0.02), NiO (0.01), SrO (0.01) and $Y_2O_3$ (0.01) in their order of abundance (Table 4.5). The rest of the major oxides like $V_2O_5$, $Cr_2O_3$, ZnO, and $Na_2O$ were below detection limit (Table 4.5).

The concentration of $SiO_2$ in coal is the dominant major oxide ranging between 3.37 Wt % (Ply C S-L) to 59.47 Wt % (Ply G S-L) (Fig. 4.7). The concentration of $Al_2O_3$, $Fe_2O_3$ and $TiO_2$ are also moderate to high ranging from 2.00 to 19.30; 0.21 to 5.26; 0.10 to 1.49 Wt % respectively (Table 4.5). The concentration of $Fe_2O_3$ in both portions of seam 10 are increasing with depth, this implies that the ferric iron is enriched with depth. In contrast, $ZrO_2$, $K_2O$, MgO, CaO, $P_2O_5$, NiO and SrO are relatively low ranging between 0.03 to 0.20; 0.01 to 0.12; 0.00 to 0.05, 0.00 to 0.02, 0.00 to 0.06, 0.00 to 0.01 and 0.01 to 0.02 Wt % (Table 4.5).

Major oxides such as $SiO_2$, Al2$O_3$, MgO and $K_2O$ are most dominant in the west far right (F-R) portion of seam 10 as compared to the south left (S-L) portion (Fig. 4.7). The concentration of $Fe_2O_3$ is dominant in the south left portion of seam 10, particularly ply E S-L and H S-L with $Fe_2O_3$ concentrations of 4.31 and 5.26 Wt% respectively (Fig. 4.7). When comparing the composite samples for both seams 11 and 10, seam 10 has a higher concentration of major oxides as compared to seam 10.

Table 4.4: Major element oxides in coal from Sekoko coal mine in Waterberg Coalfield (Wt %)

| Major Oxides (Wt %) | West far right of seam 10 | | | | | | South portion of seam 10 | | | | | | | Composites | |
|---|---|---|---|---|---|---|---|---|---|---|---|---|---|---|---|
| | PLY B-F-R | PLY C-F-R | PLY D-F-R | PLY E-F-R | PLY G-F-R | PLY H-F-R | PLY B-S-L | PLY C-S-L | PLY D-S-L | PLY E-S-L | PLY F-S-L | PLY G-S-L | PLY H-S-L | SEAM 10 | SEAM 11 |
| $SiO_2$ | 11.93 | 5.92 | 5.61 | 24.57 | 23.39 | 18.21 | 5.25 | 3.37 | 21.36 | 6.68 | 5.65 | 59.47 | 5.01 | 16.09 | 12.25 |
| $Al_2O_3$ | 6.62 | 3.26 | 3.27 | 12.60 | 12.76 | 10.18 | 3.26 | 2.00 | 14.23 | 4.19 | 3.09 | 19.30 | 2.93 | 8.90 | 7.13 |
| MgO | 0.00 | 0.00 | 0.00 | 0.04 | 0.04 | 0.03 | 0.00 | 0.01 | 0.04 | 0.00 | 0.00 | 0.05 | 0.02 | 0.02 | 0.02 |
| $Na_2O$ | 0.00 | 0.00 | 0.01 | 0.00 | 0.00 | 0.00 | 0.00 | 0.00 | 0.00 | 0.00 | 0.00 | 0.00 | 0.00 | 0.00 | 0.00 |
| $P_2O_5$ | 0.02 | 0.01 | 0.00 | 0.03 | 0.03 | 0.02 | 0.01 | 0.01 | 0.03 | 0.01 | 0.01 | 0.06 | 0.00 | 0.02 | 0.01 |
| $Fe_2O_3$ | 0.21 | 1.22 | 1.43 | 0.31 | 0.30 | 0.39 | 0.29 | 0.71 | 0.39 | 4.31 | 0.30 | 0.33 | 5.26 | 0.99 | 1.31 |
| $K_2O$ | 0.03 | 0.03 | 0.01 | 0.09 | 0.08 | 0.06 | 0.03 | 0.04 | 0.10 | 0.06 | 0.03 | 0.12 | 0.05 | 0.07 | 0.05 |
| CaO | 0.01 | 0.02 | 0.01 | 0.01 | 0.01 | 0.02 | 0.01 | 0.02 | 0.01 | 0.02 | 0.01 | 0.02 | 0.03 | 0.03 | 0.01 |
| $TiO_2$ | 0.23 | 0.21 | 0.12 | 0.53 | 0.47 | 0.40 | 0.11 | 0.10 | 0.49 | 0.31 | 0.14 | 1.49 | 0.11 | 0.36 | 0.24 |
| $V_2O_5$ | 0.00 | 0.00 | 0.00 | 0.00 | 0.00 | 0.00 | 0.00 | 0.00 | 0.01 | 0.00 | 0.00 | 0.00 | 0.00 | 0.00 | 0.00 |
| $Cr_2O_3$ | 0.00 | 0.00 | 0.00 | 0.01 | 0.01 | 0.01 | 0.00 | 0.00 | 0.01 | 0.01 | 0.01 | 0.01 | 0.02 | 0.02 | 0.01 |
| MnO | 0.00 | 0.00 | 0.00 | 0.00 | 0.00 | 0.00 | 0.00 | 0.00 | 0.00 | 0.01 | 0.00 | 0.00 | 0.00 | 0.00 | 0.00 |
| NiO | 0.00 | 0.01 | 0.01 | 0.01 | 0.01 | 0.01 | 0.01 | 0.01 | 0.00 | 0.01 | 0.01 | 0.00 | 0.01 | 0.01 | 0.01 |
| CuO | 0.00 | 0.00 | 0.00 | 0.00 | 0.00 | 0.00 | 0.00 | 0.00 | 0.00 | 0.00 | 0.00 | 0.00 | 0.00 | 0.00 | 0.00 |
| $ZrO_2$ | 0.05 | 0.06 | 0.04 | 0.13 | 0.10 | 0.10 | 0.03 | 0.04 | 0.09 | 0.05 | 0.05 | 0.20 | 0.03 | 0.10 | 0.06 |
| S | 0.00 | 0.00 | 0.00 | 0.00 | 0.00 | 0.00 | 0.00 | 0.00 | 0.00 | 0.00 | 0.00 | 0.00 | 0.01 | 0.01 | 0.00 |
| ZnO | 0.00 | 0.00 | 0.00 | 0.00 | 0.00 | 0.00 | 0.00 | 0.00 | 0.00 | 0.00 | 0.00 | 0.00 | 0.00 | 0.01 | 0.00 |
| SrO | 0.01 | 0.01 | 0.01 | 0.01 | 0.01 | 0.01 | 0.01 | 0.01 | 0.01 | 0.01 | 0.01 | 0.02 | 0.01 | 0.01 | 0.01 |
| $Y_2O_3$ | 0.01 | 0.01 | 0.01 | 0.02 | 0.01 | 0.02 | 0.00 | 0.00 | 0.01 | 0.01 | 0.01 | 0.02 | 0.01 | 0.01 | 0.01 |
| LOI | 80.86 | 89.21 | 89.45 | 61.62 | 62.76 | 70.52 | 90.96 | 93.65 | 63.22 | 84.3 | 90.66 | 18.89 | 86.47 | 73.33 | 78.87 |
| **TOTAL** | **99.98** | **99.98** | **99.98** | **99.96** | **99.99** | **99.97** | **99.97** | **99.97** | **99.99** | **99.97** | **99.98** | **99.98** | **99.97** | **99.98** | **99.99** |

Table 4.5: Descriptive statistics of major oxides (Wt %) of coal

| Major Oxides | Min | Max | Mean | SD | Standard Error | Sum | Coefficient of variation (SD/Mean) |
|---|---|---|---|---|---|---|---|
| $SiO_2$ | 3.37 | 59.47 | 14.98 | 14.31 | 3.69 | 224.76 | 0.95 |
| $Al_2O_3$ | 2.00 | 19.30 | 7.58 | 5.23 | 1.35 | 113.72 | 0.69 |
| MgO | 0.00 | 0.05 | 0.02 | 0.02 | 0.00 | 0.27 | 1.04 |
| $Na_2O$ | 0.00 | 0.01 | 0.00 | 0.00 | 0.00 | 0.01 | 3.87 |
| $P_2O_5$ | 0.00 | 0.06 | 0.02 | 0.02 | 0.00 | 0.27 | 0.87 |
| $Fe_2O_3$ | 0.21 | 5.26 | 1.18 | 1.53 | 0.40 | 17.74 | 1.29 |
| $K_2O$ | 0.01 | 0.12 | 0.06 | 0.03 | 0.01 | 0.85 | 0.52 |
| CaO | 0.01 | 0.03 | 0.02 | 0.01 | 0.00 | 0.26 | 0.43 |
| $TiO_2$ | 0.10 | 1.49 | 0.35 | 0.35 | 0.09 | 5.30 | 0.98 |
| $V_2O_5$ | 0.00 | 0.01 | 0.00 | 0.00 | 0.00 | 0.01 | 3.87 |
| $Cr_2O_3$ | 0.00 | 0.02 | 0.01 | 0.01 | 0.00 | 0.10 | 1.05 |
| MnO | 0.00 | 0.01 | 0.00 | 0.00 | 0.00 | 0.01 | 3.87 |
| NiO | 0.00 | 0.01 | 0.01 | 0.00 | 0.00 | 0.11 | 0.60 |
| $ZrO_2$ | 0.03 | 0.20 | 0.08 | 0.05 | 0.01 | 1.14 | 0.60 |
| S | 0.00 | 0.01 | 0.00 | 0.00 | 0.00 | 0.02 | 2.70 |
| ZnO | 0.00 | 0.01 | 0.00 | 0.00 | 0.00 | 0.01 | 3.87 |
| SrO | 0.01 | 0.02 | 0.01 | 0.00 | 0.00 | 0.18 | 0.26 |
| $Y_2O_3$ | 0.00 | 0.02 | 0.01 | 0.01 | 0.00 | 0.15 | 0.59 |
| LOI | 18.89 | 93.65 | 75.65 | 19.20 | 4.96 | 1134.8 | 0.25 |

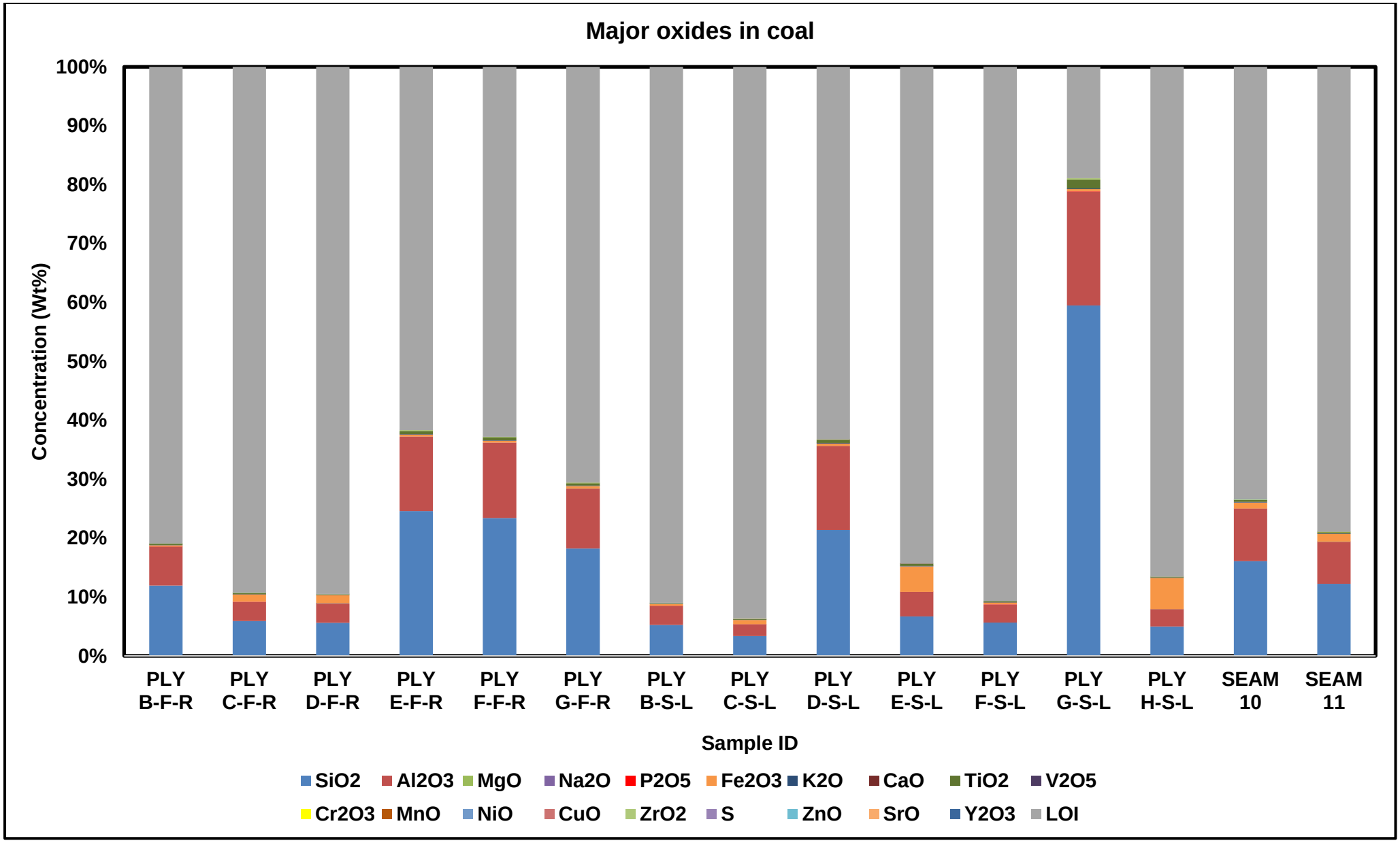


Figure 4.7: Concentration of major oxides in coal samples.

## 4.3 Organic Petrology

This section focused on the microscopic observation of six representative coal samples.

### 4.3.1 Maceral Point Count

Macerals and mineral matter of coal in Vol. % with mineral matter (inc. mm) and without mineral matter (mmf) were identified (Table 4.6). Following maceral point count coal from Sekoko coal mine was found to be dominated by inertinite, followed by vitrinite and Liptinite macerals (Fig. 4.8).

Results for maceral composition (Table 4.6) indicated that the analysed coal samples contain high concentrations of inertinite with a minimum and maximum values of 28.30 and 90.30 vol. % mmf respectively. Vitrinite are intermediate with concentrations ranging from 8 to 70.50 vol. % mmf. Liptinite is present at low concentrations with a minimum concentration of 1.2 vol. % mmf and a maximum value of 2.8 vol % mmf.

Figure 4.22 shows the distribution of macerals with depth. This shows an increase in vitrinite with increasing depth. This is evident through an increase in vitrinite from ply C S-L to ply H S-L (Fig. 4.8). There is also an increase in vitrinite from seam 11 to seam 10 (Fig. 4.8). In contrast, the inertinite macerals show a decline with increasing depth, with high concentration (> 90 vol.% mmf) in ply F S-L (Fig. 4.8). The decline of inertinite with depth is evident from seam 11 to seam 10 as well as from ply C to H S-L (Fig. 4.8).

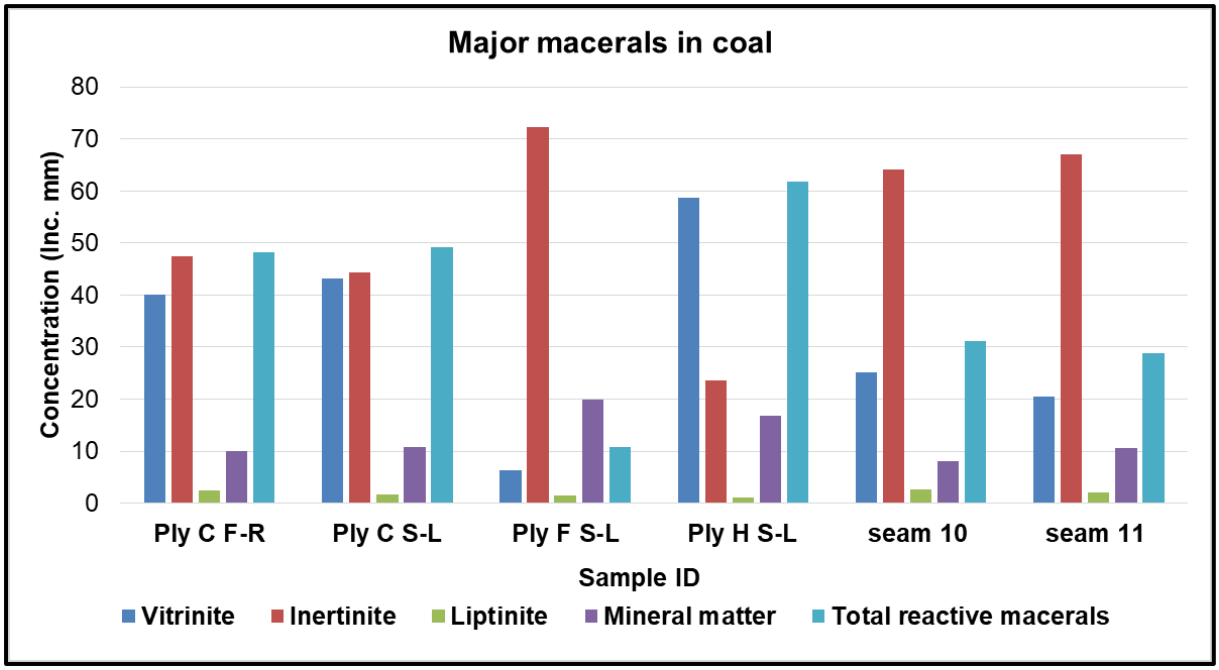


Figure 4.8: Summarised major maceral groups in selected coal samples.

Vitrinite in coal occurs in several forms. Collodetrinite is the dominant maceral with a minimum value of 4.80 vol.% mmf (Ply F S-L), a maximum value of 43.60 vol.% mmf (Ply H S-L) and an arithmetic mean of 24.78 vol. % mmf (Tables 4.6; 4.7). Collotelinite and telinite macerals are the second dominant with a minimum of 1.00 and 0.20 vol% mmf, a maximum of 14.90 and 8.40 vol. % mmf, and an arithmetic mean of 6.12 and 3.12 vol.% mmf respectively. Pseudovitrinite, corpogelinite and vitrodetrinite are present with mean concentration values of 1.62, 1.32 and 0,08 vol. % mmf respectively.

Table 4.6 shows that the concentration of collodetrinite is increasing with depth (Ply C S-L to H S-L). Inertinite in Sekoko coal samples consists mainly of inert semifusinite maceral with a minimum concentration of 11.10 vol. % mmf (Ply H S-L) and a maximum concentration of 46.8 vol% mmf (Ply F S-L) and an arithmetic mean of 32.08 vol.% mmf. Inertodetrinite I is the second dominant inertinite maceral with a minimum and maximum concentration of 1.40 (H S-L) and 33.00 (F S-L) with an arithmetic mean of 13.17 vol. % mmf. Fusinite, reactive semifusinite and secretinite macerals ranges between 1.30 to 12.60, 2.60 to 7.20 and 2.00 to 6.00 vol. % mmf with arithmetic mean of 6.35, 4.75 and 4.18 vol. % mmf respectively.

Table 4.6: Organic petrology results showing major groups, subgroups of macerals as well as the mineral matter in coal

| Sample identification | | Ply C F-R | | seam 11 | | Ply C S-L | | Ply H S-L | | seam 10 | | Ply F S-L | |
|---|---|---|---|---|---|---|---|---|---|---|---|---|---|
| | | Inc. mm | mmf | Inc. mm | mmf | Inc. mm | mmf | Inc. mm | mmf | Inc. mm | mmf | Inc. mm | mmf |
| Maceral Group | Maceral (vol %) | vol% | vol% | vol% | vol% | vol% | vol% | vol% | vol% | vol% | vol% | vol% | vol% |
| Vitrinite | telinite | 4.2 | 4.7 | 1.6 | 1.8 | 1.6 | 1.8 | 7 | 8.4 | 0.2 | 0.2 | 1 | 1.2 |
| | collotelinite | 4.8 | 5.3 | 3.6 | 4 | 5.6 | 6.3 | 12.4 | 14.9 | 4.8 | 5.2 | 0.8 | 1 |
| | vitrodetrinite | 0 | 0 | 0 | 0 | 0 | 0 | 0.4 | 0.5 | 0 | 0 | 0 | 0 |
| | collodetrinite | 27.9 | 31.1 | 12.6 | 14.1 | 34.6 | 38.8 | 36.2 | 43.6 | 15 | 16.3 | 3.8 | 4.8 |
| | corpogelinite | 1 | 1.1 | 1 | 1.1 | 1.2 | 1.3 | 2.4 | 2.9 | 1.4 | 1.5 | 0 | 0 |
| | gelinite | 0 | 0 | 0 | 0 | 0 | 0 | 0 | 0 | 0 | 0 | 0 | 0 |
| | pseudovitrinite | 2.2 | 2.4 | 1.6 | 1.8 | 0.2 | 0.2 | 0.2 | 0.2 | 3.8 | 4.1 | 0.8 | 1 |
| Inertinite | fusinite | 8 | 8.9 | 2.8 | 3.1 | 11.2 | 12.6 | 6 | 7.2 | 4.6 | 5 | 1 | 1.3 |
| | reactive semifusinite | 5.8 | 6.4 | 6.4 | 7.2 | 4.4 | 4.9 | 2.2 | 2.6 | 3.4 | 3.7 | 3 | 3.7 |
| | inert semifusinite | 23.9 | 26.6 | 36 | 40.3 | 20.2 | 22.7 | 9.2 | 11.1 | 41.4 | 45 | 37.4 | 46.8 |
| | micrinite | 1 | 1.1 | 0.2 | 0.2 | 0 | 0 | 0 | 0 | 0.8 | 0.9 | 0.6 | 0.7 |
| | macrinite | 0 | 0 | 0 | 0 | 0 | 0 | 0 | 0 | 0 | 0 | 0 | 0 |
| | secretinite | 2.4 | 2.7 | 5.2 | 5.8 | 3.4 | 3.8 | 5 | 6 | 1.8 | 2 | 3.8 | 4.8 |
| | funginite | 0 | 0 | 0 | 0 | 0 | 0 | 0 | 0 | 0 | 0 | 0 | 0 |
| | inertodetrinite R | 0 | 0 | 0 | 0 | 0 | 0 | 0 | 0 | 0 | 0 | 0 | 0 |
| | inertodetrinite I | 6.4 | 7.1 | 16.4 | 18.4 | 5.2 | 5.8 | 1.2 | 1.4 | 12.2 | 13.3 | 26.4 | 33 |
| Liptinite | sporinite | 2.2 | 2.4 | 1.8 | 2 | 1.6 | 1.8 | 1 | 1.2 | 2.6 | 2.8 | 1.4 | 1.7 |
| | cutinite | 0 | 0 | 0.2 | 0.2 | 0 | 0 | 0 | 0 | 0 | 0 | 0 | 0 |
| | resinite | 0 | 0 | 0 | 0 | 0 | 0 | 0 | 0 | 0 | 0 | 0 | 0 |
| | alginite | 0.2 | 0.2 | 0 | 0 | 0 | 0 | 0 | 0 | 0 | 0 | 0 | 0 |
| | liptodetrinite | 0 | 0 | 0 | 0 | 0 | 0 | 0 | 0 | 0 | 0 | 0 | 0 |
| | suberinite | 0 | 0 | 0 | 0 | 0 | 0 | 0 | 0 | 0 | 0 | 0 | 0 |
| | exsudatinite | 0 | 0 | 0 | 0 | 0 | 0 | 0 | 0 | 0 | 0 | 0 | 0 |
| Mineral matter | clay | 2.8 | | 6 | | 2.8 | | 2.8 | | 5.4 | | 9 | |
| | quartz | 4 | | 2.2 | | 1 | | 2 | | 1.8 | | 6.6 | |
| | pyrite | 1.4 | | 1.2 | | 5.4 | | 8 | | 0.2 | | 2.4 | |
| | carbonate | 1.6 | | 0.8 | | 1.6 | | 4 | | 0.4 | | 1.2 | |
| | other | 0.2 | | 0.4 | | 0 | | 0 | | 0.2 | | 0.8 | |
| SUMMARY TABLE | | | | | | | | | | | | | |
| MACERAL GROUP | VITRINITE | **40.1** | **44.6** | **20.4** | **22.8** | **43.2** | **48.4** | **58.6** | **70.5** | **25.2** | **27.3** | **6.4** | **8** |
| TOTALS (vol %) | INERTINITE | **47.5** | **52.8** | **67** | **75** | **44.4** | **49.8** | **23.6** | **28.3** | **64.2** | **69.9** | **72.2** | **90.3** |
| | LIPTINITE | **2.4** | **2.6** | **2** | **2.2** | **1.6** | **1.8** | **1** | **1.2** | **2.6** | **2.8** | **1.4** | **1.7** |
| | MINERAL MATTER | **10** | | **10.6** | | **10.8** | | **16.8** | | **8** | | **20** | |
| | TOTAL INERTINITE | **47.5** | **52.8** | **67** | **75** | **44.4** | **49.8** | **23.6** | **28.3** | **64.2** | **69.9** | **72.2** | **90.3** |
| | TOTAL REACTIVE MACERALS | **48.3** | **53.6** | **28.8** | **32.2** | **49.2** | **55.1** | **61.8** | **74.3** | **31.2** | **33.8** | **10.8** | **13.4** |

Micrinite occurs at lower concentrations with a maximum value of 1.10 vol. % mmf and an arithmetic mean of 0.48 vol. % mmf (Table 4.7). Fusinite, reactive semifusinite and inertodetrinite macerals are decreasing with depth, in contrast, inert semifusinite and micrinite show an increase in concentration with depth.

The Liptinite macerals have the lowest concentrations compared to other macerals. Sporinite is dominant with minimum and maximum concentrations of 1.20 and 2.80 vol. % mmf while the arithmetic mean is 1.98 vol. % mmf. Cutinite and alginite have the same concentration, both occur at lower concentrations with a minimum and maximum concentration of 0.00 and 0.20 vol.% mmf with a mean concentration of 0.03 vol.% mmf (Table 4.7).

When conducting maceral point count, the mineral matter within the coal was also investigated. Table 4.6 shows the different mineral matter present in coal, and these include clay, quartz, carbonates, and pyrite amongst other minerals. Pyrite is present in different forms within the coal. Figures (4.10B) show disseminated pyrite grains occurring within vitrinite macerals and massive pyrite occurring within cracks. Ply H S-L shows a massive pyrite occurring within cracks (Fig. 4.13D), implying that it is epigenetic. The framboidal pyrite grains within the organic matter (macerals) suggest a rather syngenetic deposition. The morphology of pyrite was studied in greater detail using scanning electron microscopy.

The overall concentration of pyrite as determined by organic petrography shows an increase with depth (Ply C S-L to H S-L; Table 4.6). This trend also applies for carbonate as the concentration increases from C S-L (1.6 vol. % inc. mm) to H S-L (4.00 vol. % inc. mm). Ply H S-L contains the highest concentration of pyrite with (8.00 vol.% inc. mm), this is also evident through the massive pyrite in Figure 4.13D. Seam 10 composite contains the lowest amount of pyrite (0.20 vol. % inc. mm). Minor Concentrations of disseminated calcite are present. They occur within fractures of pseudovitrinite (Fig. 4.12C). Calcite in this coal occurs as cleats infillings. Clay concentration in coal amounts for minimum and maximum values of 2.8 and 9.00 vol. % inc. mm (Table 4.7). Clay minerals are fine and disseminated within cracks and open voids (4.11D). Disseminated quartz grains are present in open spaces, cracks within macerals and within clay minerals (Fig. 4.11B,D).

Table 4.7: Descriptive statistics for coal macerals constituents in mineral matter free (mmf) basis

| | Macerals | Mean | SD | Min | Max |
|---|---|---|---|---|---|
| Vitrinite | Telinite | 3.02 | 3.03 | 0.20 | 8.40 |
| | collotelinite | 6.12 | 4.68 | 1.00 | 14.90 |
| | vitrodetrinite | 0.08 | 0.20 | 0.00 | 0.50 |
| | collodetrinite | 24.78 | 15.34 | 4.80 | 43.60 |
| | corpogelinite | 1.32 | 0.93 | 0.00 | 2.90 |
| | pseudovitrinite | 1.62 | 1.50 | 0.20 | 4.10 |
| Inertinite | fusinite | 6.35 | 4.10 | 1.30 | 12.60 |
| | reactive semifusinite | 4.75 | 1.76 | 2.60 | 7.20 |
| | inert semifusinite | 32.08 | 14.21 | 11.10 | 46.80 |
| | micrinite | 0.48 | 0.48 | 0.00 | 1.10 |
| | secretinite | 4.18 | 1.64 | 2.00 | 6.00 |
| | inertodetrinite I | 13.17 | 11.40 | 1.40 | 33.00 |
| Liptinite | sporinite | 1.98 | 0.56 | 1.20 | 2.80 |
| | cutinite | 0.03 | 0.08 | 0.00 | 0.20 |
| | alginite | 0.03 | 0.08 | 0.00 | 0.20 |

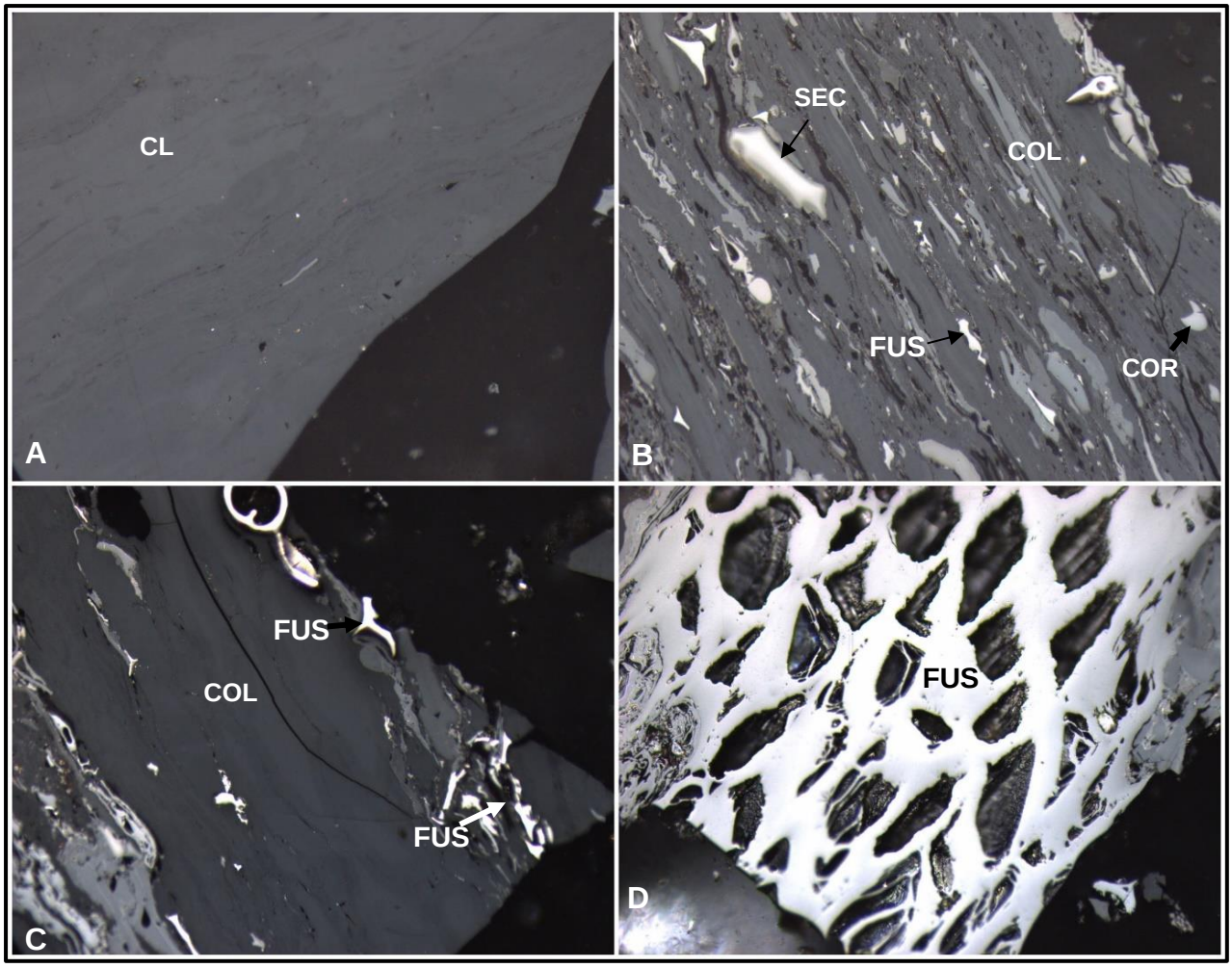


Figure 4.9: Photomicrograph of Ply C F-R: (A) alternating bands of collotelinite (B) Bimacerals showing collotelinite, fusinite, secretinite and corpogelinite, (C) shows collotelinite with fusinite enclosed within, (D) shows a white fusinite. COL= Collotelinite, COR= Corpogelinite, FUS= fusinite, SC= secretinite, F-R=West portion of seam 10 (Oil immersion at x500μm magnification).

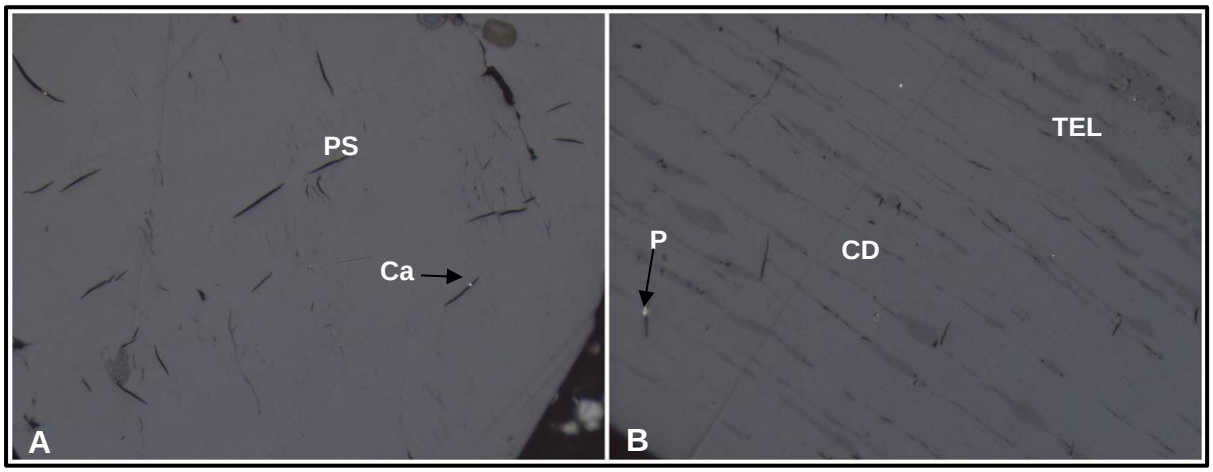


Figure 4.10: Photomicrographs of composite seam 10: (A) showing pseudovitrinite cracks and calcite within a crack, (B) shows collodetrinite alternating with telinite with pyrite within a crack.

PS= Pseudovitrinite, TEL= Telinite, CD= Collodetrinite, Ca=calcite, P=pyrite. (Oil immersion at x500 μm magnification).

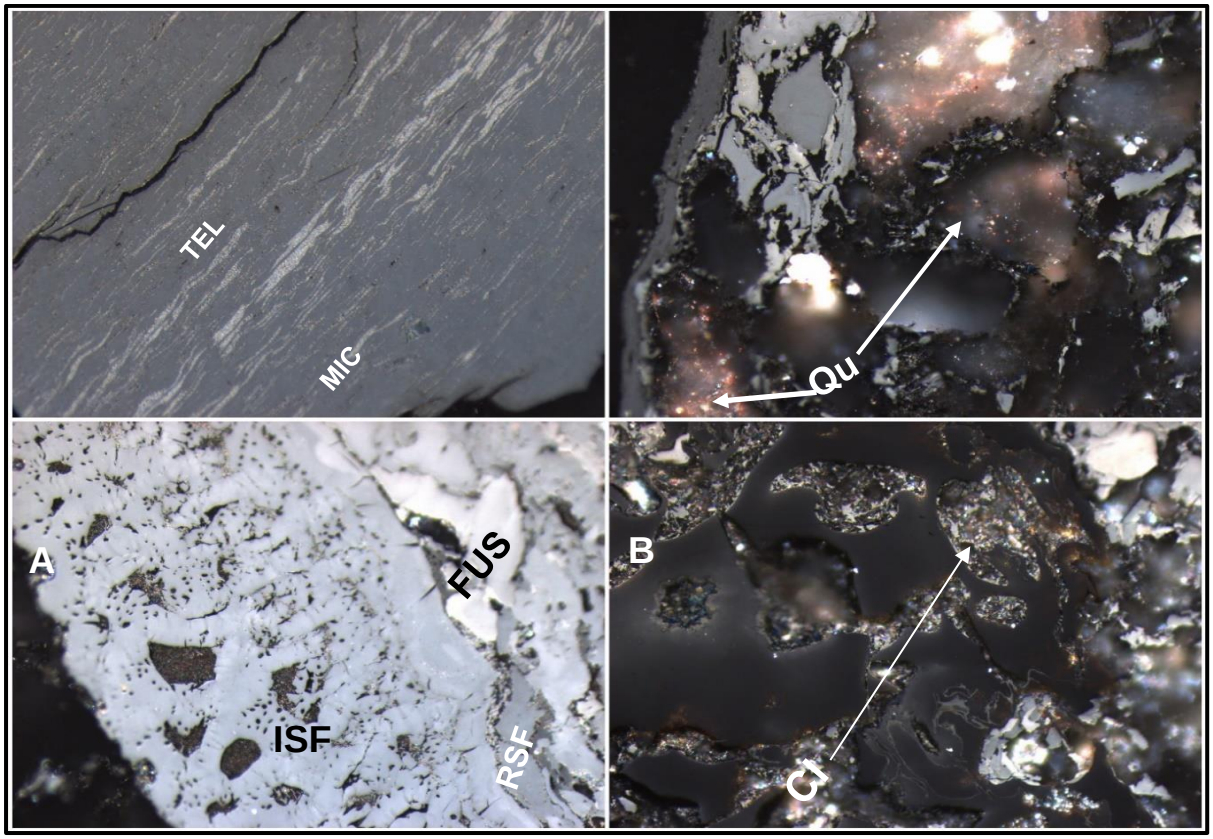


Figure 4.11: Photomicrographs of ply F S-L: (A) showing telinite and micrinite, (B) shows epigenetic quartz, (C) shows inert semifusinite with inclusions of fusinite and reactive semifusinite, (D) shows epigenetic clay minerals. TEL= Telinite, MIC=Micrinite, Qu=Quartz, ISF= Inert semifusinite, FUS= Fusinite, Cl= Clay, S-L= South portion of seam 10. (Oil immersion at 500 μm magnification).

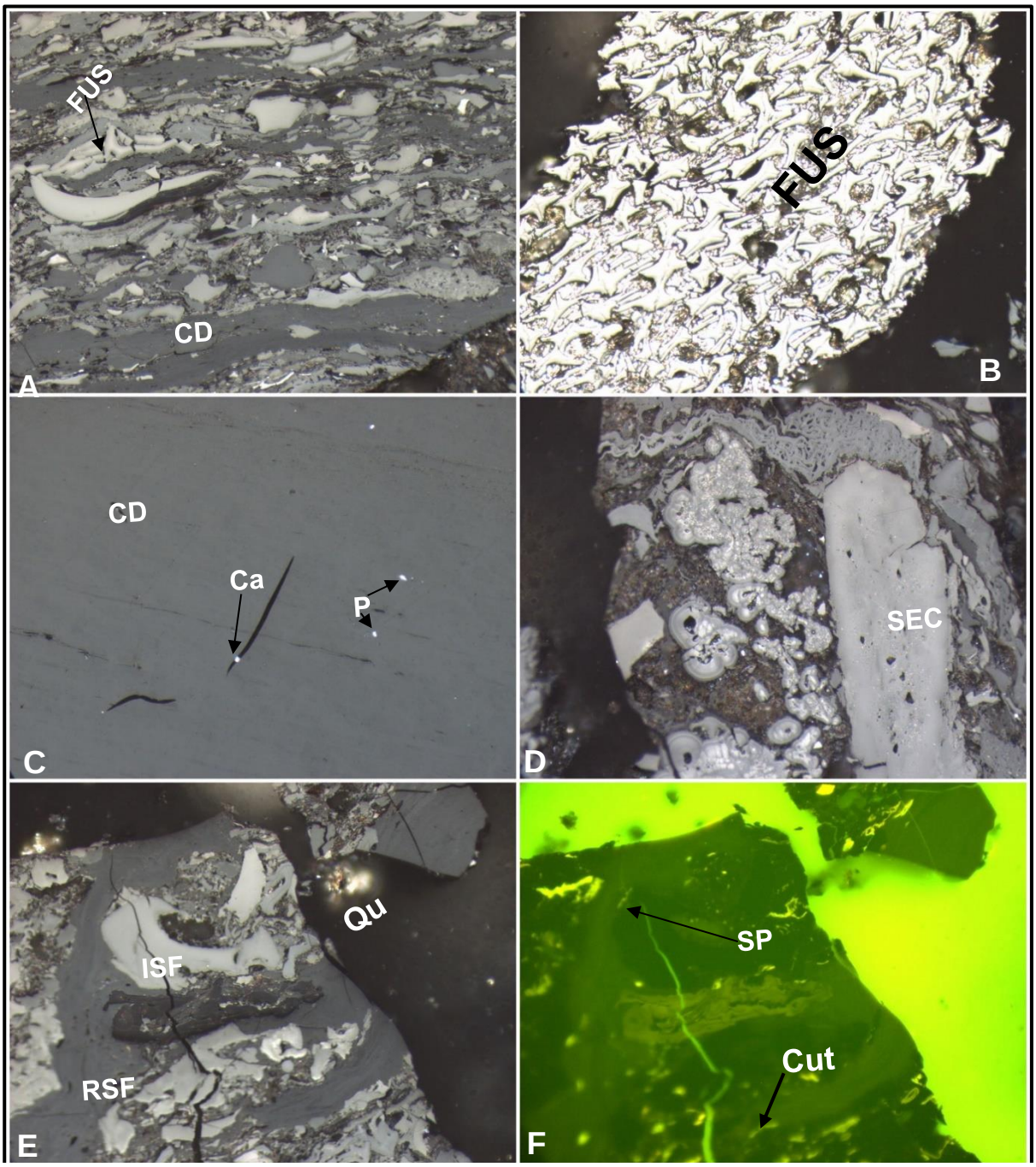


Figure 4.12: Photomicrographs of ply C S-L: (A) showing bimacerals collodetrinite and fusinite, (B) shows a white fusinite, (C) shows collodetrinite and calcite within cracks, (D) Secretinite enclosed by clay minerals, (E) shows reactive semifusinite, inert semifusinite and epigenetic quartz. Sporinite and cutinite are present in frame F. FU= fusinite, ISF= inert semi fusinite, RSF=reactive semifusinite, Cut= Cutinite, SP= Sporinite, Qu=quartz, Ca=Calcite, P=Pyrite.

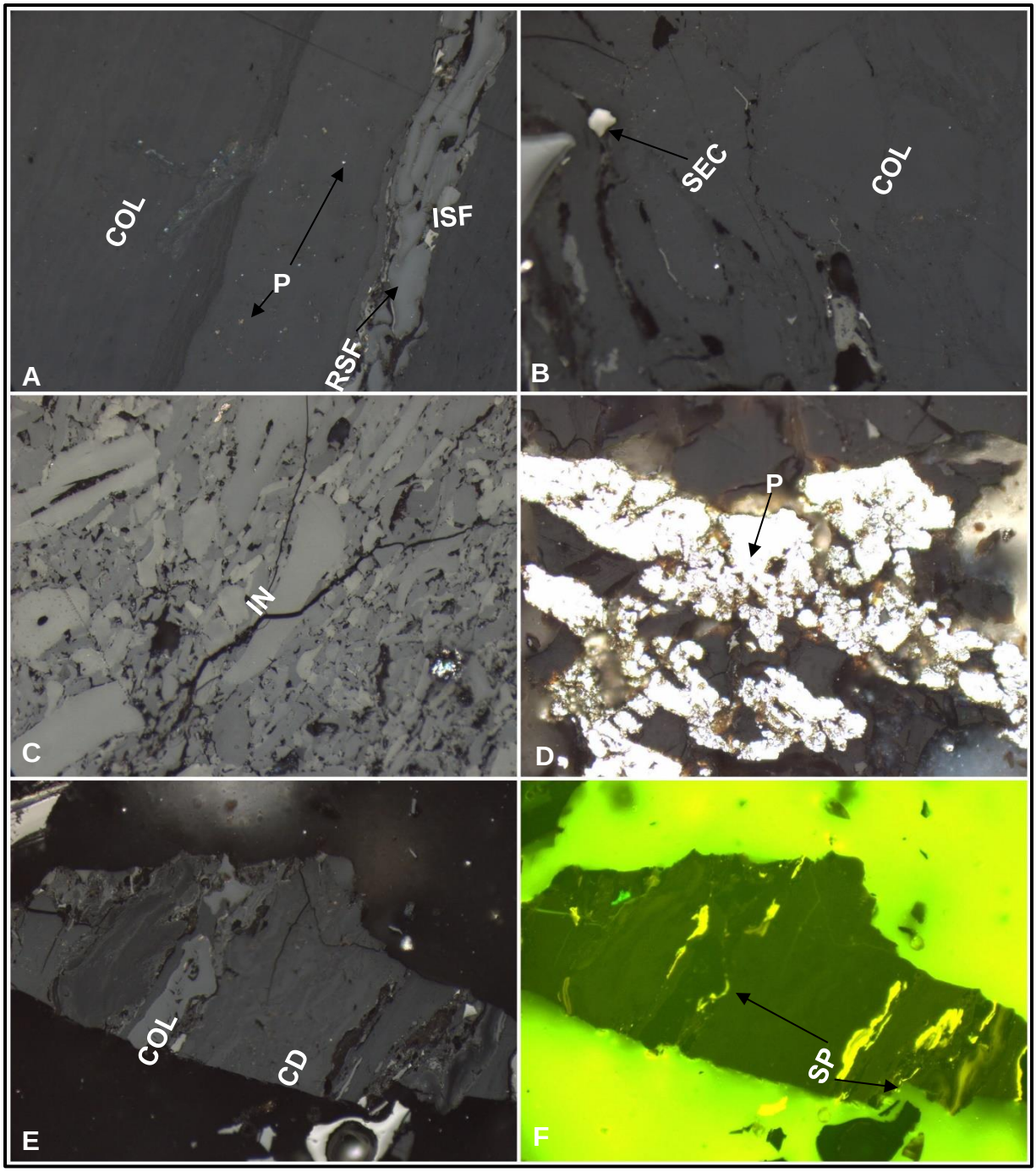


Figure 4.13: Photomicrograph of ply H S-L: (A) showing a sharp contact between collotelinite, reactive semifusinite and inert semifusinite, disseminated pyrite grains within collotelinite macerals and in the boundary between macerals, (B) shows a secretinite enclosed within collotelinite, (C) shows very fine inertodetrinite, (D) a massive framboidal pyrite occurring between cracks, (E) Collotelinite enclosed within a collodetrinite, (F) shows sporinite. Col= Collotelinite, ISF= Inert semifusinite, RSF= Reactive semifusinite, SEC= Secrenite, IN= Intertodetrinite, CD= Collodetrinite, P= pyrite.

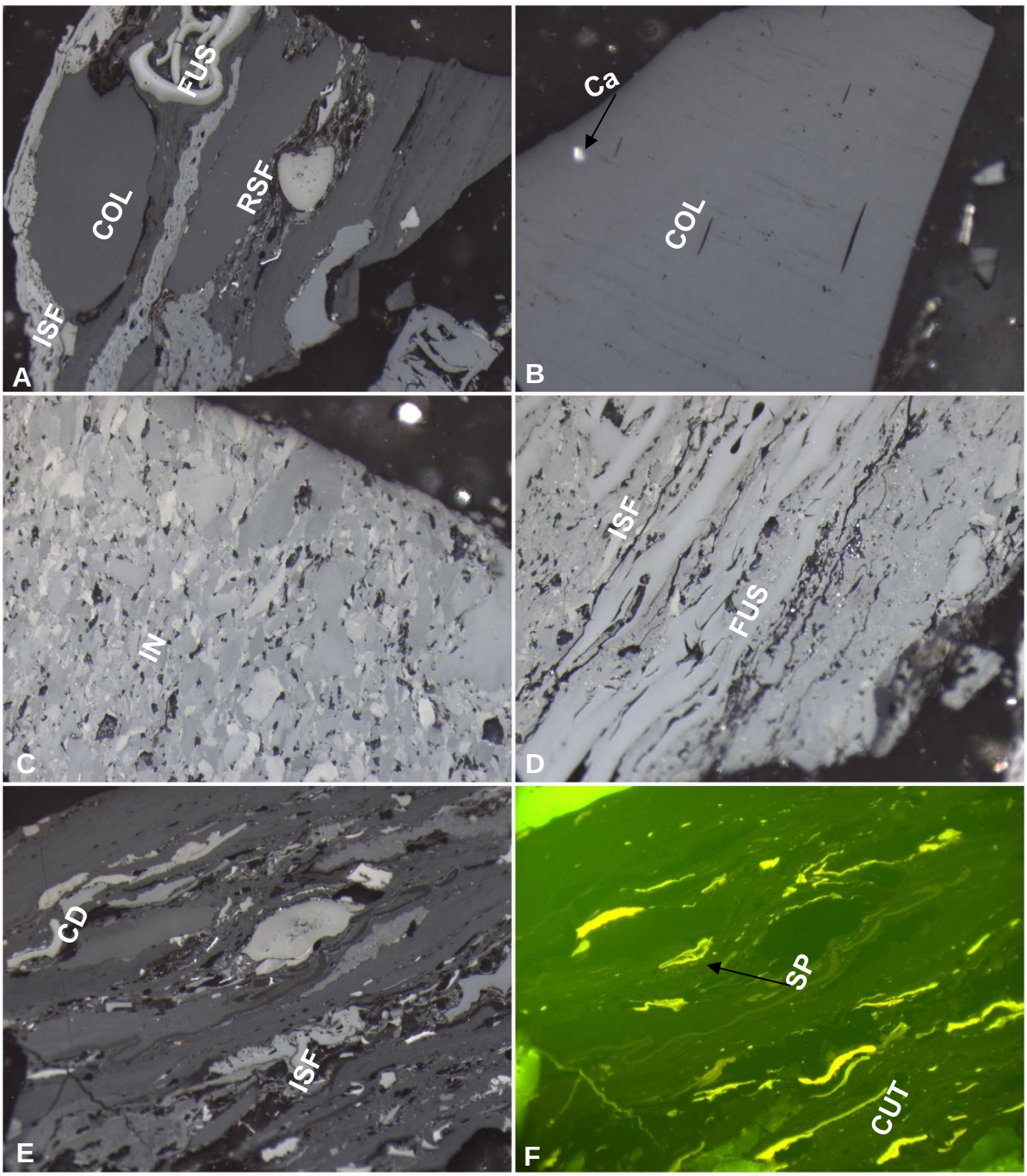


Figure 4.14: Photomicrograph seam 11 showing bimacerals with inert semifusinite surrounding collotelinite (A), Frame B shows collotelinite with calcite grain within the maceral. Frame C shows inertodetrinite with open spaces indicating epigenetic minerals. Frame D shows fusinite enclosed by inert semifusinite macerals. Frame E shows collodetrinite and inert semifusinite. Frame F shows sporinite and cutinite, Ca=Calcite.

### 4.3.2 Vitrinite Reflectance

Table 4.8 shows results for mean random vitrinite reflectance. The standard deviations as well as the number of counts are also indicated. Following reflectance measurements, coal from

Sekoko coal mine is ranked as medium-rank bituminous C following SANS 10320:2004 Standard. Following the ECE-UN classification system (1998) all coal samples except Ply C S-L are medium rank bituminous C as they have vitrinite reflectance ranging between 0.617 and 0.752 (% $RoV_{mr}$). Ply C S-L has a vitrinite reflectance of 0.593 (% $RoV_{mr}$), this implies that it is medium rank bituminous D which can be used as steam coal.

Table 4.8: Mean random vitrinite reflectance (% RoVmr) results

| Sample ID | RoV % | SD | Count |
|---|---|---|---|
| **Ply C F-R** | 0.617 | 0.043 | 0.043 |
| **Seam 11 composite** | 0.611 | 0.062 | 0.062 |
| **Ply C S-L** | 0.593 | 0.058 | 0.058 |
| **Ply H S-L** | 0.606 | 0.073 | 0.073 |
| **Seam 10 Composite** | 0.602 | 0.061 | 0.061 |
| **Ply F S-L** | 0.752 | 0.077 | 0.077 |

### 4.3.3 Characterisation of Pyrite

The purpose of the analysis was to assess the morphology of pyrite within coal samples. The collected hand specimen shows a presence of weathered framboidal pyrite (Fig. 5.1).

Figure 4.15: Hand specimen showing a dull coal with framboidal pyrite grain.

**Ply C F-R**

The concentration of sulphur ranges between 0.15 and 22.47 % with a mean concentration of 4.22%. The concentration of iron (Fe) ranges from 0 to 17.16% with a mean concentration of 2.95%. Figure 4.16 B and C show framboidal pyrite with signs of disintegration (weathering).

**Ply E S-L**

Sulphur concentrations range from 0.15 to 22.47 %, with a mean concentration of 4.22%. The iron (Fe) concentration ranges from 0.35 to 8.25%, with a mean concentration of 2.70%. Figures 4.17 B and C show framboidal pyrite with etching indicating initial stage of oxidation.

**Ply H S-L**

There is presence of disseminated pyrite grains (Fig. 4.18B,C). The pyrite grains have a framboidal morphology and are occurring on the surface of organic matter (Fig. 4.18C) The concentration of sulphur ranges from 0.37 to 8.41 with a mean concentration of 2.23. Alternatively, iron (Fe) concentration ranges from 0 to 6.78% with mean value of 1.76% (Fig. 4.18D).

**Composite Seams 11 and 10**

The concentration of both sulphur and iron (Fe) is increasing with depth as seen from seam 11 to 10 (Figs. 4.19, 4.20). Sulphur has a minimum of 0.3 and 0.24, a maximum of 1.76 and 4.2 and an arithmetic mean of 0.95 and 1.18% for seam 11 and 10 respectively. Subsequently, iron (Fe) a maximum of 1.61 and 3.4, and an arithmetic mean of 0.48 and 1.33% for seam 11 and 10 respectively (Fig. 4.19 and 4.20). The concentration of iron (Fe) is increasing from seam 11 to 10, however, the sulphur content is decreasing. This shows that there is weathering and leaching of sulphur with increasing depth. Pyrite within seam 10 composite is fine grained and appears to be embedded with the organic matter as compared to that of seam 11.

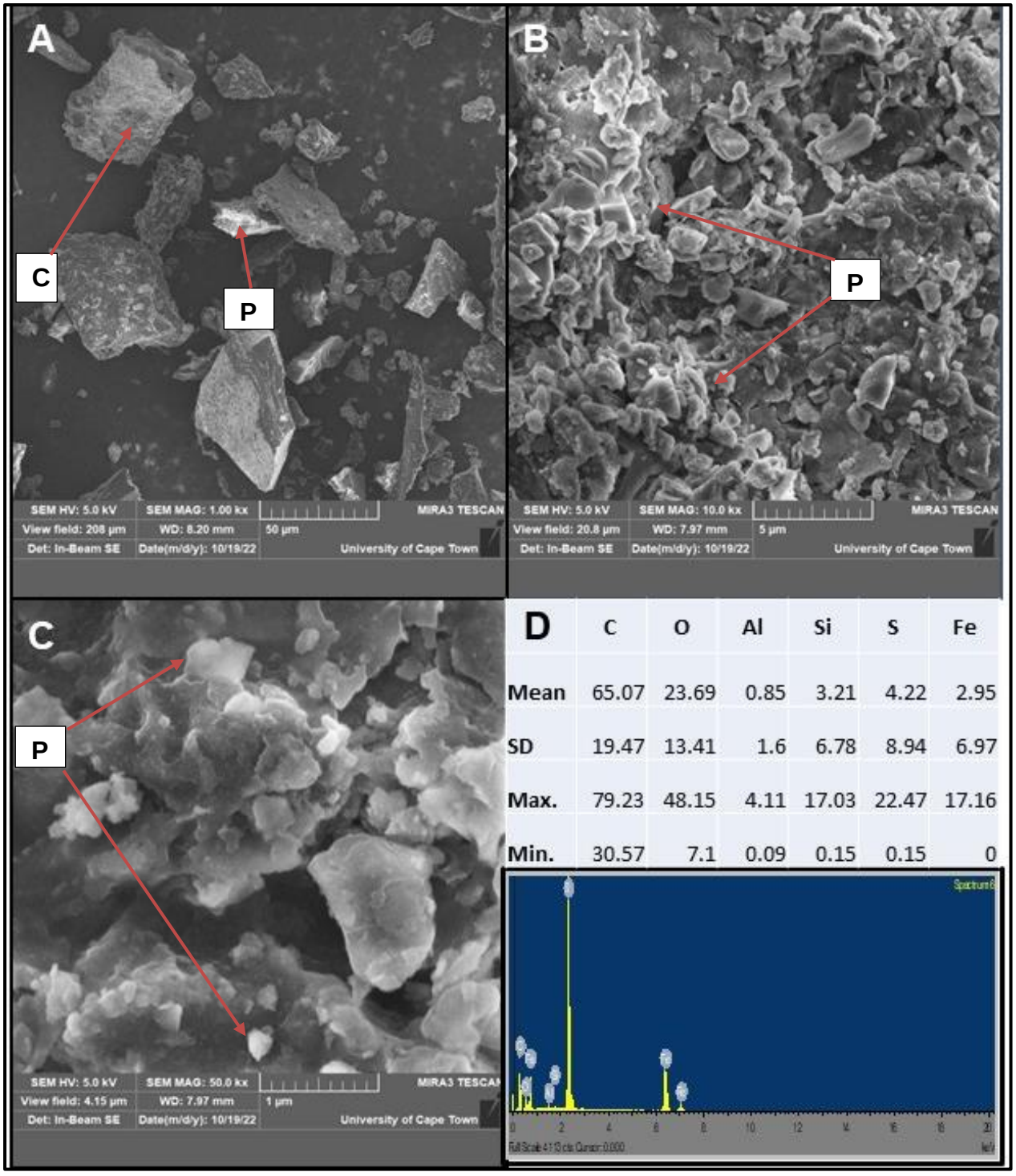


Figure 4.16: Images and results for Ply C F-R: (A) Showing organic matter and pyrite grain on a 50 µm scale, (B) Showing a cluster of pyrite grains on a 5 µm scale, (C) showing framboidal pyrite grains on a 1 µm scale, (D) shows EDX results, F-R= west portion of seam 10, C=Carbon, P=Pyrite.

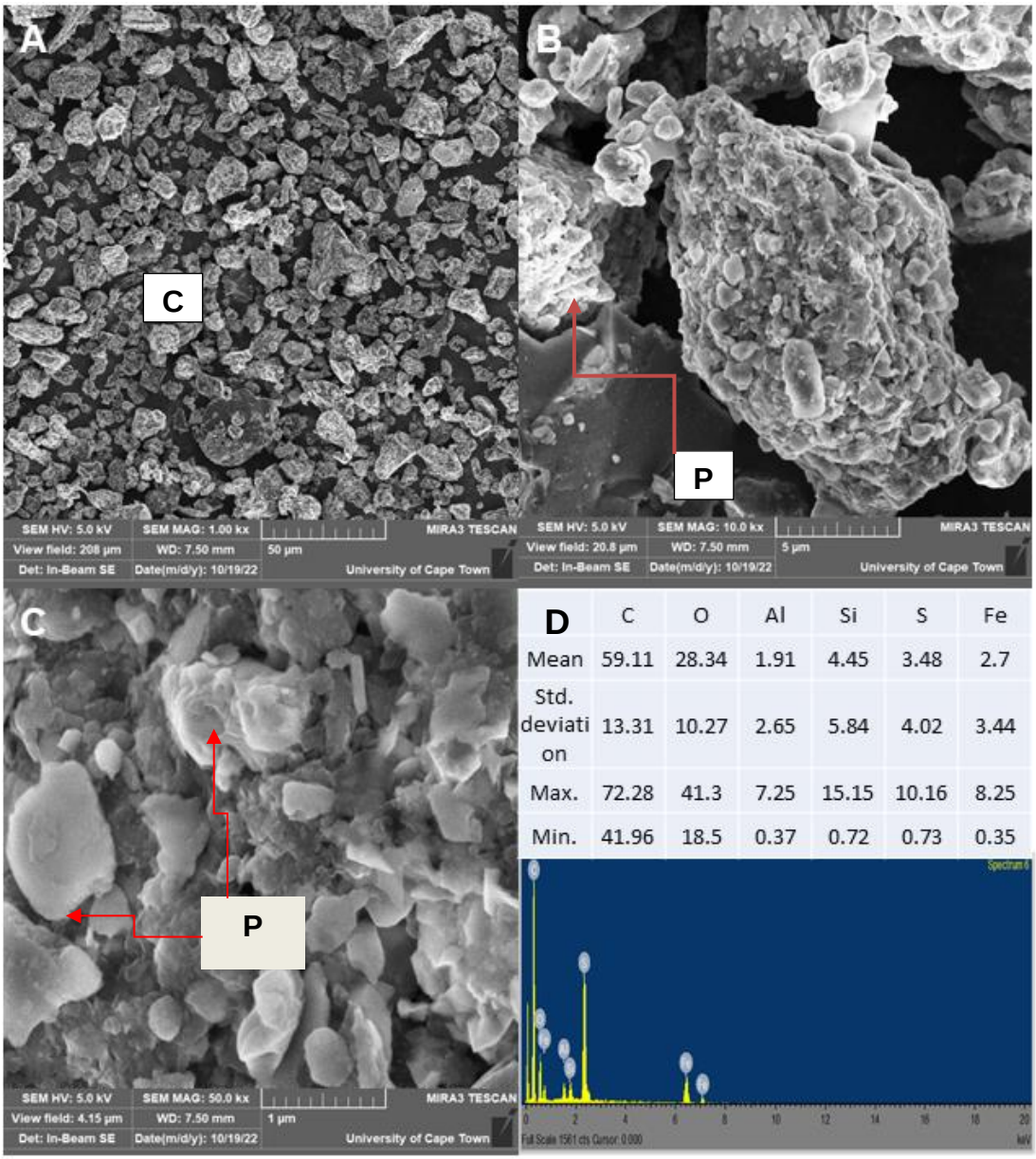


| D | C | O | Al | Si | S | Fe |
|---|---|---|---|---|---|---|
| Mean | 59.11 | 28.34 | 1.91 | 4.45 | 3.48 | 2.7 |
| Std. deviation | 13.31 | 10.27 | 2.65 | 5.84 | 4.02 | 3.44 |
| Max. | 72.28 | 41.3 | 7.25 | 15.15 | 10.16 | 8.25 |
| Min. | 41.96 | 18.5 | 0.37 | 0.72 | 0.73 | 0.35 |

Figure 4.17: Images and results for Ply E S-L: (A) Showing organic matter on a 50 µm scale, (B) Showing a cluster of pyrite grains on a 5 µm scale, (C) showing framboidal pyrite grains on a 1 µm scale, (D) shows EDX results, S-L=South portion of seam 10, C= Carbon (organic matter), P=Pyrite

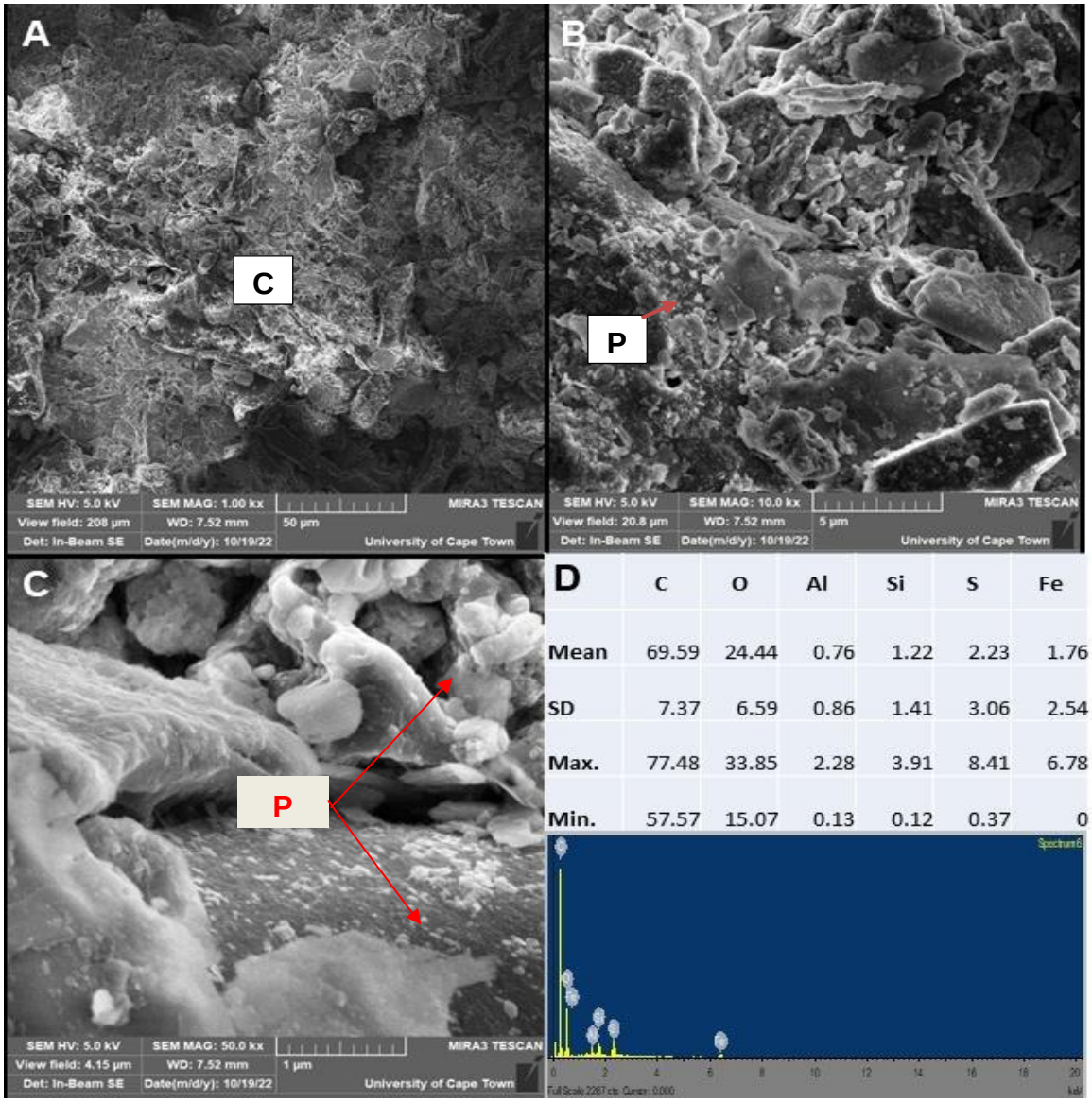


Figure 4.18: Images and results for Ply H S-L: (A) Showing fine organic matter on a 50 µm scale, (B) Showing disseminated pyrite grains on a 5 µm scale, (C) showing disseminated framboidal pyrite grains on a 1 µm scale, (D) shows EDX results, S-L= South portion of seam 10, C=Carbon (organic matter), P=Pyrite.

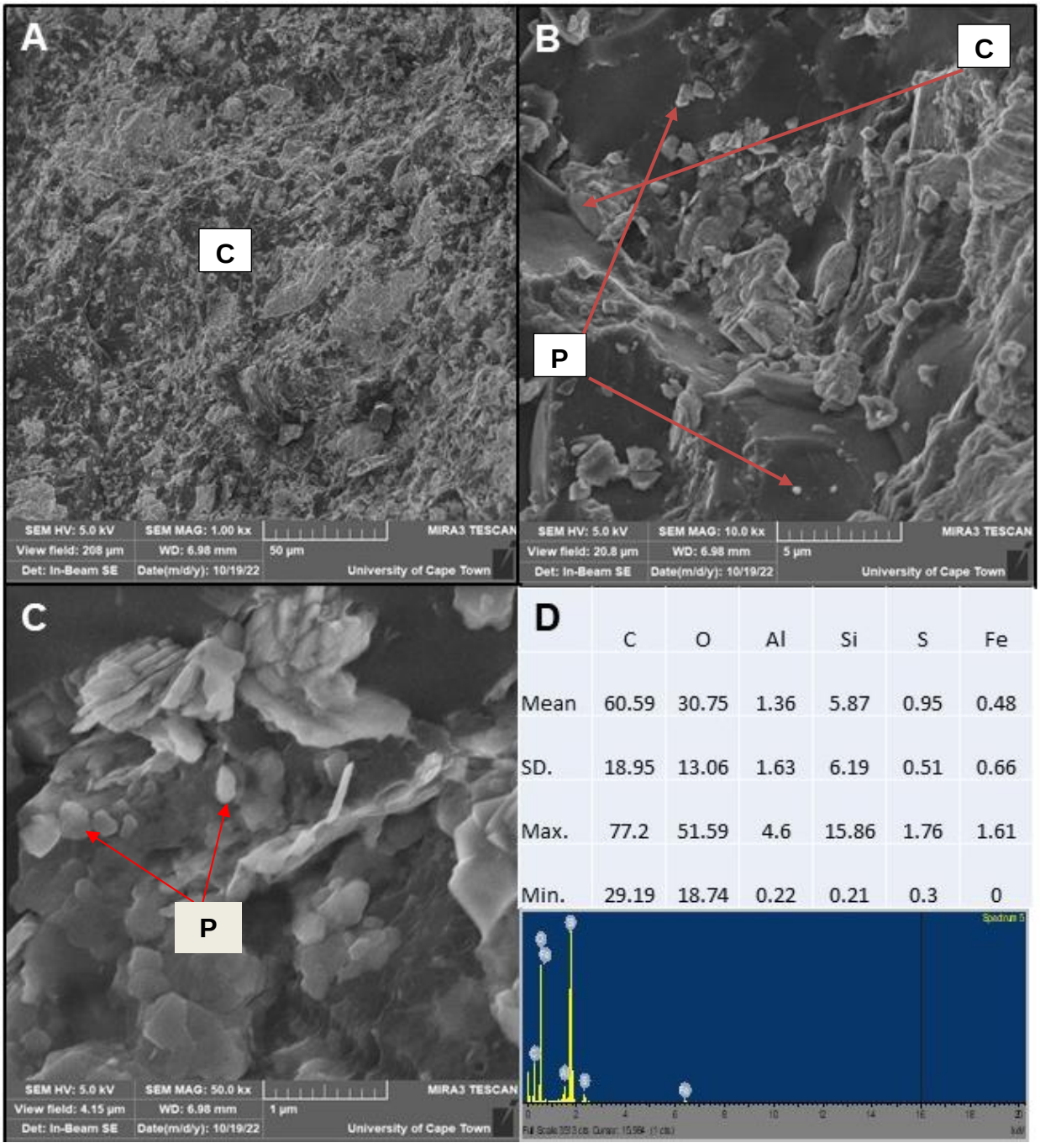


| | C | O | Al | Si | S | Fe |
|---|---|---|---|---|---|---|
| Mean | 60.59 | 30.75 | 1.36 | 5.87 | 0.95 | 0.48 |
| SD. | 18.95 | 13.06 | 1.63 | 6.19 | 0.51 | 0.66 |
| Max. | 77.2 | 51.59 | 4.6 | 15.86 | 1.76 | 1.61 |
| Min. | 29.19 | 18.74 | 0.22 | 0.21 | 0.3 | 0 |

Figure 4.19: Images and results for seam 11 composite: (A) Showing fine organic matter on a 50 µm scale, (B) Showing disseminated pyrite grains in organic matter on a 5 µm scale, (C) showing an array of framboidal pyrite grains on a 1 µm scale, (D) shows EDX results, C=Carbon (organic matter), P=Pyrite.

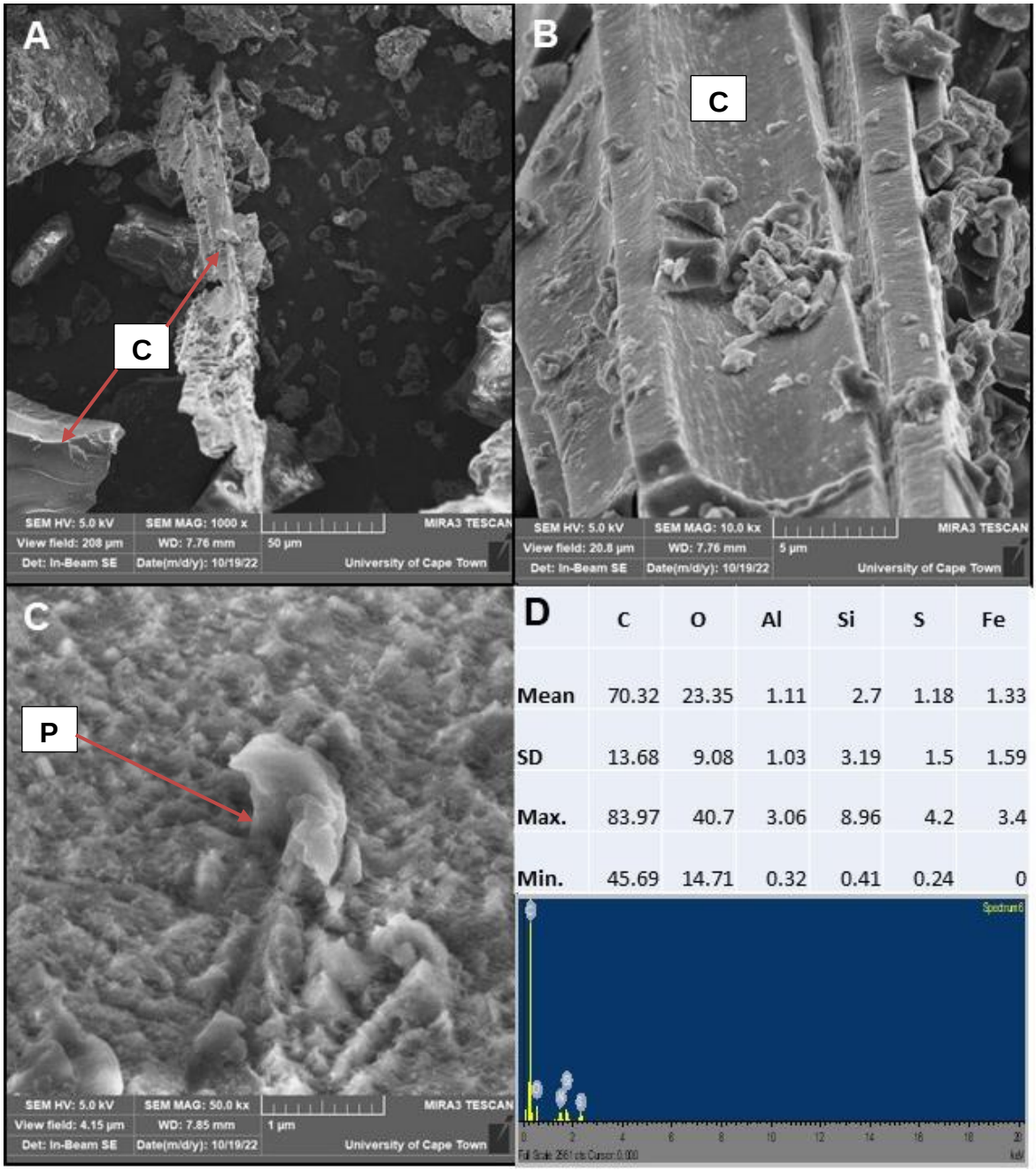


| D | C | O | Al | Si | S | Fe |
|---|---|---|---|---|---|---|
| Mean | 70.32 | 23.35 | 1.11 | 2.7 | 1.18 | 1.33 |
| SD | 13.68 | 9.08 | 1.03 | 3.19 | 1.5 | 1.59 |
| Max. | 83.97 | 40.7 | 3.06 | 8.96 | 4.2 | 3.4 |
| Min. | 45.69 | 14.71 | 0.32 | 0.41 | 0.24 | 0 |

Figure 4.20: Images and results for seam 10 composite: (A) Showing organic matter on a 50 µm scale, (B) Showing a tree bark-like organic matter a 5 µm scale, (C) showing fine grained framboidal pyrite grains on a 1 µm scale, (D) shows EDX results, C=Carbon (organic matter), P=Pyrite.

## 4.4 Coal Quality Analysis

Chemical characterisation of coal was undertaken to further investigate the coal quality. This involved proximate analysis, total sulphur, and gross calorific value (Table 4.9).

The descriptive statistics for proximate, sulphur and calorific value analyses show that samples yielded 7.72 to 62.68 Wt% in dry basis of fixed carbon content (Table 4.10). The volatile matter content in coal ranged between 10.09 and 34.40 % dry basis. The inherent moisture content (air dried) and ash (dry basis) yield of coal samples were 0.90 to 3.40 % and 7.09 to 82.19 % respectively. The high ash (82.09 %; Table 4.10) and low volatile matter and fixed carbon content were from sample (Ply G S-L) which is carbonaceous shale. The total sulphur content yielded from coal ranged between 0.18 to 4.61 % (Table 4.10). The high sulphur content is from samples collected on the south portion of seam 10. The amount of energy released from coal during combustion (calorific value) ranged from 3.08 to 29.28 MJ/kg (Table 4.10). The lower value of heat (3.08%) came from the carbonaceous shale. The mean value for calorific value adheres with the specifications outlined by Eskom (Table 4.10).

### 4.4.1 Proximate Analysis

#### Moisture Analysis

From the west far right portion of seam 10, moisture content in coal ranged from 2.6 to 3.4 % (air dried) with an arithmetic mean of 3.15% ad. The south portion of seam 10 moisture ranges from 0.9 (Ply G S-L) to 3.4 %ad (Table 4.10) with arithmetic mean of 2.83% ad. Both the west and south portion of the box-cut show a uniform decline in moisture content with depth (Fig. 4.21). Composite seam 10 contains more moisture than seam 11.

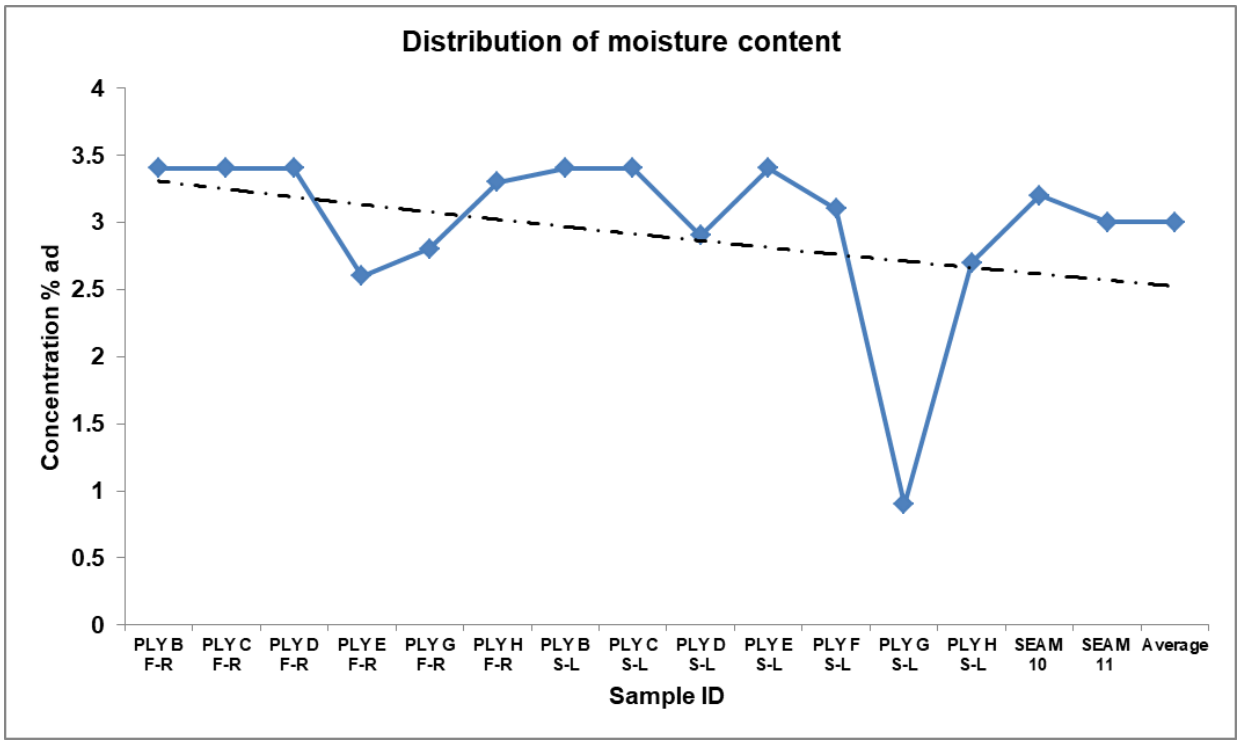


Figure 4.21: Inherent moisture content in coal from Sekoko coal mine.

**Ash Content**

The ash content of coal represents the inorganic constituent or mineral matter of coal. Following results (Table 4.9), the concentration of ash content in coal decreases with depth from Ply B (19.3 Wt% db) to D F-R (10.7 Wt% db) from the west portion of seam 10 (Fig. 4.22). The Concentration of ash content then increased exponentially from Ply D F-R (10.7 Wt% db) to Ply E F-R (38.5 Wt% db) which was then followed by a gradual decrease from Ply E (38.5 Wt% db) to H F-R (29.5 Wt% db) (Fig. 4.22). Samples from the south portion of seam 10 reported ash content of 9.5 Wt% dry basis on the top ply B S-L (Fig. 4.22). This was followed by a slight decrease in Ply C S-L. Ply D S-L underlying C S-L contains high ash content of 37.9 Wt% dry basis which then decreases to 14.1 Wt% db in H S-L (Fig. 4.22). There is no present distribution pattern of mineral matter in coal in the south portion. The elevated concentration of ash content in ply G S-L indicates that it is carbonaceous shale. The mean average value of ash content in coal from the south portion is 22.21 Wt% dry basis as compared to that of west portion which is 24.35 Wt% dry basis. Seam 10 composite (27.1 Wt% db) sample reported more ash content than the overlying seam 11 (20.9% db) this shows an overall increase in mineral matter with continuous depth (Fig. 4.22).

**Volatile Matter**

Proximate analysis results show that the volatile matter content yield (dry basis) in the west far right portion of seam 10 gradually decreases with depth from Ply B (19.5% db) to H F-R (18.2% db) (Fig. 4.22). Volatile matter content increased from Ply B to C F-R which was followed by a gradual decline to Ply H F-R. A similar pattern is observed in the south portion of seam 10 where volatile matter increases from B (30.8% db) to C (34.4% db) which was followed by a decline to 10.1% db in G S-L. The mean average volatile matter on the west far right is 21.48 % dry basis. The volatile matter on the South portion of seam 10 ranges from 10.1 (Ply G S-L) to 34.4 % db (Ply C S-L). The mean average volatile matter in the south portion of seam 10 is 26.09 Wt. % db. Ply G S-L is dominated by inorganic constituents, making up over 80%, this possibly imply that it is a carbonaceous rock. The amount of volatile matter yielded in the south is higher than the west portion of seam 10. Seam 11 composite has more volatile matter yield than seam 10, hence indicating volatile matter is decreasing with depth (Fig. 4.22).

**Fixed Carbon Content**

Tables 4.9 and 4.10 shows the results for fixed carbon content in coal in air dried, dry basis, and dry ash free basis. The dry basis and dry ash free values were used for this study. The fixed carbon content gradually decreases with depth from 61.2% db to 52.3% db from the west

portion of seam 10 (Ply B F-R to G F-R) (Fig. 4.22). The fixed carbon content is higher in the west part of seam 10 than in the south, though the difference is small. The fixed carbon content decreases overall in the south portion of seam 10 (Ply B S-L to H S-L) (Fig. 4.22). In the south portion of seam 10, fixed carbon content fluctuates from 59.7% db in Ply B S-L to a minimum of 7.7 % db in Ply G S-L (carbonaceous shale). Both seam 10 and 11 have fixed carbon content of 52.8% db (Fig. 4.22).

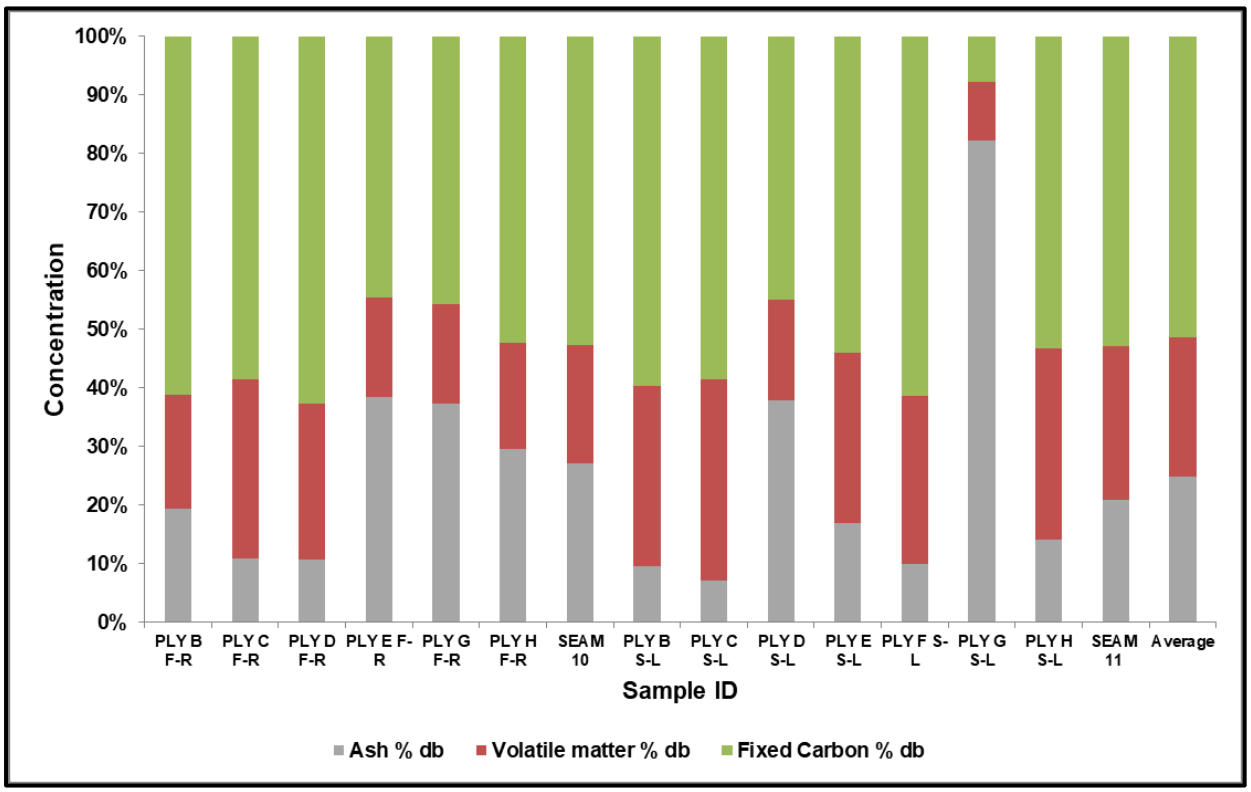


Figure 4.22: Proximate properties of coal showing the distribution of ash, volatile matter and fixed carbon content in % dry basis.

Table 4.9: Descriptive statistics for chemical and technological properties of coal (%)

| | Minimum | Maximum | Mean | SD | Eskom (Eskom, 2008) |
|---|---|---|---|---|---|
| ***Moisture (ad)*** | 0.90 | 3.40 | 2.98 | 0.64 | 10 |
| ***Ash (db)*** | 7.09 | 82.19 | 24.77 | 19.32 | 25-33 |
| ***Vm(db)*** | 10.09 | 34.40 | 23.87 | 7.26 | 20 |
| ***FC (db)*** | 7.72 | 62.68 | 51.35 | 13.47 | ND |
| ***Sulphur*** | 0.18 | 4.61 | 1.23 | 1.39 | 1 |
| ***CV*** | 3.08 | 29.28 | 22.69 | 6.86 | 21 |

Table 4.10: Chemical and technological analyses for coal samples reported in air dried, dry and dry ash free basis.

| SAMPLE ID | Proximate Analysis | | | | | | | | | Technological Properties | |
|---|---|---|---|---|---|---|---|---|---|---|---|
| | % Inherent moisture content | % Ash content | | % Volatile Matter | | | %Fixed carbon *(by calculation)* | | | % Total Sulphur | Gross Calorific Value (Mj/kg) |
| | *(air-dried)* | *(air-dried)* | *(dry basis)* | *(air-dried)* | *(dry basis)* | *(dry ash free)* | *(air-dried)* | *(dry basis)* | *(dry ash free)* | *(air-dried)* | *(air-dried)* |
| **PLY B F-R** | 3.4 | 18.7 | 19.3 | 18.9 | 19.5 | 24.2 | 59.0 | 61.2 | 75.8 | 0.34 | 24.36 |
| **PLY C F-R** | 3.4 | 10.4 | 10.8 | 29.6 | 30.6 | 34.3 | 56.6 | 58.6 | 65.7 | 1.35 | 27.91 |
| **PLY D F-R** | 3.4 | 10.4 | 10.7 | 25.7 | 26.6 | 29.8 | 60.5 | 62.7 | 70.2 | 1.23 | 27.81 |
| **PLY E F-R** | 2.6 | 37.5 | 38.5 | 16.6 | 17.0 | 27.7 | 43.3 | 44.5 | 72.3 | 0.42 | 17.48 |
| **PLY G F-R** | 2.8 | 36.3 | 37.3 | 16.6 | 17.0 | 27.2 | 44.3 | 45.7 | 72.8 | 0.41 | 18.14 |
| **PLY H F-R** | 3.3 | 28.5 | 29.5 | 17.6 | 18.2 | 25.8 | 50.6 | 52.3 | 74.2 | 0.50 | 20.36 |
| **SEAM 10 COMPOSITE** | 3.2 | 26.2 | 27.1 | 19.6 | 20.2 | 27.7 | 51.0 | 52.8 | 72.3 | 1.03 | 21.61 |
| **PLY B S-L** | 3.4 | 9.2 | 9.5 | 29.8 | 30.8 | 34.1 | 57.6 | 59.7 | 65.9 | 0.54 | 28.48 |
| **PLY C S-L** | 3.4 | 6.9 | 7.1 | 33.3 | 34.4 | 37.0 | 56.4 | 58.5 | 63.0 | 1.00 | 29.28 |
| **PLY D S-L** | 2.9 | 36.8 | 37.9 | 16.6 | 17.1 | 27.5 | 43.7 | 45.0 | 72.5 | 0.41 | 17.47 |
| **PLY E S-L** | 3.4 | 16.4 | 16.9 | 28.0 | 29.0 | 34.9 | 52.2 | 54.1 | 65.1 | 4.43 | 25.04 |
| **PLY F S-L** | 3.1 | 9.7 | 10.0 | 27.7 | 28.6 | 31.7 | 59.5 | 61.5 | 68.3 | 0.67 | 28.51 |
| **PLY G S-L** | 0.9 | 81.5 | 82.2 | 10.0 | 10.1 | 56.7 | 7.6 | 7.7 | 43.3 | 0.18 | 3.08 |
| **PLY H S-L** | 2.7 | 13.7 | 14.1 | 31.7 | 32.6 | 37.9 | 51.9 | 53.3 | 62.1 | 4.61 | 27.04 |
| **SEAM 11 COMPOSITE** | 3.0 | 20.3 | 20.9 | 25.5 | 26.3 | 33.2 | 51.2 | 52.8 | 66.8 | 1.37 | 23.78 |
| **Average** | 3.0 | 24.1 | 24.8 | 23.1 | 23.9 | 32.6 | 49.7 | 51.4 | 67.4 | 1.23 | 22.69 |

### 4.4.2 Calorific Value

The distribution of calorific value with depth is illustrated in Figure 4.23 for both samples collected from the west and south portions of the box-cut. In the west portion of seam 10 (Ply B F-R to H F-R) there is a decline in calorific values in depth from values of 24.36 to 20.36 MJ/Kg respectively (Fig. 4.23). The maximum calorific value concentration in the west side of seam 10 is 27.91 MJ/kg in Ply C F-R. Alternatively, the minimum value occurs within Ply E F-R (17.48 MJ/kg) (Fig. 4.23). Similarly, the distribution of calorific value is the same with depth in the south portion of seam 10 (Ply B S-L to H S-L) with values ranging from 28.48 to 27.04 MJ/Kg respectively (Fig. 4.23). In the south portion, the maximum concentration is 29.28 in Ply C S-L whereas the minimum value is 3.08 MJ/Kg in Ply G S-L, which is carbonaceous shale based on geochemical results.

The composite seam 11 has higher calorific value as compared to the composite seam 10 with 23.78 and 21.61 MJ/kg respectively (Fig. 4.23). Results in composite samples are in agreement with the plies, showing that the calorific value is decreasing with increasing depth.

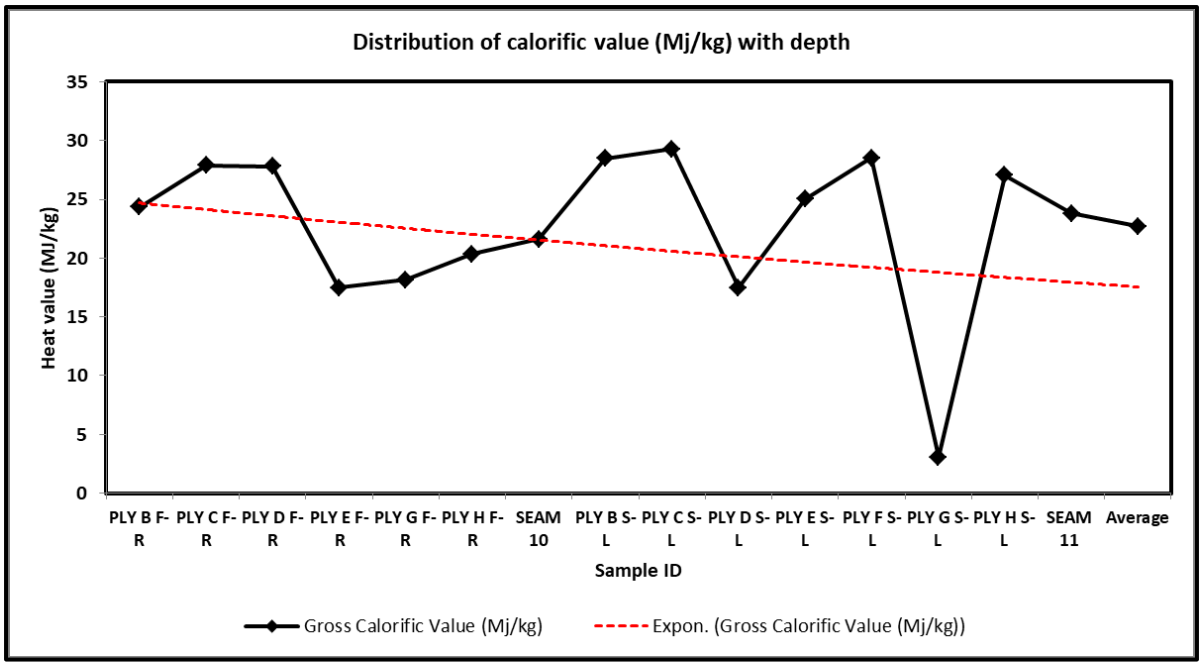


Figure 4.23: Distribution of calorific value (MJ/Kg) with depth on the west and south portions of the box-cut.

### 4.4.3 Sulphur in Coal

Table 4.9 shows the results for sulphur content in coal. Sulphur content increases from Ply B F-R (0.34 %) to Ply D F-R (1.23 %) from the west far right of seam 10 (Fig. 4.24). The sulphur content then gradually decreases to Ply G F-R. (0.50 %). In comparison to the west, the south

portion of seam 10 is sulphur enriched. Sulphur content gradually increases from Ply B S-L (0.54 %) to Ply E S-L, and ply H S-L (4.61 %) has high sulphur concentrations (Fig. 4.24). Seam 11 composite contains slightly more sulphur than seam 10 composite, being 1.37% and 1.03%, respectively (Fig. 4.24). With increasing depth, the exponential trend (Fig. 4.24) shows an increase in sulphur (Fig. 4.24).

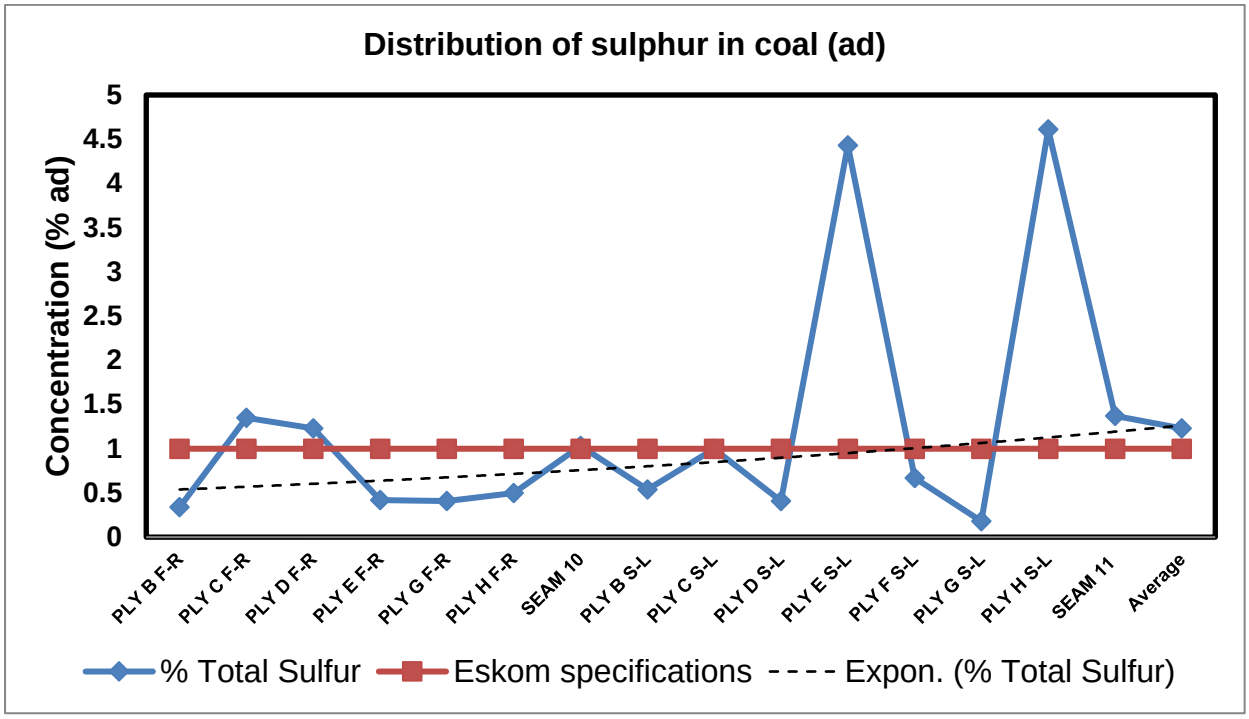


Figure 4.24: Distribution of sulphur with depth (West portion of seam 10= F-R, south portion = S-L) in coal.

**Forms of Sulphur in Coal**

Coal samples from Sekoko coal mine contain both three forms of sulphur namely; pyritic, organic and sulphate sulphur forms in their order of abundance (Table 4.11).

Table 4.11: Different forms of sulphur in coal samples from Sekoko coal mine

| Sample ID | % Pyritic Sulphur (ad) | % Sulphate sulphur (ad) | % Organic sulphur (ad) | sum |
|---|---|---|---|---|
| **Ply C F-R** | 0.7 | 0.01 | 0.64 | 1.35 |
| **Ply E S-L** | 2.68 | 0.36 | 1.39 | 4.43 |
| **Ply H S-L** | 3.33 | 0.21 | 1.07 | 4.61 |
| **Seam 10** | 0.38 | 0.46 | 0.19 | 1.03 |
| **Seam 11** | 0.56 | 0.19 | 0.63 | 1.38 |
| **Average** | 1.53 | 0.25 | 0.78 | |

Pyritic sulphur is the most abundant sulphur form in coal with an average mean of 1.53 %, a minimum and maximum concentration of 0.38 to 3.33 % respectively (Table 4.12). Organic sulphur is the second dominant form of sulphur with a minimum and maximum concentration of 0.19 to 1.39 respectively (Table 4.12). Sulphate sulphur is present in coal but in much lesser

concentrations as compared to the pyritic and organic sulphur forms. It occurs in coal at a concentration of 0.01 (minimum) to 0.46 (maximum) (Table 4.12).

Pyritic sulphur is dominant in all plies collected from the west (C F-R) and from the south portion (E and H S-L) of seam 10 (Fig. 4.25). It is exceedingly high in all samples collected from the south portion of seam 10 as compared to the west (Fig. 4.25). The composite samples (seam 10 and 11) are dominated by sulphate and organic sulphur respectively (Fig. 4.25).

Table 4.12: Descriptive statistics for forms of sulphur in coal

| | *% Pyritic sulphur (ad)* | *% Sulphate sulphur (ad)* | *% Organic sulphur (ad)* |
|---|---|---|---|
| **Minimum** | 0.38 | 0.01 | 0.19 |
| **Maximum** | 3.33 | 0.46 | 1.39 |
| **Mean** | 1.53 | 0.25 | 0.78 |
| **Standard Error** | 0.61 | 0.08 | 0.21 |
| **Standard Deviation** | 1.37 | 0.17 | 0.46 |
| **Sample Variance** | 1.88 | 0.03 | 0.21 |

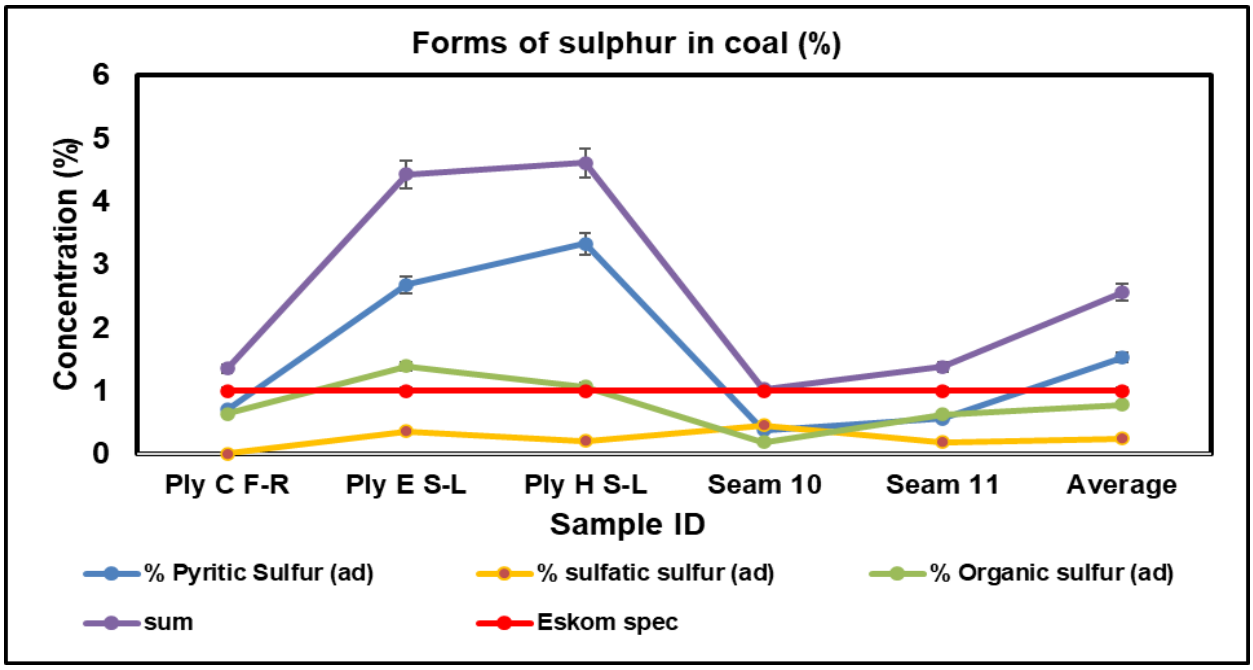


Figure 4.25: Distribution of forms of sulphur in coal from Sekoko coal mine.

## 4.5 Acid Mine Drainage Prediction

The prediction methods for acid mine water generation were the focus of this study. Paste pH, electrical conductivity, and acid base accounting tests results are indicated.

### 4.5.1 Paste pH and Electric Conductivity

Paste pH and EC were undertaken at the Earth Science Department, University of Venda, prior to acid base accounting tests. This was due to the fact that these parameters provide information of the natural acidity of samples.

The paste pH results indicate an increase in pH from Ply A F-R to shale F-R on the first day of measurement. This is followed by a sudden decline in pH from shale F-R (4.50) to ply H F-R (2.30) (Fig. 4.26). During the second day of pH measurement, both Ply A F-R and shale F-R indicate an increase in pH. This is not the case when taking into consideration ply A S-L which indicates a decline in pH over the four-day period (Table 4.13). The paste pH values are indicating a decline in pH with increasing depth on the west far right (F-R) portion of seam 10. Ply A S-L is showing an increase in pH of 4.30 as compared to ply A F-R with 3.19 (Table 4.13).

There is a decrease in pH from Ply A S-L (4.30) to C S-L (1.24). Thereafter, pH values gradually increased. Results indicate that over the four-day period, there was a significant decline in pH, particularly in the south left (S-L) portion of seam 10. Seam 11 composite contains slightly low pH values (2.22) as compared to seam 10 (Table 4.13, Fig. 4.26).

Table 4.13: Results of paste pH and EC (µs/cm) for coal and host rocks

| Date | 26/09/2022 | | 27/09/2022 | | 28/09/2022 | | 29/09/2022 | | | |
|---|---|---|---|---|---|---|---|---|---|---|
| **Site Name** | **pH** | **EC** | **pH** | **EC** | **pH** | **EC** | **pH** | **EC** | **Interpretation** | **Lithology** |
| **Ply A F-R** | 3.19 | 227 | 4.89 | 304 | 4.73 | 328 | 4.65 | 329 | Medium Risk | Gritstone |
| **Shale F-R** | 4.5 | 273 | 4.95 | 365 | 4.91 | 375 | 4.54 | 435 | Medium Risk | Shale |
| **Ply B F-R** | 3.19 | 295 | 2.77 | 486 | 2.6 | 680 | 2.55 | 576 | High Risk | Coal |
| **Ply C F-R** | 2.41 | 500 | 2.66 | 722 | 2.57 | 760 | 2.48 | 765 | High Risk | Coal |
| **Ply D F-R** | 2.27 | 1502 | 2.11 | 2180 | 2.04 | 2380 | 1.95 | 2390 | High Risk | Coal |
| **Ply G F-R** | 2.24 | 825 | 2.41 | 1183 | 2.27 | 1282 | 2.28 | 1340 | High Risk | Coal |
| **Ply H F-R** | 2.3 | 591 | 2.62 | 930 | 2.48 | 1001 | 2.43 | 1013 | High Risk | Coal |
| **Ply A S-L** | 4.3 | 772 | 3.04 | 932 | 2.9 | 1028 | 2.82 | 1042 | High Risk | Sandstone |
| **Ply B S-L** | 2.5 | 625 | 2.57 | 860 | 2.49 | 897 | 2.47 | 921 | High Risk | Coal |
| **Ply C S-L** | 1.24 | 604 | 2.66 | 886 | 2.52 | 987 | 2.47 | 999 | High Risk | Coal |
| **Ply D S-L** | 2.24 | 625 | 2.44 | 1057 | 2.31 | 1115 | 2.21 | 1185 | High Risk | Coal |
| **Ply E S-L** | 2.27 | 2440 | 1.95 | 3590 | 1.79 | 3990 | 1.77 | 4110 | High Risk | Coal |
| **Ply F S-L** | 2.02 | 1076 | 2.36 | 1559 | 2.25 | 1671 | 2.12 | 1673 | High Risk | Coal |
| **Ply G S-L** | 2.9 | 267 | 3.33 | 348 | 3.23 | 353 | 3.17 | 360 | High Risk | Coal |
| **Ply H S-L** | 2.2 | 1528 | 2.32 | 348 | 2.17 | 2220 | 2.08 | 2226 | High Risk | Coal |
| **Seam 10** | 2.45 | 1931 | 2.22 | 2100 | 2.14 | 1996 | 2.11 | 2010 | High Risk | Coal |
| **Seam 11** | 2.22 | 2970 | 1.77 | 4320 | 1.65 | 4630 | 1.63 | 1930 | High Risk | Coal |

The ability of water to conduct an electrical current is measured by its electrical conductivity. The concentration of dissolved charged chemicals in water determines the amount of electrical

current that can be conducted. The measurement of electrical conductivity (EC) showed an inverse relationship with the pH. Results for EC (Table 4.13) shows that EC is increasing exponentially from a minimum of 227 µs/cm in Ply A F-R to a maximum of 2970 µs/cm in seam 11 (Fig. 4.26). The experiment involved measuring the paste EC over a course of 4 days, the results (Table 4.13) indicate that the EC was increasing with depth from Ply A F-R (227 µs/cm) to Ply H F-R (594 µs/cm). Ply D and G F-R are indicating an elevated EC from the first day of measurement. When focusing on the South left portion of seam 10, it shows that the EC is much elevated as compared to the west far right from the first day of measurement. Although the EC in the south left portion is elevated, the trend shows a gentle decline from ply A to D S-L from day 1 to day 4 of measurement. Ply E S-L shows elevated EC values from the first day of measurement with 2240 µs/cm which then increases to 4110 µs/cm on the last day of measurement (Table 4.13). The increase in pH was also followed by an increase in electrical conductivity for samples like Ply A F-R, shale F-R, ply G S-L (Fig. 4.26).

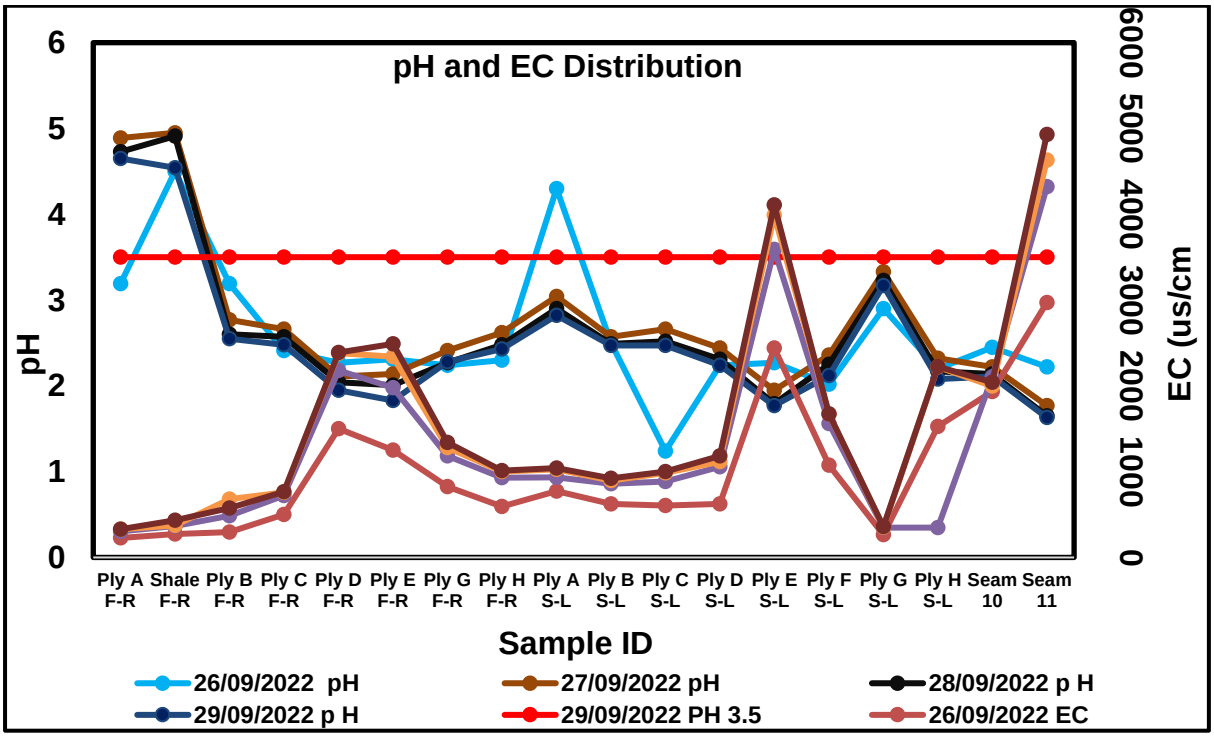


Figure 4.26: A line graph showing paste pH and EC for both coal and host rocks.

### 4.5.2 Static Acid Base Accounting

To categorize samples as acid generating or non-acid generating, total sulphur, acid generating potential, neutralizing potential, and net neutralising potential had to be determined. Table 4.14 shows the results of static acid base accounting.

#### 4.5.2.1 Acid Production Potential

The west portion of seam 10 yielded lower acid production potential with a minimum value of 5.81 kg/t in ply A F-R, maximum potential of 52 kg/t and an arithmetic mean of 19.7 kg/t (Table 4.14). The south portion of seam 10 has a higher potential for acid production with a minimum potential of 1.09 kg/t (ply A S-L), a maximum potential of 181 kg/t (ply H S-L) and an arithmetic mean of 49.58 kg/t (Table 4.14). The overall mean acid production potential is 36.14 kg/t in seam 10 plies. The potential for acid production is increasing with depth from seam 11 (61 kg/t) to seam 10 (70 kg/t). The mean acid production potential for composite samples (seam 10 and 11) is 65.5 kg/t (Table 4.14).

#### 4.5.2.2 Neutralisation Potential

Table 4.14 shows the results for neutralisation potential for all collected specimens. All specimens yielded a negative neutralisation potential values indicating that they have little to no capability to neutralise any acid that may be generated (Pinetown *et al*., 2007).

### 4.5.3 Net Neutralisation Potential

The classification used to indicate the acid generating nature (long term) of a sample is denoted by (I), whereas the intermediate (medium term acid generation) is denoted by (II), and non-acid generating is denoted by (III). According to the study's findings (Table 4.14), 13 samples (72.22%) out of 18 have a high potential for acid generation, while 5 samples (27.77%) have a moderate potential (Figure 4.27). None of the samples examined had non-acid generating potential. Negative NP values are obtained when the volume of NaOH (0.1N) titrated (pH: 8.3) is greater than the volume of HCl (1N) to reduce the pH of the sample to 2.0 – 2.5. The NNP results (Table 4.14) show that 9 of the 18 collected samples are inconclusive because they fall between +20 and -20 kg $CaCO_3$/t. Conversely, 9 samples exhibited high potential for acid generation, with NNP values as high as -190 kg $CaCO_3$/t in Ply H S-L and a mean value of -41 kg CaCO3/t (Figure 4.27). Three (37%) of eight samples from the west portion of seam 10 (Ply A -H F-R) indicate a potential for acid generation, with values of -44, -58, and -51 kg CaCO3/t for plies C,D, and E F-R, respectively. The remaining samples are inconclusive, with values ranging from -11 to -17 for plies A and H F-R, respectively.

Acid generation potential is high in samples from the south portion of seam 10 (Fig. 4.27). Four (50%) of the eight collected samples show a higher potential for acid generation when compared to the west, with values ranging from -37 to -190 for plies C and H S-L, respectively

(Fig. 4.27). The comparison of composite seams 11 and 10 (Table 4.16; Fig. 4.27) shows that seam 10 is more acidic than seam 11.

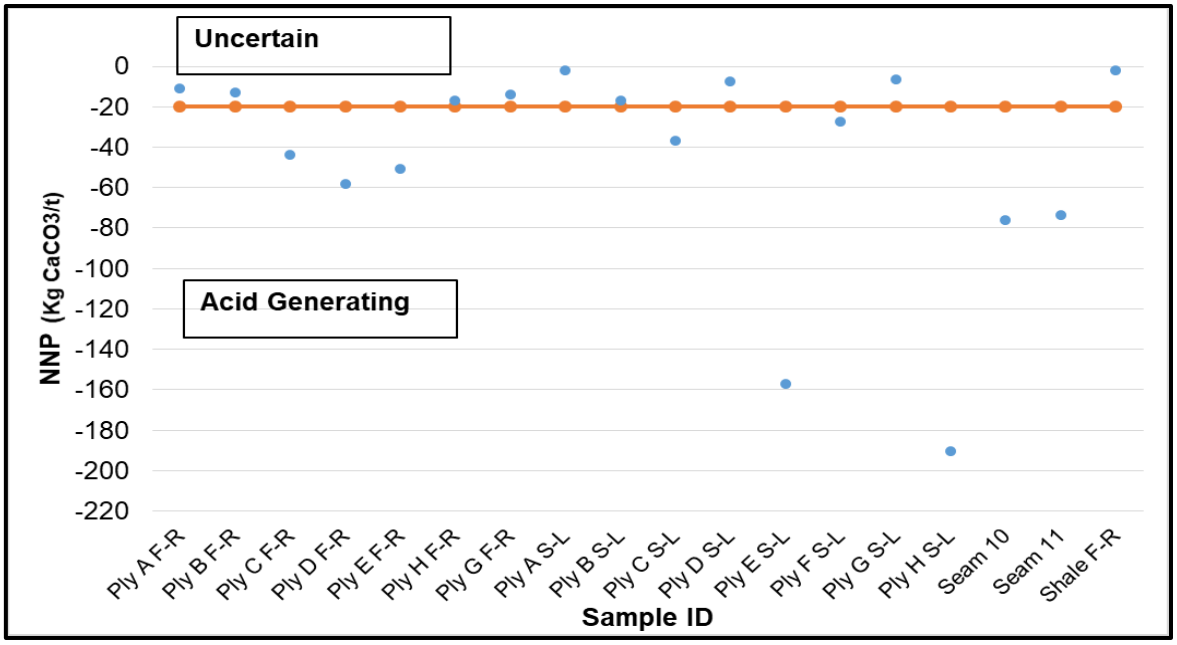


Figure 4.27: Acid mine drainage potential classification based on NNP.

Table 4.14: Static acid base accounting classification results, I (long term acid generating potential), II (Intermediate acid generating)

| Sample ID | Initial Paste pH | Total Sulphur (%) (LECO) | Acid Potential (AP) (kg/t) | Neutralization Potential (NP) | Net Neutralization Potential (NNP) | Neutralising Potential Ratio (NPR) (NP : AP) | Rock Type |
|---|---|---|---|---|---|---|---|
| **Ply A F-R** | 3.2 | 0.19 | 5.81 | -5.3 | -11 | 0.912 | II |
| **Ply B F-R** | 2.4 | 0.31 | 9.81 | -3.28 | -13 | 0.334 | I |
| **Ply C F-R** | 2.3 | 1.26 | 39 | -4.29 | -44 | 0.109 | I |
| **Ply D F-R** | 2.2 | 1.65 | 52 | -6.56 | -58 | 0.127 | I |
| **Ply E F-R** | 2.3 | 1.48 | 46 | -4.54 | -51 | 0.098 | I |
| **Ply H F-R** | 2.2 | 0.39 | 12 | -4.8 | -17 | 0.397 | I |
| **Ply G F-R** | 2.3 | 0.33 | 10 | -3.79 | -14 | 0.373 | I |
| **Shale F-R** | 4.5 | 0.04 | 1.33 | -0.76 | -2.08 | 0.568 | II |
| **Shale F-R** | 4.5 | 0.04 | 1.35 | -0.76 | -2.11 | 0.559 | II |
| **Mean F-R** | 2.88 | 0.63 | 19.70 | -3.79 | -23.58 | 0.39 | |
| **Ply A S-L** | 4.3 | 0.04 | 1.09 | -1.01 | -2.1 | 0.921 | II |
| **Ply B S-L** | 2.5 | 0.41 | 13 | -4.04 | -17 | 0.317 | I |
| **Ply B S-L** | 2.5 | 0.4 | 13 | -4.04 | -17 | 0.32 | I |
| **Ply C S-L** | 2.2 | 1.03 | 32 | -4.8 | -37 | 0.149 | I |
| **Ply D S-L** | 2.3 | 0.13 | 4.17 | -3.28 | -7.45 | 0.787 | II |
| **Ply E S-L** | 2 | 4.54 | 142 | -15 | -157 | 0.105 | I |
| **Ply F S-L** | 2.3 | 0.78 | 24 | -3.28 | -28 | 0.135 | I |
| **Ply G S-L** | 2.9 | 0.13 | 4.09 | -2.52 | -6.61 | 0.617 | II |
| **Ply H S-L** | 2.2 | 5.79 | 181 | -9.59 | -190 | 0.053 | I |
| **Mean S-L** | **2.5** | **1.59** | **49.58** | **-6.01** | **-55.65** | **0.34** | |
| **Overall Mean** | **2.7** | **1.16** | **36.14** | **-4.98** | **-41.12** | **0.358** | **I** |
| **Seam 10** | 2.2 | 2.25 | 70 | -5.55 | -76 | 0.079 | I |
| **Seam 11** | 2.1 | 1.95 | 61 | -13 | -74 | 0.207 | I |
| **Composite Mean** | **2.15** | **2.1** | **65.5** | **-9.275** | **-75** | **0.143** | |

### 4.5.4 Neutralisation Potential Ratio

Results for acid production (AP) and neutralisation potential (NP) (Table 4.14) were used to calculate the neutralisation potential ratio in open and closed system (Table 4.15). To determine the NPR in uncontrolled (open) and controlled (closed) environment, the acid production potential (Table 4.16) was multiplied by 2 to obtain values in a closed system (Price, 1997). The NPR in open system was obtained by dividing the NP by AP in Tables 4.14, results are shown in Table 5.5. The NPR in a closed system was determined following the same procedure only that, the NP was divided by AP in a closed system (Table 4.15).

The NPR results were used to generate MS Excel plot (Fig. 4.28) using 1 as a screening criterion (Price, 1997). This criterion indicates that all the values below 1 are acid generating, however, values above 1 but below 3 are categorised as inconclusive whereas values above 3 are categorised as non-acid generating (Price, 1997).

Using this criterion, all the samples (100%) in open and closed system are below the dotted line (Fig. 4.28) thus indicating that they are acid generating as indicated by the interpretation in Table 4.15. The acid generation potential on the west far right increases with depth from ply A F-R to E F-R (Fig. 4.28). The overall trend on the south left indicates that the acidity increases with depth (Fig. 4.28).

Figure 4.28 shows that all the samples fall within the acid generation range, it doesn't however, indicate the intensity of acid generation, hence, Figure 4.29 was plotted using ABACUS tool using 1:1, 2:1, and 4:1 screening criterion as indicated by Price (1997). From the 18 analysed samples, 7 (38.9%) shows a high potential for acid generation as they fall above the 1:1 ratio (Fig. 4.28). A total of 4 samples (22.22%) occur within 1:1 and 2:1 (Fig. 4.29) indicating that they possibly can generate acid on the basis that there is insufficient neutralising material (Price, 1997). The remaining 7 samples (38.9%) occur within 2:1 and 4:1 ratio (Fig. 4.29), this shows that these samples have a low potential for acid generation. The only case where acid generation can prevail is when there is a presence of reactive sulphide minerals. Following the NPR results and the screening criteria by Price (1997) none of the samples showed a potential for acid neutralisation.

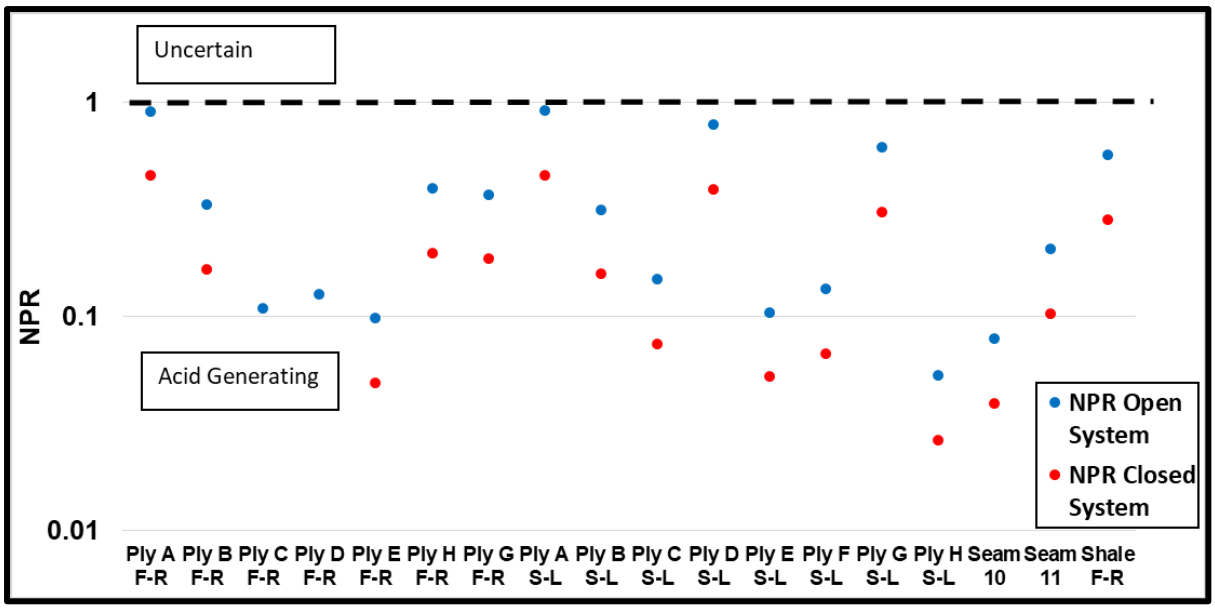


Figure 4.28: Acid mine drainage potential classification showing net neutralising ratio in open and closed system.

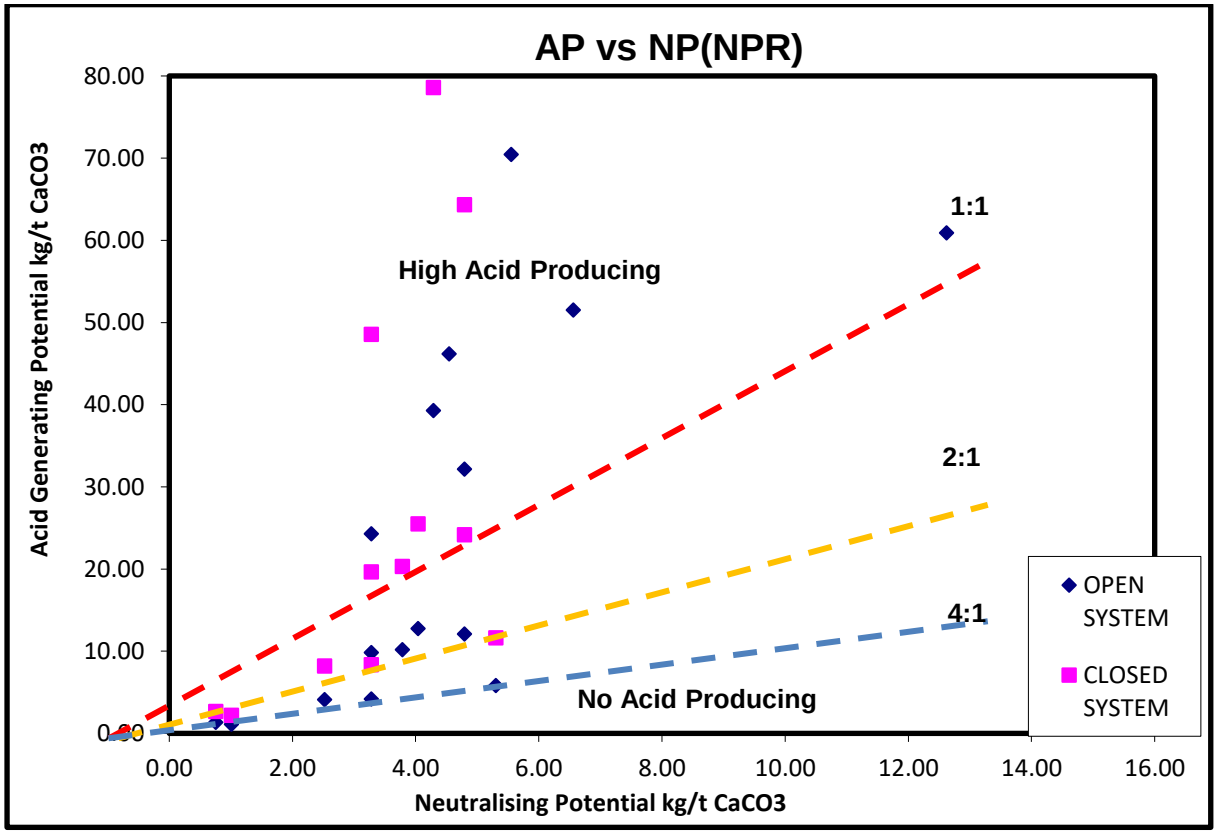


Figure 4.29: Acid mine drainage classification using AP vs NP, showing values above 1:1 as highly acid generating, between 1:1 and 2:1 as potentially acid generating, 2:1 and 4:1 showing low potential for acid generation and below 4:1 indicating no potential for acid generation.

### 4.5.5 Neutralising Potential Ratio (NPR) vs Sulphur

Results from Table 4.16 were used to generate NPR vs %s plot (Fig. 4.30). Figure 4.30 indicates that from the 18 samples, 13 (72.22%) show a potential for acid generation as they occur within the red box (below NPR of 1). The generated plot shows that 72.22% of the analysed samples have sufficient sulphur for long term acid generation (Price, 1997; Usher *et al.*, 2003). From the 18 analysed samples, 5 samples (27.8%) are in the grey area, this doesn't necessarily imply that they are uncertain, they have low sulphur content, this implies that they may generate acid water but not for a long period of time. Results generated by all the screening criterions were put together and a verdict was made (Appendices A.10). The verdict shows that 13 (72.22%) of the 18 analysed samples have a high acid production potential. Conversely, the remaining 5 (27.77%) requires the long-term kinetic tests to determine if minerals don't leach and generate acid (Usher *et al.*, 2003).

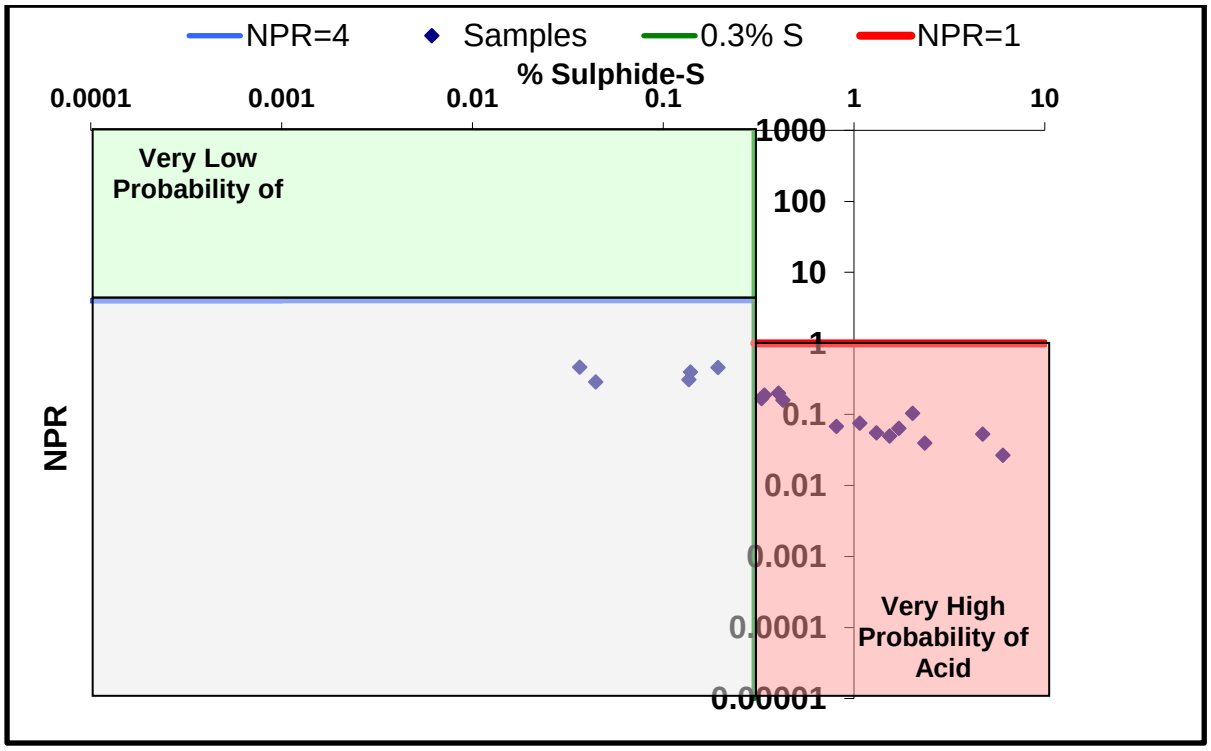


Figure 4.30: Acid mine water classification through comparison of NPR and sulphur, samples with NPR below 1 (red line) and sulphur beyond 0.3 (green line) are acid generating.

Table 4.15: NPR results with interpretations in open and closed systems

| Sample ID | AP (Open System) | AP(Closed System) | NP | NPR Open System | NPR Closed System | Interpretation Open System | Interpretation Closed System |
|---|---|---|---|---|---|---|---|
| **Ply A F-R** | 5.81 | 11.63 | -5.30 | 0.91 | 0.46 | Likely Acid Generator | Likely Acid Generator |
| **Ply B F-R** | 9.81 | 19.63 | -3.28 | 0.33 | 0.17 | Likely Acid Generator | Likely Acid Generator |
| **Ply C F-R** | 39.29 | 78.58 | -4.29 | 0.11 | 0.05 | Likely Acid Generator | Likely Acid Generator |
| **Ply D F-R** | 51.52 | 103.04 | -6.56 | 0.13 | 0.06 | Likely Acid Generator | Likely Acid Generator |
| **Ply E F-R** | 46.15 | 92.31 | -4.54 | 0.10 | 0.05 | Likely Acid Generator | Likely Acid Generator |
| **Ply H F-R** | 12.09 | 24.18 | -4.80 | 0.40 | 0.20 | Likely Acid Generator | Likely Acid Generator |
| **Ply G F-R** | 10.16 | 20.32 | -3.79 | 0.37 | 0.19 | Likely Acid Generator | Likely Acid Generator |
| **Ply A S-L** | 1.09 | 2.19 | -1.01 | 0.92 | 0.46 | Likely Acid Generator | Likely Acid Generator |
| **Ply B S-L** | 12.74 | 25.49 | -4.04 | 0.32 | 0.16 | Likely Acid Generator | Likely Acid Generator |
| **Ply C S-L** | 32.15 | 64.30 | -4.80 | 0.15 | 0.07 | Likely Acid Generator | Likely Acid Generator |
| **Ply D S-L** | 4.17 | 8.34 | 3.28 | 0.79 | 0.39 | Likely Acid Generator | Likely Acid Generator |
| **Ply E S-L** | 141.90 | 283.79 | -14.90 | 0.10 | 0.05 | Likely Acid Generator | Likely Acid Generator |
| **Ply F S-L** | 24.28 | 48.55 | -3.28 | 0.14 | 0.07 | Likely Acid Generator | Likely Acid Generator |
| **Ply G S-L** | 4.09 | 8.18 | -2.52 | 0.62 | 0.31 | Likely Acid Generator | Likely Acid Generator |
| **Ply H S-L** | 180.90 | 361.81 | -9.59 | 0.05 | 0.03 | Likely Acid Generator | Likely Acid Generator |
| **Seam 10** | 70.45 | 140.90 | -5.55 | 0.08 | 0.04 | Likely Acid Generator | Likely Acid Generator |
| **Seam 11** | 60.88 | 121.76 | -12.62 | 0.21 | 0.10 | Likely Acid Generator | Likely Acid Generator |
| **Shale F-R** | 1.33 | 2.66 | -0.76 | 0.57 | 0.28 | Likely Acid Generator | Likely Acid Generator |

# CHAPTER 5: DISCUSSION

This chapter focused on the discussion of the results. The different analyses conducted were used to determine how the collected specimens can produce acidic mine water. There are various factors that play a role in the production of acidic mine water, and these encompass a range of parameters such as mineralogy, petrography, and geochemistry, and will be discussed here following the results presented in chapter 4.

## 5.1 Mineralogy of Host Rocks and Coal

Host Rocks:

A sandstone that contains significant concentration of clay material is characterised as argillaceous sandstone (Minerals Database, 2022). De Jager (1986) indicated that there is no reported presence of sandstone layers or channels within the 70 m of the Grootegeluk coal-mudstone sequence in the Waterberg basin.

The presence of the overlying sandstone within the Sekoko coal mine could possibly imply high energy depositional environment for the host rocks. This is also evident through the presence of muscovite which indicates mechanical weathering of rocks in the source area and minimal chemical alteration (Faure, 1993). Muscovite unlike quartz and feldspar is more susceptible to chemical alteration, thus the presence of muscovite in ply A S-L indicate rapid deposition or deposition in less acidic environment (Pettijohn, 1975). Kaolinite occurs as cementing material in the sandstone as determined by petrographic studies. Clay minerals of detrital origin originate from influxes of sediment rich water (Faure, 1973). Clay minerals according to Pettijohn (1975) are the end products of chemical weathering of primary minerals, whereas quartz and feldspars are more of mechanical weathering in sedimentary rocks. This implies that the kaolinite within the sandstone was inherited from chemical weathering of the source rock under acidic and low cation activity environment as proposed by Garrels and Christ (1965); Curtis (1983) and Faure (1993).

The occurrence of K-feldspar in the gritstone (ply A F-R) also implies that deposition occurred under alkaline (less acidic) environments or possibly deposition occurred rapidly in close proximity with the source rock such that the degree of weathering was minimal. This is following that K-feldspar can easily be weathered and altered. Muscovite unlike quartz and feldspar is more susceptible to chemical alteration; the presence of muscovite indicates rapid deposition or deposition in less acidic environment.

Quartz is a residual mineral, resistant to chemical weathering, hence, the presence of quartz indicates mechanical weathering of the source rock to form the host rocks. Quartz in these specimen suggests high depositional energy environment (Faure, 1993). Tucker (2001) indicated that the origin of quartz determines its size and shape. Quartz grains in both samples revealed sub-angular to sub-rounded shape, which implies that grains were transported from a distal crystalline source rock. Quartz grains from pre-existing sedimentary rocks tend to be more rounded while those from the original crystalline rocks are characterised by angular shapes (Tucker, 2001). The roundness of rock fragments is chiefly due to the transport medium and distance of transportation. Since this specimen (Shale F-R) is dominated by kaolinite (clay) that forms in acidic and low cation activities (Curtis, 1983; Faure, 1993), the quartz could have been introduced in the shale as stream and/or wind deposit as suggested by Renton (1982). Faure (1993) reported that the upper portion of the Grootegeluk Formation is more alkaline and less acidic, this possibly imply that the shale lithology was formed through deposition of sediments from a distal source rock.

Coal Mineralogy:

A substantial portion of the Grootegeluk and Swartrant Formations consists of mudstones and sandstones respectively. The mineral matter present within these Formations is most likely to be present in the underlying coal beds but at much lesser concentrations. Coal samples are dominated by three mineral phases, namely; kaolinite, quartz and pyrite in their order of abundance. Renton (1982) explained that the clay within some coal beds may be of vegetal chemical origin formed from aluminosilicate materials contained within plants in the swamp. However, the elevated concentration of kaolinite in coal suggests that it is of detrital origin. K-feldspar was chemically altered from the source rock which was distal from the depositional environment to form kaolinite as a secondary mineral (Faure, 1993). The selected coal samples contain significant pyrite concentration which may cause acid mine drainage, particularly the south portion of seam 10 with 9.40 Wt% in Ply H S-L. Pyrite possibly formed at more or less the same time with coal through deposition of iron into the peat swap which then gets reduced by sulphate-reducing bacteria into pyrite (Taylor and Macquaker, 2011).

## 5.2 Geochemistry of Host Rocks and Coal

Major Oxides of Host Rocks:

Baiyegunhi *et al.* (2017) stated that clastic sedimentary rocks contain information about the composition as well as the evolution of the continental crust. When normalised against Taylor and McLennan (1985) UCC values (Fig. 5.1), the $SiO_2$ content for all samples is above 1 indicating that they are enriched in silica content (Taylor and McLennan, 1985). The

concentration of $Al_2O_3$ is also moderate to high ranging from 7.89 to 23.48 Wt %. When normalised against the UCC values of Taylor and McLennan (1985), only shale F-R is enriched in $Al_2O_3$ whereas others are depleted (Fig. 5.1). The concentration of $TiO_2$ for all samples with the exception of shale F-R were depleted (Fig. 5.1), when normalised against the UCC values, all samples were deficient of $Fe_2O_3$ with a ratio less than 0.20 (Fig. 5.1). Ply A F-R (Gritstone) is the only specimen enriched in $P_2O_5$.

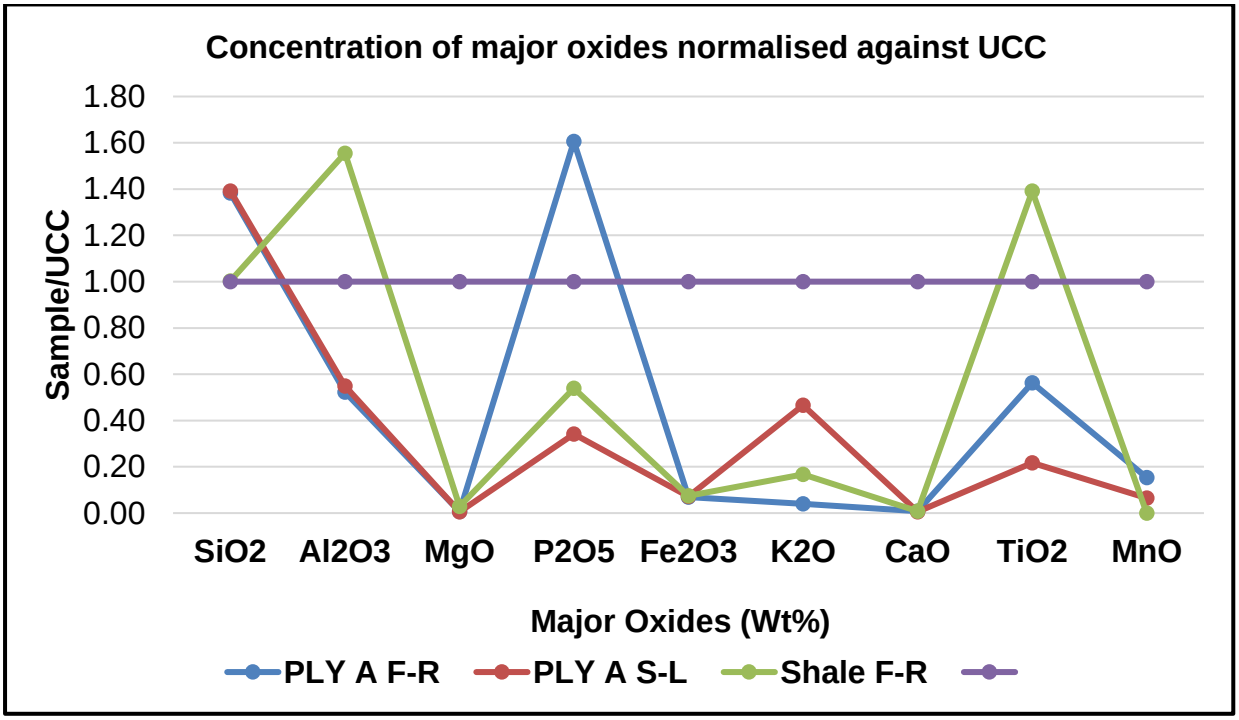


Figure 5.1: Spider plot of major oxides in clastic sedimentary rocks normalised against UCC values after Taylor and McLennan (1985).

Coal oxide ratio:

The coal oxide ratio of $SiO_2/Al_2O_3$ yields values ranging from 2.62 to 10.78 and 1.50 to 3.08 for host rock and coal respectively (Tables 5.1; 5.2). According to Yossifova *et al.* (2009); Zhao *et al.* (2015) and Ameh (2019), low values of $SiO_2/Al_2O_3$ imply that coal was deposited under stable conditions. This concurs with the findings of Snyman (1998) who indicated that majority of the coal seams in South Africa were deposited under stable conditions. Alternatively, the host rock material may have been deposited under unstable conditions as the $SiO_2/Al_2O_3$ ratio is higher compared to that of coal. Harnois (1998); McLennan *et al.* (1993) and Chen *et al.* (2016) indicated that Al and Ti cannot be easily mobilised by weathering hence, $Al_2O_3$ and $TiO_2$ in source rocks are preserved. The oxides ratio of $Al_2O_3/TiO_2$ in clastic sedimentary rocks ranges from 20.60 to 56.08 with a mean value of 33.83 (Table 5.1) while in coal it ranges from 12.95 to 29.59 and has a mean value of 23.74 (Table 5.2).

Chen *et al.* (2016) elucidated that $Al_2O_3/TiO_2$ as a discrimination criterion to distinguish different types of source rocks. They further indicated that $Al_2O_3/TiO_2$ ratio of 3 to 8 with $SiO_2$ (45.52%) is for mafic igneous rocks, 8 to 21 with SiO2 (53 to 66%) is for intermediate igneous rocks and 21 to 70 with $SiO_2$ (66 to 76%) for felsic igneous rocks. The ratio of $Al_2O_3/TiO_2$ for host rocks ranges between 20.60 and 56.08 (Table 5.1) while coal samples ranges from 12.95 to 29.59 with an average value of 23.74 (Table 5.2). This could possibly imply that intermediate to felsic igneous rock was the source rock of the detrital sediments in coal and host rocks.

Several authors have proposed indices of weathering. These include the chemical index of alteration (CIA), the chemical index of weathering (CIW) and plagioclase index of alteration (PIA). Chemical index of alteration (CIA) as proposed by Nesbitt and Young (1982) is a good measure of the intensity of weathering and can be obtained by calculation (Equation 22):

$$CIA= [Al_2O_3/(Al_2O_3 + CaO + Na_2O + K_2O] * 100 \quad \text{Equation (22)}$$

According to Nesbitt and Young (1982) and Baiyegunhi *et al.* (2017) the CIA value provides a measure of the ratio of primary and secondary minerals such as clay. Fresh unaltered alibite, anorthite and potassic feldspar has CIA value of 50 whereas diaposide has a value of 0. Fresh basalt sample ranges between 30 and 45 in CIA values, whereas granite and granodiorite have much higher values ranging between 45 and 55 (Nesbitt and Young, 1982). Muscovite samples give a value of 75 while illite ranges between 75 and 85. They further indicated that kaolinite and chlorite have CIA values close to 100. Following the results of this study, the CIA value ranges between 97.19 and 99.43 with an average value of 98.72 for coal (Table 5.2), whereas for host rock it ranges between 87.82 to 98.27 (Table 5.1). This implies that there was high degree of chemical weathering in the source area for minerals in coal and host rocks. The high values of CIA indicate high presence of clay mineral and absence of detrital feldspars. This concurs with the findings of this study as kaolinite is present as a secondary mineral.

The Chemical index of weathering (CIW) can be determined by calculation as proposed by Harnois (1988) (Equation 23):

$$CIW= [Al_2O_3/ (Al_2O_3+CaO + Na_2O)] *100 \quad \text{Equation (23)}$$

The chemical index of weathering also indicates the degree of weathering in the source area. According to Harnois (1988), the CIW index is superior because it includes a limited number of components that are known to have consistent geochemical behaviour during weathering. The CIW values for the host rocks and coal studied range from 99.46 to 99.81, with an average mean of 99.63 (Table 5.1), and from 98.92 to 99.94, with an average mean value of 99.61

(Table 5.2). These CIW values for both host rock and coal samples indicate that the source rock had experienced extensive chemical weathering.

Plagioclase index of alteration (PIA) was proposed by Fedo *et al.* (1995) and can be determined by calculation (Equation 24):

$$PIA= [(Al_2O_3 –K_2O)/Al_2O_3 + CaO + Na_2O – K_2O)] * 100 \quad \text{Equation (24)}$$

According to Fedo *et al.* (1995) and Baiyegunhi *et al.* (2017), the PIA determines the progressive weathering of feldspars to form clay minerals. Fully altered feldspars have a PIA value of 100, whereas weathered plagioclase has a PIA value of 50. According to the findings of this study, the PIA values for both host rocks and coal range between 99.46 and 99.80, with a mean value of 99.61 (Table 5.1), and between 98.90 and 99.94, with a mean value of 99.60 (Table 5.2). These findings point to intense weathering of feldspars to form clay minerals like kaolinite. Because the concentration of kaolinite is slightly high, these results agree with the mineralogy of the collected samples.

Table 5.1: Major oxides ratio for clastic sedimentary rocks

| Sample ID | $SiO_2/Al_2O_3$ | CaO/MgO | Cao + MgO/$K_2O$ +$Na_2O$ | $Al_2O_3/TiO_2$ | CIA | PIA | CIW |
|---|---|---|---|---|---|---|---|
| **PLY A-F-R** | 10,78 | 1,82 | 0,29 | 20,60 | 98,27 | 99,46 | 99,46 |
| **PLY A-S-L** | 10,31 | 1,43 | 0,05 | 56,08 | 87,82 | 99,57 | 99,62 |
| **SHALE F-R** | 2,62 | 0,43 | 0,31 | 24,82 | 98,13 | 99,80 | 99,81 |
| **Mean** | 7,91 | 1,23 | 0,21 | 33,83 | 94,74 | 99,61 | 99,63 |

Table 5.2: Major oxides ratios for coal samples

| Sample ID | $SiO_2/Al_2O_3$ | CaO/MgO | Cao + MgO/$K_2O$ +$Na_2O$ | $Al_2O_3/TiO_2$ | CIA | PIA | CIW |
|---|---|---|---|---|---|---|---|
| **PLY B-F-R** | 1,80 | <0.01 | 0,01 | 29,29 | 99,43 | 99,89 | 99,89 |
| **PLY C-F-R** | 1,82 | <0.01 | 0,02 | 15,52 | 98,40 | 99,43 | 99,43 |
| **PLY D-F-R** | 1,72 | <0.01 | 0,02 | 26,37 | 98,81 | 99,26 | 99,26 |
| **PLY E-F-R** | 1,95 | 0,33 | 0,44 | 23,82 | 99,21 | 99,90 | 99,90 |
| **PLY F-F-R** | 1,83 | 0,29 | 0,53 | 27,09 | 99,25 | 99,90 | 99,90 |
| **PLY G-F-R** | 1,79 | 0,56 | 0,59 | 25,45 | 99,28 | 99,82 | 99,82 |
| **PLY B-S-L** | 1,61 | <0.01 | 0,01 | 28,85 | 98,74 | 99,57 | 99,58 |
| **PLY C-S-L** | 1,69 | 2,23 | 0,25 | 20,68 | 97,19 | 99,02 | 99,04 |
| **PLY D-S-L** | 1,50 | 0,20 | 0,46 | 29,22 | 99,26 | 99,94 | 99,94 |
| **PLY E-S-L** | 1,59 | <0.01 | 0,02 | 13,65 | 97,98 | 99,45 | 99,46 |
| **PLY F-S-L** | 1,83 | <0.01 | 0,01 | 21,91 | 98,71 | 99,60 | 99,61 |
| **PLY G-S-L** | 3,08 | 0,42 | 0,42 | 12,95 | 99,29 | 99,90 | 99,90 |
| **PLY H-S-L** | 1,71 | 2,02 | 0,35 | 26,64 | 97,27 | 98,90 | 98,92 |
| **SEAM 10** | 1,81 | 1,37 | 0,40 | 25,07 | 98,91 | 99,63 | 99,64 |
| **SEAM 11** | 1,72 | 0,89 | 0,31 | 29,59 | 99,11 | 99,81 | 99,81 |
| **Mean** | 1,83 | 0,92 | 0,26 | 23,74 | 98,72 | 99,60 | 99,61 |

Major Oxides of Coal from Sekoko Mine:

The major oxides and trace elements present in coal form part of its inorganic constituents (Wagner *et al.*, 2018; Ameh, 2019). These major oxides and trace elements may also be part of coal organic constituent through authigenic or biogenic processes (Ward, 2016). The presence of such inorganic constituents in coal indicates that they were sourced chiefly from terrigenous origin. Furthermore, the abundance of $Al_2O_3$ (Tables 4.2) could imply that there was surplus detrital material in the peat as well as high degree of weathering of source rock (Ameh, 2019). Minerals containing aluminium are typically produced by the weathering of rocks containing aluminium, such as granites or shales, on land. Due to the presence of aluminium oxide, it is likely that surrounding rocks or terrestrial sources of sediment input had an impact on the coal-forming environment (Taylor *et al*., 1998). The $Al_2O_3$ in coal samples is from the kaolinite mineral determined through XRD. Coal in this area could have formed in freshwater or low salinity conditions. This agrees with the findings of Finkelman (1994) who indicated that the enrichment of $Al_2O_3$ in coal indicates that coal deposition was influenced freshwater sources. Ward (2002) further elaborated that the abundance of $Al_2O_3$ also indicates oxidizing environment for coal deposition as the presence of oxygen supports the weathering and oxidation of aluminium rich minerals to form aluminium oxide.

The terrestrial origin of inorganic matter in coal is also supported by the dominant occurrence of $SiO_2$. This is supported by Taylor *et al*. (1998), Kalkreuth (2004) and Ward (2016) whose findings indicated that enriched $SiO_2$ in coal indicates terrestrial origin. Ward (2016) further elaborated that inorganic matter in coal may also be from authigenic or vegetal origin. The collected coal specimens also reveal the presence of $Fe_2O_3$. This iron oxide may be derived from pyrite which according to Ward (2016) contains (Fe) and (S). Taylor *et al*. (1998) indicated that pyrite can get oxidised and produce $Fe_2O_3$. This further support the freshwater depositional environment as well as the elevated oxygen level to support the oxidation of pyrite.

## 5.3 Coal Petrology

The prevalence of inertinite in coal offers indications regarding the conditions of the coal-forming processes as well as the paleoenvironment in which the plants grew. It provides ideas about the prevailing environmental circumstances during coal formation by pointing to the presence of particular plant species or groups that were more resistant to deterioration and preservation (Diessel, 1992). Coal with a greater inertinite content likely contains plant matter that is more resistant to decay and breakdown (Scott, 2009). The presence of vitrinite is a reflection of the preservation of woody tissues and a sign that trees and shrubs with lignin-rich structures were present in the prehistoric environment (Taylor *et al*., 1998). Coal from Sekoko coal mine has vitrinite reflectance ranging between 0.593 to 0.752 (% $RoV_{mr}$). A reflectance value of 0.7 indicates that the coal has been subjected to extreme heat and pressure, which is frequently linked with deep burial or tectonic activity as indicated by Taylor *et al.* (1998). Lower liptinite content in coal may indicate a higher rank or degree of thermal maturity. Liptinite macerals are more vulnerable to thermal alteration, this implies that as coal receives increasing heat and pressure during coalification, this would have resulted in decreased liptinite concentration (Scott, 2009).

## 5.4 Coal Quality

Proximate Analysis:

Coal from Sekoko coal mine meets the requirements for utilisation in South African power stations. The moisture content in the analysed coal specimens is below the rejection specification of 10 % (Eskom, 2008, Steyn and Minnit, 2010). The ratio of coal quality value by Eskom requirements yielded 0.30 for moisture content, this further shows that moisture content is lower in coal. Low inherent moisture in coal indicates that coal will yield increased heat values (ASTM, 2018). The maximum requirement for ash content is coal ranges between

25 -33 % db (Table 5.3), the rejection value for ash content in coal is above 35 % (Steyn and Minnit, 2010). The analysed ash content has mean value of 24.77 % db which does not exceed the rejection values stipulated by Eskom (2008). Following the ASTM D388 (1997) coal from Sekoko coal mine can be classed as bituminous coal and it can be grouped as high volatile A bituminous coal as the fixed carbon is less than 69 % daf and the volatile matter content is greater than 31 % daf on average (Table 4.9; ASTM D388, 1997).

Table 5.3: Comparison of coal quality with Eskom requirements for utilisation

| | Min | Max | Mean | SD | Eskom (2008) | Mean/Eskom |
|---|---|---|---|---|---|---|
| **Moisture (ad)** | 0.9 | 3.4 | 2.98 | 0.64 | 10 | 0.30 |
| **Ash (db)** | 7.09 | 82.19 | 24.77 | 19.32 | 25 | 0.99 |
| **VM (db)** | 10.09 | 34.4 | 23.87 | 7.26 | 20 | 1.19 |
| **FC (db)** | 7.72 | 62.68 | 51.35 | 13.47 | ND | ND |
| **Sulphur** | 0.18 | 4.61 | 1.23 | 1.39 | 1 | 1.23 |
| **CV (Mj/kg)** | 3.08 | 29.28 | 22.69 | 6.86 | 21 | 1.08 |

Sulphur in Coal:

The average or mean concentration of sulphur in coal is 1.23 %, which is above 1.00% of the required specification for utilization by Steyn and Minnitt (2010). Coal from the Sekoko coal mine contains more sulphur than the average sulphur concentrations in the Waterberg coalfield (0.99%) (Wagner *et al.*, 2018). According to Gilligan (1986) and Greenshields (1986), the sulphur content of the Free State and Ermelo coal fields is slightly higher than that of the Sekoko coal mine, with 1.4 and 1.3%, respectively. Coal from Sekoko coal mine within the Waterberg coalfield exceeds the 0.40 to 1.29 % from the Highveld coalfield as specified by Wagner and Hlatshwayo (2005). The mean concentration of sulphur at Sekoko coal mine (1.23%) is higher than the documented average of 0.9% in the Waterberg Coalfield as indicated by Wagner *et al.* (2018).

Caloric Value:

The overall mean value of the amount of heat yielded (calorific value) in Mj/kg is 22.69 (Table 5.3). The ratio of mean value of CV (Mj/kg) with Eskom requirements is 1.08 (Table 5.3). This shows that coal from Sekoko Coal mine meet the requirements for utilisation as it exceeds the minimum CV of 21 Mj/kg (Steyn and Minnitt, 2010). The mean CV value of 22.69 Mj/kg indicates that this this coal can yield significant amount of heat energy when combusted

making it suitable for energy production (Moazzem *et al*., 2012). Following Steyn and Minnitt (2010), coal from Sekoko coal mine can be classified as below grade D, using proximate values and calorific value.

Calorific value and ash content have a strong negative correlation, with an $R^2$ of 0.9957 (Fig. 5.2). Figure 5.2 depicts the dependence of calorific value on ash content, demonstrating that as ash content (mineral matter) increases, the heat value yielded during coal combustion decreases (Wagner *et al.*, 2018). Ply G S-L contains more than 80% ash (mineral matter), but the calorific value drops to less than 5 Mj/kg; hence, it can be classified as a carbonaceous rock. The linear regression equation in Figure 5.3 shows a positive correlation between fixed carbon and calorific value of coal from Sekoko coal mine. Figure 4.18 shows $R^2$= 0.9031 indicating a very strong correlation. This implies that an increase in fixed carbon will be accompanied by increase in calorific value.

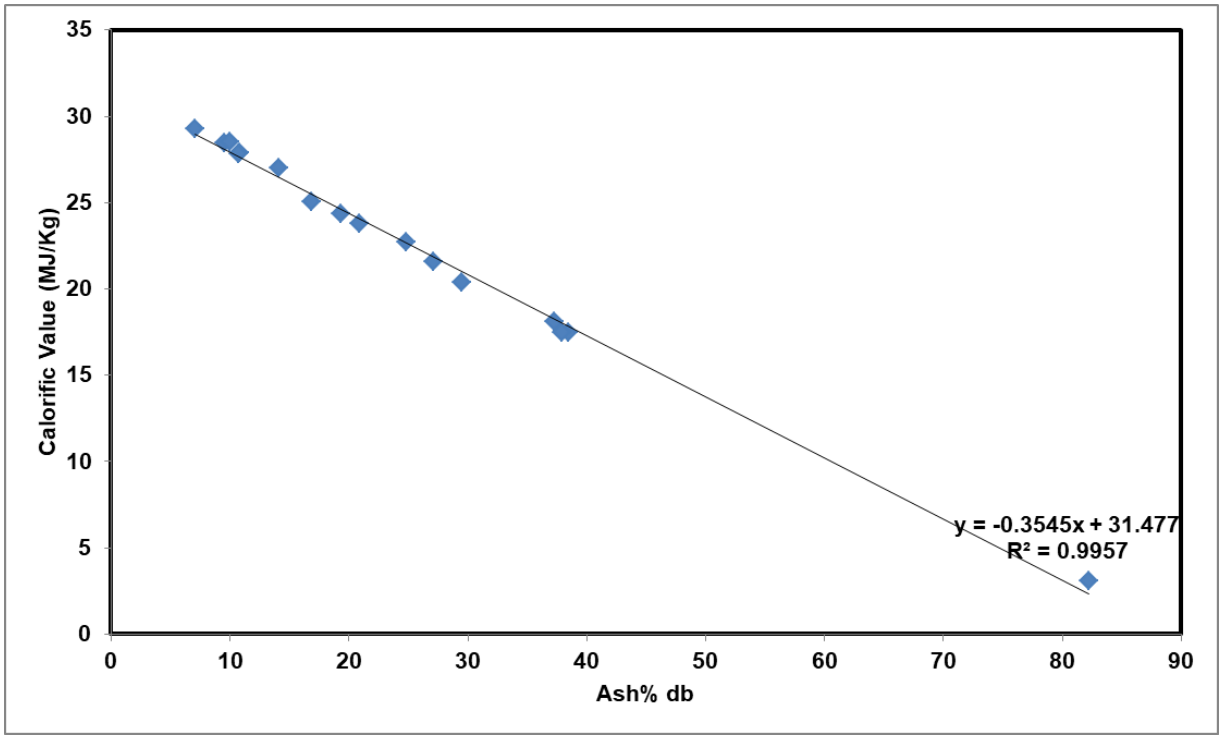


Figure 5.2: Strong Negative relationship between Calorific value (MJ/Kg) and ash content (% d.b).

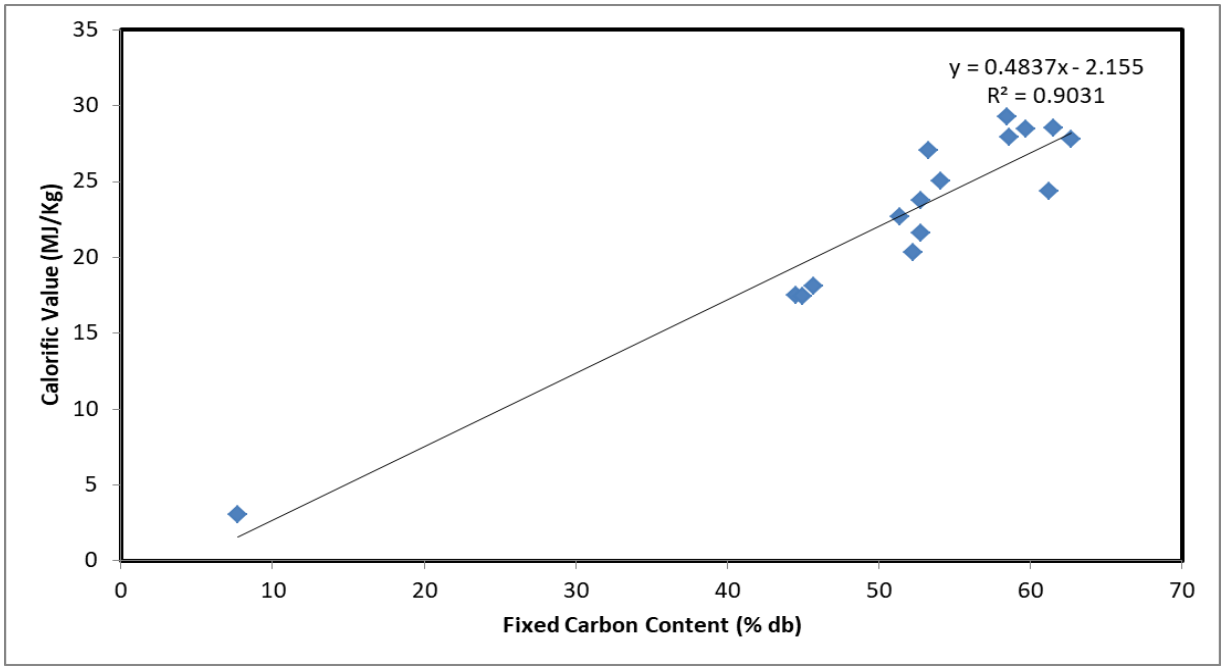


Figure 5.3: Strong positive relationship between calorific value (Mj/kg) and fixed carbon content (% d.b).

## 5.5 Potential for Acid Mine Water Mine Generation

Paste pH and Electrical Conductivity:

Interpretation on whether the sample is acid generating or not was given based on whether the pH was above or below 5 and 3.5 as indicated by Usher (2003) and Thwala (2020) respectively. From the 18 samples tested, all samples yielded paste pH below 5 whereas 16 samples were below 3.5 (Table 4.14). Based on the screening criteria by Usher (2003) of 3.5, 88 % of these samples have a potential for acid generation (all coal samples except the host rocks).

The increase in pH in ply A F-R and shale F-R could be from the dissolution of oxides such as (CaO and MgO) as seen from whole rock geochemistry results (Table 4.2). The oxide minerals in these samples occur in less quantity which explains why the pH started to gradually decrease from day 3 to 4. When checking the exponential trend, it shows that pH is decreasing from the west far right portion to the south left portion of seam 10 indicating that the south left portion has a greater potential for acid generation compared to the west far right.

Acid Mine Water Generation Potential:

Coal from Sekoko coal mine has a great potential to generate acidic mine water. The NNP of over 72% of the collected specimen exceed -20 kg $CaCO_3$/t indicated by (Price, 1997; Usher *et al.*, 2003). The coal is more acidic than the overlying host rocks as supported by Deysel

(2015) who indicated that the upper part of the overlying rock formations of the Grootgeluk Formation are less likely to generate acid when compared to the coal.

Implications of Geochemistry on Acid Mine Water Generation:

The geochemical characteristics of host rocks and coal can affect how acidic mine water forms. The oxide of interest is particularly the iron oxide as it has a relationship with the pyrite determined through XRD. Pinetown *et al*. (2007) indicated that correlation between $Fe_2O_3$ and acid production is insignificant as the major source of $Fe_2O_3$ in the Highveld coalfield is siderite. However, this is not the case at Sekoko coal mine. Figure 5.4 shows a strong positive correlation between APP and $Fe_2O_3$. This correlation is significant because pyrite is the source of $Fe_2O_3$. This evident through X-Ray diffraction spectroscopy results, which shows that pyrite is the only mineral with iron detected. This relationship shows that an increase in $Fe_2O_3$ will cause an increase in acid production potential. Geochemistry results also reveal trace amounts of oxides and carbonates. This explains why the neutralisation potential for all specimen was negative. This signifies that there is little carbonates to neutralise the acid that may be produced by these rock units. The decrease in pH with depth can be linked with the increase in $Fe_2O_3$ with depth as established by geochemical analysis. The decrease of pH with depth is most likely due to an increase in hydrogen ($H^+$) ions caused by hydrolysis of $Fe^{3+}$ and $Al^{3+}$ as indicated by (Masindi, 2015). The increase in EC in these samples is more likely related to the hydrolysis of cations like $K^+$ and $Mg^+$ as supported by Miraj *et al.* (2017). The EC in the south left portion of seam 10 exceeds 600 µs/cm (WHO, 1984). Hence, indicating that the effluents and leachates from the pit can cause server surface and groundwater pollution.

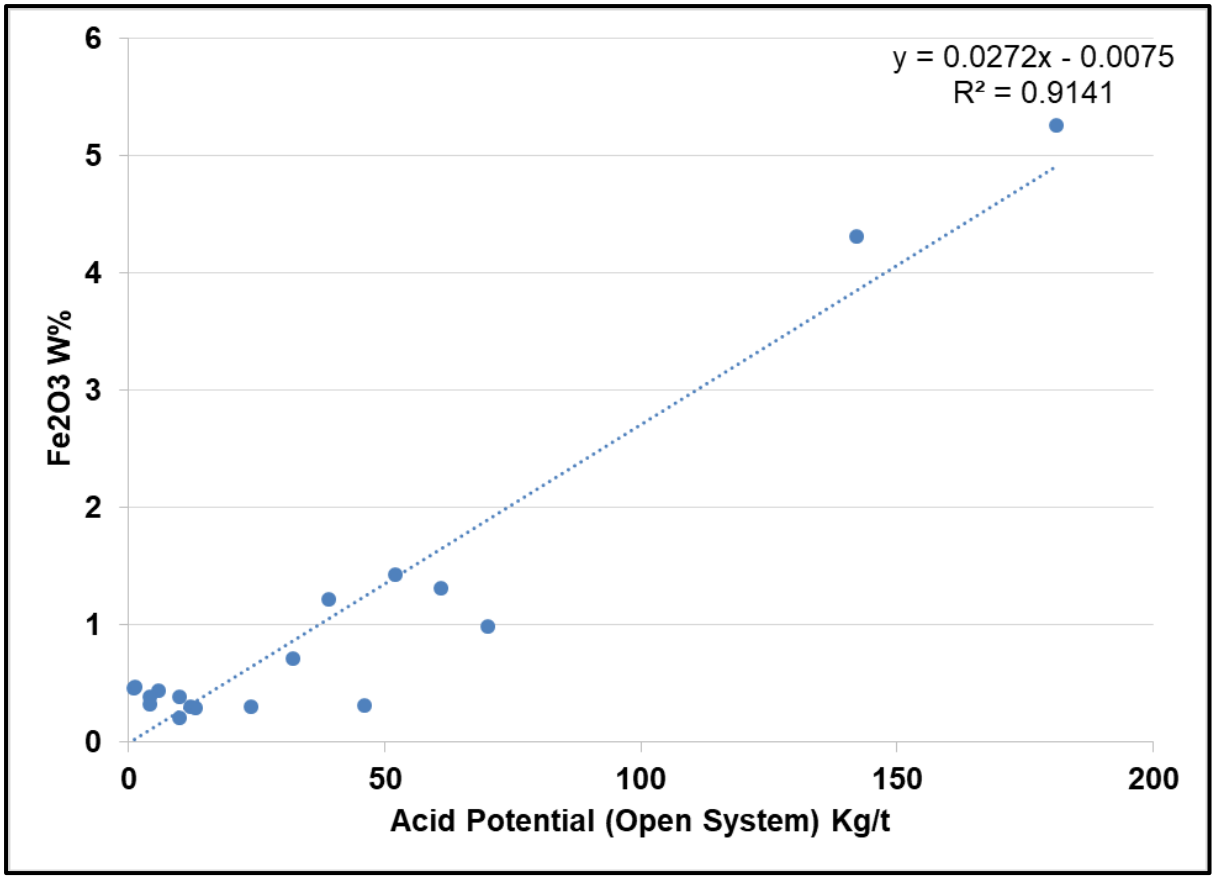


Figure 5.4: Strong positive relationship between acid potential (open system) and $Fe_2O_3$, showing the dependency acid production potential on $Fe_2O_3$.

Implication of Organic Matter on Acid Mine Water Generation:

This study also investigated the relationship between macerals and pyrite and how this influences acid mine water generation. The relationship between organic matter of coal and sulphur content was investigated by Roberts (1988). The study investigated the relationship between macerals and sulphur content of South African Permian coals. Roberts (1988) indicated a positive correlation between vitrinite macerals and sulphur, in contrast, there was a negative correlation between inertinite and sulphur content. The results of this study indicates that a positive correlation with $R^2$=0.6251 was established between vitrinite and sulphur (Fig. 5.5). This concurs with the increase in vitrinite with depth, as an increase in pyrite with depth is also witnessed. The high sulphur content in vitrinite macerals is due to rise of water levels in the swamp which causes an increase in pH and decrease in Eh, hence promoting anaerobic bacterial activities (Roberts, 1988). Smyth (1970) indicated that rise in water levels causes variations in redox potential in peat forming environments. In contrast, Figure 5.6 shows a negative correlation between inertinite and total sulphur in coal. This concurs with the findings of Roberts (1988). Stach *et al.* (1975) and Casagrande *et al.* (1976)

further elucidated that inertinite macerals formed when the water table was low, with high redox potentials influenced by oxygen respiration organisms.

Although the result of this study concurs with the findings of Roberts (1988) it is important to note that correlation between macerals and sulphur content works better when the depositional setting (syngenetic and epigenetic) of pyrite is known. Organic petrology results indicate pyrite grains occurring restrictively within cracks and vitrinite. This suggests that certain pyrite deposits may have formed simultaneously with organic matter (syngenetic), while pyrite observed within cracks indicates an epigenetic origin due to periodic seawater flooding following peat formation.

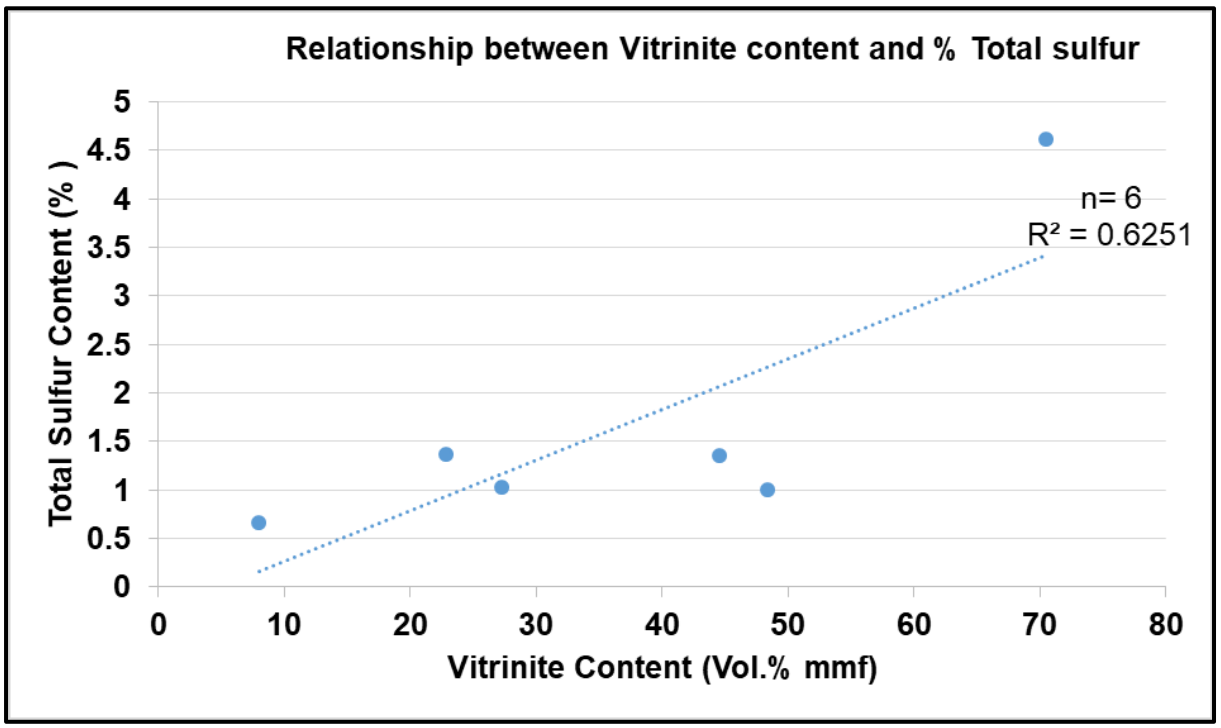


Figure 5.5: Positive relationship between vitrinite content and total sulphur.

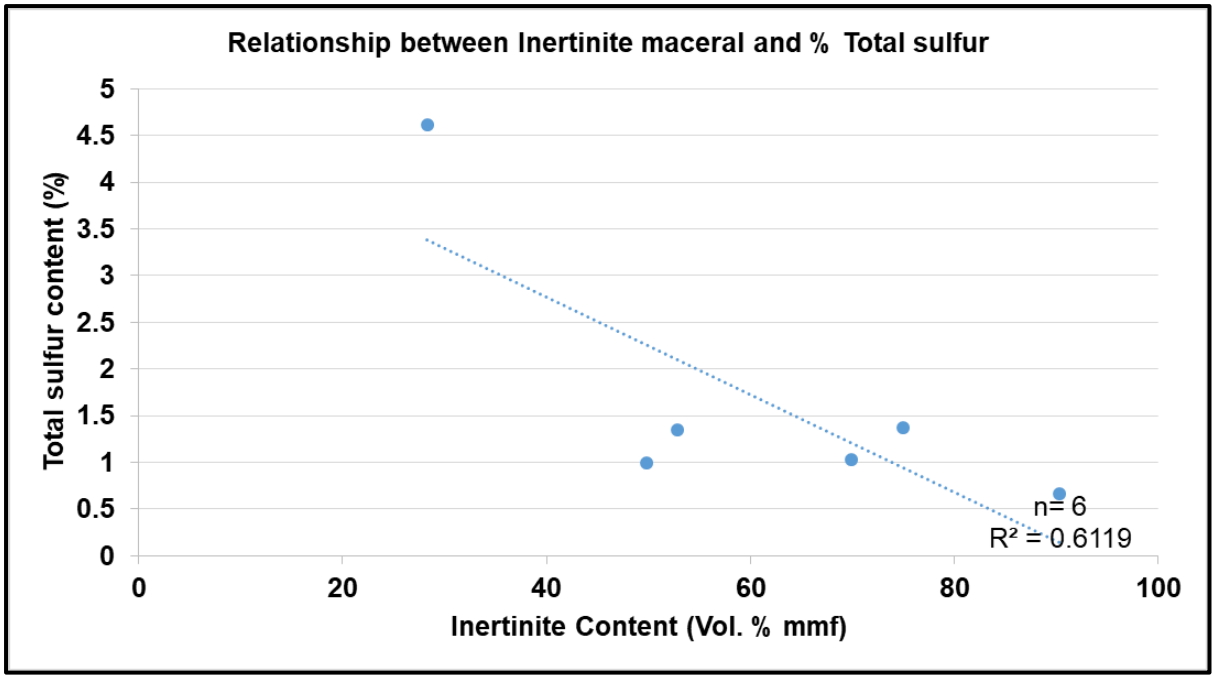


Figure 5.6: Negative relationship between inertinite macerals and total sulphur.

Implication of Mineralogy on Acid Mine Water Generation:

The formation of acidic mine water is substantially influenced by the makeup and properties of the minerals found in host rocks and coal. When exposed to air and water, different minerals have different capacities to produce acidity. According to Robertson *et al.* (2015), mineralogical and geochemical data can be utilised to anticipate environmental concerns. Sulphuric acid is produced when pyrite ($FeS_2$) is exposed to oxygen and water (Nengovhela *et al*., 2006; Udayabhanu and Prasad, 2010). The preliminary acid production potential (APP) was calculated using the Abates V. 1.4 estimation tool (Table 5.4). This was achieved because some minerals, such as pyrite, can produce more sulphuric acid than their original mass (Earth Systems, 2012). When 1 kg of pyrite undergoes oxidation, it can generate 1.63 kg of sulphuric acid using the balanced Equation 25.

$4FeS_2 + 15O_2 + 8H_2O \rightarrow 2Fe_2O_8 + 8H_2SO_4$ Equation (25)

4 mol 8 mol

4 x 120 g (mass) 8 x 98 g

1000 g of pyrite generates $\frac{8\ X\ 98}{4\ X120}\ X\ 1000$ = 1.63 kg $H_2SO_4$

This tool is used to provide a preliminary acid generating and neutralising potential, but it doesn't eliminate results from acid base accounting and kinetic tests. The assumptions of the program are as follows:

- The mineralogy is in weight percentage.
- All reactions have undergone complete reaction (which is difficult to achieve in a natural environment).
- The iron (Fe) in sulphide minerals has been oxidized to ferric iron ($Fe^{3+}$).

Earth Systems (2012) and Fey (2003) also elucidated that whenever the acid production potential exceeds 20 kg/tonne of rock, the material is most likely to generate acid. In contrast, where the neutralising potential is below 20 kg/tonne, the material is unlikely to generate acid. Net neutralisation values between – 20 and 20 indicate inconclusive results which need further testing using other methods.

To calculate the acidity generated by each sulphide mineral, the number of moles of sulphuric acid generated from the sulphide mineral (pyrite) were calculated following Equation 26. Thereafter, the mass of sulphuric acid generated was calculated following Equation 27 (Earth Systems, 2012). Results of preliminary acid production potential are indicated in Table 5.6.

$$FeS_2 + 15/4O_2 + 7/2H_2O \rightarrow Fe(OH)_3 + 4H^- + 2SO_4 \quad \text{Equation (26)}$$

$$\text{Acidity} = \frac{((\text{mass of mineral}) \text{x} (\text{mol mass of H2SO4})) \; x \; no. \; of \; mol \; of \; \text{H2SO4 generated}}{\text{molar mass of mineral}} \quad \text{Equation (27)}$$

Table 5.4: Potential for acid production potential from quantitative mineralogy using Earth Systems' ABATES V.1.4 program

| Sample ID | Wt % of sulphide minerals (pyrite) | Mass of $H_2SO_4$ (kg/tonne rock) | Acid Producing Potential (APP) |
|---|---|---|---|
| **Ply E S-L** | 6.90 | 112.82 | Likely to generate acid |
| **Ply H S-L** | 9.40 | 153.69 | Likely to generate acid |
| **Ply C F-R** | 1.30 | 21.26 | Likely to generate acid |
| **Seam 10** | 1.30 | 21.26 | Likely to generate acid |
| **Seam 11** | 1.10 | 17.99 | Additional tests through Static acid base accounting required. |

Results from ABATES tool indicates that there is a greater likelihood of acid generation from selected coal samples. Plies H and E collected from the south left (S-L) part of seam 10 yielded extremely high concentrations for acid generating potential of 153.69 and 112.82 kg/tonne

respectively. Ply C collected from the west far right (F-R) part of seam 10 does have a potential for acid generation, but at much lower concentrations as compared to the south left samples (Price, 1997). Composite sample from seam 10 has a great potential for acid generation as compared to the overlying seam 11. Most sulphide minerals are commonly (pyrite) known for generating acid when exposed to oxygen and water (Nengovhela *et al.*, 2006).

Pyrite is particularly common because of its ability to generate sulphuric acid twice it's mass. Abates tool uses sulphides and carbonates minerals to determine the acid generating potential of samples. The mineralogy of the selected samples only shows pyrite as the only sulphide mineral. Through chemical equations from Abates tool, pyrite was used to investigate the acid generating potential of selected coal samples. The results from Abates V. 1.4 indicate coal samples from Sekoko coal mine are most likely to generate acid. The lithology from the roof (clastic sedimentary rocks) doesn't have any pyrite or sulphide mineralization which concurs with the findings by Deysel (2015) that overburden materials are less likely to generate acid. However, additional methods from acid base accounting are required to ensure accuracy of the results as these tests takes precedents on the mineralogical estimation.

The south portion of seam 10 can generate a combined mass of sulphuric acid of 266.51 kg/tonne of coal. Compared to the south portion, the west portion of seam 10 is less acidic with a mass of sulphuric acid of 21.26 kg/tonne (Table 5.4). Ply C F-R does exceed 20 kg/tonne indicating that it is a likely generator of acid just like the composite seam 10 (Table 5.4). This concurs with the screening criteria by Usher *et al.* (2003). The mass for seam 11 composite varies between -20 and 20 kg/tonne, indicating that further analysis using acid base accounting methods is required. Mineralogically, there are no carbonate minerals in both coal and clastic rock samples, hence the neutralisation potential is assumed to be zero, however, further analysis using static acid base accounting is required.

Although quantitative mineralogy was used to calculate the influence of pyrite (Wt %) on acid production potential (Table 5.4), it is important to know how these preliminary findings differ from the acid production potential determined through ABA tests. Figure 5.18 shows the relationship between acid production potential (APP) generated using mineralogy and APP in open system generated by acid base accounting. A strong positive relationship between APP (mineralogy) and APP (open system) was established with an $R^2$=0.9628. This simply shows that mineralogy can be used to give a preliminary understanding of the acid generating nature of samples as it has a strong relationship with acid production potential generated through static acid base accounting tests.

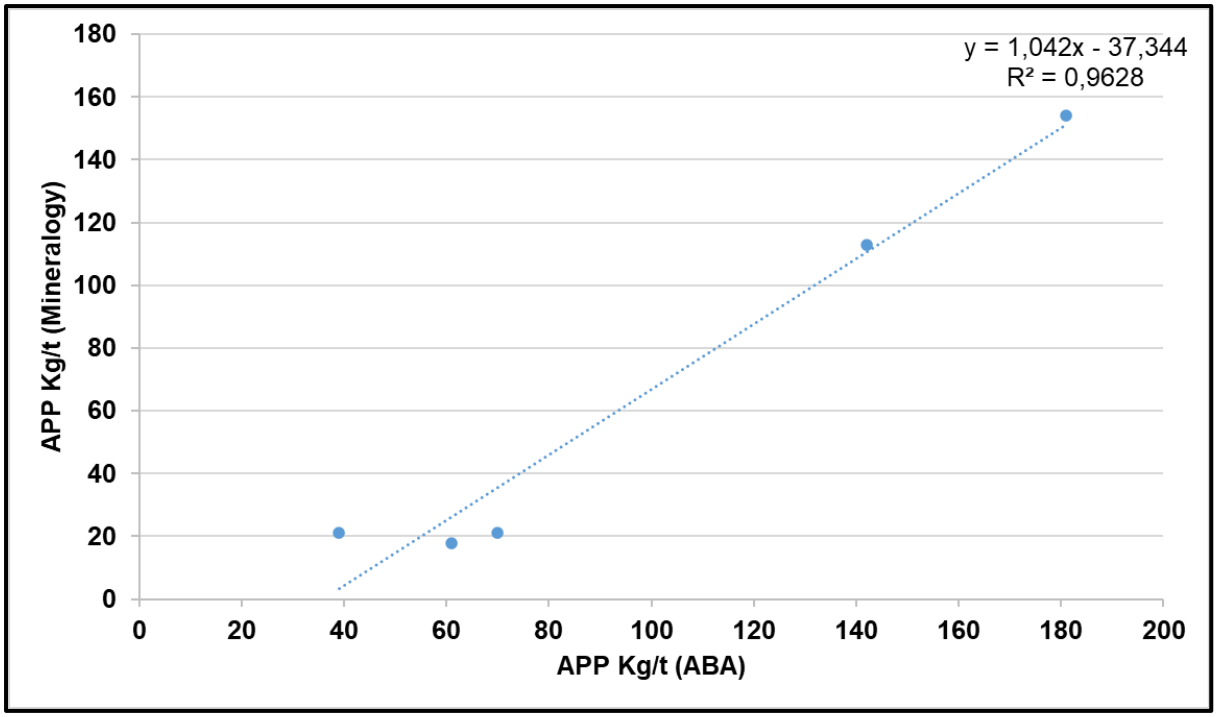


Figure 5.7: Strong positive relationship between acid production potential (Mineralogy) and acid production potential (ABA).

Form of Sulphur and Its Influence of Acid Mine Water Generation:

The production of acidic mine water is also dependent on the type of sulphur present in coal. Sulphur in coal occurs in three forms namely, pyritic, organic and sulphate sulphur. Pyritic sulphur is the dominant form of sulphur, and it is more elevated in the south portion of the box-cut. The west portion does contain pyritic sulphur but based on the field conditions some of it might have been weathered to form elemental sulphur (yellow stains). The correlation matrix (Table 5.5) of forms of sulphur with acid production potential shows a strong positive correlation between pyritic sulphur and acid production potential. This concurs with the findings by several authors such as Caruccio and Geidel (1978); Caruccio *et al.* (1981); Casagrande *et al.* (1989) and Deysel (2015) who elucidated that pyrite is the primary source of acid mine water generation in coal mines. The organic sulphur also has a strong positive correlation with both acid production potential and pyritic sulphur (Table 5.5).

Organic sulphur had been concluded to be a potential contributor in acid generation (Frederick *et al.*, 1957; Schnitzer and Fransway, 1982; Dollhoph and Russell, 1984; Fisher and Munshower, 1984). However, Casagrande *et al.* (1989) in their experimental laboratory tests indicated that organic sulphur is a non-participant in acid generation. This was later supported by Skousen (1995) that organic sulphur is not chemically reactive, thus has no effect in acid production potential.

Sulphate sulphur occurs in lower quantities in coal from the Sekoko coal mine. The presence of sulphate sulphur may be due to the weathering or oxidation of pyritic (sulphide) sulphur as indicated by Skousen (1995). Since sulphate sulphur is a reaction product of pyritic sulphur, it is a non-participant in acid generation. This concurs with the findings of this study as the sulphate sulphur has a weak positive correlation with the acid generation potential (Table 5.5).

Table 5.5: Pearson correlation matrix of sulphur forms and acid generation potential

| | *% Pyritic Sulphur* | *% sulphate sulphur* | *% Organic sulphur* | *APP (kg/tonne)* |
|---|---|---|---|---|
| **% Pyritic Sulphur** | 1.00 | | | |
| **% sulphate sulphur** | 0.07 | 1.00 | | |
| **% Organic sulphur** | 0.86 | -0.08 | 1.00 | |
| **APP (kg/tonne)** | 0.99 | 0.13 | 0.90 | 1.00 |

A perfect positive correlation between total sulphur and acid production potential with $R^2$=1 is shown in Figure 5.8. Leco analysed sulphur concurs with the acid production potential (open system). This relationship simply implies that an increase in sulphur will be followed by an increase in acid production potential. This concurs with the findings of Pinetown *et al*. (2007). It is important to note that an increase in sulphur (pyritic) will cause an increase in acid generation as the correlation study above shows that pyritic sulphur is the dominant participant in acid mine water generation.

The abundance of sulphur in coal is largely controlled by the degree of seawater influence during peat accumulation and post-depositional changes (Chou, 2012). The abundant sulphur in coal from Sekoko coal mine implies that there was either partial inundation of seawater into the peat mire or the seawater flooded the peat swamp after it was deposited (White, 1913; Chou, 2012). Sulphur could have been introduced into the peat through seawater sulphate during and after the early stages of diagenesis and thereafter diffused into the peat and was then reduced by bacteria into hydrogen sulphide, polysulphide, and elemental sulphur. The reason behind this is that the major oxides ratio for coal indicates that coal was deposited in a quiet depositional environment. Hydrogen sulphide would have reacted with ferrous iron to produce pyrite crystals and mackinowite, which would then react with elemental sulphur to produce greigite and framboidal pyrite (Chou, 2012).

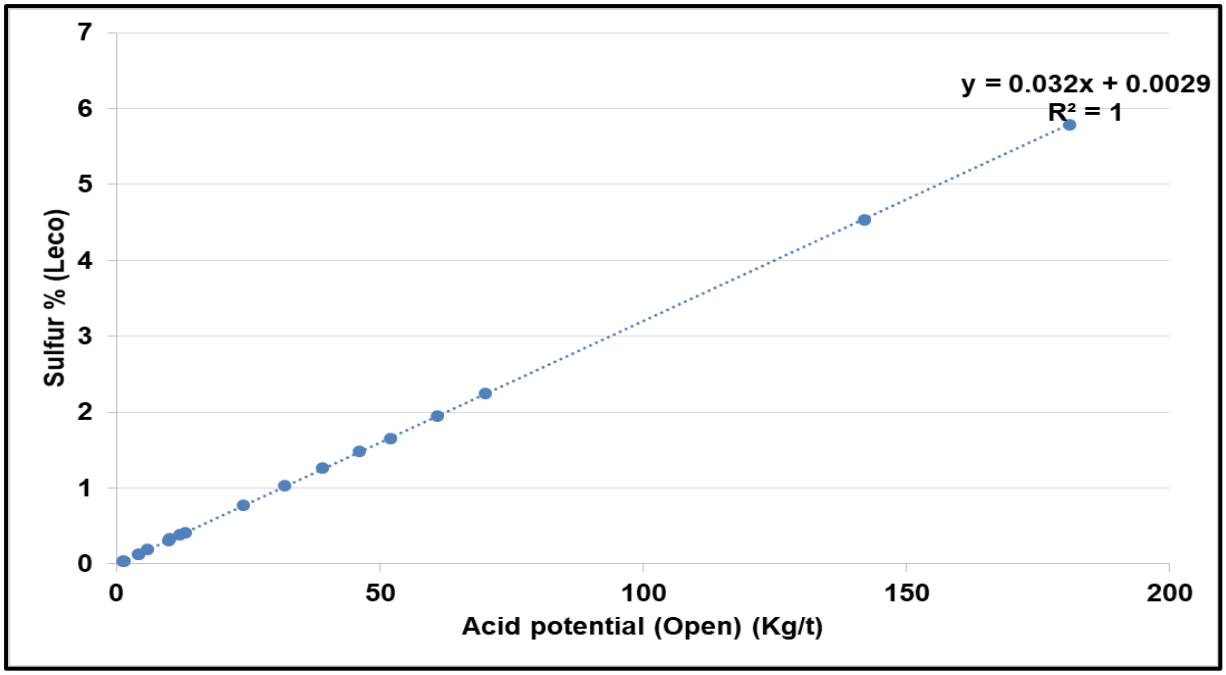


Figure 5.8: A perfect positive relationship between total sulphur and acid production potential (open system) showing the dependency of acid production on sulphur content.

Influence of Pyrite Morphology on Acid Mine Water Generation:

The rate of acid generation is influenced by several factors including the proportion of sulphides and carbonate minerals, their morphology, the surface area of minerals as well as the mineral dissemination (Evangelou, 1998; Maiyana, 2003). The morphological analysis of coal provides useful insights on the physical features of pyrite such as the existence of etching and weathering. All these analysed specimens reveal that the presence of framboidal pyrite. This section focused on sulphides (pyrite) because there is no significant presence of carbonates minerals as shown by XRD results. Framboidal crystal structure (first defined by Rust, 1935) is found in deformed grains. Weber *et al*. (2004) reported that framboidal pyrite grain is more reactive than euhedral forms. They further elucidated that this is influenced by the greater specific area of framboidal pyrite. According to Maiyana (2003) euhedral pyrite grains are less susceptible to weathering because they are formed with minimal instability. This implies that framboidal pyrite can easily oxidise and generate acid mine water. This appears to be the case with coal collected for this study.

Scanning electron microscopy microphotographs indicate that framboidal pyrite is the dominant morphology of pyrite. Pyrite grains exceed 1 µm (as seen from the scale of photomicrographs) and mainly occur in a disseminated manner as opposed to the array of closely packed pyrite crystals proposed by Love and Amstutz (1966). The oxidation of pyrite causes disintegration of its morphology. This possibly explains the disseminated occurrence

of pyrite in coal. The framboidal pyrite shows signs of oxidation as etching can be seen in the analysed microphotographs.

Shamshuddin *et al.* (2004) conducted SEM-EDX analyses to investigate the oxidation of pyrite. The study outlines that un-oxidised pyrite has a ratio of 1:2 (Fe:S). Pyrite that is oxidised or is undergoing oxidation will have an increase in iron (Fe) to sulphur (S) ratio. This concurs with the findings of this study. The ratio of Fe:S is indicated in Table 5.6 and it shows that there is oxidation of pyrite as the ratio of Fe:S is below 1:2. Table 5.6 shows an increase in oxidation of pyrite with increasing depth. This is evident through the decrease in sulphur and increase in iron (Fe) in the ratio with depth (Ply E S-L to H S-L and Seam 11 to Seam 10).

Table 5.6: Fe:S ratio to assess oxidation of pyrite

| Sample ID | Mean Fe (%) | Mean S (%) | Fe:S ratio |
|---|---|---|---|
| **Ply C F-R** | 2.95 | 3.21 | 1 : 1.43 |
| **Ply E S-L** | 2.7 | 3.48 | 1 : 1.29 |
| **Ply H S-L** | 1.76 | 2.23 | 1 : 1.26 |
| **Seam 11** | 0.48 | 0.95 | 1 : 1.98 |
| **Seam 10** | 1.33 | 1.18 | 1 : 0.88 |

# CHAPTER 6: CONCLUSIONS AND RECOMMENDATIONS

This chapter focused on the study's findings and recommendations for corrective and mitigating actions to address the identified environmental problems.

## 6.1 Conclusions

The purpose of the research was to determine the acid mine water generation potential of the Sekoko coal mine lithostratigraphy within the Waterberg coalfield. The overall outcome of the study shows that coal has a potential for long-term acid generation whereas host rock has low potential for acid generation. The following conclusions are reached.

- The coal studied contains significant concentrations of pyrite with minimum and maximum concentrations of 1.10 and 9.40 Wt % respectively. The south portion of seam 10 contains more pyrite than the west portion. Mineralogical and optical studies of host rock revealed no evidence of pyrite. In addition, no carbonate minerals were found in host rocks and coal.
- Pyrite is abundant in coal, from seam 11 to seam 10, the concentration of pyrite increases with depth. Scanning electron microscopy revealed that pyrite in coal has a framboidal morphological structure. Because of this it is more susceptible to weathering and oxidation, framboidal pyrite exhibits etching. The Fe:S ratio indicates that pyrite is being oxidized with increasing depth.
- The results of X-ray fluorescence spectroscopy show that coal is enriched in $Fe_2O_3$, with a mean concentration of 1.18 Wt%. However, host rocks are depleted in $Fe_2O_3$, with a mean concentration of 0.45 Wt%.
- The ratio of major oxides in both coal and host rocks indicates that deposition occurred under stable conditions. Furthermore, the chemical index of alteration, plagioclase index of alteration, and chemical index of weathering indicate that the source rock was severely weathered. Based on the Plagioclase index of alteration, kaolinite occurs as a secondary mineral as a by-product of chemical weathering. The $Al_2O_3/TiO_2$ ratio demonstrates that the detrital material in both coal and host rocks came from a felsic to intermediate rock.
- Proximate analyses show that the moisture content of coal is low (2.98) and within Eskom's specified maximum of 10%. Pearson's correlation matrix reveals that fixed carbon content and calorific value have a strong positive relationship (0. 95). This simply means that an increase in fixed carbon content is accompanied by an increase in coal heating value. Ash content and calorific value have a perfect negative correlation (-1). Both volatile matter and fixed carbon content have a strong negative relationship with ash

content. This translates to an increase in calorific value, fixed carbon, and volatile matter with decreasing ash content.

- Coal from the Sekoko coal mine in the Waterberg coalfield is classified as medium sulphur coal with an average sulphur content of 1.53%. The mean concentration of total sulphur in coal exceeds Eskom's specified requirement of 1.00%, but it is also below the 2.00% rejection range. According to the results of the sulphur form analysis, pyritic sulphur is the dominant form of sulphur, followed by organic sulphur and, at much lower concentrations, sulphate sulphur. The sulphur in coal is most likely caused by sulphate-rich seawater flooding of the peat mire on occasion.
- The average amount of heat produced (calorific value) in MJ/Kg was found to be 22.69. The average value meets the recommended value of 21 MJ/Kg for domestication of South African coal. Sekoko coal falls below grade D in terms of proximate and calorific value.
- According to organic petrology, coal is dominated by inertinite macerals, specifically inert semifusinite. According to a mean random reflectance study, coal from the Sekoko coal mine can be classified as medium rank bituminous C with potential applications as soft coking coal. Pyrite is abundant within cracks, indicating epigenetic deposition. Pyrite grains are present with vitrinite macerals, indicating a syngenetic deposition. When compared to total sulphur, vitrinite macerals have a strong positive correlation, whereas inertinite has a negative correlation. This relationship works best when the depositional environment of pyrite is the same as that of coal (syngenetic).
- The initial measurement of paste pH and EC shows that coal underwent oxidation because the initial pH was less than 3.5. Acid can be produced by coal and host rock samples. The revealed that NNP values were less than - 20 kg $CaCO_3$. The neutralisation potential ratio (NPR) showed that coal has a potential to generate acid.
- The results of static acid base accounting were supported by a correlation of acid production potential with total sulphur, sulphur forms, and $Fe_2O_3$ concentrations. Pyritic sulphur has a strong positive correlation with acid production potential (0.99. This implies that pyritic sulphur is the primary contributor to acid formation. With $R^2$=1, there is a strong positive correlation between sulphur and acid production potential.

- Iron oxide ($Fe_2O_3$) was found to have a strong positive correlation with acid production; it is more likely that the $Fe_2O_3$ concentration is related to pyrite. The high acid production potential and negative neutralising potential led to the conclusion that there aren't enough carbonates to buffer the acid produced. The acid production potential generated through quantitative mineralogy has a strong positive correlation with the acid production potential generated through acid base accounting with $R^2$=0.9628. This shows that quantitative

mineralogy can be used to give preliminary results on the acid generating nature of host rocks and coal.

## 6.2 Recommendations

Following the results, this study recommends:

- Further testing the material using the long period kinetic tests.
- Using phreeQC to simulate the oxidation and weathering of pyrite to determine its state and form.
- Drastic modelling to determine groundwater vulnerability to the acid mine water generated.
- Screening and washing of coal prior utilization can help improve coal quality.

## REFERENCES

Agarwal, A., and Narain, S. 1991. Global Warming in an Unequal World. *International Sustainable Development*. Vol.1, pp. 98-104.

Akcil, A., and Koldas, S. 2006. Acid Mine Drainage (AMD): Causes, Treatment and Case Studies. *Journal of Cleaner Production*, Vol. 14, pp. 1139-1145.

Alberts, B.C. 1982. The Planning and Establishment of the Grootegeluk Coal Mine. *Journal of South African Institute of Minerals and Metallurgy*, Vol. 82 (12), pp. 341-352.

Ameh, E.G. 2019. Geochemistry and Multivariate Statistical Evaluation of Major Oxides, Takcrace and Rare Earth Elements. In: Coal Occurrences and Deposits around Kogi East, Northern Anambra Basin, Nigeria. *International Journal of Coal Science and Technology*, Vol. *6* (2), pp. 260-273.

American Society for Testing and Materials (ASTM). 1997. Standard Classification of Coals by Rank, Method D388. Annual Book of ASTM Standards, Vol. 5(5), Gaseous Fuels, Coal and Coke, pp. 225-230.

American Society for Testing and Materials. 2018. ASTM D5865/D5865M-18: Standard Test Method for Gross Calorific Value of Coal and Coke. ASTM International.

Andrew, M.W. 2004. Standard Operating Procedure for X-ray Fluorescence Analysis of PM2.5 Deposits on Teflon Filters. Environmental and Industrial Measurements Division Research Triangle Institute. Research Triangle Park. North Carolina. 16p.

Baiyegunhi, C., Liu, K. and Gwavava, O. 2017. Geochemistry of Sandstones and Shales from the Ecca Group, Karoo Supergroup, in the Eastern Cape Province of South Africa: Implications for Provenance, Weathering and Tectonic Setting. *Open Geosciences*, Vol. *9*(1), pp. 340-360.

Bangert, B., Stollhofen, H., Lorenz, V., Armstrong, R. 1999. The Geochronology and Significance of Ash-Fall Tuffs in the Glaciogenic Carboniferous–Permian Dwyka Group of Namibia and South Africa. *Journal of African Earth Sciences*, Vol. 29 (1), pp. 33–49.

Bega, S. 2022. Acid Mine Spill will take Years to Fix: Toxic Water in the Wilge River System from Thungela's Colliery is a Catastrophic Event. Mail Guardian. Ecology. Water Security, Available from "www.pressreader.com/South-africa/mail-guardian/20220401/281586654111762": [Accessed 13 April 2022] available online.

Bell, F.G. Halbich, T.F.J., and Bullock, S.E.T. 2001.The Effects of Acid Mine Drainage from an Old Mine in the Witbank Coalfield, South Africa. *Journal of Engineering Geology and Hydrogeology*, Vol. 35, pp. 265-278.

Beuhler. 2012. Preparation of Petrographic Thin Sections. 3p.

Beukes, N.J. 1985. Sedimentologie van die Ellisrassteenkoolveld. Finale Verslag, WNNR, KWP, NGP: Steenkoolgeologieprojek. (Report to the CSIR Coal Geology Project), 15p.

Beukes, N.J., 1969. Die Sedimentologie van die Etage Holkranssandsteen, Sisteem Karoo. Unpublished MSc Dissertation, University of Free State, Bloemfontein, 138p.

Beukes, N.J., Siepker, E.H., Naudé, F. 1991. Genetic Stratigraphy of the Waterberg Coalfield. Unpaginated Abstract, Conference on South Africa's Coal Resources. Geological Society of South Africa.

Brady, K.B.C., Perry, E.F., Beam, R.L., Bisko, D.C., Gardner, M.D., and Tarantino, J.M. 1994. Evaluation of Acid-Base Accounting to Predict the Quality of Drainage at Surface Coal Mines in Pennsylvania, USA. In: *Proceedings of the International Land Reclamation and Mine Drainage Conference*, Vol. 1, pp. 138 – 147.

Brandl, G. 1996. The Geology of the Ellisras area: Explanation of the Sheet 2326, Geological Survey of South Africa, 49 pp.

Bredenkamp, G., Granger, J.E., Van Rooyen, N. 1996. Moist Sandy Highland Grassland. In: Low, A.B and Robelo, A.G (Eds.). *Vegetation of South Africa, Lesotho and Swaziland*. Department of Environmental Affairs and Tourism, Pretoria.

Buchholz, K. 2021. The World's Biggest Coal Exporters. Statista. Available from "https://www.statista.com/chart/20587/biggest-coal-exporters/" [Accessed 19 August 2021].

Cadle, A. B., Cairncross, B., Christie, A. D. M., Roberts, D. L. 1993. The Karoo Basin of South Africa: Type Basin for the Coal-Bearing Deposits of southern Africa. *International Journal of Coal Geology*, Vol. 23, pp. 117-157.

Cadle, A.B. 1982. Controls on Coal Distribution. In: Cadle, A.B. (Ed.), Coal Exploration, Economics and Assessment. University of the Witwatersrand, Johannesburg, 36p.

Cairncross, B. 2001. An overview of the Permian (Karoo) Coal Deposits of southern Africa. *Journal of African Earth Sciences*, Vol. 33, pp. 529-562.

Caruccio, F.T. and Geidel, G. 1978. Geochemical Factors Affecting Coal Mine Drainage Quality. *Reclamation of Drastically Disturbed Lands*, pp. 129-148

Caruccio, F.T. and Geidel, G. 1985. Acid mine drainage: Surface mine treatment and in-situ abatement technology. In *Perspectives on Nonpoint Source Pollution: Proceedings of a National Conference, Kansas City, Missouri, May 19-22, 1985*, Vol. 85 (1), pp. 307, US Environmental Protection Agency, Office of Water Regulations and Standards.

Caruccio, F.T., Geidel, G. and Pelletier, M. 1981. Occurrence and Prediction of Acid Drainages, *Journal Energy Division ASCE*, 107: No.EY1, Proceedings Paper 16228, pp. 167-178.

Casagrande, D.J., Finkelman, R.B. and Caruccio, F.T. 1989. The Non-Participation of Organic Sulphur in Acid Mine Drainage Generation. *Environmental Geochemistry and Health*, Vol. 11(3), pp.187-192.

Casagrande, D.J., Siefert, K., Berschinski, C. and Sutton, N., 1976. Sulphur in Peat-Forming Systems of the Okefenokee Swamp and Florida Everglades. *Geochem. Cosmochim. Acta*, Vol. 40, pp. 161- 167.

Catuneanu, O., Wopfner, H., Eriksson, P. G., Cairncross, B., Rubidge, B. S., Smith, R. M. H., Hancox, P. J. 2005. The Karoo Basins of South-Central Africa. *Journal of African Earth Sciences*, Vol. 43, pp. 211-253.

Chabedi, C.K. 2013. Analysis of Technical Factors for Underground Mining of Deep Waterberg Coal Resources, Dissertation for Master Of Science in Engineering, Faculty Of Engineering And Built Environment, University of Witwatersrand, South Africa, Johannesburg.

Chamber of Mines. 2018. National Coal Strategy for South Africa. Chamber of Mines, 30p.

Chauhan, A. and Chauhan, P. 2014. Powder XRD Technique and its Applications in Science and Technology. *Journ. Anal. Bioanal. Tech*, Vol. *5*(5), pp. 1-5.

Cheepurupalli, N. and Anuradha, B. 2019. Proximate and Ultimate Characterisation of Coal Samples from Southwestern Part of Ethiopia. *International Journal of Engineering and Advanced Technology.* Vol. 9, pp. 1643-1648.

Chen, B., Liu, G., Wu, D., and Sun, R. 2016. Comparative Study on Geochemical Characterization of the Carboniferous Aluminous Argillites from the Huainan Coal Basin, China. *Turk. Journal of Earth Sciences*, Vol. 25, pp. 274–287

Chou, C.L. 2012. Sulphur in coals: A Review of Geochemistry and Origins. *International journal of Coal Geology*, Vol. 100, pp. 1-13.

Chou, C.L., 1997. Geologic Factors Affecting the Abundance, Distribution, and Speciation of Sulphur in Coals. In: Yang, Q. (Ed.), Geology of Fossil Fuels, Proceedings of the 30th International Geological Congress: Part B, VSP, Utrecht, The Netherlands, vol. 18, pp. 47–57.

Cole, D.I. 1992. Evolution and Development of the Karoo Basin. In: De Wit, M.J., Ransome, I.G.D. (Eds.). *Inversion Tectonics of the Cape Fold Belt. Karoo and Cretaceous Basins of Southern Africa*. A.A. Balkema, Rotterdam, pp. 87–99.

Cox, K.G., 1992. Karoo Igneous Activity and the Early Stages of the Break-Up of Gondwanaland. In: Story, B.C., Alabaster, T., Pankhurst, R.J. (Eds.). *Magmatism and the Causes of Continental Break-up*. *Geological Society Special Publication*, Vol. 68, pp. 137–148.

Craig, J.R. and Vaughan, D.J. 1994. Ore Microscopy and Ore Petrography. 2nd edition. John Wiley and Sons, Inc. New York, 424 pp.

Creamer Media's Mining Weekly. 2010. A Brief Look at SA'S Coal-Mining Industry 3rd September 2010. Available from "http://www.miningweekly.com/article/a-brief-look-at-sas-coal-mining-industry-2010-09-03" [Accessed 20 September 2020].

Creamer, M. 2021. More Sales of South African Coal to China Expected as Price Rises. Polity, Available from "https://m.polity.org.za/article/sa-coal-exports-2021-01-14" [Accessed 19 August 2021].

Creswell, M. 2019. South Africa's coal miners still have a relevant future for decades to come. Mining Review Africa. Available from "https://www.miningreview.com/coal/coal-miners-have-a-future-for-decades-to-come-in-south-africa/?amp=1" [Accessed 18 June 2021].

Cruywagen, L.M. 1999. Static Geochemical Methods in determining Acid Mine Drainage. MSc Dissertation, (Unpublished). University of the Orange Free State.

Curtis, C.D. 1983. Geochemistry of Porosity Enhancement and Reduction in Elastic Sediments. In: Brooks J. (Ed.). Petroleum geochemistry and exploration of Europe. The Geological Society. Blackwell, London, pp. 113-125.

De Jager, F. S. J. 1983. The Geology of the Springbok Flats, Waterberg, Soutpansberg and Limpopo Coal Fields, Unpublished Report 1983-0120, Pretoria (South African Geological Survey), 11 pp.

De Jager, F.S.J. 1976. Coal. In: Coetzee, C.B. (Ed.), Mineral Resources of the Republic of South Africa. Handbook of the Geological Survey of South Africa, Vol. 7, 478p.

De Jager, F.S.J. 1986. Coal Occurrences of the Central, North-Western, Northern, and Eastern Transvaal. In: Anhaeusser, C.R. and Maske, S. (Eds.). *Mineral and Deposits of Southern Africa*. Vols 1 and 2. Geological Society of South Africa, Johannesburg. Pp. 2047-2056.

Demchark, J., Morrow, T., and Skousen, J. 2001. Treatment of Acid Mine Drainage by Four Vertical Flow Wetlands in Pennsylvania. *Geochem. Explore. Env*. Vol. 1, pp. 71-80.

Deysel, L.M. 2015. Environmental Geochemistry of the Waterberg Coalfield. PhD Thesis. Bloemfontein, South Africa, University of Free State. 290p.

Diessel, C.F. 1992. Coal facies and depositional environment. Coal-bearing depositional systems, pp. 161-264.

Dollhoph, D.J. and Russell, L J, 1984. Assessment of Acid Producing Materials in the Northern Plains. Symposium on Surface Coal Mining and Reclamation in the Northern Great Plains, Billings, Montana.

Donahue, C.J. and Rais, E.A. 2009. Proximate Analysis of Coal. Journal of chemical education. Vol. 86(2), pp. 222-224.

Dreyer, C. 1994. An Overview of the Geology of the Waterberg Coalfield: Implications for Future Exploitation. Unpublished Conference Abstract, FFF Waterberg Coal Conference.

Du Toit, A.L. 1954. The Geology of South Africa. Oliver and Boyd, Edinburgh, United Kingdom, 611p.

Earth Systems. 2012. Acid Drainage, Earth Systems RSS. Available at: http://www.earthsystems.com.cn/?page_id=3940&lang=en [Accessed 10 June 2022].

EPA. 1994. Acid Mine Drainage Prediction. USA, Washington, EPA 530-R-94-036, 44p.

Eriksson, P.G., 1981. Aeolian Dune and Alluvial Fan Deposits in the Clarens Formation of the Natal Drakensberg. Trans. Geological Society of South Africa Vol. 89, pp. 389–394.

Eskom. 2008. Eskom Annual Report 2008. Available from "www.Eskom.co.za" [Accessed 20 April 2020].

Evangelou, V.P. 1998. Pyrite Chemistry: The Key for Abatement of Acid Mine Drainage. In *Acidic Mining Lakes.* Springer, Berlin, Heidelberg, pp. 197-222.

Exxaro. 2018. Grootegeluk. Available from "http://www.exxaro.com/index.php/where-we-operate/coal/grootegeluk/" [Accessed 20 April 2020].

Falcon, R.M.S, and Ham, A. J. 1988. The Characteristics of Southern African coals, *Journal of the South African Institute of Mining and Metallurgy*, Vol. 88, pp. 145-161.

Falcon, R.M.S. 1989. Macro-and Micro-Factors Affecting Coal-Seam Quality and Distribution in Southern Africa with Particular Reference to the No. 2 Seam, Witbank coalfield, South Africa. *International Journal of Coal Geology*, Vol. *12*(1-4), pp. 681-731.

Falcon, R.M.S. 2013. Coal petrography. In: *The coal handbook: towards cleaner production*, Woodhead Publishing, pp. 53-79.

Falcon, R.M.S. and Snyman, C.P. 1986. An Introduction to Coal Petrography: Atlas of Petrographic Constituents in the Bituminous Coals of Southern Africa. *Geological Society of Southern Africa*, Johannesburg. 27p.

Falcon, R.M.S., Ham, A.J. 1988. The characteristics of Southern African coals. Journal of the South African Institute of Mining and Metallurgy. Vol. 88(5), pp. 145–161.

Faure, K., Willis, J. P., Dreyer, J. C. 1996. The Grootegeluk Formation in the Waterberg Coalfield, South Africa: Facies, Paleo-Environment and Thermal History-Evidence from Organic and Clastic matter. *International Journal of Coal Geology*. Vol. 29, pp. 147-186.

Fedo, C.M., Nesbitt, H.W., and Young, G.M. 1995. Unravelling the Effects of Potassium Metasomatism in Sedimentary Rocks and Palesols, with Implications for Paleoweathering Conditions and Provenance, Vol. 23, pp. 921-924.

Ferguson, K. D., and Morin, K. A. 1991. The Prediction of Acid Rock Drainage Lessons from the Database. In: *Second International Conference on the Abatement of Acidic Drainage*. Conference Proceedings. Vol. 1 - 4, Montreal, Canada.

Ferguson, K.D. and Erickson, P.M. 1988. Pre-Mine Prediction of Acid Mine Drainage. In: *Environmental Management of Solid Waste*. Springer, Berlin, Heidelberg. pp. 24-43.

Fey, D.L. 2003. Acid-Base Accounting. Assessing the Toxicity Potential of Mine-waste piles workshop. Billings Symposium. USGS, 34p.

Finkelman, R.B., 1994. Modes of occurrence of potentially hazardous elements in coal: levels of confidence. Fuel processing technology, Vol. 39(1-3), pp. 21-34.

Fisher, S.E. and Munshower, F.F. 1984. Extremely Acid Soils, Overburden and Minerals in the Great Plains. Symposium on Surfacing Coal Mining and Reclamation in the Northem Great Plains, Billings, Montana.

Ford, C.T. 1974. Use of limestone in AMD treatment. In Proc. Fifth Symp. *Coal Mine Drainage Res*. Preprints, Vol. 205.

Fossil Fuel Foundation (FFF). 2013. The South African Coal Roadmap. Pretoria, South Africa, 37p.

Fourie, C.J.S., Henry, G. and Maré, L.P. 2014. The structure of the Karoo-age Ellisras Basin in Limpopo Province, South Africa, in the Light of New Airborne Geophysical Data. *South African Journal of Geology*, Vol. 117(2), pp.193-210.

Frederick, L.R., Starky, R.L. and Segal, W. 1957. Decomposability of Some Organic Sulphur Compounds in Soil. *Soil Science Society of American*, Proceeding, Vol. 21, pp. 287-292.

Fuge, R., Laidlaw, I.M.S., Perkins, W.T. and Rogers, K.P. 1991. The Influence of Acidic Mine and Spoil Drainage on Water Quality in the Mid-Wales Area. Environmental Geochemistry and Health, Vol. 13, pp. 70-75.

Gandolphe, S.C. 2019. Status of global coal markets and major demand trends in key regions. Center for Energy. Etades de l'Ifri, 58p.

GARD. 2009. Global Acid Rock Drainage Guide (GARD Guide). The International Network for Acid Prevention. Available from "http://www.gardguide.com" [Accessed 1 April 2022].

Garrels, R.I. and Christ C.L. 1965. Solutions, Minerals and Equilibria. Freeman. Cooper and Co., San Francisco. 405p.

Garside, M. 2021. Leading Countries Based on Hard Coal Production 2018. Statista, Available from "https://www.statista.com/statistics/264775/top-10-countries-based-on-hard-coal-production/" [Accessed 19 August 2021].

Gassen, N., Hyari, M.A., Hiasat, T., Hanbali, B. 2013. Delineation of Groundwater Protection Zones for Aidan Well Field. Technical report No.3. German-Jordanian Technical cooperation, pp. 18.

Geldenhuis, S., and Bell, F.G. 1998. Acid Mine Drainage at a Coal Mine in the Eastern Transvaal, South Africa. Environmental Geology, Vol. 34 (2-3), 9p.

Geology Wiki. 2022. *Gritstone*. [online] Available from "https://geology.fandom.com/wiki/Gritstone" [Accessed 30 July 2022].

Gilligan, R.N. 1986. OFS-Vierfontein Coalfield. In: *Mineral Deposits of Southern Africa*, pp. 1929-1937.

Glasspool, I.J. 2003. Hypautochtonous-Allochthonous Coal Deposition in the Permian, South African, Witbank Basin, No. 2 Seam, a Combined Approach using Sedimentology, Coal Petrology and Palaeontology. *International Journal of Coal Geology*, Vol. 53(2), pp. 81-135.

Goswami, S. 2013. Need for Clean Coal Mining in India. *Environmental Research Engineering and Management*, Vol. 4(66), pp. 79-84.

Goswami, S. 2015. Impact of Coal Mining on the Environment. *European Researcher*. Vol. 92(3), pp. 185-196.

Gray, R. J., Rhoades, A. H., King, D. T. 1976. Detection of Oxidized Coal and the Effect of Oxidation on the Technological Properties. *Transactions of the Society of Mining Engineers*. AIME; (United States). Vol. 260, pp. 2-31.

Greenshields, H.D. 1986. Eastern Transvaal Coalfield. In: *Mineral Deposits of Southern Africa*, pp. 1995-2010.

Grootegeluk. 2007. Available from "https://web.archive.org/web/20070223181025/http://www.exarro.com/content/ops/coal_grootegeluk.asp" [Accessed 07 August 2021].

Hancox, P. J., and Götz, A. E. 2014. South Africa's Coalfields-A 2014 perspective. *International Journal of Coal Geology*. Vol. 132, pp. 170-254.

Hancox, P.J. 1998. A Stratigraphic, Sedimentological and Palaeo-Environmental synthesis of the Beaufort-Molteno contact in the Karoo Basin. Unpublished PhD. Thesis, University of the Witwatersrand, Johannesburg, 404p.

Harnois, L. 1988. The CIW Index: A New Chemical Index of Weathering. *Sedimentary Geology*, Vol. 55(3-4), pp. 319-322.

Haughton, S.H. 1969. Karroo System. In: Geological History of Southern Africa, *Geological Society of Southern Africa*, pp. 349–415.

Hawley, J.R. 1977. The problem of acid mine drainage in the province of Ontario. Special Projects Section (Mining), Industrial Wastes Branch, Ministry of the Environment, 338p.

Helgen, S.O. and Davis, A. 2000. Quantifying Metal Contributions from Multiple Sources to the Clark Fork River, Montana, USA. *Journal of Environmental Forensics*, Vol. 1, pp. 55 – 62.

Henderson, R.E. 1986. South Rand Coalfield. In: Anhausser, C.R., and Maske, S. (Eds), *Mineral Deposits of Southern Africa, II*. *Geological Society of South Africa*, pp. 1953–1961.

Hobbs, P., Oelofse, S.H.H., Rascher, J. 2008. Management of Environmental Impacts from Coal Mining in the Upper Olifants River Catchment as a Function of Age and Scale. *Water Resources Development*, Vol. 24(3), pp. 417-431.

Hossner, L.R., and Brandt, J.E. 1997. Acid/Base Account and Mine Soils: A review. Proceedings America Society of Mining and Reclamation, pp. 128-140.

Hou, X. and Jones, B.T. 2000. Field Instrumentation in Atomic Spectroscopy. *Microchemical Journal*, Vol. 66, (1-3), pp. 115-145.

Hower, J.C., Wagner, N.J., O'Keefe, J.M., Drew, J.W., Stucker, J.D. and Richardson, A.R. 2012. Maceral Types in Some Permian Southern African Coals. *International Journal of Coal Geology*, Vol. 100, pp. 93-107.

ICCP. 1998. The New Vitrinite Classification. International Committee for Coal and Organic Petrology (ICCP). *Fuel*. Vol. 80, pp. 349-358.

ICCP. 2001. The New Inertinite Classification (ICCP System 1994). Fuel, 80, 459-471. Available from http://dx.doi.org/10.1016/S0016-2361(00)00102-2 [Accessed 04 July 2023].

IEA. 2019. Coal information overview. Statistics. 11 pp.

International Committee for Coal Petrology (ICCP). 1957. International Handbook of Coal Petrography: 1st edition. Paris.

International Committee for Coal Petrology. 1971. International Handbook of Coal Petrography: Supplement to the 2nd Edition, 1st supplement. Paris, 300 pp.

International Energy Agency. 2022. International Thermal Coal Prices Hit Three All-Time Peaks in The Space of Nine Months. Available from https://www.iea.org/reports/coal-market-update-july-2022/prices [Accessed 07 July 2022].

Jambor, J.L., and Blowes, D.W. 1998. Theory and Applications of Mineralogy in Environmental Studies of Sulphide Bearing Mine Wastes. Environmental Mineralogy, Mineral Association of Canada. Short Course. Vol. 27. Ottawa, Ontario, pp. 367-401.

Jeffrey, L. Challenges associated with further development of the Waterberg Coalfield. *Journal of the Southern African Institute of Mining and Metallurgy*, Vol.105 (6), pp. 453-457.

Jeffrey, L., 2005. Challenges Associated with Further Development of the Waterberg Coalfield. *Journal of the Southern African Institute of Mining and Metallurgy*, Vol. 105(6), pp. 453-457.

Johnson, D.B., and Hallberg, K.B. 2005. Acid Mine Drainage Remediation Options: A review. *Sci. Total Env*. Vol. 338(1-2), pp. 3-14.

Johnson, M.R. 1966. The Stratigraphy of the Cape and Karoo Systems in the Eastern Cape Province. Unpublished MSc Thesis, Rhodes University, Grahamstown, 125p.

Johnson, M.R. 1976. Stratigraphy and Sedimentology of the Cape and Karoo Sequences in the Eastern Cape Province. Unpublished PhD Thesis, Rhodes University, Grahamstown, 336p.

Johnson, M.R., Van Vauuren, C.J., Hegenberger, W.F., Key, R., Shoko, U. 1996. Stratigraphy of the Karoo Supergroup in southern Africa: An Overview. *Journal of African Earth Sciences*, Vol. 23, pp. 3-15.

Johnson, M.R., Van Vuuren, C.J., Visser, J.N.J., Cole, D.I., Wickens, H., de, V., Christie, A.D.M., Roberts, D.L., Brandl, G. 2006. Sedimentary Rocks of the Karoo Supergroup. In: Johnson, M.R., Anhaeusser, C.R., Thomas, R.J. (Eds.), *The Geology of South Africa*. Johannesburg/Council for Geoscience, Pretoria, pp. 461–499.

Jordan, J. 1986. Highveld Coalfield. In: C. Anhaeusser, C. and Maske, S. (Eds). *Mineral Deposits of Southern Africa*. Johannesburg: The Geological Society of South Africa, pp. 1985-1994.

Kalkreuth, W.D., 2004. Coal facies studies in Canada. International journal of coal geology, 58(1-2), pp.23-30.

Kannan, M. 2018. Scanning Electron Microscopy: Principles, Components and Applications. *A textbook on fundamentals and applications of nanotechnology*, pp. 81-92.

Kemezys, M. and Taylor, G.H. 1964. Occurrence and Distribution of Minerals in Some Australian Coals. *Journal of the Institute of Fuel*, Vol. 37.

Kleinmann, R. 1990. Acid Mine Water Treatment using Engineered Wetlands. Mine Water and the Environment. *International Mine water Association*, Vol. 2006, pp. 85-96.

Lepakko, K. 1993. Predictive Testing for Mine Waste Drainage Quality. In: Mine Operation and Closure Short Course. Sponsored by EPA and others. Helena, MT.

Lishman, K.L. 2009. The Acid Mine Drainage Potential of the Platreef, Northern Limp of the Bushveld complex, South Africa, Master of Sciences, University of Witwatersrand, 70p.

Love, L.G., and Amstutz, G.C. 1966. Review of Microscopic Pyrite from the Devonian Chattanooga Shale and Rammelserg Banderz. *Fortschr Mineral*, Vol. 43, pp.

MacRae, C.S, 1988. Palynostratigraphic Correlation between the Lower Karoo Sequence and the Waterberg and Pafuri coal-bearing Basins and the Hammanskraal Plant Macrofossil Locality, Republic of South Africa. Memoir/Memorie 75. *Geological Survey*. 9p.

Mahooana, P.E., Moroeng, O.M. and Wagner, N.J. 2022. Petrology of the A and B Seams, Ermelo Coalfield (South Africa): Indications for Changing Palaeo-Environmental and Sedimentary Conditions. *International Journal of Coal Geology*, Vol. 263, p.104135.

Maiyana, A. 2003. Evaluation and Validation of Geochemical Prediction Techniques for Underground Coal Mines in the Highveld Regions: Mineralogical characterisation of pyrite for Long Term Prediction of Acid Rock Drainage in S7 Compartment, Brandspruit Colliery, Sasol Secunda, Masters of Earth Sciences, University of Venda, 70p.

Mamurekli, D. 2010. Environmental Impacts of Coal Mining and Coal Utilisation in the UK, Acta. Mantanistica. Slovaca, pp. 134-144.

Mamurekli, M. 1997. Removing Pyritic Sulphur and Trace Element From UK Coal by Coal Beneficiation Techniques. Nottingham University. Ph.D Thesis, 312p.

Maromo, J. 2011. Sekoko secures R250 M from IDK for Waterberg coal mine. IOL, Available from "Sekoko secures R250m from IDC for Waterberg coal mine (iol.co.za)" [Accessed 05 June 2022].

Martinez, M. and Escobar, M. 1995. Effect of Coal Weathering on some Geochemical Parameters. *Organic geochemistry*, Vol. 23 (3), pp. 253-261.

Masindi, V. 2015. Remediation of Acid Mine Drainage using Magnesite and its Bentonite Clay Composite, (Doctoral dissertation, University of Venda), 233p.

Matshusa, K.P. 2007. Socio-Economic and Environmental Impacts of Tshikondeni Coal Mine: A Case Study of Ha-Makomawabani and Makuya Park Area in the Limpopo Province. Dissertation for the Degree of Master in Environmental sciences and geology. RSA. University of Venda.

McCabe, P.J. 1984. Depositional Environments of Coal and Coal-Bearing Strata. In: Rahmani, R.A. and Flores, R.M. (Eds.). Sedimentology of Coal and Coal-bearing Sequences, Special Publication 7, *International Association of Sedimentologists*, Blackwell Scientific Publications, Oxford, pp. 13–42.

McCarthy, T.S. 2011. Impact of Acid Mine Drainage in South Africa. *South African Journal of Science*, Vol. 107, pp. 1-7.

McGinnes, S. 1999. Treatment of Acid Mine Drainage. Science and Environment Section. House of Commons Library. 36p.

McHugh, E. A., Diessel, C. F., Kutzner, R. 1991. Use of Fluorescence Microscopy in the Detection of Level Oxidation in Bituminous Coals. *Fuel*. Vol. 70, pp. 647-653.

McLennan, S.M. and Taylor, S.R. 1982. Geochemical Constraints on the Growth of the Continental Crust. *The Journal of Geology*, Vol. 90(4), pp. 347-361.

McLennan, S.M., 1993. Weathering and Global Denudation. *The Journal of Geology*, Vol. 101(2), pp. 295-303.

Minerals Database. 2022. Sandstone - Minerals Education Coalition. [online] Minerals Education Coalition. Available from "https://mineralseducationcoalition.org/minerals-database/sandstone/#:~:text=Sandstone%20is%20a%20sedimentary%20rock,called%20arkose%20or%20arkosic%20sandstone" [Accessed 30 July 2022].

Mining Review Africa. 2011. Sekoko Coal Lands Eskom Coal Supply Agreement, Available from "Sekoko Coal lands Eskom coal supply agreement - Miningreview.com" [Accessed on 05 June 2022].

Miraj, A., Pal, S., Bhattacharya, S., Chakraborty, K., Miraj, A., Pal, S. and Chakraborty, K. 2017. Observation on the TDS and EC Values of Different Water Bodies at Cooch Behar, West Bengal, India. *International Journal of Theoretical & Applied Sciences*, Vol. 9(2), pp. 106-113.

Moazzem, S., Rasul, M.G. and Khan, M.M.K. 2012. A review on technologies for reducing CO2 emission from coal fired power plants (Vol. 11, pp. 227-254). chapter.

Modis, K., Adam, K., Panagopoulos, K., Kontopoulos, A. 1998. Development and Validation of a Geostatistical Model for Prediction of Acid Mine Drainage in Underground Sulphide Mines. *Journal of Trans. Instn. Min. Metall*. (Sec A: Min industry). A102-A107.

Moumakwa, M. 2009. The Future role of the Waterberg Coalfield in South Africa's coal Industry. Department of Mineral Resources, Report R76/2009.

Mtimkulu, N. 2009. A Provisional Basinal Study of the Waterberg-Karoo. Masters Dissertation. South Africa, University of Pretoria. 134p.

Munnik, V., Hochmann, G., Hlabane, M. and Law, S. 2010. The Social and Environmental Consequences of Coal Mining in South Africa: A Case Study. Environmental Monitoring Group. Cape Town, 24p.

Murdoch, S. 2018. The Distribution and Qualities of Radioactive Trace Elements in Particular Uranium and Thorium within the Waterberg Coalfield. Masters Dissertation. Johanesburg, South Africa: University of Witwatersrand. 84p.

Natarajan, K.A. 2008. Microbial Aspects of Acid Mine Drainage and its Bioremediation. *Trans. Nonferrous met. Soc. China*. Vol. 18, pp. 1352-1360.

Nengovhela, A.C., Yibas, B. and Ogola, J.S. 2006. Characterisation of Gold Tailings Dams of the Witwatersrand Basin with Reference to their Acid Mine Drainage Potential, Johannesburg, South Africa. *Water SA*, Vol. 32(4).

Nephalama, A and Muzerengi, C. 2016. Assessment of the Influence of Coal Mining on Ground water Quality: Case Study of Masisi village in the Limpopo province of South Africa: Thohoyandou, South Africa, pp. 430-438.

Nesbitt, H. and Young, G.M. 1982. Early Proterozoic Climates and Plate Motions Inferred from Major Element Chemistry of Lutites. *Nature*, Vol. 299 (5885), pp. 715-717.

Netshitungulwana, R., Yibas, B., Novhe, O., and Motlakeng, T. 2013. Stream Sediment Geochemistry of Areas Impacted by Mining around Emalahleni (Formerly known as Witbank), South Africa: Fingerprinting AMD potential point sources. *Annual International Mine water Association Conference*. *Reliable Mine water Technology*, Vol. 118, pp. 122-134.

Pettijohn, F.J. 1975. Sedimentary Rocks, New York: Harper and Row, Vol. 3, 628p.

Pinetown, K.L., Ward, C.R. and Van der Westhuizen, W.A. 2007. Quantitative Evaluation of Minerals in Coal Deposits in the Witbank and Highveld Coalfields, and the Potential Impact on Acid Mine Drainage. *International Journal of Coal Geology*, Vol. *70*(1-3), pp. 166-183.

Plumstead, E.P. 1957. Coal in Southern Africa. Witwatersrand University Press. 29p.

Plumstead, E.P. 1966. The Story of South Africa's coal. *Optima*, Vol. 16, pp. 186-202.

Price, W.A., Morin, K. and Hutt, N. 1997. Guidelines for the Prediction of Acid Rock Drainage and Metal leaching for Mines in British Columbia: Part 11. Recommended Procedures for Static and Kinetic testing. In: *Proceedings of the Fourth International Conference on Acid Rock Drainage,* Vol. 1, pp. 15 – 30.

Ramane, L. 2014. South Africa's coal industry overview. Department of Mineral Resources. Report R111/2014, 30 pp.

Renton, J.J. 1982. Mineral Matter in Coal. Coal structure, pp. 283-326.

Roberts, D.L. 1988. The Relationship between Macerals and Sulphur Content of some South African Permian coals. *International journal of coal geology*, Vol. 10(4), pp. 399-410.

Robertson, A., Kawashima, N., Smart, R and Schumann, R. 2015. Management of Pyrrhotite Tailings at Savannah Nickel Mine: A Decade of Experience and Learning. *10th International Conference on Acid Rock Drainage and International Mine Water Association Annual Conference.Santiago, Chile*. pp. 362-372.

Roux, L. 2015. Personal Communication. GLK Mining, Grootegeluk.

Rowsell, D.M., Connan, J. 1979. Oil Generation, Migration and Preservation in the Middle Ecca Sequence near Dannhauser and Wakkerstroom. Geological Society of South Afrika, Special Publication, Vol. 6, pp. 131-150.

SANS 10320:2004. South African Guide to the Systematic Evaluation of Coal Resources and Coal Reserves. South African National Standard (SANS).

SANS 5925:2007. Moisture Content of Coal Samples Intended for General Analysis (Air-Oven Method): Second Edition; South African National Standard (SANS).

SANS 7404-2:2015 Methods for the Petrographic Analysis of Coals - Part 2: Method of Preparing Coal samples. South African National Standard (SANS).

SANS 7404-3:2016. Methods for the Petrographic Analysis of Coals Part 3: Method of Determining Maceral Group Composition. South African National Standard (SANS).

SANS 7404-5:1994 Methods for the Petrographic Analysis of Coals - Part 5: Method of Determining Microscopically the Reflectance of Vitrinite. South African National Standard (SANS).

Schapiro, N., Gray, R.J. and Eusner, G.R. 1964. The use of Coal Petrography in Coke Making. *Journal of the Institute of Fuel*, Vol. 11(30), pp. 234-242.

Schnitzer, E.F., and Fransway, D.F. 1982. Strip Mine Reclamation Problems Associated with the Oxidation of Surface Spoils in Wyoming. LEQ-LQD Acid Base Seminar on June 11, Cheyenne, Wyoming.

Scott, A. C. 2002. Coal Petrology and the Origin of Coal Macerals: a way ahead?. *International Journal of Coal Geology*. Vol. 50, pp. 119-134.

Scott, A.C. 2009. Forest fire in the fossil record. CRC Press.

Shamshuddin, J., Muhrizal, S., Fauziah, I. and Van Ranst, E. 2004. A laboratory Study of Pyrite Oxidation in Acid Sulphate Soils. *Communications in Soil Science and Plant Analysis*, Vol. 35 (1-2), pp. 117-129.

Siepker, E.H. 1986. Genetiese Stratigrafie en Sedimentologie van die Opeenvolging Karoo in die Westelike en Noordelike Deel van die Waterbergsteenkoolveld. Unpublished Master of Science Dissertation, University of Pretoria.

Skousen, J.G. 1995. Acid Mine Drainage. *Green Lands*, Vol. 25 (2), pp. 52-55.

Smith, D. and Whittaker, R. 1986. The Springs-Witbank Coalfield. In: Anhaeusser, C. and Maske, S. (Eds). Mineral Deposits of Southern Africa. Johannesburg: *Geological Society of South Africa*, pp. 1969-1984.

Smith, R. M. H., Eriksson, P. G., Botha, W. J. 1993. A Review of the Stratigraphy and Sedimentary Environments of the Karoo-aged Basins of Southern Africa. *Journal of African Earth Sciences (and the Middle East).* Vol. 16, pp. 143-169.

Smyth, M. 1970. Type Seam Sequences for some Permian Australian coals. *Proc. Aust. Inst. Min. Metall.*, Vol. 233, pp. 7-15.

Snyman, C. P., and Botha, W. J. 1993. Coal in South Africa. *Journal of African Earth Sciences (and the Middle East).* Vol. 16, pp. 171-180.

Snyman, C.P. 1986. A comparison between the Petrography of South African and some other Palaeozoic coals. Publications of the University of Pretoria 15 (N Series), pp. 1-37.

Sobek, A.A., Schuller, W.A., Freeman, J.R. and Smith, R.M. 1978. Field and Laboratory Methods Applicable to Overburdens and Mine Soils. EPA-600/2-78-054. USEPA. Cincinnati. Ohio.

Soregaroli, B.A. and Lawrence, R.W. 1998. Update on Waste Characterisation Studies. *Proc. Mine Design, Operations and Closure Conference*. Polson, Montana.

South African Committee for Stratigraphy (SACS). 1980. Stratigraphy of South Africa. Part 1 (Comp. L.E. Kent). Lithostratigraphy of the Republic of South Africa, South West

Africa/Namibia and the Republics of Bophuthatswana, Transkei and Venda. *Handb. Geol. Surv. S. Afr*. Vol. 8, 690p.

South African Weather Service (SAWS). 2016. Climate of South Africa-WB42-Lephalale-Climate Statistics 1981-2010.

Speight, J. G. 2005. Handbook of Coal Analysis; John Wiley and Sons: Hoboken, 222p.

Stach, E., Mackowsky, M.T., Teichmuller, M., Taylor, G.H., Chandra, D., Teichmuller, R., Bwnfraeger, G., Berlin, S., Cloth, D.M., Hacquebard, P.A. and Darfmoufh, N.S. 1982. Stach's Textbook of Coal Petrology. Gebruder borntraeger, 535p.

Stach, E.M. 1975. Coal Petrology. Gebruder Borntraeger, Berlin, Stuttgart, 428p.

Steyn, M., and Minnitt, R.C.A. 2010. Thermal Coal Products in South Africa. *The Journal of South African Institute of Mining and Metallurgy*, Vol. 110, 7p.

Sua´rez-Ruiz, I., and Ward, C.R. 2008. Basic Factors Controlling Coal Quality and Technological Behaviour of Coal. In: Suárez-Ruiz, I., and Crelling, J. C. (Eds.). Applied coal petrology: the role of petrology in coal utilization. Academic Press, pp. 173-192.

Sullivan, J., Brink, V. and Sullivan, D. 1994. The Soutpansberg Coalfields. Johannesburg. Geological Society of South Africa, pp. 165-170.

Syed, N.A., Kumar, L., Sharma, N., and Bhuyan, P. 2017. Sample preparation techniques for electron microscopy 50 years of SEM and beyond!. Microscopy and imaging Science: Practical approaches to applied research and education, pp. 723-726.

Taggart, J.E. Lindsay, J.R., Scott, B.A., Vivit, D.V., Bartel, A.J. and Stewart, K.C. 1987. Analysis of Geologic Materials by Wavelength-Dispersive X-Ray Fluorescence Spectrometry. In Methods for Geochemical Analysis, Vol. 1770, Denver, CO, USA: US Geological Survey Bulletin, pp. 1-19.

Taylor, G.H., Mackowsk, M.T., and Alpern, B. 1967. Behaviour of Inertinite during Carbonization. *Fuel*, Vol. 46(6), 431p.

Taylor, G.H., Teichmuller, M., Davis, A., Diessel, C.F.K., Littke, R. and Robert, P. 1998. Organic Petrology, Gebruder Borntraeger, Berlin, 704p.

Taylor, S.R. and McLennan, S.M. 1985. The continental crust: its composition and evolution, 312p.

Teichmuller, M. 1989. The Genesis of Coal from the Viewpoint of Coal Petrology. *International Journal of Coal Geology*, Vol. 12, pp. 1–87.

Teichmuller, M. and Teichmuller, R. 1982. The Geological Basis of Coal Formation. In: Stach, E., Mackowski, M.T.H., Teichmuller M., Taylor, G.H., Chandra, D. and Teichmuller, R. (Eds). Stach's Book of Coal Petrography, 3rd edn, Gebruder Borntraeger, Berlin, pp. 5–86.

Theunissen, N. 2012. Waterberg Coalfields. Mining Mirror. 28p.

Thiessen, G. 1945. Forms of Sulphur in Coal. In: *Chemistry of Coal Utilization*, Vol. 1, New York: John Wiley.

Thiessen, R. 1920. Compilation and Composition of Bituminous coals. Journal of Geology. Vol. 28, pp. 185–209.

Thomas, L. 2013. Coal Geology. Wiley-Blackwell: United Kingdom, 457p.

Thwala, K. 2020. Geochemical Characterisation of the Witbank coalfields, South Africa, Master of dissertation, University of the Free State, 133p.

Tlou-Sebola, M.J. 2018. Weathering of coals from the Waterberg and Limpopo Coalfields, South Africa. Master of Science dissertation. University of Witwatersrand, Johannesburg, 160p.

Trading Economics. 2023. Projection of Coal Price. Available from https://tradingeconomics.com/commodity/coal [Accessed 04 July 2023].

Tucker, M.E. Ed. 2001. Sedimentary Petrology: An Introduction to the Origin of Sedimentary Rocks. John Wiley and Sons, 291p.

Udayabhanu, S.G., and Prasad, B. 2010. Studies on Environmental Impact of Acid Mine Drainage Generation and its Treatment: An Appraisal. *Indian journal of Environmental Protection*, Vol. 30(11), pp. 953-967.

Usher, B.H., Cruywagen, L.M., De Necker, E. and Hodgson, F.D.I. 2003. Acid-Base Accounting, Techniques and Evaluation (ABATE): Recommended Methods for Conducting and Interpreting Analytical Geochemical Assessments at Opencast Collieries in South Africa. Water Research Commission Report No 1055/2/03. Pretoria.

Vassilev, S. V., and Vassilev, C. G. 1996. Occurrence, Abundance and Origin of Minerals in Coals and Coal ashes. *Fuel Processing Technology*, Vol. 48, pp. 85-106.

Veevers, J.J., Cole, D.I., Cowan, E.J. 1994. Southern Africa: Karoo Basin and Cape Fold Belt. In: Veevers, J.J., Powell, J.J., McA, C. (Eds.). Permian Triassic Pangean Basins and

Fold belts Along the Panthalassan Margin of Gondwanaland. *Geological Society of America Memoir*. Vol. 184, pp. 223–279.

Visser, J.N.J. 1990. The Age of the Late Palaeozoic Deposits in Southern Africa. *South African Journal of Geol*ogy, Vol. 93, pp. 366-375.

Wagner, N.J. 2007. The Abnormal Condition Analysis used to Characterize Weathered Discard Coals. *International journal of coal geology*, Vol. *72*(3-4), pp. 177-186.

Wagner, N.J. and Hlatshwayo, B. 2005. The Occurrence of Potentially Hazardous Trace Elements in Five Highveld Coals, South Africa. *International Journal of Coal Geology*, Vol. 63(3-4), pp. 228-246.

Wagner, N.J., Falcon, R.M.S., Malumbazo, N. 2018. Southern African Coals and Carbons: Definitions and Applications of Organic Petrology, Struik Nature, 248p.

Wang, Z., Xu, Y., Zhang, Z., and Zang, Y. 2021. Review: Acid mine drainage (AMD) in Abandoned Coal Mines of Shanxi, China. Water. Vol. 13 (8), 21p.

Ward, C.R. 1984. Coal Geology and Coal Technology. Blackwell Science.

Ward, C.R. 2016. Analysis, origin and significance of mineral matter in coal: An updated review. *International Journal of Coal Geology*, Vol. 165, pp.1-27.

Waterberg Municipality. 2013. Final IDP. South Africa: Waterberg District. pp. 75-76.

Weber, P.A., Stewart, W.A., Skinner, W.M., Weisener, C.G., Thomas, J.E. and Smart, R.S.C. 2004. Geochemical Effects of Oxidation Products and Framboidal Pyrite Oxidation in Acid Mine Drainage Prediction Techniques. *Applied Geochemistry*, Vol. 19(12), pp.1953-1974.

Weldode, J.M. 2020. Analysis of Coal. Chemistry Hunt. Available from "Https://drive.google.com/open?Id=1oHuO27T2kE2Wy8grnHHwnfj9znEcsH7i" [Accessed 10 April 2021].

White, D. and Thiessen, R. 1913. The Origin of Coal. US Government Printing Office, 390p.

WHO (World Health Organization). 1984. Guidelines for Drinking Water Quality, Recommendations, Geneva. Vol. 1, pp. 130.

Wilmoth, R.C., Scott, R.B. and Hill, R.D. 1972. Combination Limestone-Lime Treatment of Acid Mine Drainage. Norton Mine Drainage Field Site.

World Coal Association. 2015. Coal Facts 2014. *London: World Coal Association*.

Wu, C. 2021. Acid Mine Drainage Prediction Techniques and Geochemical Modelling: Case Study on Gold Tailing dams, West Rand, Witwatersrand Basin Area, South Africa. Doctoral Thesis, University of Western Cape, 237p.

Yossifova, M., Lerouge C., Deschamps Y. 2009. Mineral matter and trace elements in the Vulche pole coal, Bulgaria. Geolines Vol. 22, pp. 89–94

Younger, P.L, Banwart, S.A., Hedin, R.S. 2002. Mine Water: Hydrology, Pollution, Remediation. Kluwer Academic Publishers, Boston

Zero Hedge. 2021. Coal Demand is Spiking in 2021. Available from "https://oilprice-com.cdn.ampproject.org/v/s/oilprice.com/Energy/Coal/Coal-Demand-Is-Spiking-In2021.amp.html?amp_js_v=a6&amp_gsa=1&usqp=mq331AQIKAGwASCAAgM%3D#aoh=16278601788909&csi=0&referrer=https%3A%2F%2Fwww.google.com&amp_tf=From%20%251%24s&ampshare=https%3A%2F%2Foilprice.com%2FEnergy%2FCoal%2FCoal-Demand-Is-Spiking-In-2021.html" [Accessed 02 August 2021].

Zhao, L, Ward C.R., French, D., Graham, I.T. 2015. Major and Trace Element Geochemistry of Coals and Intra-seam Claystones from the Songzao Coalfield, SW China. *Minerals*, Vol. 5, pp. 870–893.

Zhu, Q. 2014. Coal Sampling and Analysis Standards. IEA Clean coal Center. United Kingdom, pp. 17-107.

Zipper, C., Skousen, J., Jage, C. 2018. Passive Treatment of Acid Mine Drainage. Virginia Cooperate Extension. *Virginia State University Publication*, Vol. 460 (133), 14 pp.

# APPENDICES

A.1: Ethical Clearance Certificate

ETHICS APPROVAL CERTIFICATE

RESEARCH AND INNOVATION
OFFICE OF THE DIRECTOR

NAME OF RESEARCHER/INVESTIGATOR:
**Mr KT Ramphabana**

STUDENT NO:
17002715

PROJECT TITLE: **Lithostratigraphic and geochemical characterisation of the Waterberg coalfield: implications to acid mine drainage, Limpopo province, South Africa.**

ETHICAL CLEARENCE NO: **FSEA/22/GES/08/0206**

SUPERVISORS/ CO-RESEARCHERS/ CO-INVESTIGATORS

| NAME | INSTITUTION & DEPARTMENT | ROLE |
|---|---|---|
| Dr HR Mundalamo | UNIVEN, Earth Sciences | Supervisor |
| Prof Emeritus. JS Ogola | UNIVEN, Earth Sciences | Co - Supervisor |
| Mr R Netshitungulwane | Council for Geoscience, Economic geology and Geochemistry unit | Co - Supervisor |
| Mr KT Ramphabana | University of Venda | Investigator – Student |

Type: **Masters Research**
Risk: **Straightforward research without ethical problems (Category 1)**
Approval Period: **June 2022 – June 2024**

**The Animal, Environmental and Biosafety Research Ethics Committee (AEBREC) hereby approves your project as indicated above.**

General Conditions
While this ethics approval is subject to all declarations, undertakings and agreements incorporated and signed in the application form, please note the following.

- The project leader (principal investigator) must report in the prescribed format to the REC:
  - Annually (or as otherwise requested) on the progress of the project, and upon completion of the project
  - Within 48hrs in case of any adverse event (or any matter that interrupts sound ethical principles) during the course of the project.
  - Annually a number of projects may be randomly selected for an external audit.
- The approval applies strictly to the protocol as stipulated in the application form. Would any changes to the protocol be deemed necessary during the course of the project. The project leader must apply for approval of these changes at the REC. Would there be deviated from the project protocol without the necessary approval of such changes, the ethics approval is immediately and automatically forfeited.
- The date of approval indicates the first date that the project may be started. Would the project have to continue after the expiry date; a new application must be made to the REC and new approval received before or on the expiry date.
- In the interest of ethical responsibility, the RECs retains the right to:
  - Request access to any information or data at any time during the course or after completion of the project.
  - To ask further questions; Seek additional information; Require further modification or monitor the conduct of your research or the informed consent process.
  - withdraw or postpone approval if:
  - Any unethical principles or practices of the project are revealed or suspected.
  - It becomes apparent that any relevant information was withheld from the REC or that information has been false or misrepresented.
  - The required annual report and reporting of adverse events was not done timely and accurately.
  - New institutional rules, national legislation or international conventions deem it necessary

ISSUED BY:
UNIVERSITY OF VENDA, RESEARCH ETHICS COMMITTEE
Date Considered: April 2022

Name of the AEBREC Chairperson of the Committee: **Prof Irene Barnhoorn**

Signature

University of Venda
PRIVATE BAG X5050, THOHOYANDOU, 0950, LIMPOPO PROVINCE, SOUTH AFRICA
TELEPHONE (015) 962 8504/8313 FAX (015) 962 9060
*"A quality driven financially sustainable, rural-based Comprehensive University"*

UNIVERSITY OF VENDA
OFFICE OF THE DIRECTOR
RESEARCH AND INNOVATION
2022-06-07
Private Bag X5050
Thohoyandou 0950

A.2: X-ray diffraction patterns for Ply A S-L

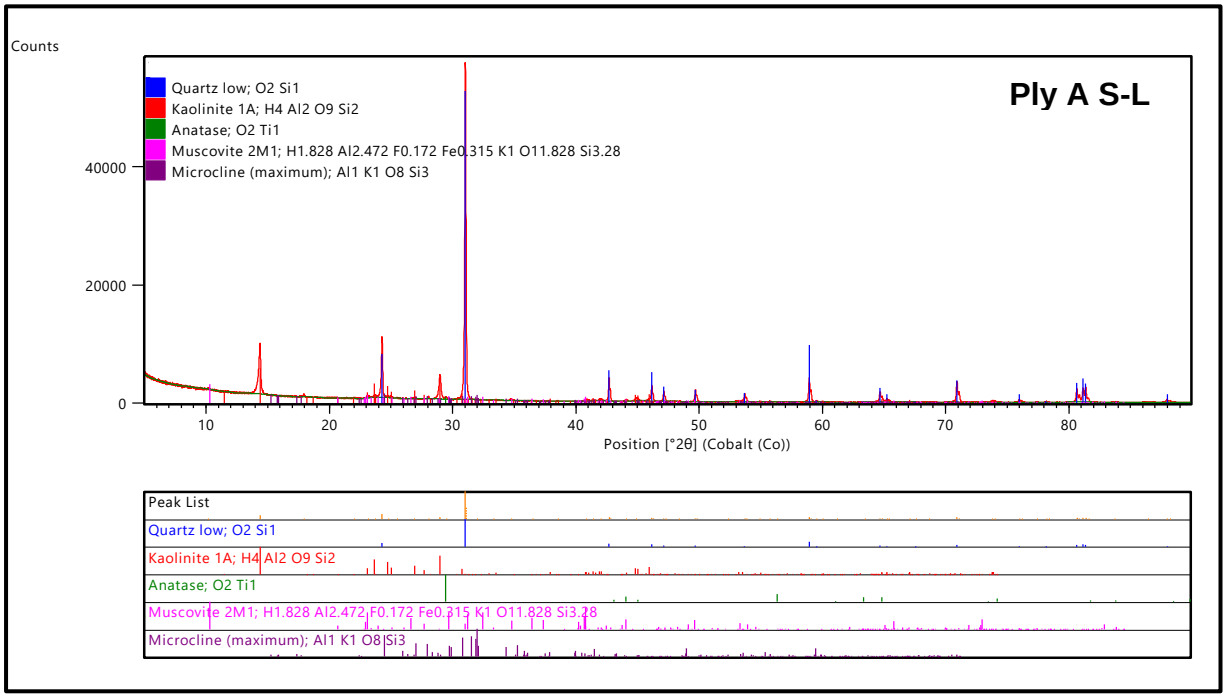


A 3: X-Ray diffraction patterns for ply A F-R.

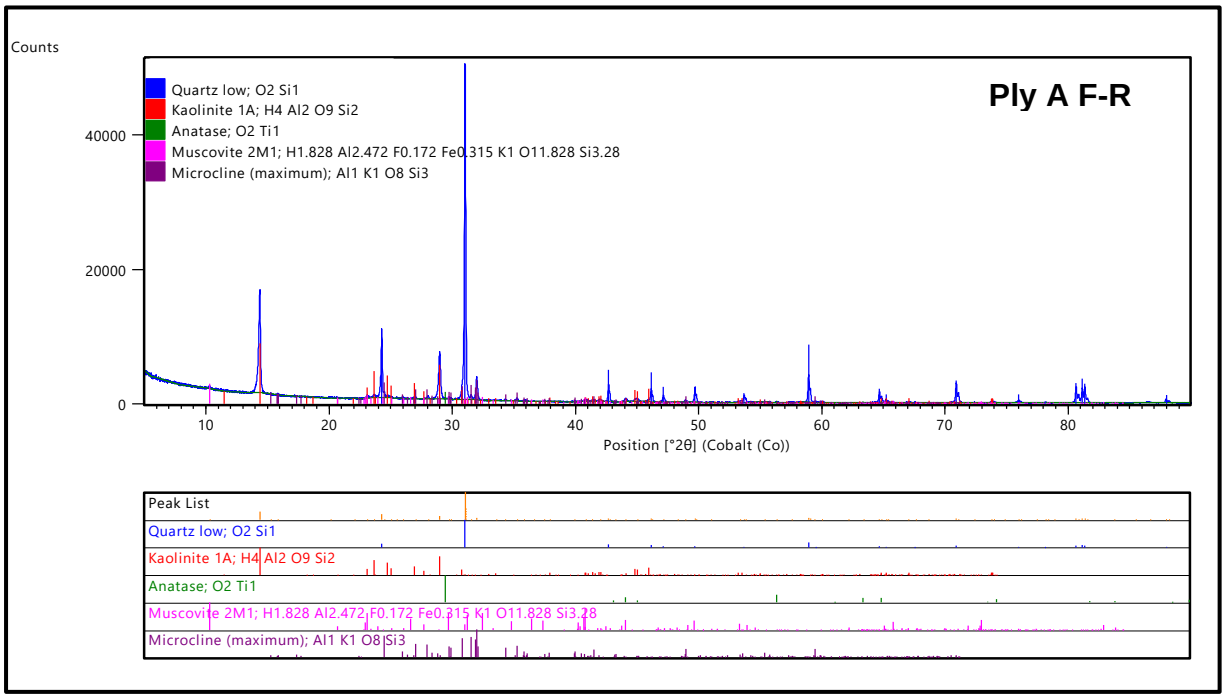

A 4: X-ray diffraction patterns for shale F-R.

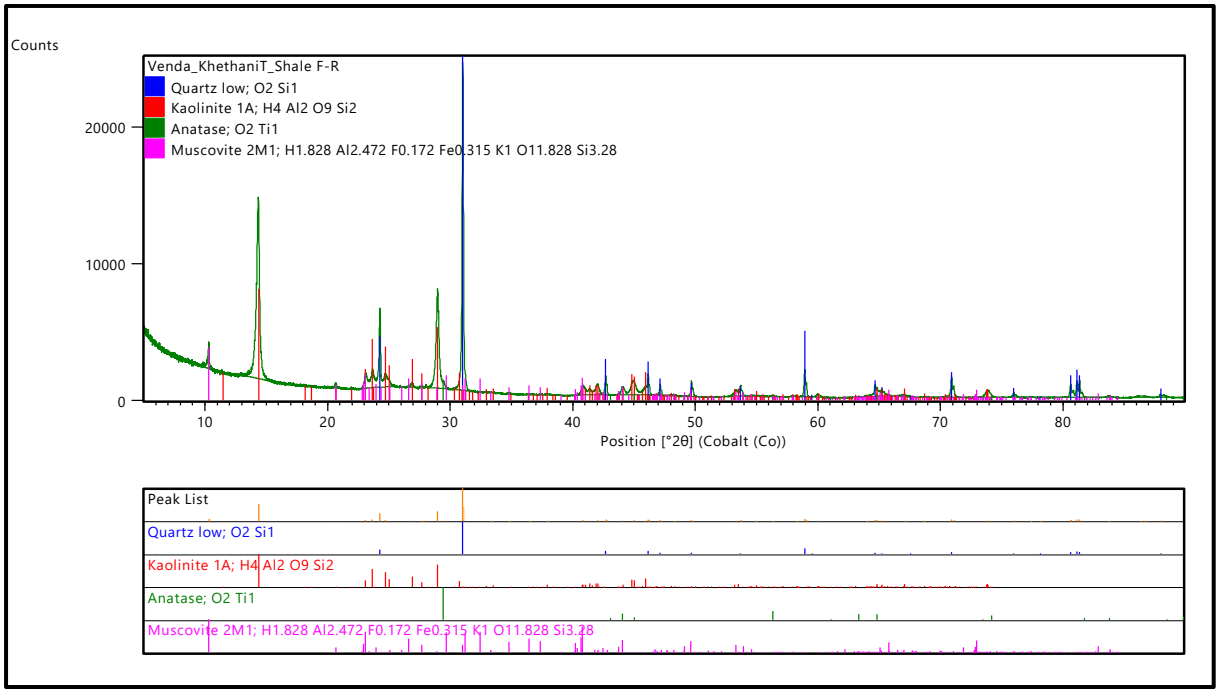


A 5: X-ray diffraction patterns for Ply C F-R

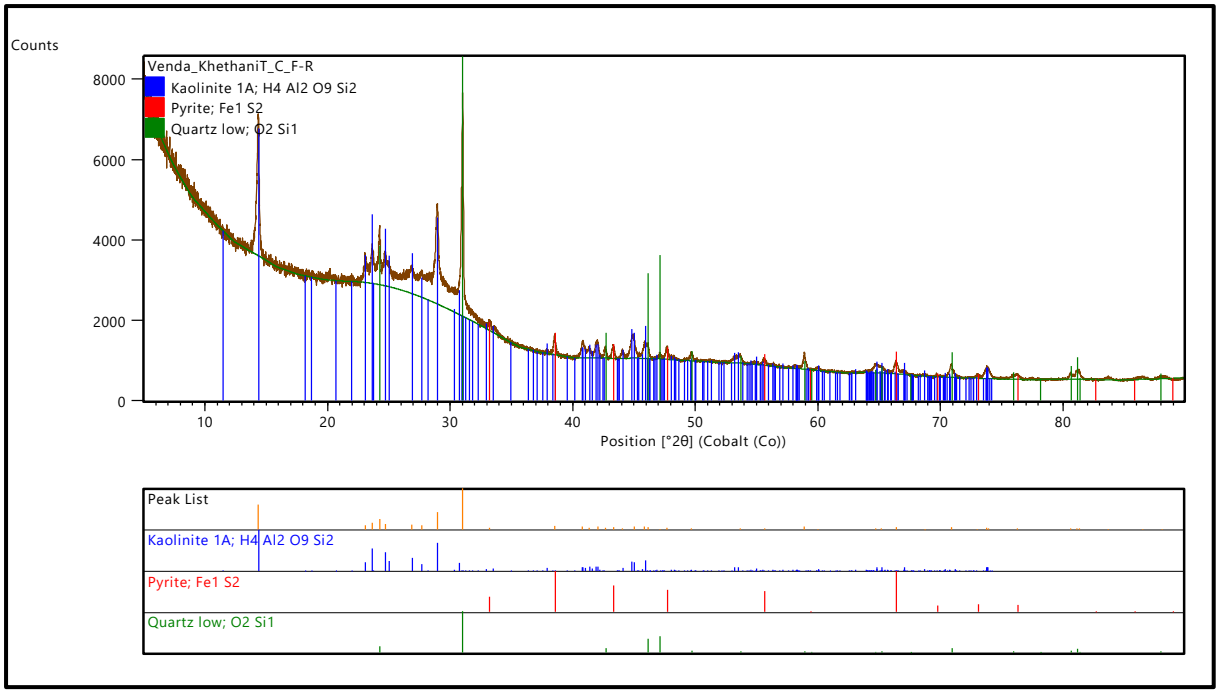

Appendix 6: X-ray diffraction patterns for Ply E S-L

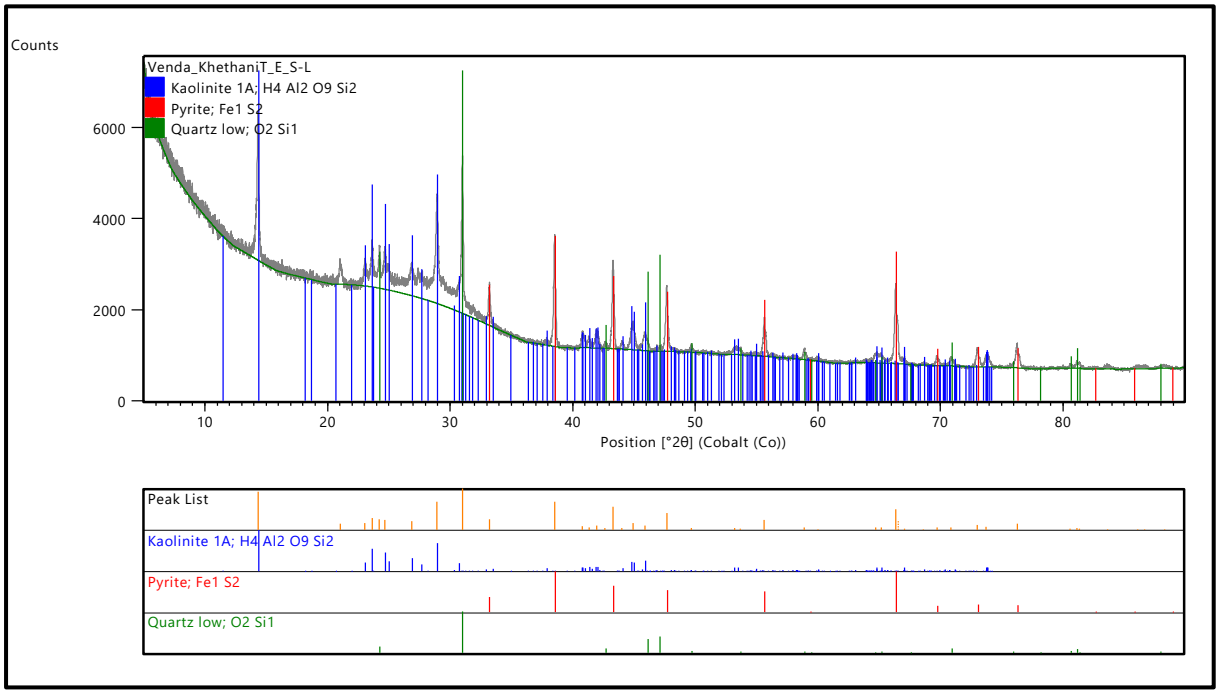


Appendix 7: X-ray diffraction patterns for Ply H S-L

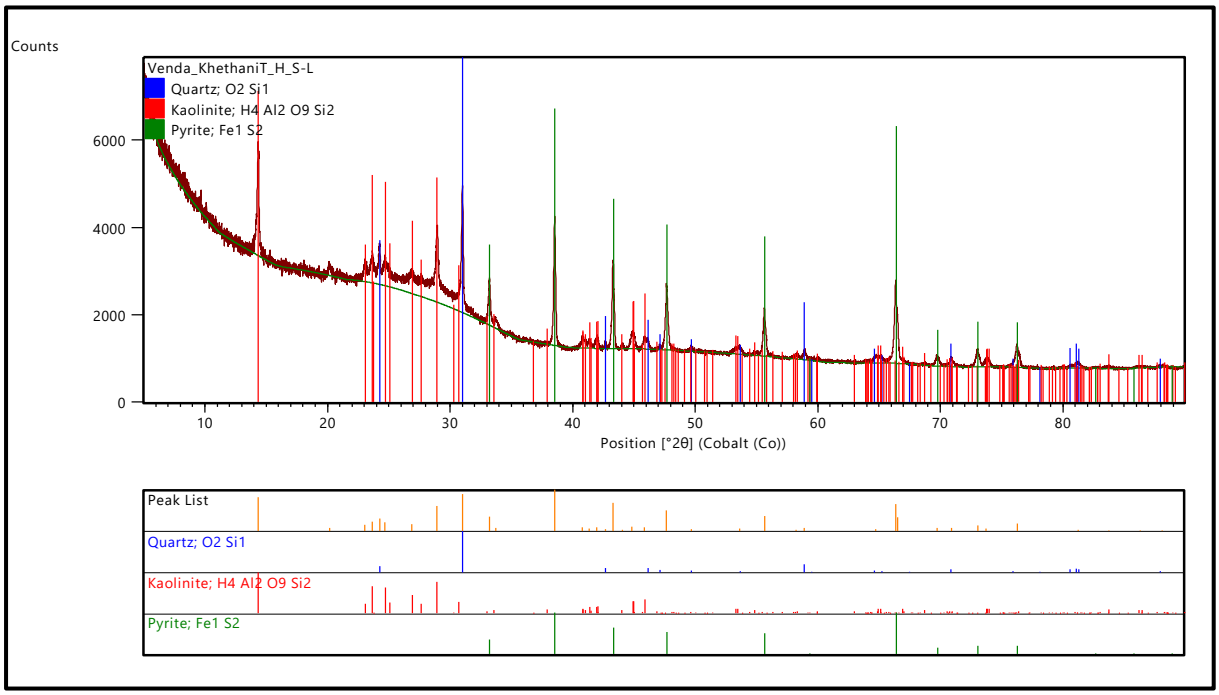

Appendix 8: X-ray diffraction patterns for Seam 10 composite

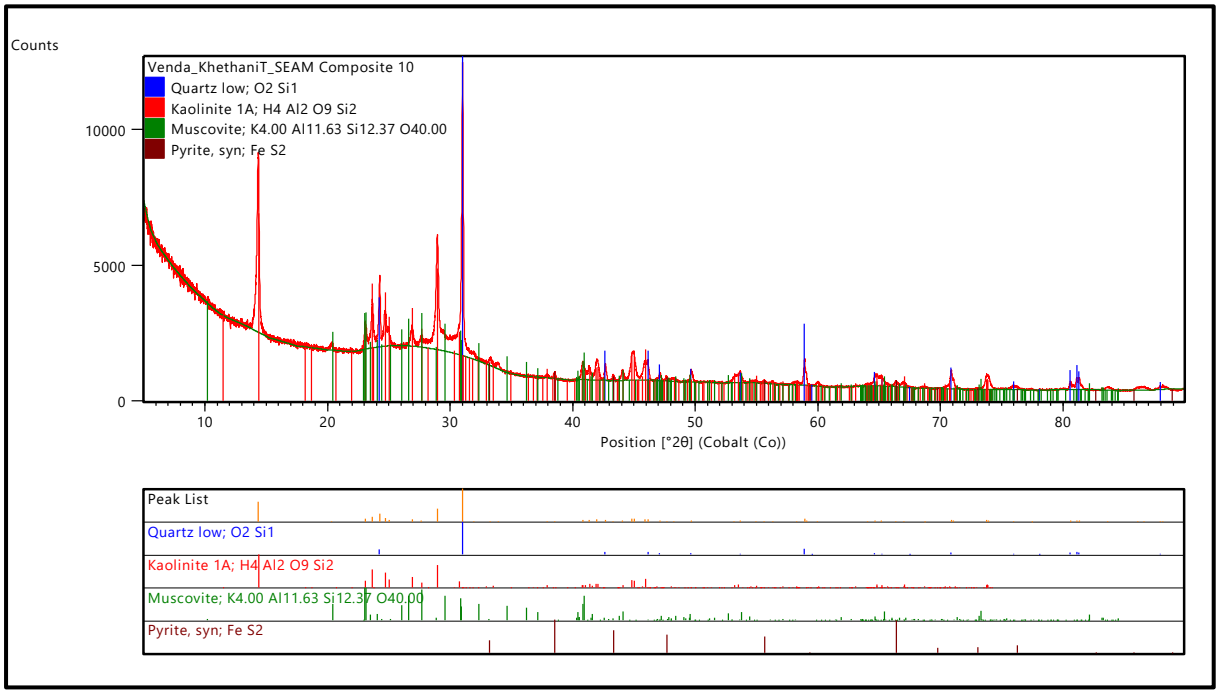


Appendix 9: X-ray diffraction patterns for Seam 11 composite

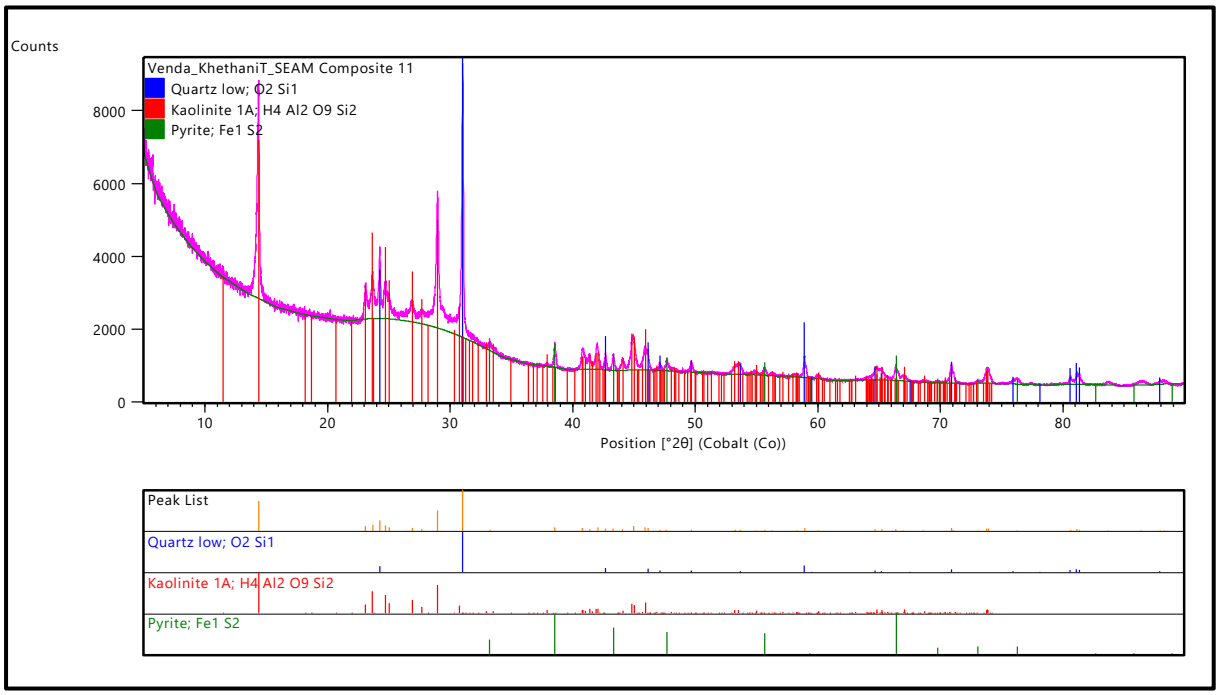

A.10: Combined Static Acid Base Accounting Screening Parameters with a Verdict

| Site Number | pH values | Net Neutralising Potential | NPR (Open System) | NPR (Closed System) | %S and NPR Method (Soregali and Lawrence,1997) | ABA INDEX | VERDICT |
|---|---|---|---|---|---|---|---|
| **Ply A F-R** | Higher Risk Acid Generation | Verify with other tests | Likely Acid Generator | Likely Acid Generator | Too little S to create sustained acidity | **15** | **Do Further Testing** |
| **Ply B F-R** | Higher Risk Acid Generation | Potential Acid Generator | Likely Acid Generator | Likely Acid Generator | Additional Confirmation of Acidity | **55** | **High Acid Potential** |
| **Ply C F-R** | Higher Risk Acid Generation | Potential Acid Generator | Likely Acid Generator | Likely Acid Generator | Additional Confirmation of Acidity | **607** | **High Acid Potential** |
| **Ply D F-R** | Higher Risk Acid Generation | Potential Acid Generator | Likely Acid Generator | Likely Acid Generator | Additional Confirmation of Acidity | **688** | **High Acid Potential** |
| **Ply E F-R** | Higher Risk Acid Generation | Potential Acid Generator | Likely Acid Generator | Likely Acid Generator | Additional Confirmation of Acidity | **787** | **High Acid Potential** |
| **Ply H F-R** | Higher Risk Acid Generation | Potential Acid Generator | Likely Acid Generator | Likely Acid Generator | Additional Confirmation of Acidity | **58** | **High Acid Potential** |
| **Ply G F-R** | Higher Risk Acid Generation | Potential Acid Generator | Likely Acid Generator | Likely Acid Generator | Additional Confirmation of Acidity | **52** | **High Acid Potential** |
| **Ply A S-L** | Higher Risk Acid Generation | Verify with other tests | Likely Acid Generator | Likely Acid Generator | Too little S to create sustained acidity | **3** | **Do Further Testing** |
| **Ply B S-L** | Higher Risk Acid Generation | Potential Acid Generator | Likely Acid Generator | Likely Acid Generator | Additional Confirmation of Acidity | **75** | **High Acid Potential** |
| **Ply C S-L** | Higher Risk Acid Generation | Potential Acid Generator | Likely Acid Generator | Likely Acid Generator | Additional Confirmation of Acidity | **371** | **High Acid Potential** |

| | | | | | | | |
|---|---|---|---|---|---|---|---|
| **Ply D S-L** | Higher Risk Acid Generation | Verify with other tests | Likely Acid Generator | Likely Acid Generator | Too little S to create sustained acidity | **12** | **Do Further Testing** |
| **Ply E S-L** | Higher Risk Acid Generation | Potential Acid Generator | Likely Acid Generator | Likely Acid Generator | Additional Confirmation of Acidity | **2276** | **High Acid Potential** |
| **Ply F S-L** | Higher Risk Acid Generation | Potential Acid Generator | Likely Acid Generator | Likely Acid Generator | Additional Confirmation of Acidity | **307** | **High Acid Potential** |
| **Ply G S-L** | Higher Risk Acid Generation | Verify with other tests | Likely Acid Generator | Likely Acid Generator | Too little S to create sustained acidity | **14** | **Do Further Testing** |
| **Ply H S-L** | Higher Risk Acid Generation | Potential Acid Generator | Likely Acid Generator | Likely Acid Generator | Additional Confirmation of Acidity | **5603** | **High Acid Potential** |
| **Seam 10** | Higher Risk Acid Generation | Potential Acid Generator | Likely Acid Generator | Likely Acid Generator | Additional Confirmation of Acidity | **1487** | **High Acid Potential** |
| **Seam 11** | Higher Risk Acid Generation | Potential Acid Generator | Likely Acid Generator | Likely Acid Generator | Additional Confirmation of Acidity | **519** | **High Acid Potential** |
| **Shale F-R** | Medium Risk Acid Generation | Verify with other tests | Likely Acid Generator | Likely Acid Generator | Too little S to create sustained acidity | **4** | **Do Further Testing** |